AD-A049 077 NAVAL UNDERSEA CENTER SAN DIEGO CALIF F/G 17/1
SURFACE-DUCT SONAR MEASUREMENTS (SUDS I - 1972).(U)
NOV 76 E R ANDERSON
UNCLASSIFIED NUC-TP-463 NL

| OF 3
AD A049077

NUC TP 463

SURFACE-DUCT SONAR MEASUREMENTS (SUDS I - 1972) TECHNICAL REPORT

by

E. R. Anderson

Undersea Sciences Department

M. A. Pedersen

Undersea Surveillance Department

November 1976

Approved for public release; distribution unlimited.

NAVAL UNDERSEA CENTER, SAN DIEGO, CA. 92132

AN ACTIVITY OF THE NAVAL MATERIAL COMMAND

R. B. GILCHRIST, CAPT, USN
Commander

HOWARD L. BLOOD, PhD
Technical Director

ADMINISTRATIVE INFORMATION

During February 1972 the Naval Undersea Center conducted a series of 18 propagation loss experiments in three deep-water areas off the coast of California. These experiments are known as the SUrface Duct Sonar Measurements (SUDS I – 1972). This work was originally supported by the then Naval Ships Systems Command, Sonar Technology Division, PMS-302-4 and partly supported by the Office of Naval Research, code 102-OSC. The preparation of this report began in April 1973 under the sponsorship of the Naval Sea Systems Command, code 06H1-4, problem SF 52-552-602, task 19344. This report covers work from March 1971 to August 1976 and was approved for publication on 23 November 1976.

Technical reviewers for this report were R. F. Hosmer and P. G. Hansen.

Released by

H. E. MORRIS, Head
Ocean Sciences Group

Under authority of

B. A. POWELL, Head
Undersea Sciences Department

ACKNOWLEDGMENTS

The SUDS I program was a coordinated effort involving personnel from the Undersea Sciences and the Undersea Surveillance Departments. Also participating in the oceanographic measurement program were personnel from the Lockheed Ocean Laboratory. The program was basically an Acoustic Propagation Division project developed by H. P. Bucker and H. S. Aurand.

The Principal Investigator for the SUDS experiments was J. Cummins. H. P. Bucker was the Senior Scientist for the CW pulse measurements, D. L. Keir Senior Scientist for the explosive measurements, P. G. Hansen and K. W. Nelson co-Senior Scientists for the oceanographic measurements program, and D. P. Hamm Principal Investigator for the Lockheed Ocean Laboratory. R. W. McGirr was in charge of the planning aspects of acoustic modeling. Additional contributions were made to experiment planning by J. R. Lovett and J. D. Pugh.

Preliminary analysis of the acoustic data was done by H. P. Bucker and H. E. Morris. Assisting in the preliminary data reduction and analysis of the acoustic data was J. L. Thompson, an exchange scientist from RANRL, Sidney, Australia, and R. W. Townsen. Preliminary analysis of the environmental data was done by K. W. Nelson.

H. P. Bucker was the Scientist-in-Charge aboard the *DeSteiguer*, D. E. Good Scientist-in-Charge aboard the *Lee*, and P. A. Hanson Scientist-in-Charge aboard the *Cape*. Assisting with the acoustic measurements at sea were T. E. Stixrud, C. K. Lisle, N. J. Martini, D. White, and R. F. Hosmer. Assisting with the oceanographic measurements at sea were A. E. Diamond, H. L. Hascall, C. T. Smallenberger, and W. M. Woods. The assistance of the officers and men of the *DeSteiguer*, *Lee*, and *Cape* in making the propagation loss and oceanographic measurement program a success is acknowledged.

The following assisted in a consulting and planning capacity: M. A. Pedersen, K. V. Mackenzie, D. F. Gordon, D. Murdock, E. R. Anderson, P. A. Barakos, O. S. Lee, W. F. Potter, R. H. Allen, M. J. Hoernemann, and L. A. Smothers.

The assistance of C. L. Barker and C. D. Curtis in calibrating the teletherm buoy sensors, of K. W. Nelson, S. L. Speidel, D. White, D. F. Gordon, and G. L. Crutcher in the data reduction and computer aspects of the work, and of O. S. Lee in the spectral analysis of the Waverider buoy measurements is gratefully acknowledged.

Additional acknowledgments are: Pacific Missile Range, Geophysics Division, Point Mugu, CA, furnished the Datawell Waverider buoy system; Fleet Numerical Weather Central, Monterey, CA, furnished the expendable bathythermograph probes; Fleet Weather Facility, San Diego, CA, arranged for air-dropped expendable bathythermographs in the SUDS I areas prior to the ships moving from station 2 to station 3; the Naval Oceanographic Office, Pacific Support Group, San Diego, CA, provided personnel to make environmental measurements and to assist aboard the *DeSteiguer*; and the Navy Electronics Laboratory Center, Communications Facilities Support Branch, provided the shore-based portions of the ship-to-shore communications. The Lockheed Ocean Laboratory, with L. D. Coates as Program Manager, constructed the Teletherm buoy system, operated the system at sea, and provided the initial reduction of the data.

UNCLASSIFIED

SECURITY CLASSIFICATION OF THIS PAGE (When Data Entered)

REPORT DOCUMENTATION PAGE	READ INSTRUCTIONS BEFORE COMPLETING FORM
1. REPORT NUMBER: NUC-TP-463	2. GOVT ACCESSION NO. / 3. RECIPIENT'S CATALOG NUMBER
4. TITLE (and Subtitle): SURFACE-DUCT SONAR MEASUREMENTS (SUDS I-1972) TECHNICAL REPORT.	5. TYPE OF REPORT & PERIOD COVERED: Research & Development Rept. March 1971 – August 1976 / 6. PERFORMING ORG. REPORT NUMBER
7. AUTHOR(s): E. R. Anderson	8. CONTRACT OR GRANT NUMBER(s)
9. PERFORMING ORGANIZATION NAME AND ADDRESS: Naval Undersea Center, San Diego, California 92132	10. PROGRAM ELEMENT, PROJECT, TASK AREA & WORK UNIT NUMBERS: SF 52-552, Task 19344
11. CONTROLLING OFFICE NAME AND ADDRESS: Naval Sea Systems Command, Washington, D.C. 20360	12. REPORT DATE: November 1976 / 13. NUMBER OF PAGES: 199
14. MONITORING AGENCY NAME & ADDRESS (if different from Controlling Office): 12 199p.	15. SECURITY CLASS. (of this report): Unclassified / 15a. DECLASSIFICATION/DOWNGRADING SCHEDULE
16. DISTRIBUTION STATEMENT (of this Report): Approved for public release; distribution unlimited. 16 F52552 17 SF5255202	
17. DISTRIBUTION STATEMENT (of the abstract entered in Block 20, if different from Report)	
18. SUPPLEMENTARY NOTES	
19. KEY WORDS (Continue on reverse side if necessary and identify by block number): Sonar; Underwater sound propagation; Seawater sound speed; Propagation loss; Ocean temperature; Ocean salinity	

20. ABSTRACT (Continue on reverse side if necessary and identify by block number)

During 9-24 February 1972 a series of 18 propagation loss experiments were conducted in three deep-water areas located southwest of San Diego, California. These measurements were designed to measure near-surface continuous wave (CW) pulse propagation losses and propagation losses for explosive sources out to ranges of 45 kyd and to obtain detailed supporting environmental measurements. Measurements were made at

DD FORM 1 JAN 73 1473 EDITION OF 1 NOV 65 IS OBSOLETE

UNCLASSIFIED

SECURITY CLASSIFICATION OF THIS PAGE (When Data Entered)

390 458

KB

20. (Continued)

CW frequencies of 0.4, 1.0, 1.5, 2.5, 3.5, and 5.0 kHz. The explosive measurements were analyzed at 0.40, 0.63, 1.00, 1.60, 2.50, 3.15, 5.00, and 10.00 kHz.

This is the first in a series of three NUC Technical Papers reporting the results of these measurements. This report includes a brief historical background of near-surface propagation loss measurements, a summary of the experimental plan designed to accomplish the SUDS I objectives, and an analysis and discussion of the environmental and propagation loss measurements. Included, for selected propagation loss runs, are comparisons of the measured propagation losses with theoretical propagation losses computed using inputs derived from the environmental measurements.

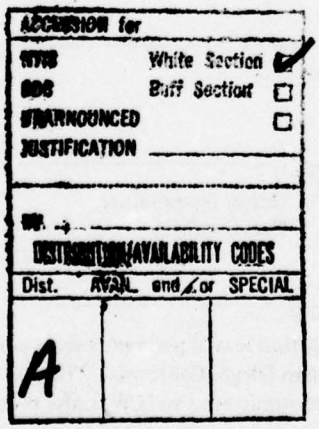

SUMMARY

PROBLEM

Develop a data base by obtaining near-surface propagation loss measurements complete with relevant supporting environmental measurements.

Specifically, the SUDS I experiments were designed to measure near-surface continuous wave (CW) pulse propagation losses and propagation losses for explosive sources out to ranges of 45 kyd and to obtain detailed supporting environmental measurements in three deep-water areas off the west coast of southern California. This report contains a brief historical background of near-surface propagation loss measurements, a summary of the experimental plan designed to accomplish the SUDS I objectives, and an analysis and discussion of the environmental and propagation loss measurements. Included, for selected propagation loss runs, are comparisons of the measured propagation losses with theoretical propagation losses computed using inputs derived from the environmental measurements.

RESULTS

- Because of surface-decoupling effects, theory predicts that the 0.4-kHz propagation loss for the shallowest receiver (4 to 6 m) is greater than at the next shallowest receiver (17 to 34 m) and that at 5.0 kHz the propagation loss is comparable for the two receiver depths. A comparison of the propagation losses measured by the two shallowest receivers suggests that at 5.0 kHz the propagation loss at the shallowest receiver, corresponding to the depth of a surface-ship hull-mounted sonar, was comparable to the propagation loss measured at the next deeper receiver. However, there appears to be some performance degradation at the shallowest receiver, even at 3.5 kHz, with the degradation becoming progressively greater at lower frequencies.
- Two of the 0.4-kHz and 1.0-kHz propagation loss runs were made in the presence of similar oceanographic and acoustic parameters. Despite the similarity, the propagation loss measurements for comparable receiver depths showed marked differences. Some of the differences are explained in terms of the number of modes trapped in the near-surface channels. However, there still remain some marked differences which the theoretical calculations did not support. For example, the combination of exceedingly small propagation losses measured by the shallow receivers at 0.4 kHz and the exceedingly large propagation losses measured by the deep receivers at 1.0 kHz is difficult to explain in terms of present understanding for nonrange-dependent sound-speed profiles.
- Theoretical propagation losses calculated using the n-layer normal-mode model are relatively insensitive to sound-speed profile inputs for receivers located in the main thermocline as compared to receivers located above the thermocline.
- Comparison of theoretical and measured propagation losses suggests that acoustically important features of the sound-speed profiles present during some propagation loss

runs represent critical regimes, requiring much greater accuracy than can be obtained from a consideration of a few XBT measurements.

- Examination of the average sound-speed profiles derived from thermistor chain measurements at standard hydrographic cast depths indicates that they can be categorized into seven general types. The most prevalent average profile was a surface channel over a depressed channel and the least prevalent a surface channel over two depressed channels. The classical bilinear surface channel, used by most propagation loss models, was the second most prevalent type.
- A comparison of sound-speed profiles derived from XBT profiles read with a digitizer and thermistor chain measurements suggests that XBT profiles read at standard hydrographic cast depths do not provide adequate sound-speed inputs to presently used propagation loss models. Better agreement between thermistor chain- and XBT-derived sound-speed profiles was obtained by digitizing the XBT profiles at 5-m depth intervals from the surface to the top of the main thermocline.
- Initial analysis indicated that nine of the propagation loss runs were characterized by single sound-speed profiles, suggesting spatial and temporal homogeneity in sound speed (Ref. 2). A few of these runs were re-analyzed using one-half hour averages of the thermistor chain measurements. These one-half hour average sound-speed profiles, based on 180 thermistor chain temperature profiles, showed progressive changes within one profile type and, in some cases, a change to a different profile type. This suggests that perhaps the sound-speed profiles for none of the propagation loss runs are spatially or temporally homogeneous.
- Customary methods of converting temperature and salinity measurements into sound-speed profiles utilize measurements at standard hydrographic cast depths and certain special depths, such as the depth of surface channels and depressed channels. Detailed examination of the thermistor chain measurements indicates that the average temperatures for the individual thermistor chain sensors represent a capability for greatly increasing the accuracy of critical input parameters to propagation loss models.

RECOMMENDATIONS

- Reduce, analyze, and report the bottom-reflected measurements made during all propagation loss runs, the short-pulse fluctuation measurements made for 10-min samples at various fixed ranges, and the bistatic reverberation measurements made with source and receiver 1.0 kyd apart.
- Apply the new approaches of this report, as well as the simple models presently in general use, to all of the SUDS I propagation loss runs.
- Study the sensitivity of propagation loss models to the details of the sound-speed profile inputs. Once the sensitivity is established, determine an optimum sample size of the thermistor chain measurements that averages out scatter but preserves trends and, utilizing average thermistor chain temperatures, develop a computerized technique for statistically fitting functions appropriate to the propagation loss model being employed.
- Study the application of the parabolic equation model to complex environmental situations such as those present during station 2 run 1. Since the basic method allows

the introduction of an unlimited number of sound-speed profiles, it could be applied with varying degrees of refinement.

- Plan and conduct an experiment to investigate the effect of a temperature frontal surface on propagation loss.
- Determine whether or not theoretical propagation loss calculations can be brought into closer agreement with the station 3 run 3 and station 1 run 2 experimental propagation losses by using sound-speed profiles derived from one-half hour averages of thermistor chain temperature measurements as inputs to the parabolic equation model.
- Investigate the penalty paid for a shallow source, or receiver, by subjecting the experimental data to a detailed comparison on a pulse-to-pulse basis by utilizing a computer and making normal-mode calculations to determine the optimum receiver or source depth for each of the SUDS I propagation loss run sound-speed profiles and for each frequency. Comparison of the theoretical losses at the optimum depth with the theoretical losses for the 4- to 6-m receiver depths would establish the penalty for a hull-mounted sonar.
- Develop techniques for the quantitative comparison between experiment and theory that will adequately account for a displacement between experimental and theoretical beats.
- Study the problem of finding mode eigenvalues for multiple-channel profiles and for negative-gradient profiles, such as were encountered in the SUDS I propagation loss runs.

CONTENTS

CONTENTS (Continued)

CONTENTS (Continued)

FIGURES

FIGURES (Continued)

TABLES

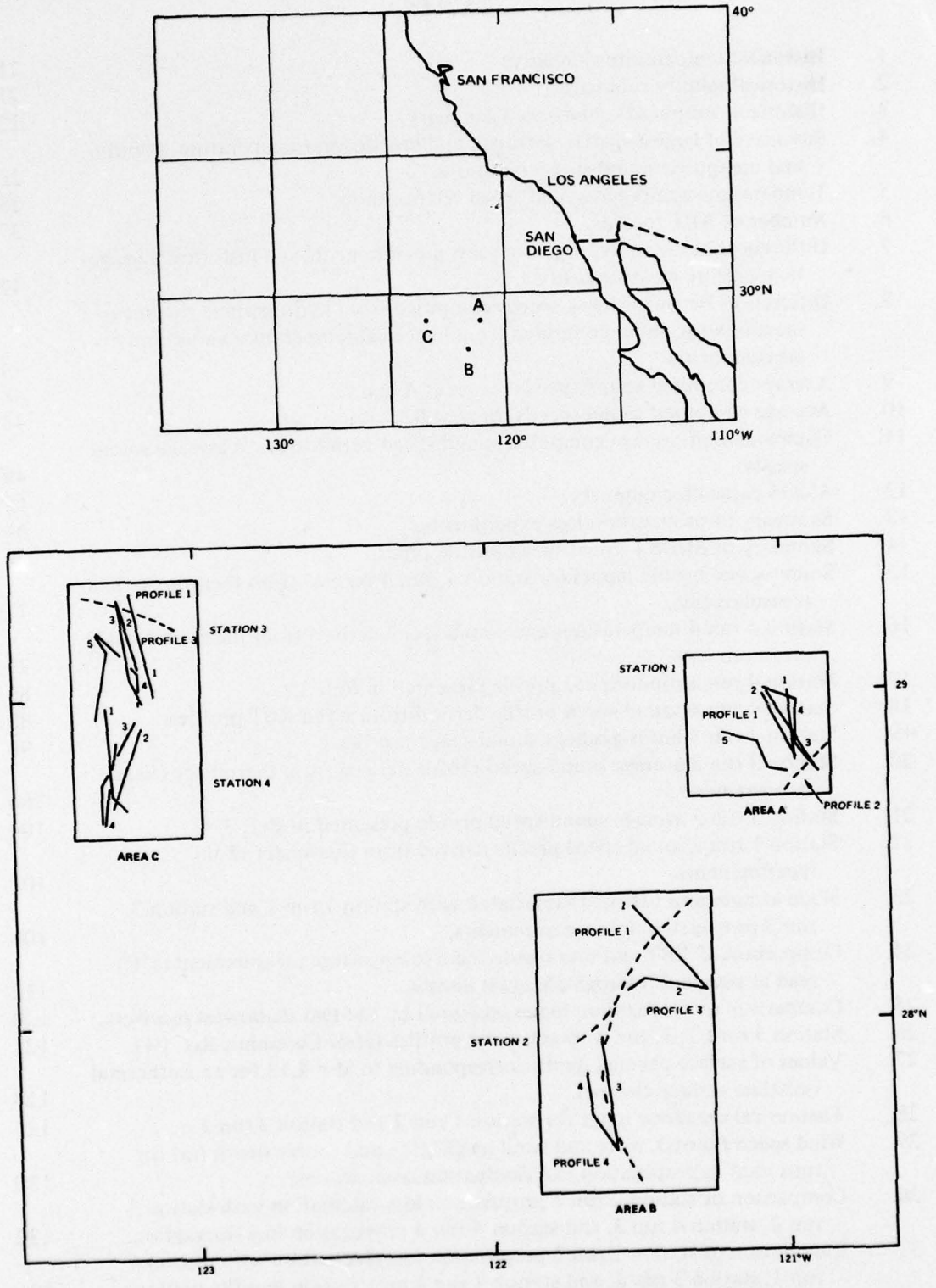

Figure 1. Location of experiments and sound-speed profile boundaries.

INTRODUCTION

The Naval Undersea Center made measurements of near-surface propagation losses in three deep-water areas off the west coast of southern California from 9 to 24 February 1972. In addition, bottom reflection, reverberation, and short and long CW-pulse fluctuation measurements were made. The propagation loss measurements were made at four acoustic stations, with either 4 or 5 propagation loss runs made during each station for a total of 18 propagation loss runs. Collectively these measurements are known as the SUrface Duct Sonar Measurements (SUDS I – 1972). The locations of the experimental areas, acoustic stations, and propagation loss runs are shown in Fig. 1. The dashed lines show the locations of sound-speed profile shape boundaries crossed during the propagation loss runs.

The objectives of the SUDS I program were to:

1. Measure propagation losses, at frequencies below 10.0 kHz, for acoustic energy traveling in near-surface propagation paths – direct, surface channel, depressed channel, and diffraction.

2. Measure bottom reflection, reverberation, and short and long CW-pulse fluctuation as functions of range, receiver depth, and frequency.

3. Measure all oceanographic parameters necessary to describe the temporal and spatial distribution of sound speed and sea-surface roughness present during the propagation loss measurement runs.

The purposes of the SUDS I measurement program were to:

1. Provide data necessary to improve the Navy Interim Surface Ship Sonar Prediction Model (NISSM), especially for frequencies below 10.0 kHz.

2. Provide data to evaluate recently developed near-surface propagation loss prediction models.

3. Provide data for the NAVSEA Ocean Environmental Acoustic DAta Bank (NAVDAB).

This is the first in a series of three NUC Technical Papers reporting on the propagation loss and supporting environmental measurements made during the SUDS I propagation loss measurement runs. The second report in the series, NUC TP 464 (Ref. 1), contains the propagation loss measurements made during the four acoustic stations. It consists of five volumes. Volume I describes the instrumentation used to make the propagation loss measurements and the data reduction procedures. Volumes II–V, one volume for each acoustic station, are detailed reports containing a summary of the environmental measurements, plots of propagation loss versus range, and comments pertinent to a specific propagation loss run. All comments and comparisons are qualitative, being based on a visual comparison of propagation loss plots. Due to a lack of funds, the bottom reflection, reverberation, and fluctuation measurements were not analyzed and, hence, are not included in this report. The third report in this series, NUC TP 465 (Ref. 2), contains the supporting environmental measurements made during the four acoustic stations. This report also consists of five volumes.

Volume I discusses the instrumentation used to make the required environmental measurements, the data reduction procedures, an accuracy analysis of the final measurements, and the method of reconstruction of the experimental track charts. Volumes II–V, one volume for each acoustic station, are detailed reports containing all of the environmental measurements applicable to each propagation loss run. A summary of preliminary results has been reported by Cummins (Ref. 3). The data contained in the present series of reports supersede the data reported in Ref. 3. Comparisons of propagation loss models with the SUDS I experimental data were reported by Morris (Ref. 4).

This report provides a brief historical background of near-surface propagation loss measurements, a summary of the experimental plan designed to accomplish the SUDS I objectives, and an analysis and discussion of the environmental and propagation loss measurements. Included, for selected propagation loss runs, are comparisons of the measured propagation losses with theoretical propagation losses computed using inputs derived from the environmental measurements.

Participating in these experiments were the USNS *S. P. Lee* (TAG-192), the USNS *DeSteiguer* (T-AGOR-12), and the R/V *Cape*. The *Lee* was the source ship, the *DeSteiguer* the receiving ship, and the *Cape* operated and monitored environmental sensors.

BACKGROUND

This section contains a brief historical review of selected sets of propagation loss measurements of acoustic energy traveling in near-surface acoustic paths. For purposes of this discussion, near-surface propagation is defined as acoustic energy traveling in the upper few hundred meters of the ocean via direct, surface channel, depressed channel, combined surface channel and depressed channel, and diffraction propagation paths.

AMOS MEASUREMENTS

The AMOS (Acoustic, Meteorological, and Oceanographic Survey) measurements of near-surface propagation loss were made during 10 cruises from June 1949 to April 1953. During these cruises propagation loss measurements were made at 192 acoustic stations in the North Atlantic Ocean. Most of the measurements were made at 2.2, 8.0, 16.0, and 25.0 kHz, with fewer measurements made at frequencies down to 70 Hz using an underwater siren and a Mk 4v noisemaker. The unclassified studies based on these measurements were published by Marsh and Schulkin (Ref. 5). The major study, Study A (Ref. 5), was an analysis of all AMOS data in the 2.0- to 25.0-kHz frequency band. Based on this analysis, equations and charts that, for a given frequency and source and receiver depth, are functions of surface layer depth, depth of axis of depressed channels, sea state, bottom depth, and surface water temperature were prepared and presented. Collectively these equations and charts are referred to as the AMOS near-surface propagation loss prediction model and are presently in widespread use for providing estimates of near-surface propagation losses.

NEL MEASUREMENTS

The Navy Electronics Laboratory (NEL) made four limited sets of near-surface propagation loss measurements during the period from 1953 to 1964. The first set of measurements (using a 0.53-kHz source) was made in March 1953, out to a range of 85 nm, in a well-defined surface channel (Ref. 6). This set of measurements initiated a low-priority project into investigating the applicability of normal-mode theory applied to surface channel propagation (Ref. 7). A second set of measurements using 0.53- and 1.03-kHz sources was made in January 1955. Although these measurements were never published independently, they were used to test improved and refined normal-mode theories (Ref. 8). A third set of measurements, also unpublished, was made in December 1963. At that time NEL was asked to investigate by means of normal-mode theory the optimum source depth for below-layer targets. The December 1963 measurements were made to verify certain conclusions made as a result of this investigation (Ref. 9). The fourth set of NEL measurements was made in December 1964. Due to the low priority of surface channel propagation work at NEL, the A. D. Little Company was employed under contract to analyze and report the results (Ref. 10).

LOCKHEED MEASUREMENTS

The second attempt, after AMOS, to obtain a large-scale, comprehensive set of near-surface propagation loss measurements was undertaken by the Lockheed-California Company in 1965. As a result of the NEL studies, BUSHIPS contracted with Lockheed in early 1965 to investigate the sound field in and below surface ducts as a function of source depth

and frequency and to assess the adequacy of the normal-mode approach under various environmental conditions, particularly the effect of a rough surface (Ref. 11).

EXPERIMENTAL PLAN

Initial planning for the SUDS I experiments began in March 1971 with a scientific plan, completed in January 1972. The final plan, in addition to providing for acoustic measurements using both CW and explosive sources, contained provisions for a detailed set of oceanographic measurements designed to describe the temporal and spatial variation in sound speed and sea-surface roughness.

EVENT SCHEDULE

The plan called for acoustic and supporting environmental measurements to be made at four acoustic stations. At each station the following events were planned:

Event	Description	Hours
A	Temperature profile survey	6
B	Sound-speed profile survey	6
C	Deploy Teletherm buoy line Measure sound-speed profiles	12
D	Explosive propagation loss run	3
E	CW-pulse propagation loss runs *(4 runs of 5 hours each)*	20
F	Reverberation	2
G	Fluctuation	8
H	Recover Teletherm buoy line Measure sound-speed profiles	15
	Station duration	72

ACOUSTIC MEASUREMENTS

In order to meet the major objectives and purposes of the SUDS program, the plan provided for measurements of propagation loss, reverberation, and fluctuation as functions of frequency, source depth, receiver depth, and acoustic range. The plan provided for five propagation loss runs out to a minimum range of 24.0 kyd, with four of the runs being made using CW pulse sources and one run using explosive sources during each acoustic station. These runs were to be made in deep water off the coast of southern California in areas selected just prior to the execution of the experiments. For these experiments the *DeSteiguer* was the receiver ship and the *Lee* the source ship.

CW Pulse Propagation Loss Measurements

CW frequencies to be used were 0.4, 1.0, 1.5, 2.5, 3.5, and 5.0 kHz, with projectors towed at 3 knots at depths of 6 m or 0.7 of the surface layer depth. Receiver depths were to be 6 m and 0.4, 0.8, 1.3, and 2.0 of the surface layer depth. Two frequencies – 0.4 and

1.0 kHz, 1.5 and 2.5 kHz, or 3.5 and 5.0 kHz – were used during each CW run. At each frequency four 0.5-sec pulses were transmitted during each minute of the run. Acoustic ranges were obtained by measuring the time difference between an acoustic CW pulse and a radio pulse transmitted simultaneously with the acoustic pulse. This time difference was then multiplied by the near-surface sound speed to obtain the acoustic range. The arrivals were recorded on strip chart and magnetic tape recorders.

Explosive Propagation Loss Measurements

Mk 61 Signal Underwater Sound (SUS) charges detonated at 0.5-nm intervals at a depth of 18 m were used as sound sources during these runs. Receiver depths were the same as used during the CW runs. Acoustic ranges were obtained in the same way as obtained during the CW runs. The explosive arrivals were recorded broadband on magnetic tape recorders.

Reverberation Measurements

The reverberation measurements were made with the *Lee* maintaining a position as near to the *DeSteiguer* as practical. With the projector at a depth of 0.7 the surface layer depth, 5-sec pulses at 1-min intervals were hand-keyed. Ten CW pulses for each of the six frequencies were to be transmitted and recorded on the same recorder used during the CW propagation loss runs.

Fluctuation Measurements

Fluctuation measurements using short (0.5 sec) and long (10.0 min) pulses were to be made. The measurements consisted of four runs with the *Lee* drifting at ranges of 6.0, 12.0, 18.0, and 24.0 kyd from the *DeSteiguer*. The projector depth was 0.7 of the surface layer depth and receiver depths and recording techniques the same used during the CW pulse propagation loss runs.

OCEANOGRAPHIC MEASUREMENTS

The nature of the acoustic experiment should dictate the type and extent of the environmental measurement program designed to support the experiment. Past experience at NUC suggests that for the type of experiments designed to meet the major SUDS I objectives, the primary environmental variables are the vertical and horizontal distribution of sound speed and sea-surface roughness. Additionally, past experience has shown that because of instrumentation malfunction and accuracy limitations, redundancy in temperature and salinity measurements is essential. This redundancy provides a means of detecting and identifying erroneous and biasing measurements. The distribution of sound speed can be calculated from measurements of temperature and salinity as a function of depth and sea-surface roughness from measurements of wave height as a function of time.

The environmental data acquisition plan contained provisions for all ships to acquire environmental data. The types of environmental data to be acquired by each ship during the indicated event were:

	Event							
	A	B	C	D	E	F	G	H
Lee								
Hydrographic casts		x	x					x
STD/SV		x	x					x
XBT	x	x	x	x	x	x	x	x
Thermistor chain	x		x	x	x			x
Datawell Waverider buoy				x	x	x	x	
Stilwell wave system				x	x	x	x	
DeSteiguer								
Hydrographic casts		x	x					x
STD/SV		x	x					x
XBT	x	x	x	x	x	x	x	x
Cape								
Teletherm buoy line			x	x	x	x	x	x
XBT	x		x	x	x	x	x	
NUC wave spar buoy				x	x	x	x	

The hydrographic cast and the STD/SV were used to measure temperature and salinity from the surface to the bottom, and the XBT, thermistor chain, and the Teletherm buoy line were used to measure temperature to depths of 450, 242, and 125 m, respectively. The Datawell Waverider buoy, the Stilwell wave system, and the NUC spar buoy were used to measure surface wave heights as a function of time. In addition to the above measurements all ships were required to maintain a 2-hour weather observation log and a radar log of all ship contacts acquired during the acoustic data acquisition periods.

PHYSICAL OCEANOGRAPHY OF THE EXPERIMENTAL AREA

The SUDS I experimental areas were located in the southwestern edge of the California Current. The California Current is the eastern limb of the wind-driven subtropical anticyclone of the North Pacific Ocean. The name applies to the southeastward flow of water from the West Wind Drift to join the North Equatorial Current. Its eastern boundary is the coast of North America. It has no well-defined western boundary, but is common to define one arbitrarily at a distance of 1000 km (540 nm) from shore. The California Current may be visualized as a mass of water volumes sluggishly moving in a southeastern direction. These volumes are in the process of mixing; hence, both horizontal and vertical eddies of all sizes are present. At any given time and place the current may be flowing in any direction. However, over a long period of time the resultant current direction is southeast. By the time these water volumes reach 18–20°N latitude the mixing process has essentially been completed and a homogeneous water mass, Pacific Equatorial Water, has been formed. The active mixing process in the California Current extends to a depth of 1200–1500 m. At depths greater than this the water volume is essentially stable, with little spatial or temporal variability in oceanic properties.

To describe the time and space distribution of any property (i.e., temperature, salinity, sound speed, or density) in the SUDS I experimental areas the water volume may be thought of as one volume extending from the surface to 1200–1500 m, in which the variation of any property is a function of time and space, and a second volume extending from that depth to the bottom, in which the variation of any property is a function of space only. The time-space-dependent volume consists of two sub-volumes, one, extending from the surface to a few tens or hundreds of meters, containing periodic variations (diurnal and seasonal), and another overlapping volume extending from the surface to several hundred meters and containing aperiodic variations. In the SUDS I areas the first volume extends to 200–300 m and the second to 1200–1500 m. The diurnal variation extends to a few tens of meters and is most pronounced when calm to near-calm wind conditions are present. Under the influence of wind the diurnal variation is neutralized. The seasonal variation is the most important cyclical variation. In this area considerable year-to-year variation is observed, making it virtually impossible to estimate the distribution, in this layer, of any oceanic property from historical data. The aperiodic variability is also difficult to estimate from historical data. At the greater depths the variability of physical properties is small and for most applications can be estimated from a consideration of historical measurements.

HISTORICAL AVERAGE TEMPERATURE, SALINITY, AND COMPUTED SOUND SPEED

The temporal and spatial variability in temperature, salinity, and computed sound speed expected to be observed in the experimental area may be established from an analysis of historical hydrographic cast measurements of temperature and salinity as a function of depth. In this study computed sound speeds are determined from the hydrographic cast measurements of temperature, salinity, and depth and are based on Anderson's sound-speed equation (Ref. 12). Figure 2 shows, by the symbols (•, X), the locations of 94 hydrographic casts made in 16 different years between 1939 and 1964. Measurements were made in all months of the year. The depths of hydrographic casts deeper than 2000 m are also indicated on Fig. 2. Beginning in 1949 Scripps Institution of Oceanography began hydrographic cast measurements at selected locations off the west coast of North America. The lettered

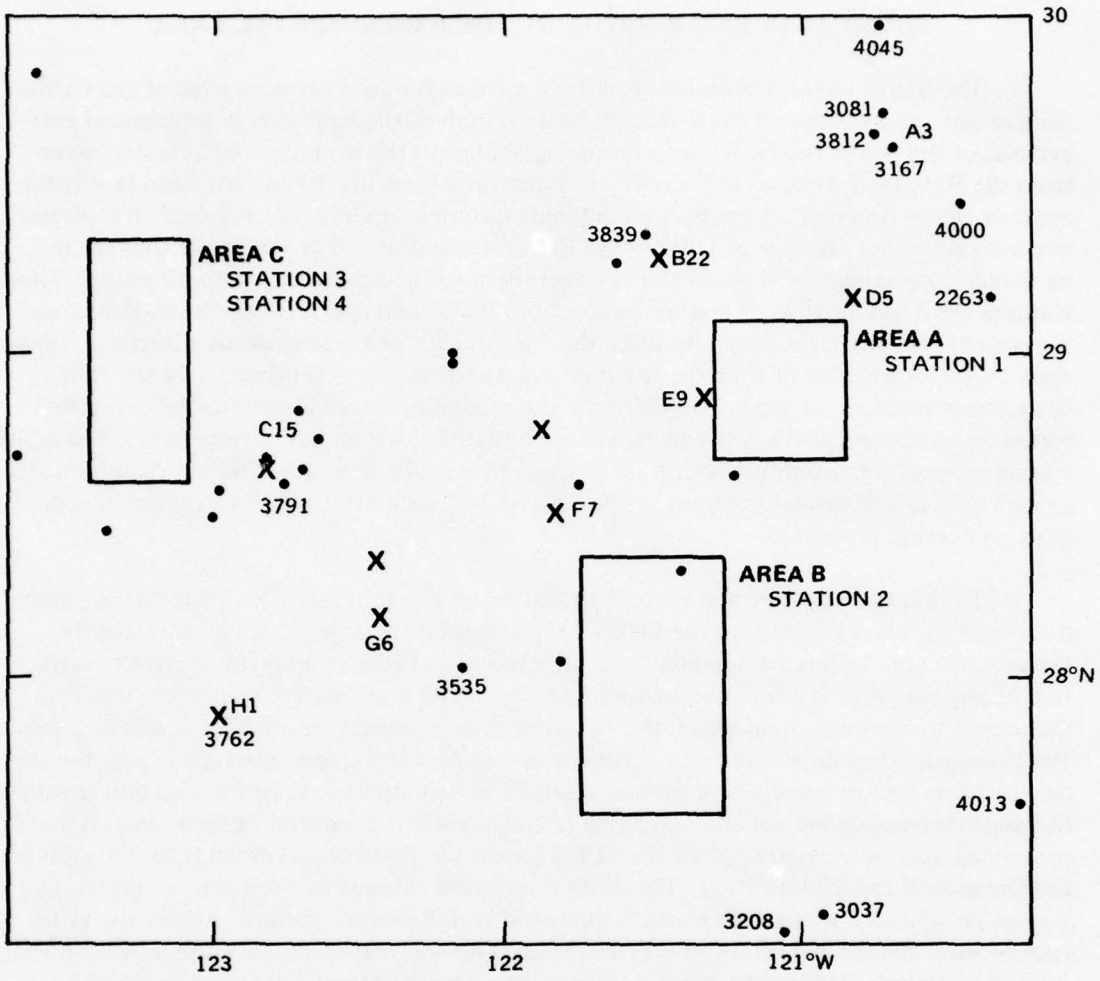

Figure 2. Location of historical hydrographic casts and the SUDS I experimental areas.

locations (X) show the positions of Scripps' locations pertinent to this analysis. The number of hydrographic casts made at these locations is also indicated. Also shown are the locations of the SUDS I experimental areas.

Average Temperature, Salinity, and Sound Speed

To obtain a general impression of the average temperature, salinity, and computed sound speed, and the associated variability, all hydrographic cast data shown in Fig. 2 were averaged and the standard deviation computed for standard hydrographic cast depths. These data together with the domains and ranges of the indicated variable are summarized in Tables 1 to 3. The variability in temperature and computed sound speed shows distinct changes between 150 and 250 m and between 800 and 1500 m, whereas the variability in salinity shows a more gradual decrease with increasing depth. Other studies of the distribution of these variables (Ref. 13) in the California Current show a marked decrease in variability at a depth of 1200 to 1500 m.

Table 1. Historical temperature summary (°C)

Depth, m	Number Observations	Average	Standard Deviation	Domain	Range
0	94	17.65	1.65	[14.60, 20.64]	6.04
10	94	17.54	1.56	[14.65, 20.42]	5.77
20	94	17.48	1.58	[14.46, 20.02]	5.56
30	93	17.35	2.44	[14.84, 20.00]	5.16
50	94	16.74	1.37	[13.13, 19.88]	6.75
75	94	15.74	1.19	[12.09, 17.88]	5.79
100	94	14.81	1.43	[11.16, 17.73]	6.57
125	94	13.42	1.39	[10.34, 16.79]	6.45
150	94	11.96	1.22	[9.63, 14.72]	5.09
200	94	9.73	0.60	[8.41, 11.35]	2.94
250	94	8.71	0.46	[7.68, 10.22]	2.54
300	93	7.96	0.48	[7.07, 9.60]	2.53
400	94	6.86	0.44	[5.98, 8.11]	2.13
500	93	6.08	0.34	[5.55, 7.03]	1.48
600	71	5.51	0.25	[5.03, 6.15]	1.12
800	63	4.65	0.19	[4.37, 5.59]	1.22
1000	59	3.97	0.10	[3.80, 4.22]	0.42
1200	34	3.46	0.07	[3.35, 3.61]	0.26
1500	15	2.86	0.05	[2.79, 2.94]	0.15
2000	15	2.12	0.03	[2.08, 2.19]	0.11
2500	13	1.80	0.02	[1.75, 1.84]	0.09
3000	13	1.64	0.03	[1.59, 1.70]	0.11
4000	3	1.59	0.02	[1.57, 1.60]	0.03

Table 2. Historical salinity summary (ppt)

Depth, m	Number Observations	Average	Standard Deviation	Domain	Range
0	94	33.68	0.20	[33.22, 34.20]	0.98
10	94	33.67	0.19	[33.21, 34.11]	0.90
20	94	33.67	0.20	[33.21, 34.18]	0.97
30	93	33.69	0.20	[33.21, 34.20]	0.99
50	94	33.69	0.20	[33.18, 34.13]	0.95
75	94	33.67	0.20	[33.05, 34.09]	1.04
100	94	33.68	0.22	[33.08, 34.14]	1.06
125	94	33.66	0.19	[33.12, 34.20]	1.08
150	94	33.64	0.15	[33.27, 34.00]	0.73
200	94	33.79	0.13	[33.53, 34.25]	0.72
250	94	33.97	0.10	[33.72, 34.40]	0.68
300	93	34.07	0.09	[33.89, 34.40]	0.51

Table 2. Continued.

Depth, m	Number Observations	Average	Standard Deviation	Domain	Range
400	94	34.16	0.08	[33.98, 34.46]	0.48
500	93	34.25	0.06	[34.03, 34.45]	0.42
600	71	34.32	0.05	[34.20, 34.42]	0.22
800	63	34.42	0.04	[34.30, 34.50]	0.20
1000	59	34.48	0.04	[34.40, 34.61]	0.21
1200	34	34.53	0.03	[34.45, 34.60]	0.15
1500	15	34.57	0.03	[34.52, 34.64]	0.12
2000	15	34.63	0.02	[34.60, 34.69]	0.09
2500	13	34.65	0.03	[34.59, 34.73]	0.14
3000	13	34.66	0.03	[34.61, 34.73]	0.12
4000	3	34.69	0.02	[34.68, 34.71]	0.03

Table 3. Historical computed sound-speed summary (m/sec)

Depth, m	Number Observations	Average	Standard Deviation	Domain	Range
0	94	1513.6	5.0	[1504.0, 1522.3]	18.3
10	94	1513.4	4.7	[1504.4, 1521.7]	17.3
20	94	1513.3	4.8	[1503.9, 1521.1]	17.2
30	93	1513.1	4.8	[1502.6, 1521.1]	18.5
50	94	1511.6	4.3	[1500.0, 1521.4]	21.4
75	94	1509.0	3.9	[1496.8, 1515.8]	19.0
100	94	1506.4	4.8	[1493.7, 1516.0]	22.3
125	94	1502.3	4.8	[1491.3, 1513.7]	22.4
150	94	1497.8	4.3	[1489.3, 1507.5]	18.2
200	94	1490.9	2.1	[1486.3, 1496.7]	10.4
250	94	1488.3	1.7	[1484.5, 1494.9]	10.4
300	93	1486.4	1.9	[1482.9, 1492.7]	9.8
400	94	1483.9	1.8	[1480.4, 1488.9]	8.5
500	93	1482.6	1.4	[1480.4, 1486.5]	6.1
600	71	1482.1	1.1	[1480.1, 1484.6]	4.5
800	63	1481.9	0.6	[1480.8, 1483.7]	2.9
1000	59	1482.6	0.4	[1481.8, 1483.6]	1.8
1200	34	1483.8	0.3	[1483.3, 1484.4]	1.1
1500	15	1486.3	0.2	[1486.0, 1486.6]	0.6
2000	15	1491.7	0.1	[1491.5, 1492.0]	0.5
2500	13	1498.9	0.1	[1498.7, 1499.0]	0.3
3000	13	1506.9	0.1	[1506.6, 1507.0]	0.4
4000	3	1524.3	0.1	[1524.2, 1524.3]	0.1

Spatial Variation

Information on the spatial variation is obtained from the hydrographic cast measurements made at different distances apart but on the same day of the year. One such set of measurements were contained in the historical data set. Figure 3 shows differences in temperature, salinity, and computed sound speed for pairs of hydrographic cast measurements taken on 13 August 1949. These measurements were taken at locations E, F, G, and H (Fig. 2). The differences are for distances between hydrographic casts made at E and F, E and G, E and H – 35, 70, 105 nm apart, respectively. The differences are shown on the abscissa, the selected depths are indicated on the ordinate, and the distance apart are ordered for each depth as indicated at the 10 m depth. If the difference is positive, the parameter value is largest at location E. These data show, at least on 13 August 1949, little spatial variability from the surface to 30 m. The largest differences in temperature, salinity, and computed sound speed were 0.21°C, 0.09 ppt, and 0.7 m/sec, respectively. For depths greater than 30 m there appears to be little systematic variability related to the distance between measurements. The largest differences observed were 1.66°C, 0.34 ppt, and 5.2 m/sec for temperature, salinity, and computed sound speed, respectively.

Seasonal Variation

In 1949, 31 hydrographic casts were made at approximately monthly intervals from March through November at the locations indicated on Fig. 2 by the symbol (**X**). All but three of the measurements were made at the Scripps' locations D, E, F, G, and H. These data are used to obtain an estimate of the expected seasonal variation in temperature, salinity, and computed sound speed. Appendix A summarizes the observed season variability in temperature and salinity from the surface to 600 m and computed sound speed from the surface to 1000 m. The systematic cyclical nature of the seasonal variability is obvious from the surface to 50 m, while from 75 m to 200 m it is less obvious. For depths greater than 200 m, systematic seasonal variation is not observed. Thus, at least in 1949, the seasonal variation extended to a depth of about 200 m.

Year-to-Year Variation

An estimate of the year-to-year variation is obtained from hydrographic casts made at the same location on the same day of the year but in different years. The historical data set contained 12 pairs of hydrographic casts made at location B within 6 days of each other and 1 to 14 years apart in time, and 4 pairs made at location C within 4 days of each other and 4 to 12 years apart in time. Figure 4 summarizes the largest differences in temperature, salinity, and computed sound speed as a function of standard hydrographic casts depths for these data sets. The upper line is for location B and the lower for location C. In general, the largest differences (4.14°C, 1.02 ppt, and 14.5 m/sec) are observed at 100 m, with the differences at depths greater than 500 m decreasing to about 0.24°C, 0.10 ppt, and 1.0 m/sec.

Summary

The averages of 94 hydrographic cast measurements of temperature, salinity, and computed sound speed taken during all months of the year in 16 different years from 1939 to 1964 in the SUDS I experimental areas show that the major variability in these parameters, from all causes, will be observed from the surface to about 250 m depth. For depths greater than 1200 m the water column shows little variability in these parameters.

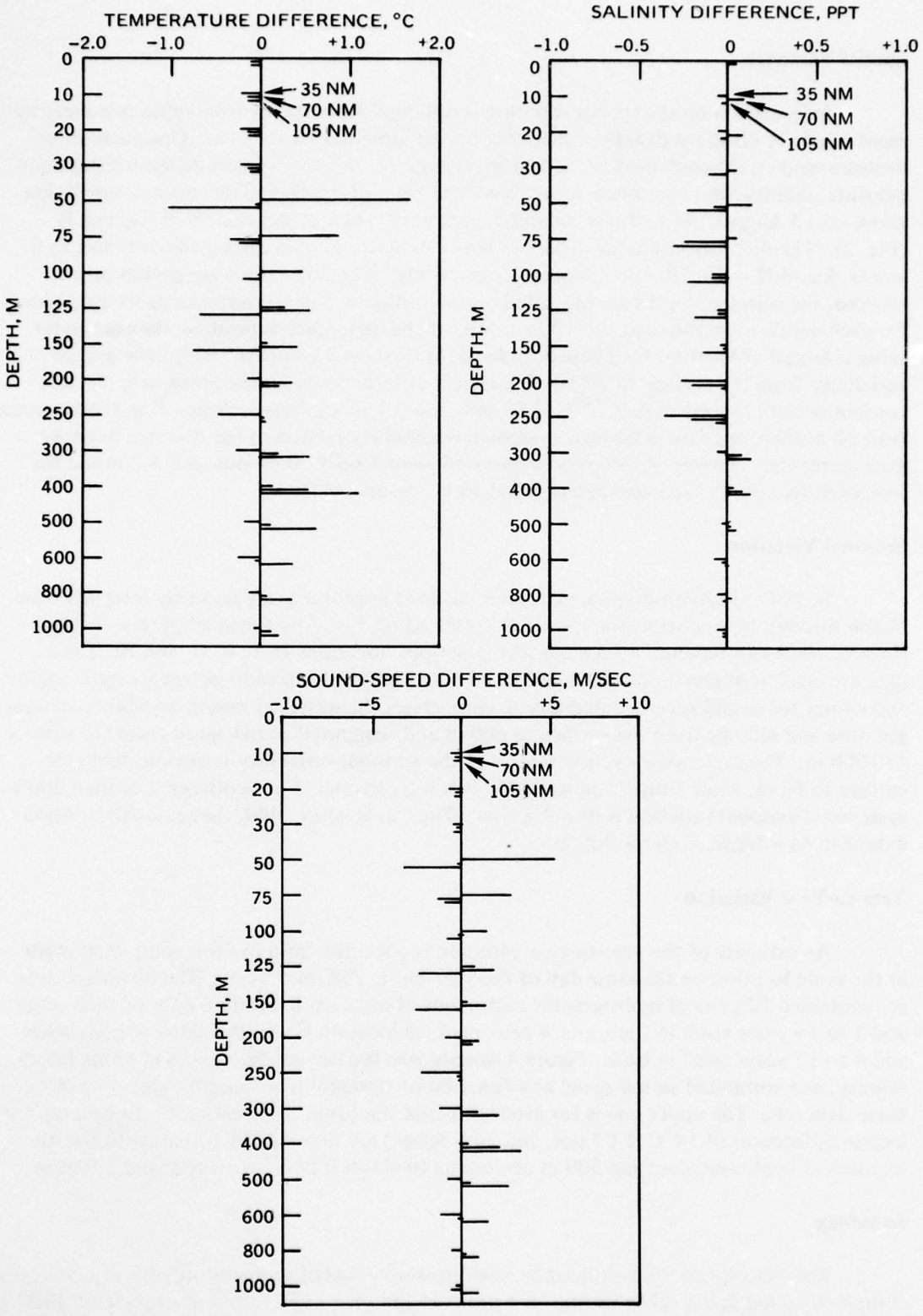

Figure 3. Spatial variability in temperature, salinity, and computed sound speed observed on 13 August 1949.

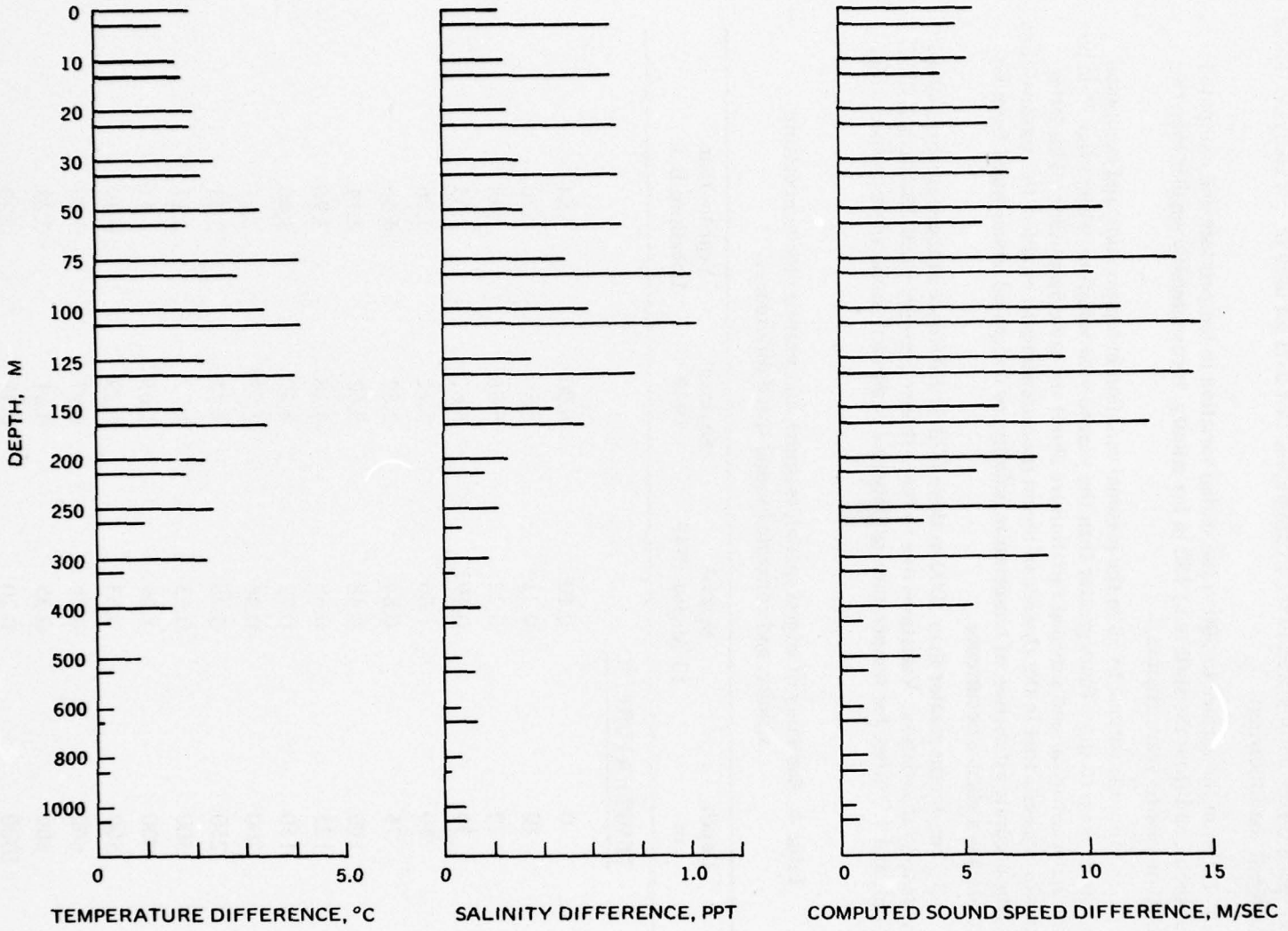

Figure 4. Year-to-year variations in temperature, salinity, and computed sound speed at locations B and C.

Table 4 summarizes the largest spatial (up to 105 nm on 13 August 1949), seasonal (during 1949), and year-to-year (locations B and C) temperature, salinity, and computed sound speed variations observed in the hydrographic cast data set used in this analysis. These data suggest the following:

1. From the surface to 500 m the spatial variation in temperature and computed sound speed, and from the surface to 150 m for salinity, is considerably smaller than the seasonal or year-to-year variation.

2. From the surface to 50 m the seasonal variation in temperature and computed sound speed is up to three times greater than the year-to-year variation, while from 75 m to 400 m the year-to-year and seasonal variation are about the same magnitude. This latter conclusion suggests that in the absence of recent measurements to establish the seasonal time scale, the accurate estimation of temperature, salinity, or computed sound speed from historical data is a chance occurrence.

3. For depths greater than 1000 m there is little difference in the seasonal, spatial, and year-to-year variation. Variations due to these three causes are small, less than 0.30°C, 0.12 ppt, and 1.7 m/sec for temperature, salinity and computed sound speed, respectively.

Table 4. Summary of largest spatial, seasonal, and year-to-year temperature, salinity, and computed sound-speed differences.

Depth, *m*	Spatial 13 August 1949	Seasonal 1949	Year-to-Year Locations B, C
TEMPERATURE, °C			
0	0.10	6.00	1.64
10	0.21	5.36	1.70
20	0.22	5.56	1.94
30	0.19	5.62	2.35
50	1.66	5.72	3.26
75	0.84	2.82	4.06
100	0.48	3.62	4.14
125	0.68	4.28	3.96
150	0.72	3.67	3.40
200	0.36	2.73	2.15
250	0.48	1.73	2.33
300	0.53	1.72	2.17
400	1.09	1.65	1.47
500	0.63	1.29	0.79
600	0.36	0.97	0.19
800	0.35	0.61	0.23
1000	0.20	0.39	0.20

Table 4. Continued.

Depth, m	Spatial 13 August 1949	Seasonal 1949	Year-to-Year Locations B, C
SALINITY, ppt			
0	0.05	0.76	0.67
10	0.09	0.63	0.67
20	0.07	0.80	0.69
30	0.11	0.83	0.70
50	0.23	0.69	0.71
75	0.30	0.61	0.99
100	0.22	0.52	1.02
125	0.18	0.46	0.77
150	0.13	0.60	0.56
200	0.26	0.56	0.26
250	0.34	0.43	0.21
300	0.13	0.35	0.18
400	0.13	0.33	0.14
500	0.05	0.32	0.12
600	0.07	0.16	0.12
800	0.05	0.18	0.06
1000	0.05	0.12	0.08
COMPUTED SOUND SPEED, m/sec			
0	0.3	18.3	5.4
10	0.6	16.3	5.1
20	0.7	17.2	6.4
30	0.5	17.3	7.6
50	5.2	17.7	10.6
75	2.7	9.6	13.5
100	1.4	12.2	14.5
125	2.4	14.5	14.2
150	2.6	12.5	12.4
200	0.9	9.6	7.9
250	2.2	6.7	8.8
300	2.1	6.7	8.3
400	3.4	6.6	5.2
500	2.6	5.2	3.1
600	1.5	4.0	1.0
800	1.0	2.6	1.0
1000	0.8	1.7	0.7

DIRECT CONVERSION OF TEMPERATURE TO SOUND SPEED

In any oceanic water mass the temporal and spatial variations in salinity are small. At any depth a significant relationship between computed sound speed and temperature exists. The effect of the small salinity changes is included in the computed sound speed. The historical hydrographic cast data set used to establish the historical temperature, salinity, and computed sound-speed distributions for the SUDS I experimental areas may also be used to establish a computed sound speed versus temperature relationship. At each standard hydrographic cast depth from the surface to 150 m, a second-degree polynomial was least-square fitted to the 94 historical hydrographic cast data sets. For depths from 200 m to 500 m, a first-degree polynomial was used. The applicable coefficients are listed in Table 5 along with the temperature domains for which the relationships are valid. In the right-hand column of Table 5 are the standard deviations of the data points about the regression relationships. Figure 5 is a plot of these relationships for the indicated depths. The coefficients in Table 5 are used to convert the XBT, thermistor chain, and Teletherm buoy temperature measurements directly into computed sound speed.

Table 5. Temperature-computed sound-speed relationship, $C_c = a + bT + cT^2$

Depth, m	a	b	c	Temperature Domain, °C	σ m/sec
0	1448.45	4.35878671	-0.03783127523	[14.6, 20.6]	0.21
10	1448.34	4.38862700	-0.03864440131	[14.8, 20.1]	0.21
20	1448.53	4.38184549	-0.03832009244	[14.4, 20.0]	0.21
30	1449.09	4.33192655	-0.03668241277	[14.0, 20.0]	0.20
50	1449.76	4.26903442	-0.03695678230	[13.1, 19.8]	0.20
75	1450.95	4.10190029	-0.02623654397	[12.0, 17.8]	0.16
100	1449.47	4.35375572	-0.03394354120	[11.1, 17.7]	0.14
125	1452.61	3.98520682	-0.02077373949	[10.3, 16.7]	0.15
150	1454.84	3.69033463	-0.00826872973	[9.6, 14.7]	0.17
200	1456.36	3.55553957		[8.4, 11.3]	0.15
250	1455.38	3.77478121		[7.6, 10.2]	0.12
300	1455.10	3.93064373		[7.0, 9.6]	0.09
400	1456.11	4.05159974		[5.9, 8.1]	0.08
500	1457.65	4.10099745		[5.6, 7.0]	0.07

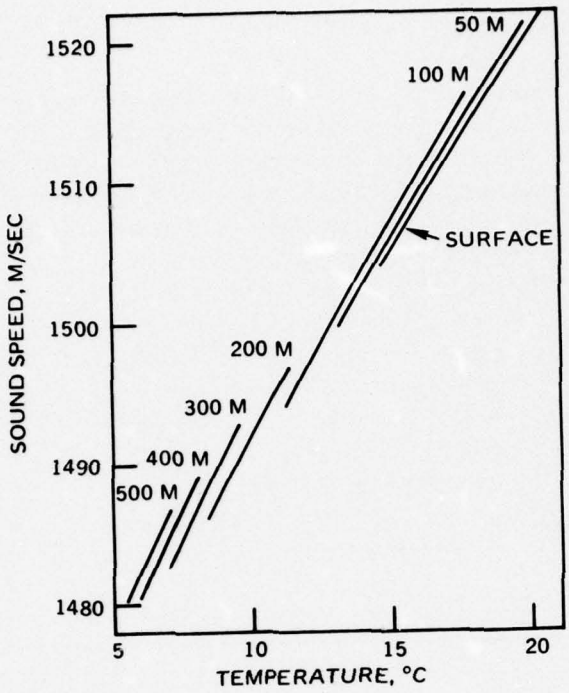

Figure 5. Relationship between computed sound speed and temperature at selected depths for the *SUDS I* experimental areas.

RECONSTRUCTION OF EXPERIMENTAL TRACK CHARTS

The details of the method used in reconstructing the experimental track charts are included in Ref. 2. This section summarizes this information.

Satellate navigation, celestial navigation, and dead reckoning were employed for absolute positioning, and radar ranges and bearings and acoustic ranges were used for relative positioning. Each ship was required to maintain a position fix log, a maneuvering log, and a radar range and bearing log during all experimental runs. The satellite fixes gave the most accurate absolute positions and the acoustic ranges gave the most accurate relative range determinations. All absolute positioning was adjusted to the satellite fixes and all relative positioning to the acoustic range measurements.

Only the *Lee* was equipped with satellite navigation equipment. The first step in reconstructing the experimental track charts was to determine the position of the *Lee* during each of the experimental runs and for periods between runs when environmental data were taken. The satellite fixes were plotted and the maneuvering logs, courses, and speeds used to determine the position of the *Lee*, both backward and forward in time, relative to the satellite fixes. Celestial fixes were used in the absence of satellite fixes. Because of a marked and variable drift from the northwest caused by ocean currents and wind, it was often necessary to adjust the track so it would agree reasonably well with the satellite fixes. In the absence of satellite or celestial fixes, it was necessary to use dead reckoning for absolute positioning. When this was done, the absolute positioning of the *Lee* is uncertain, with the uncertainty increasing as a function of elapsed time since the last satellite or celestial fix. There were times when the *Lee* was hove to and drifting or when there were frequent course and speed changes, which meant it was impossible to reconstruct its track. This was particularly true between the conclusion of the station 1 experiments on 12 February 1400 LST and the beginning of the station 2 experiments on 14 February 1822 LST. At these times arbitrary straight-line interpolation between satellite or celestial fixes was used in the reconstruction. During each run the *Lee*, *DeSteiguer*, and *Cape* took radar range and bearing measurements on each other every 20 min. The second step in the reconstruction process was to use these measurements to determine the position of the *DeSteiguer* and the *Cape* with respect to the *Lee* for each experimental run. During the first deployment of the Teletherm buoy line, no positioning measurements were made on the line. Therefore, it was not possible to determine the position of the buoys with respect to the experimental track during this deployment. During the second deployment of the buoy line, the *Cape* made frequent range and bearing measurements on buoys 1, 4, and 8 and from 20 February 1350 LST to 23 February 0400 LST made measurements on all eight buoys. The third step in the reconstruction was to use these data to locate the position of the buoy line with respect to the *Cape*.

OCEANOGRAPHIC MEASUREMENTS

A detailed discussion of the instrumentation used to make the required supporting environmental measurements, the data reduction procedures, an accuracy analysis of the final measurements, and a detailed reporting of all the environmental measurements applicable to each propagation loss run is contained in Ref. 2. This section summarizes the information contained in Ref. 2, compares the SUDS I hydrographic cast and STD/SV measurements with the historical temperature, salinity, and computed sound speeds, and compares the STD/SV measured sound speeds with sound speeds computed from the STD/SV simultaneously measured temperatures and salinities.

Figure 6 summarizes, as a function of time, the oceanographic measurements made in support of the propagation loss measurements. Shown are the times in the experimental areas, the times each of the four acoustic stations were occupied, and the times each propagation loss run was made. The width of the shaded areas indicates the time intervals over which the propagation loss run or the indicated oceanographic measurement was made. The number of the hydrographic cast or STD/SV is shown at the top of the shaded area. The small number at the left or right of the shaded area is the maximum depth. in meters, of the observation. For the Datawell Waverider buoy measurements, the vertical line within a shaded area indicates a 1-min break in the record. For the XBTs, the number is the number of acceptable XBT profiles made during the indicated station and between stations. Only a limited amount of data was obtained by the Stilwell wave system and the NUC wave spar buoy. It is not included in this report.

HYDROGRAPHIC CAST MEASUREMENTS

The hydrographic cast is an internationally standardized technique used by oceanographers to obtain measurements of temperature and salinity at discrete preselected depths from the surface to the bottom. Description of the instrumentation may be found in any physical oceanography textbook. The generally accepted overall accuracy of the technique is: temperature ±0.02°C, salinity ±0.02 ppt, and depth ±5 m for depths less than 1000 m and ±0.5 percent for depths greater than 1000 m.

Thirteen hydrographic casts were completed. Five were made in area A, six in area C, none in area B, and two between areas A and B. In determining the distribution of sound speed these measurements are the primary measurements of temperature, salinity, and depth and are the standard for comparison of other measurements of these parameters using other instrumentation.

STD/SV MEASUREMENTS

Simultaneous salinity, temperature, depth, and sound-speed measurements were obtained using a Plessey Environmental Systems 9040-4C profiling system. The Plessey system provides both an analog and digital output. The analog output is a continuous trace of the measured variables as functions of depth, and the digital record is on magnetic tape, with a sample rate of 0.2 sec for each measured variable. According to the manufacturer the overall system error is: ±0.02°C, ±0.02 ppt, ±0.30 m/sec, and ±4.0 m for depths less than 500 m and ±6.0 m for depths greater than 500 m.

Twelve STD/SV profiles were completed Five were made in area A, five in area C, none in area B, and two were made between the experimental areas. In order to obtain *in situ* accuracy checks on the STD/SV measurements, the original planned observational program included independent measurements of temperature, salinity, and depth utilizing hydrographic cast measurements. Six hydrographic casts were taken close enough in time and space to obtain useful comparisons. Reversing thermometers and sampling bottles attached to the STD/SV cable just above the sensor unit were also used to obtain temperature, salinity, and depth measurements at the maximum depth of selected STD/SV profiles. Attempts were made on 7 of the 12 STD/SV profiles. Satisfactory measurements were obtained on 2 of the 7 attempts. In addition, an attempt was made to obtain temperature and salinity measurements at several depths on STD/SV 6 by attaching a rosette sampler just above the sensor unit. This attempt failed to produce any useful information.

A comparison of the quasi-simultaneous STD/SV and hydrographic cast measurements showed that for depths greater than 200 m the STD/SV measured temperatures were consistently 0.02°C lower than the hydrographic cast temperatures. The salinity comparison showed that at all depths the STD/SV measured a higher salinity than the hydrographic cast, with the difference being a function of depth from the surface to 1000 m. For depths greater than 1000 m the difference was a constant difference of 0.06 ppt. A similar depth bias has been reported by other investigators utilizing similar STD/SV systems (Ref. 14). Six comparisons of depth measured by the STD/SV system and the thermometric depth calculated from the temperature measurements made using the reversing thermometers attached just above the STD/SV sensor unit showed excellent agreement between the two determinations. The differences varied from −2.0 m to +3.0 m at 2000 m and −8.0 m to −1.0 m at 3800 m. The temperature and salinity corrections were added to all STD/SV measurements to bring them into agreement with the hydrographic cast measurements.

XBT MEASUREMENTS

Temperature measurements as a function of depth were obtained by means of a Sippican Corporation R-603 XBT system. The output of this system is an analog record of temperature as a function of depth to a maximum depth of 460 m. According to Sippican, the system accuracy is: temperature ±0.2°C, depth ±4.6 m from the surface to 230 m and ±2.0% from 230 m to 460 m.

A total of 462 XBT temperature profiles were attempted in the experimental areas. Table 6 summarizes the number of XBT records made by each ship in each of the operating areas. A visual examination of the XBT records sufficed to determine those XBT records that were catastrophic failures (no usable temperature measurements) and those that were partial failures (usable temperature measurements did not extend to 450 m). Out of a total of 462 recorded XBT profile attempts, 52 (11.3 percent) and 25 (5.4 percent) were catastrophic or partial failures, respectively. Eliminating the 52 catastrophic failures left 410 XBT temperature profiles as being visually acceptable.

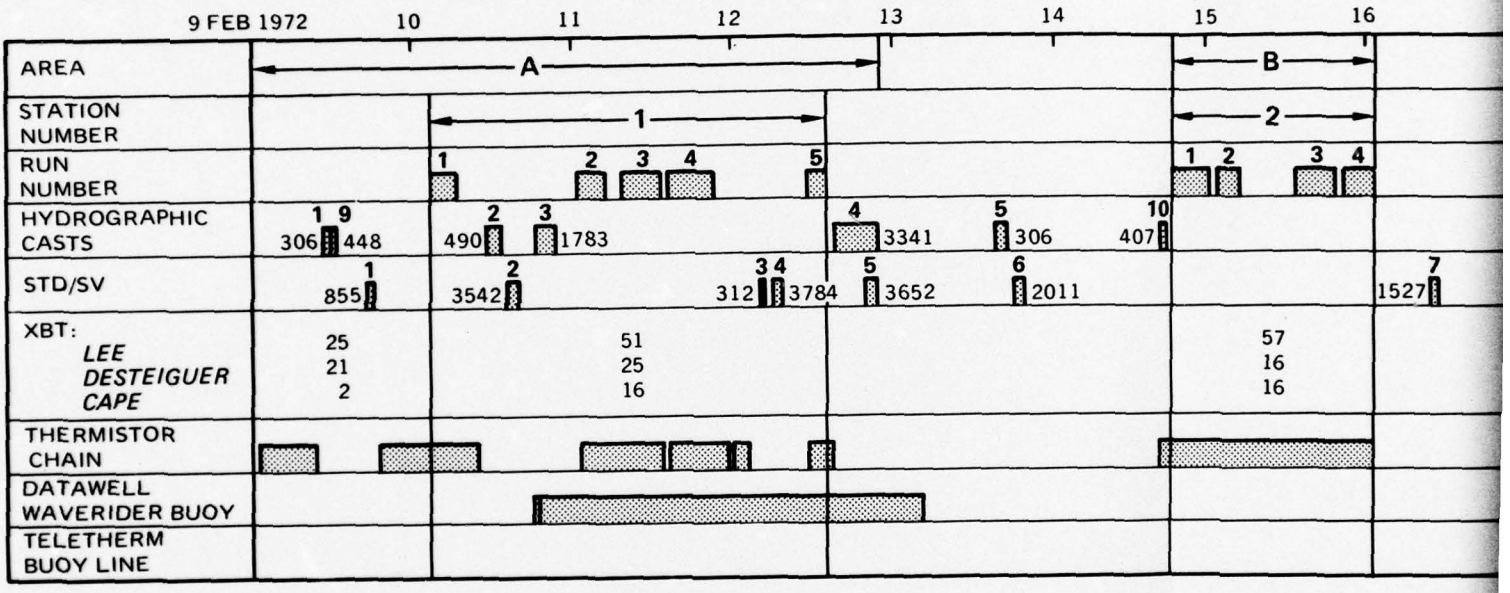
9 FEB 1972
10
11
12
13
14
15
16
AREA
A
B
STATION NUMBER
1
2
RUN NUMBER
1
2
3
4
5
1
2
3
4
HYDROGRAPHIC CASTS
1 9
306
448
2
3
490
1783
4
3341
5
306
10
407
STD/SV
1
855
2
3542
3 4
312
3784
5
3652
6
2011
7
1527
XBT:
LEE
DESTEIGUER
CAPE
25
21
2
51
25
16
57
16
16
THERMISTOR CHAIN
DATAWELL WAVERIDER BUOY
TELETHERM BUOY LINE

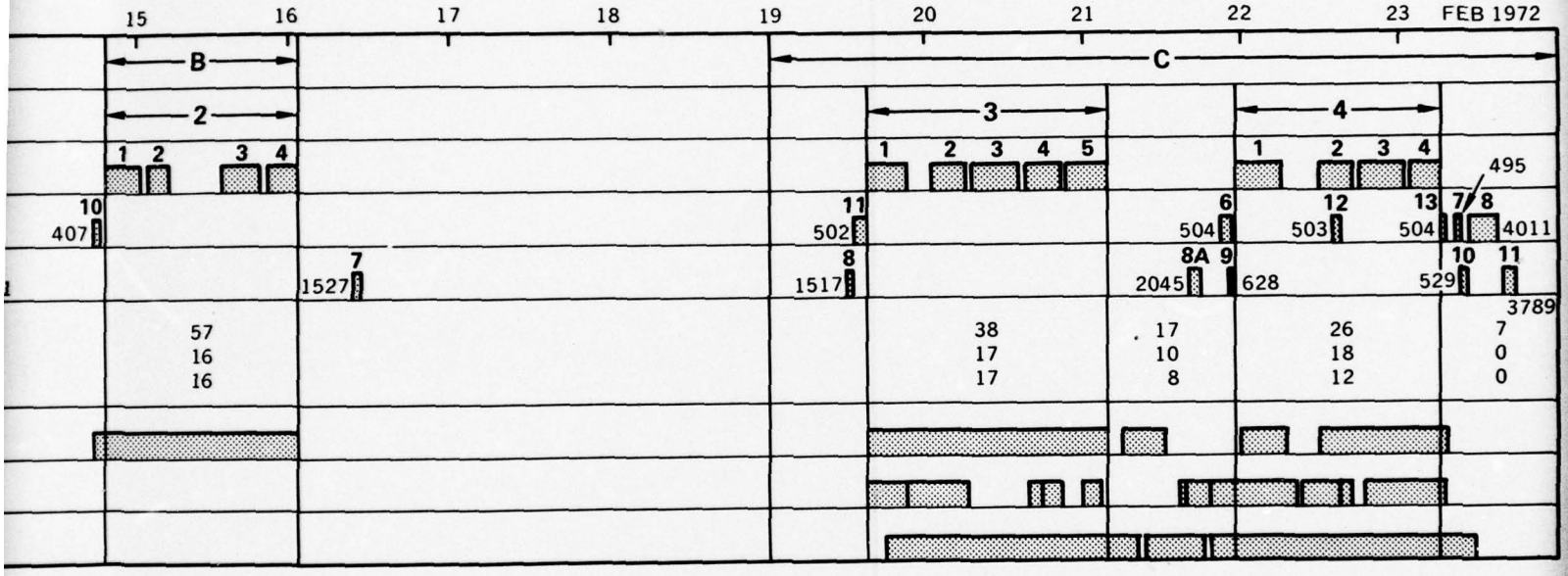

Figure 6. Summary of oceanographic measurements.

Table 6. Number of XBT records.

Ship	Area A	Area B	Area C
Lee	89	66	104
DeSteiguer	49	21	50
Cape	19	18	46
Total	157	105	200

Previous comparisons of XBT temperature measurements with simultaneous and independent temperature measurements made using hydrographic cast and STD/SV systems show that some visually acceptable XBT profiles result in temperatures that are higher than those made by the hydrographic cast and/or STD/SV systems (Ref. 14). Since the observed difference is an increasing function of depth, the acceptance and use of such measurements results in a systematic biasing of the vertical temperature gradient. To detect XBT profiles that might possibly contain such gradient biasing errors, the 200- and 400-m measurements were used. For each ship and area the average temperature and standard deviation was obtained for these two depths. If, for a given XBT, both the 200- and 400-m temperatures were within three standard deviations of the average temperature, the XBT record was considered to be correct. If the temperature at either depth was greater than or equal to three standard deviations of the average temperature, the profile was considered in error and eliminated from further analysis. A total of 9 out of the 410 visually acceptable XBT records (2.2 percent) failed to meet this criterion. The final accuracy check was to compare the average XBT 200- and 400-m temperature with the STD/SV and hydrographic cast 200- and 400-m average temperatures. Two of the 401 XBTs failed to meet the criterion of not exceeding plus or minus three standard deviations of the average hydrographic cast and STD/SV temperatures at 200 and 400 m. In addition, one XBT could not be used since the time was not recorded on the trace. Thus, out of the original 462 XBT profiles, 399 (86.4 percent) were finally accepted as being accurate temperature profiles.

XBT temperature profiles were made within 45 min of the time nine of the hydrographic casts and STD/SV profiles were made. A comparison of the XBT temperatures with the hydrographic cast temperatures at 13 selected depths from the surface to 400 m showed that out of a total of 114 differences, 94 (82.5 percent) were less than ±0.2°C, the XBT specified temperature accuracy. In general, the larger differences were associated with depths where the temperature gradients were the greatest. The average difference was +0.08°C, with 87 (76.3 percent) being positive and 27 (23.7 percent) being negative,

suggesting that there is a tendency for the XBT system to measure a higher temperature, at any given depth, than the hydrographic cast or STD/SV. This tendency has been observed in other temperature measurement programs involving the XBT system (Ref. 15). The XBT system does not measure depth directly but rather measures time, with depth being obtained by assuming a rate of fall. A possible explanation for this tendency to record higher temperatures than other systems is that the XBT probe falls at a slower rate than assumed, thereby measuring a temperature at a depth shallower than calculated.

THERMISTOR CHAIN MEASUREMENTS

The thermistor chain is a towed device used for measuring temperature from the surface to a maximum depth of 242 m. It consists of 44 thermistors spaced 5.6 m apart plus shipboard equipment consisting of a winch and the necessary electronics for recording the temperature as measured by the 44 thermistors. The instrument is designed to measure vertical temperature profiles every 10 sec with an estimated accuracy of about ±0.1°C. At a 3-knot towing speed this results in a vertical temperature profile every 17 yd. Additionally, a depth sensor records the depth of the deepest thermistor. Unfortunately during the SUDS I experiments, the depth sensor was inoperative. As a result, the sensor depths were empirically determined from comparisons with temperatures measured by other systems. For all experiments, except station 1 run 5, the towing speed was 3 knots. For the station 1 run 5 experiment the towing speed was 6 knots. It was hoped that at the slow 3-knot towing speed the chain would be vertical in the water, with the depth of the deepest sensor at 242 m. The system provides both an analog and a digital output. The analog output is a contour chart showing integer isotherms as a function of depth and range along the tow track, and the digital record is a magnetic tape containing the output of each vertical scan of the temperature and depth sensor.

Between runs 4 and 5 of station 1, temperatures were measured simultaneously by the thermistor chain, hanging vertically in the water (zero tow speed), and the STD/SV system. STD/SV 3 was made to a depth of 312 m in 10 min, starting at 0415 LST on 12 February 1972. During the period 0418-0425 LST, the thermistor chain made 45 scans of its sensors. A comparison of these measurements revealed two features of interest: (a) Relatively large differences centered at a depth of 100 m. These large differences are related to the strong negative temperature gradients observed between 80 and 135 m. A small change in depth changes the temperature considerably. For example, the largest difference of −0.46°C at 100 m is accounted for by a depth change of only 2 m. (b) From the surface to 80 m and from 135 m to 242 m, where the temperature gradients are small, the differences show that the thermistor chain is measuring a temperature slightly higher than the STD/SV system. The average difference for these two layers is 0.03°C. Thus, all thermistor chain measurements are reduced by 0.03°C to bring them more nearly into agreement with the hydrographic cast and STD/SV measurements.

As noted, the thermistor chain depth sensor was inoperative during the time of the SUDS I experiments. As a result, accurate information on the depth of the thermistor chain sensors is unavailable. To obtain some information on the sensor depths when towing at 3 knots, the average hydrographic cast and STD/SV temperatures made in area A and area C were compared with the average temperatures measured by the thermistor chain for all

acoustic runs made in these two areas. The comparisons for the area C measurements suggest agreement, on the average, between the hydrographic cast and STD/SV measurements and the thermistor chain measurements. The area A comparisons showed good agreement for depths greater than or equal to 150 m, with the average thermistor chain measurements being higher than the hydrographic cast and STD/SV average measurements at shallower depths. However, all average thermistor chain measurements fell within the hydrographic cast and STD/SV measured range of temperature. Since these comparisons showed no consistent evidence of shoaling at the 3-knot towing speed, it is assumed that the chain is being towed nearly vertically, with the deepest sensor very close to 242 m.

Comparison of the average hydrographic cast and STD/SV temperature measurements made in area A with the average temperature measured by the thermistor chain for the 6-knot tow made during station 1 run 5 showed that the average chain temperatures were all higher than the highest recorded hydrographic cast and STD/SV temperature measurements. This suggests that the thermistor chain sensors are at a depth shallower than assumed. Experience in towing the thermistor chain at 6 knots indicates that the depth of the 242-m sensor is about 221 m. A depth correction was obtained by assuming the deepest sensor is 21 m shallower than the maximum depth, the surface sensor is at the correct depth, and the depths of the remaining sensors are linearly adjusted. Application of this depth correction improved the agreement between the two sets of measured temperatures by making most of the average thermistor chain temperatures fall within the measured range of hydrographic cast and STD/SV temperatures. In any use of the thermistor chain measurements made during station 1 run 5 this depth correction was applied.

TELETHERM BUOY MEASUREMENTS

Under contract to the Office of Naval Research, the Lockheed Ocean Laboratory designed, constructed, calibrated, and operated the Teletherm buoy system (Ref. 16). At the completion of the at-sea measurements, Lockheed performed the preliminary data reduction and provided NUC with a set of magnetic tapes containing the pertinent measurement information. The Teletherm buoy line consisted of 10 Lockheed Model 9-TB-10T Teletherm buoys. The 10 buoys were tethered 2 kyd apart, forming an 18-kyd-long line. The experimental plan called for deploying the line from the vicinity of the *DeSteiguer* in the direction of the expected propagation path, thereby providing 10 simultaneous temperature profiles along the first 18 kyd of the propagation path. Each buoy measured temperatures, using thermistor beads as sensors, at 10 equally spaced depths from the surface to 125 m. A complete temperature profile was measured every 10 sec for each buoy. The data were transmitted to the *Cape* via a radio link and recorded on magnetic tape in digital format. According to the manufacturer the overall system accuracy is 0.034°C. No depth sensor was included in the system. Details of the system are reported in Ref. 15.

The *DeSteiguer* deployed the buoy line with a large float at one end. At intervals of 2 kyd were connector shackles, onto which the 10 Teletherm buoys were attached by the *Cape*. To keep the buoy line straight, several configurations of drogue chutes and sea anchors were attached to the system. The buoy line was deployed twice. The first deployment was during acoustic stations 1 and 2 and the second during stations 3 and 4. All 10 buoys were used during the first deployment. During this deployment the tether line parted

several times, disrupting the integrity of the array and the measurements. Several times nonlinear configurations of the buoy line were noted. A wind shift at one time caused the buoy line to double back on itself. As a result of problems caused by strong winds, heavy seas, unfamiliarity of personnel with a new complex temperature measuring system, and the lack of a station-keeping capability, no useful measurements were obtained during this deployment. For the second deployment the line was reconfigured to a 14-kyd line containing eight buoys. Additionally, radar reflectors were installed on each buoy for station keeping. During this deployment the *Cape* took radar range and bearing measurements on buoys 1, 4, and 8 every 20 min during the propagation loss runs. Radar measurements were made on all eight buoys, during nighttime hours, at 1- to 2-hour intervals from 20 February 1350 LST to 23 February 0400 LST.

The first step in the data reduction process was to prepare plots of temperature versus time for all buoys and all depths and compute the average and standard deviation for each data set. These plots and computations showed a marked buoy-to-buoy variability in data quality, with buoys 5 and 6 yielding high-quality data for all propagation loss runs. No usable data were obtained from buoys 1, 7, and 8. Usable data for some runs were obtained from buoys 2, 3, and 4. The Teletherm buoy system did not have a depth sensor. It was assumed that the thermistor string hung vertically in the water, with the sensors equally spaced from the surface to 125 m. This assumption may be valid under calm or near-calm wind conditions but invalid when the wind causes the system to drift through the water, resulting in a shoaling of all sensors. To check the validity of this assumption, 19 XBTs, taken within 2 kyd of a Teletherm buoy, were compared with the buoy measurements made at the same time as the XBT measurements. Comparisons at seven depths in the surface layer showed that the buoys have a temperature about 0.1°C higher than the XBTs. The 125-m sensor was located in the thermocline. On the average, this sensor measured temperatures 0.8°C higher than the XBTs. Of the 19 comparisons at this depth only 2 were negative. The differences varied from −0.4°C to 2.4°C, with six of the differences greater than 1.0°C. This strongly suggests that the buoy sensors were at a depth shallower than assumed. Since the amount of shoaling is variable, being a function of wind and ocean currents, it was not possible to correct the assumed depths. Consequently, only the measurements made in the surface layer, where vertical gradients are small or nonexistent, are valid. The primary value of these measurements is as an indicator of temporal stability in the surface layer.

DATAWELL WAVERIDER BUOY MEASUREMENTS

The Datawell Waverider buoy system was used to obtain a measure of sea-surface roughness. The system, manufactured by the Datawell-Laboratory for Instrumentation, a Netherlands concern, measures wave height versus time in both analog and digital formats. The system consists of a telemetering buoy, employing accelerometers to sense sea-surface height variations, and shipboard receiving and recording equipment. Wave height is measured at a rate of 120 measurements per min. According to the manufacturer the system will measure waves of periods 1.25 to 16.7 sec with an accuracy of about 3 percent for waves up to a maximum wave height of 20 m.

During the first deployment of the Teletherm buoy line, the Waverider buoy was attached to Teletherm buoy 5, and during the second deployment it was attached to

Teletherm buoy 4. The measurements were telemetered to the *Lee* and recorded on magnetic tape. Complete measurement sets (no breaks in sampling) were obtained for station 1 runs 2, 3, 4, and 5; station 3 run 2; and station 4 runs 1 and 4. Incomplete sets were obtained for station 3 runs 1, 4, and 5 and station 4 runs 2 and 3. No measurements were obtained for station 2 and station 3 run 3. During station 1 and 2 the Waverider buoy was attached to the Teletherm buoy line from a ring on the bottom of the buoy. This method of attachment could cause the buoy to be tilted during periods of high wind speeds. For the station 3 and 4 measurements, the buoy was attached from a ring on the side of the buoy, thereby eliminating the possibility of tilting.

In 1969 the Nearshore Processes Group at Scripps Institution of Oceanography checked the Datawell Waverider buoy by making simultaneous measurements with two such buoys and a wave-height sensor that they had some faith in. They concluded "the buoys they used measured near-shore waves with sufficient accuracy and precision to allow an energy spectrum to be calculated which is statistically valid between 0.055 Hz and 1.0 Hz. However, the response . . . is not reliable for frequencies less than about 0.055 Hz . . ."*

To check the record for continuity and to determine times of good record, the wave-height measurements were plotted as a function of time. At present, the sea-surface roughness parameter most useful as an input to acoustic models is RMS wave amplitudes. At a sample rate of 120 data points per min more detail on surface roughness is available than can be used in any realistic application. After experimenting with averaging times up to 30 min it was arbitrarily decided that a 3-min averaging time would preserve enough detail for most current applications. A more detailed analysis of the wave-height measurements was made employing fast Fourier transform techniques (Ref. 17). These calculations generated a table of variance as a function of wave frequency. To determine if any change in surface roughness occurred during an acoustic run, the data were subdivided into periods approximately 1-hour in length. The spectra for the 1-hour samples were computed and examined. If no significant time change was noted the spectra were ensemble averaged into a single spectrum. This type of analysis is useful in that it determines the wave periods where most of the variance (surface roughness) is concentrated.

COMPARISON OF HYDROGRAPHIC CAST MEASUREMENTS WITH HISTORICAL MEASUREMENTS

The analysis of the historical hydrographic cast measurements suggested that most of the temperature, salinity, and computed sound speed variability in the SUDS I areas extends to depths of about 1200 m. For depths greater than 1200 m, the water column is stable with respect to temperature and salinity. Table 7 summarizes the differences between the hydrographic cast temperature and salinity measurements and the historical average temperature and salinity. The hydrographic casts are grouped by area and are ordered from north to south within each area. For comparison, column 3 shows the value of three standard deviations of the historical average temperature and salinity. Differences greater than or equal to three standard deviations are shown in italics. In area A the observed

Personal communication to K. W. Nelson

Table 7. Differences between measured and historical average temperature (°C) and salinity (ppt).

Depth, m	n	3σ	Area A				Between Areas A & B		Area C					
			9	1	2/3	4	5	10	11	6	7/8	12	13	
250	94	1.38	1.19	1.25	1.11	0.89	1.23	-0.21	0.06	-0.20	0.09	-0.03	0.26	Temperature
300	93	1.44	*1.48*	*1.72*	1.36	1.12	1.14	0.17	-0.03	-0.24	-0.06	-0.13	0.04	
400	94	1.32	*1.64*		1.18	1.15		0.57	-0.23	-0.39	-0.29	-0.36	-0.16	
500	93	1.02			0.99	0.96			-0.12	-0.31	-0.18			
600	71	0.75			0.71	0.71					-0.24			
800	63	0.57			0.29	0.46					-0.22			
1000	59	0.30			0.26	*0.36*					-0.12			
1200	34	0.21			0.16	0.21					-0.14			
1500	15	0.15			0.12	0.08					-0.14			
2000	15	0.09				0.02					-0.05			
2500	13	0.06				-0.01					0.00			
3000	13	0.09				-0.02					-0.01			
4000	3	0.06									-0.05			
250	94	0.30	*0.30*	*0.34*	*0.31*	0.21	-0.03	-0.01	0.01		-0.14	-0.17	-0.03	Salinity
300	93	0.27	*0.28*	*0.29*	*0.29*	0.18	*0.28*	-0.01	-0.08		-0.13	-0.02	-0.06	
400	94	0.24	0.20		0.19	0.16		-0.07	-0.06		-0.06	-0.05	-0.06	
500	93	0.18			0.09	0.10			-0.04		-0.03	-0.06	-0.07	
600	71	0.15			0.03	0.05					-0.02			
800	63	0.12			-0.01	-0.02					0.00			
1000	59	0.12			-0.02	-0.03					0.01			
1200	34	0.09			-0.03	-0.03					0.01			
1500	15	0.09			-0.02	0.00					0.01			
2000	15	0.06				-0.02					0.00			
2500	13	0.09									0.00			
3000	13	0.09									0.00			
4000	3	0.06									0.00			

temperatures are all higher than the historical average temperature, with a tendency for the differences to be largest for the northernmost set of measurements. In area C the differences are all within one standard deviation of the historical average, with the majority of differences being slightly negative. These observations suggest that area A was occupied by a large mass of warm water centered in depth at 300 to 400 m. The differences for hydrographic casts 5 and 10 suggest that the boundary of this warm-water mass is between these two hydrographic casts. The salinity of the warm-water mass is higher than the historical average salinity to depths of about 600 m. For depths greater than 600 m the observed salinity is very close to the historical average and are all within one standard deviation of it.

Table 8 summarizes the differences between sound speeds computed from the measured temperature, salinity, and depth using Anderson's sound-speed equation (Ref. 12) and the historical average sound speeds also computed using Anderson's sound-speed equation. The format is similar to that used in Table 7, except differences for the standard hydrographic cast depths from the surface to 200 m are included, and all differences greater than or equal to two standard deviations are shown in italics. Differences greater than or equal to three standard deviations are also underlined. From the surface to 150 m the computed sound speeds are considerably less than the historical average sound speeds. This is not unexpected. The historical average sound speeds contain sound speeds for all months of the year and for several different years, thereby masking any seasonal variation. The SUDS I measurements were made in February, when near-surface temperatures, and thus sound speeds, are well below the historical averages. The distribution of the differences in area A is quite different from the distribution of differences in area C from 200 m to about 1500 m. The differences in area A are all positive, i.e., SUDS I sound speed greater than the historical average sound speed. From 250 to 1500 m all differences are greater than or equal to two standard deviations of the historical average, with some differences for hydrographic casts 8, 1, and 4 greater than or equal to three standard deviations of the historical average. This is the result of the previously identified warm, high-salinity mass of seawater present in this area during the experiments. It is judged that area C does not contain this water mass since most of the differences are within one standard deviation of the historical averages.

COMPARISON OF MEASURED AND COMPUTED SOUND SPEEDS

This section compares the measured sound speeds with sound speeds computed from the STD/SV measured temperature, salinity, and depth by means of Anderson's sound-speed equation (Ref. 12). Figure 7 presents the differences between computed and measured sound speeds as a function of depth for the 12 STD/SV profiles. The average value at each depth is indicated by the vertical line. The shaded area contains differences that are less than or equal to ±0.2 m/sec. The left-hand figure shows the differences from the surface to 300 m, and the right-hand figure shows the differences from 300 to 3000 m. The large differences, centered at about 100 m, are associated with the thermocline and halocline, where it is difficult to obtain accurate measurements of temperature, salinity, and sound speed since small variations in depth are associated with large variations in the measured parameters. Of major interest is the systematic increase in the difference with depth for depths greater than 250 m. At 250 m the difference is 0.02 m/sec, increasing to 0.21 m/sec at 1000 m and to 0.26 m/sec at 3000 m. Over this depth interval the measured

Table 8. Differences (m/sec) between sound speeds computed from hydrographic cast measurements and those computed from historical temperature and salinity measurements.

			Area A				Between Areas A & B		Area C			
Depth, m	n	σ	9	1	2/3	4	5	10	11	7/8	12	13
0	94	5.0	-8.9	-9.3	-8.2	-7.1	-8.5	-9.4	-7.1	-6.6	-4.9	-6.8
10	94	4.7	-9.0	*-9.8*	-9.3		-8.8	-9.0	-7.6	-6.5	-5.7	-6.3
20	94	4.8	-8.8	*-9.6*	-9.3		-8.9	-8.8	-8.0	-6.3	-5.8	-6.0
30	93	4.8	-8.5	-9.3	-9.0		-8.9	-9.0	-7.8	-6.1	-5.5	-5.8
50	94	4.3	-6.6	-8.1	-7.4		-7.5	*-8.9*	-6.0	-4.7	-3.8	-4.4
75	94	3.9	-4.1	-7.6	-6.5		-5.5	-7.6	-3.1	-2.3	-2.1	-2.3
100	94	4.8	-6.0	*-10.5*	-9.0		-5.0	*-9.7*	-0.9	-0.3	-2.7	-0.3
125	94	4.8	-7.3	-9.2	-8.1		-5.1	-8.7	–	-0.4	–	–
150	94	4.3	-4.1	-4.7	-4.7		-4.5	-6.1	-0.9	-0.2	-3.1	-2.7
200	94	2.1	2.1	3.1	2.0	1.9	2.2	-1.8	0.4	-1.0	-0.4	0.7
250	94	1.7	*4.7*	*5.0*	*4.5*	*3.5*	*4.8*	-0.6	0.2	0.1	-0.4	0.9
300	93	1.9	*5.9*	*6.8*	*5.4*	*4.2*	*4.6*	0.6	-0.2	-0.4	-0.5	0.1
400	94	1.8	*6.5*		*4.8*	*4.6*		-0.7	-1.0	-1.2	-1.5	-0.7
500	93	1.4			*4.0*	*3.9*			-0.5	-0.8	-0.2	-0.1
600	71	1.1			*2.8*	*2.9*				-1.0		
800	63	0.6			*1.3*	*1.9*				-0.8		
1000	59	0.4			*0.9*	*1.3*				-0.7		
1200	34	0.3			*0.6*	*0.9*				*-0.6*		
1500	15	0.2			*0.5*	*0.4*				*-0.6*		
2000	15	0.1				0.0				*-0.3*		
2500	13	0.1				0.1				0.0		
3000	13	0.1				*-0.2*				-0.1		
4000	3	0.1								*-0.2*		

sound speeds are consistently and systematically lower than the computed sound speeds. For depths greater than 500 m all individual differences are positive. It is concluded that Anderson's equation gives sound speeds that are systematically greater than the measured sound speeds for depths greater than 250 m. An additional comment is in order. The results obtained using Anderson's equation agree with results obtained using STD/SV measurements made in the Gulf of Alaska in 1971 (Ref. 18). The Gulf of Alaska analysis considered 90 STD/SV profiles. This comparison showed that differences between average computed and average measured sound speed were zero at the surface, with the measured sound speed being systematically less than the computed sound speed at all depths to 5000 m. At 3000 m the measured sound speed was 0.62 m/sec less than the computed sound speed.

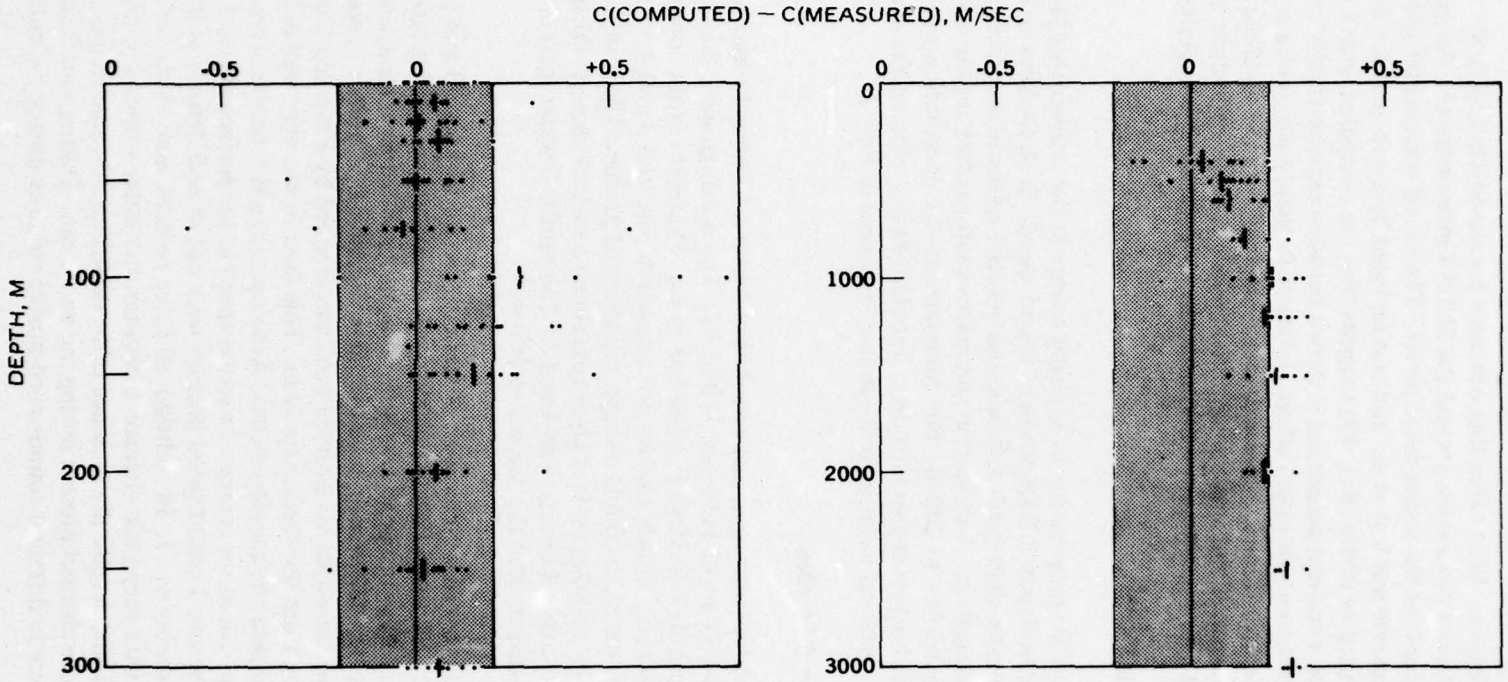

Figure 7. Differences between sound speed computed from STD/SV measured temperature, salinity, and depth using Anderson's sound-speed equation and STD/SV measured sound speed.

The difference at 3000 m was about twice that obtained for the SUDS I STD/SV measurements. In the Gulf of Alaska measurements and the SUDS I measurements, the same STD/SV system was used except for the sound velocimeter. The sound velocimeter used for the Gulf of Alaska measurements was lost at sea and was replaced by a new unit for the SUDS I experiments. Other limited evidence (Ref. 19) suggests that the computed sound speeds are correct. In this evidence, excellent agreement is shown between experimentally measured acoustic parameters and theoretical values where the input to theory was sound-speed data computed from temperature, salinity, and depth using Anderson's sound-speed equation. On the basis of this evidence, sound speeds computed from Anderson's equation will be used in developing the sound-speed profiles present during the propagation loss experiments.

SOUND-SPEED PROFILES

Of importance to the propagation of acoustic energy in the near-surface layers of the ocean is the vertical and horizontal distribution of sound speed. Such features as water-mass boundaries, surface channels, depressed channels, and negative near-surface sound-speed gradients govern the propagation. This section summarizes information on the distribution of sound speed from the surface to 200 m. For completeness the distribution of sound speed from 200 m to the bottom is also included. Tabulations and plots of the average sound-speed profiles for each propagation loss run may be found in Ref. 2.

Near-Surface Sound-Speed Profiles

Five propagation loss runs were made at station 1 over a 59-hour 11-min period from 10 February 0251 LST to 12 February 1400 LST. The oceanographic measurements showed a sound-speed profile boundary (dashed line in Fig. 1) present in the southeast portion of the experimental area. This boundary was crossed during runs 3 and 4, with runs 1, 2, and 5 made in a water mass containing a single sound-speed profile. The profile 1 water mass was characterized by an 80-m surface layer containing a surface channel during runs 1, 2, and 3 and a depressed channel during runs 4 and 5. The profile 2 water mass contained a negative sound-speed gradient from the surface to 200 m.

Four propagation loss runs were made at station 2 over a 30-hour 30-min period from 14 February 1822 LST to 16 February 0052 LST. The oceanographic measurements showed the experimental area contained two water masses separated by a transitional water mass (dashed line in Fig. 1). The transition water mass, designated as profile 2, was involved in all runs. For run 1 the transition water mass was characterized by a marked temperature frontal surface extending from the surface to 79 m. This feature was very well defined by the thermistor chain temperature measurements. Accompanying this temperature discontinuity was an abrupt 2.8-m/sec increase in sound speed in the surface channel. The boundaries separating the run 3 sound-speed profiles were not as well defined as the boundary encountered during run 1. In addition, all three profiles were characterized by 30-m surface channels, with very little difference between the water volumes in the absolute value of sound speed. Thus, despite the presence of three different profile shapes, there was a continuous 30-m surface channel present during the entire run. During runs 2 and 4 the sources and receivers were in different sound-speed-profile volumes during the entire run.

Five propagation loss runs were made at station 3 over a 37-hour period from 19 February 1500 LST to 21 February 0400 LST. The oceanographic measurements suggested the experimental area contained two water masses separated by a transitional water mass (dashed line in Fig. 1). The transition water mass is designated as profile 2. During runs 1, 2, and 3 most of the propagation loss measurements were made in the profile 3 volume. Runs 4 and 5 were both conducted in the profile 3 volume. During runs 1, 2, 3, and 4 the profile 3 volume was characterized by a depressed channel. During runs 2, 3, and 4, profile 3 also exhibited a 6-m surface sound channel. During run 5, profile 3 was characterized by a 6-m surface sound channel underlain by a weak negative sound-speed gradient to a depth of about 80 m. During runs 1, 2, and 3, the profile 1 volume was characterized by two depressed channels, with a 6- to 11-m surface channel developing during runs 2 and 3.

Four propagation loss runs were made at station 4 over a 30-hour 50-min period from 21 February 2342 LST to 23 February 0632 LST. The oceanographic measurements showed the experimental area contained a single water mass. The average sound-speed profiles for runs 1 and 4 had 17- and 10-m surface sound channels, respectively. For runs 2 and 3 the average sound-speed profiles were characterized by negative sound-speed gradients from the surface to the depth of the deep sound-speed minimum at 700 m.

Deep Sound-Speed Profiles

Sound speeds for both the hydrographic cast and STD/SV temperature, salinity, and depth measurements were computed using Anderson's sound-speed equation (Ref. 12). In the discussion of the temperature and salinity distributions, it has already been noted that the seasonal variability in temperature and salinity extends to a depth of about 200 m, that the distribution of temperature and salinity in area A is markedly different from that observed in area C from 200 m to 1500 m, and that no spatial difference was noted for depths greater than 1500 m.

Table 9 contains the average computed sound speeds for area A and area C from 200 to 1500 m and the average computed sound speeds for all data from 2000 to 4000 m. The number of observations, the standard deviations, and the differences between computed and sound speeds for area A and area C are also included. No hydrographic cast or STD/SV measurements were made in the experimental area B. However, two hydrographic casts and two STD/SV profiles were made nearby. Table 10 contains the average computed sound speeds, the standard deviation, and the number of observations for these four sets of measurements. Figure 8 contains plots of the average sound-speed data presented in Tables 9 and 10 for the 200- to 1500-m depth interval. The sound-speed profile difference between the experimental areas is marked and obvious. Column 2 of Table 11 shows the differences between the average computed sound speeds and the average expected sound speeds for this area from 2000 to 4000 m, and column 3 shows a similar comparison with average computed sound speeds presented by Anderson (Ref. 13) for the California Current sound-speed profile volume. All differences, except at 4000 m, are within one standard deviation of the average historical values. The 4000-m average is within two standard deviations of the average historical values. The average sound speeds presented in Table 9 for depths greater than 1500 m should be used in any acoustic application requiring sound-speed profiles for depths greater than 1500 m.

Table 9. Average computed sound speeds (m/sec).

Depth, m	Area A n	Area A C	Area A σ	Area C n	Area C C	Area C σ	Difference, m/sec
200	9	1493.3	0.47	9	1491.1	0.58	-2.2
250	9	92.8	0.43	9	88.4	0.40	-4.4
300	8	92.3	0.73	9	86.0	0.33	-6.3
400	7	89.7	1.15	9	82.9	0.27	-6.8
500	6	87.2	0.77	9	81.8	0.31	-5.4
600	6	85.5	0.72	5	81.4	0.36	-4.1
800	6	83.6	0.29	4	81.3	0.15	-2.3
1000	5	83.5	0.19	4	82.2	0.22	-1.3
1200	5	84.6	0.13	4	83.5	0.22	-1.1
1500	5	86.7	0.09	4	86.0	0.22	-0.7

	All Data		
Depth, m	n	C	σ
2000	8	1491.6	0.14
2500	6	98.9	0.04
3000	6	1506.8	0.06
3500	6	15.2	0.09
4000	1	24.1	—

Table 10. Average computed sound speeds for area B.

Depth, m	Number of Observations	Average Sound Speed, m/sec	Standard Deviation
200	4	1491.0	2.16
250	3	90.6	2.88
300	4	89.0	1.73
400	3	85.9	1.62
500	2	84.1	2.13
600	2	83.5	0.71
800	2	82.6	0.73
1000	2	83.0	0.36
1200	2	84.2	0.39
1500	2	86.4	0.30

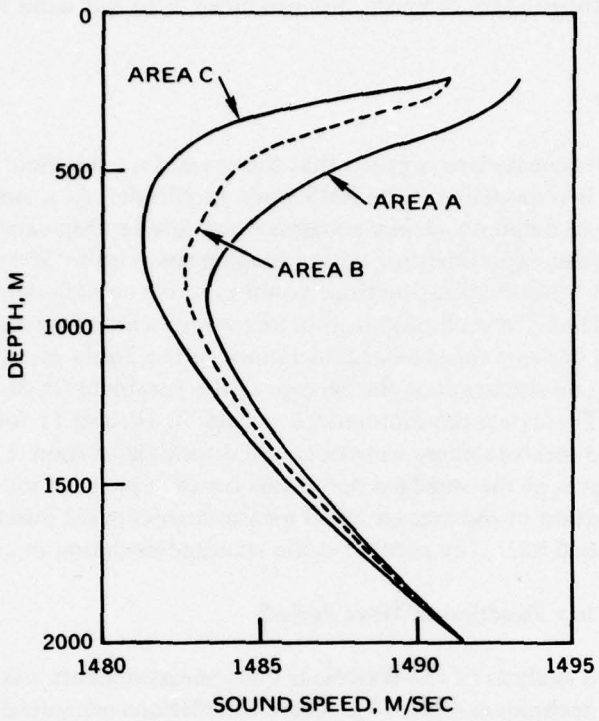

Figure 8. Average computed sound-speed profiles for areas A, B, and C.

Table 11. Difference of average computed sound speed with historical average sound speeds.

Depth, m	Average Historical, m/sec	NUC TP 264, m/sec
2000	-0.1	0.1
2500	0.0	0.2
3000	-0.1	0.2
4000	-0.2	0.3

SEA-SURFACE ROUGHNESS

Information on sea-surface roughness was obtained from the ship's weather logs and from the Datawell Waverider buoy sea-surface roughness measurements. The ship's logs contained measurements of wind speed and visual estimates of wave and swell heights. The ship's logs showed that mild weather prevailed during the time the propagation loss measurements were made at stations 1, 3, and 4. Adverse weather conditions were encountered during station 2. During stations 1, 3, and 4 the wind speed, varying from near calm to

12 knots, produced 1- to 2-ft wind waves accompanied by 3- to 5-ft swell. During station 2 the wind speed varied from 12 to 22 knots, and produced 3- to 8-ft wind waves accompanied by 6- to 10-ft swell.

RMS Wave Amplitudes

Discussion with acousticians suggests that the sea-surface roughness parameter most useful for propagation loss modeling is the RMS wave amplitude. At a sample rate of 120 data points per min more detail on surface roughness is available than can be used in any realistic application. After experimenting with averaging times up to 30 min, it was arbitrarily decided that a 3-min averaging time would preserve enough detail for most present applications. Thus, for each propagation loss run in which Waverider buoy measurements were made, a table of the standard deviations of the 3-min averages was generated together with the standard deviation of the average of the complete set of measurements made during the run. These data are summarized in Figs. 9, 10, and 11 for stations 1, 3, and 4, respectively. No measurements were obtained during the station 2 propagation loss runs. Presented are ogives of the standard deviations for each propagation loss run. In addition, the standard deviation of the average of all measurements made during the run is shown as a vertical dashed line. The number is the standard deviation in centimeters.

Wave-Height Variance as a Function of Wave Period

A more detailed analysis of the Waverider buoy measurements was made employing fast Fourier transform techniques (Ref. 17). These calculations generated a table of variance (standard deviation squared) as a function of wave frequency (reciprocal of the wave period). The final data were summarized as plots of standard deviation versus wave period from 1.25 to 16.7 sec. This type of analysis is useful in that it determines the wave periods in which most of the surface roughness (variance) is concentrated. The results of these analyses are summarized in Figs. 12, 13, and 14 for stations 1, 3, and 4, respectively.

During station 1 most of the wave energy was in the 10.0- to 16.0-sec wave-period band of swell, with lesser amounts in the 1.5- to 3.5-sec wave-period band of wind waves. During runs 2, 3, and 5 there was no change in the spectra over the duration of the run. However, during run 4 there was a change in the spectra with time. At the beginning of the run, 1.7-sec wind waves were present, with the period increasing to 3.2 sec as the run progressed. During the beginning of the run, a 9.7-sec swell was also present. This swell tended to decay during the run, although it was still detectable at the end of the run. During the last 2 to 3 hours, a 14.4-sec swell began to move into the area. The station 3 spectra showed most of the wave energy in the 12.0- to 15.0-sec wave-period band of swell with smaller amounts in the 1.5–4.5 sec wave-period band of wind waves during runs 4 and 5. For all runs there was no detectable change in the spectra during the runs. The station 4 spectra showed changes with time during runs 1, 2, and 4 but did not change with time during run 3. During station 4 most of the wave energy was in the 11.0- to 16.0-sec band of swell. However, the predominant swell periods varied from run to run.

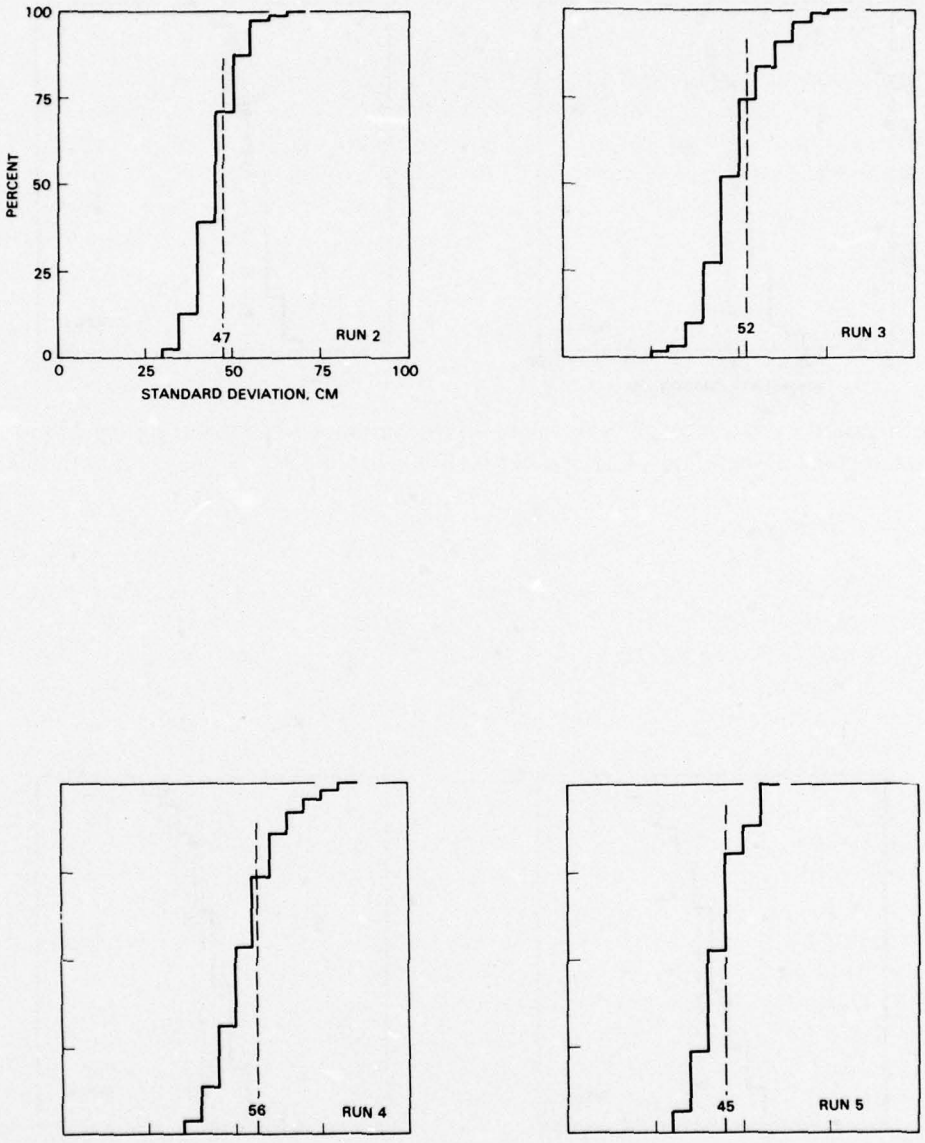

Figure 9. Ogives of standard deviation of surface wave height for 3-min average wave heights measured during station 1.

Figure 10. Ogives of standard deviation of surface wave height for 3-min average wave heights measured during station 3.

Figure 11. Ogives of standard deviation of surface wave height for 3-min average wave heights measured during station 4.

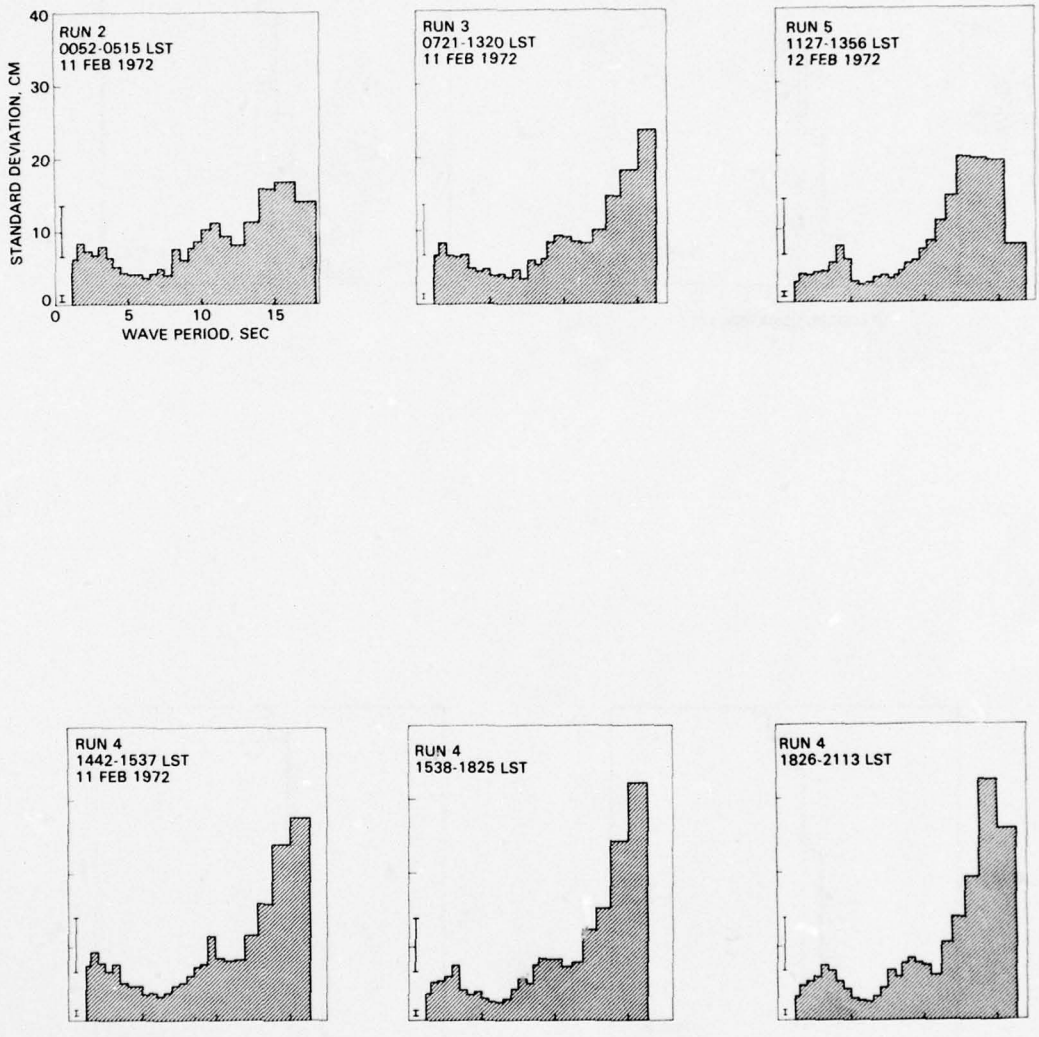

Figure 12. Standard deviation of wave height as a function of wave period for station 1.

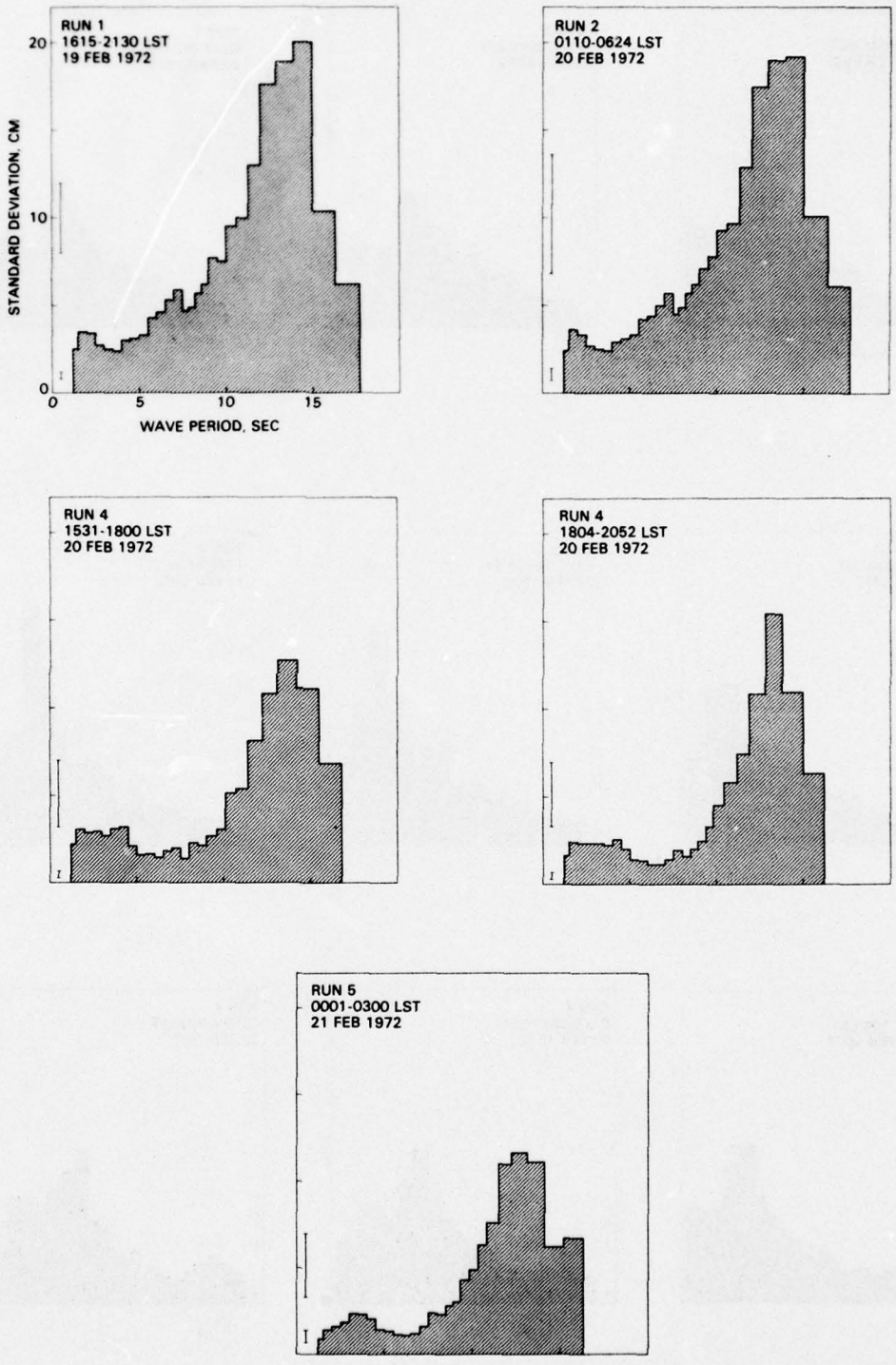

Figure 13. Standard deviation of wave height as a function of wave period for station 3.

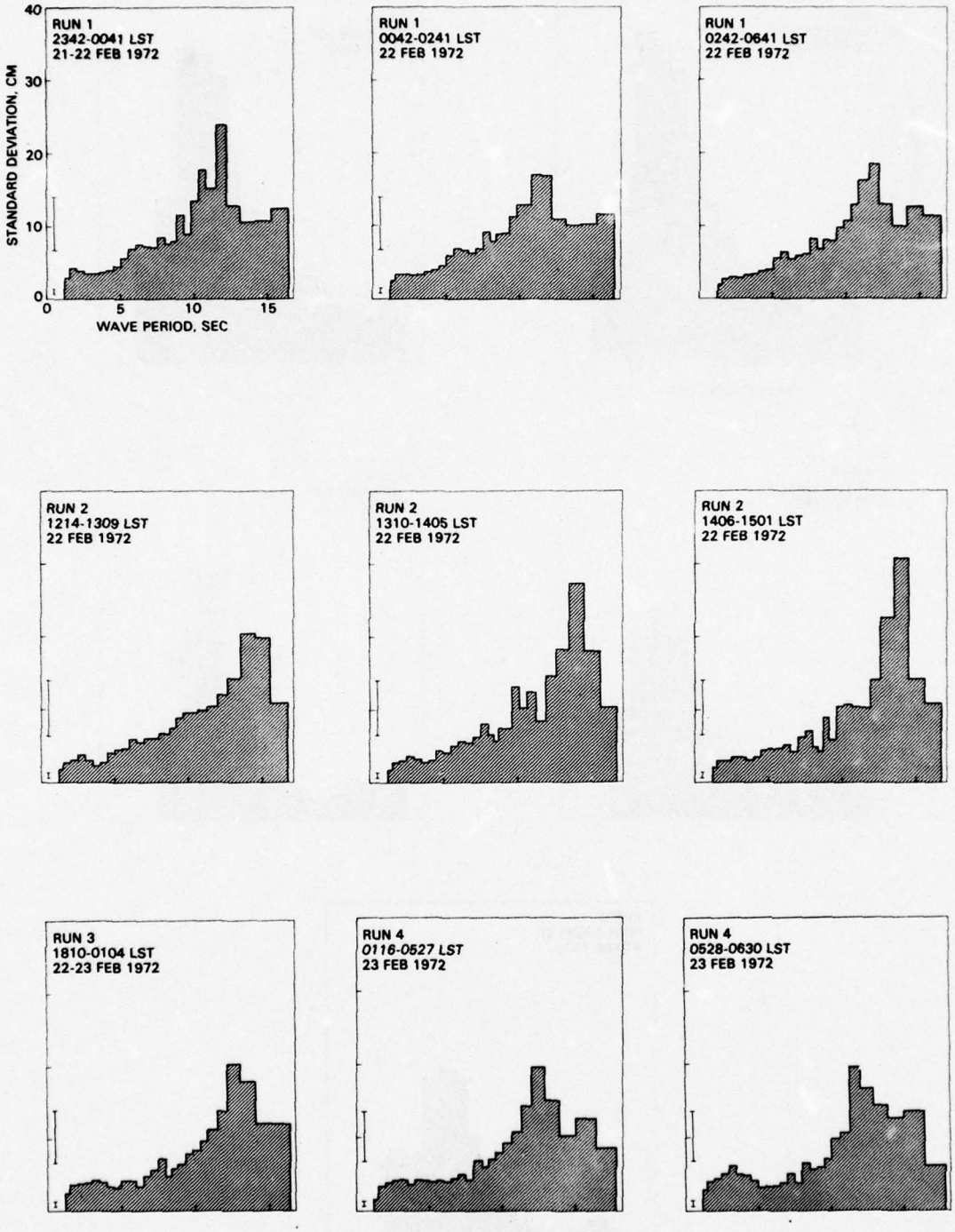

Figure 14. Standard deviation of wave height as a function of wave period for station 4.

AMOS PARAMETERS

The AMOS near-surface propagation loss prediction model requires single average values of isothermal layer depth, depressed channel depth, sea state, and sea-surface temperature as inputs (Ref. 5). The isothermal layer depth is defined as the depth below the surface at which the temperature gradient from the surface is greater than $-0.3^{\circ}F/100$ ft. The depressed channel is formed by an isothermal layer (as defined above) within the water column. This latter vertical temperature structure results in a sound-speed minimum near the top of the isothermal layer because of the effect of pressure on sound speed. The width of the depressed channel is approximately equal to the depth of the channel axis (Ref. 5). Figure 15 aids in defining these parameters.

Figure 16 contains, for each acoustic station, plots of the average temperatures derived from the thermistor chain measurements made during the indicated propagation loss run. The length of the horizontal bar is the standard deviation of the average for the number of observations shown below the run number. Table 12 summarizes the average values of the AMOS parameters. These averages are based upon the averages used in Fig. 16. Also tabulated are the number of observations and the maximum acoustic range for which the AMOS model is valid. For station 2 runs 2 and 4 the use of the AMOS model is invalid since the sources and receivers were in water masses characterized by different sets of parameters during each entire run. Included in the SUDS I data set are propagation loss measurements made in water volumes characterized during five runs by a single surface channel, one run by a single depressed channel, six runs by a surface channel and a depressed channel, and four runs by a negative sound-speed gradient starting at the surface.

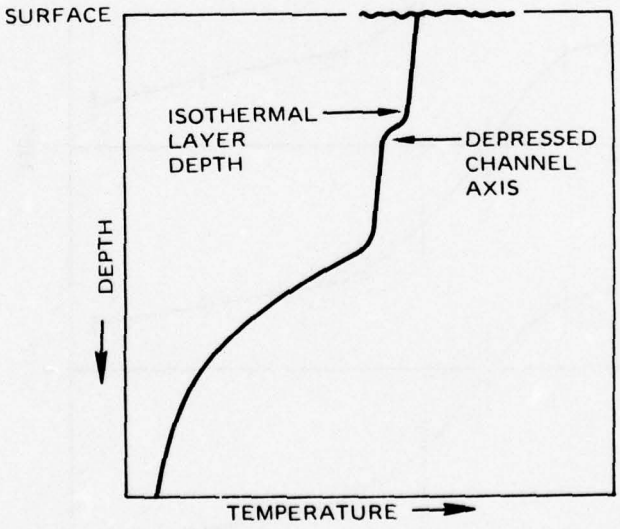

Figure 15. Vertical temperature profile.

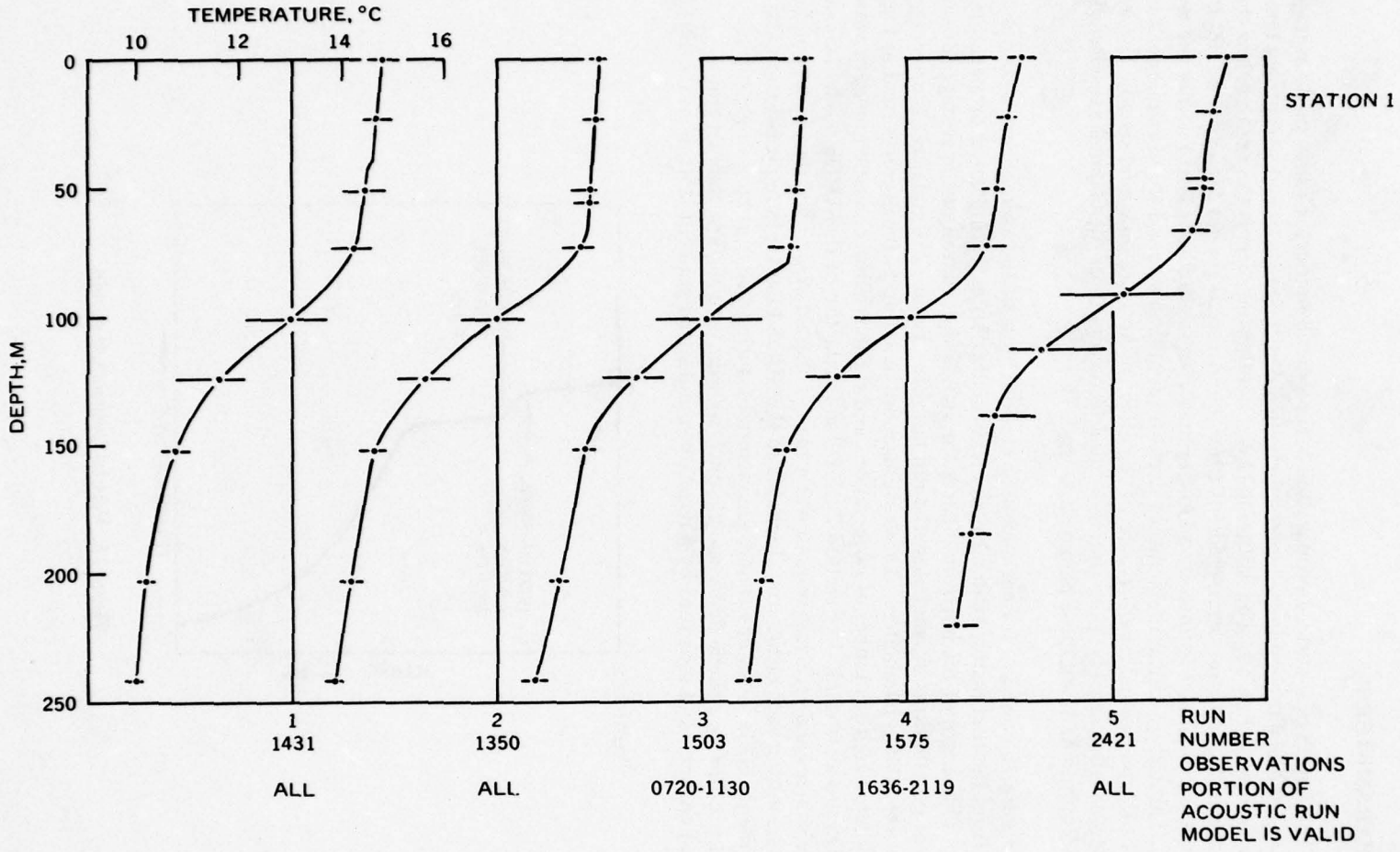

Figure 16. Environmental parameters for AMOS acoustic model derived from average thermistor chain temperature measurements. Times shown are LST.

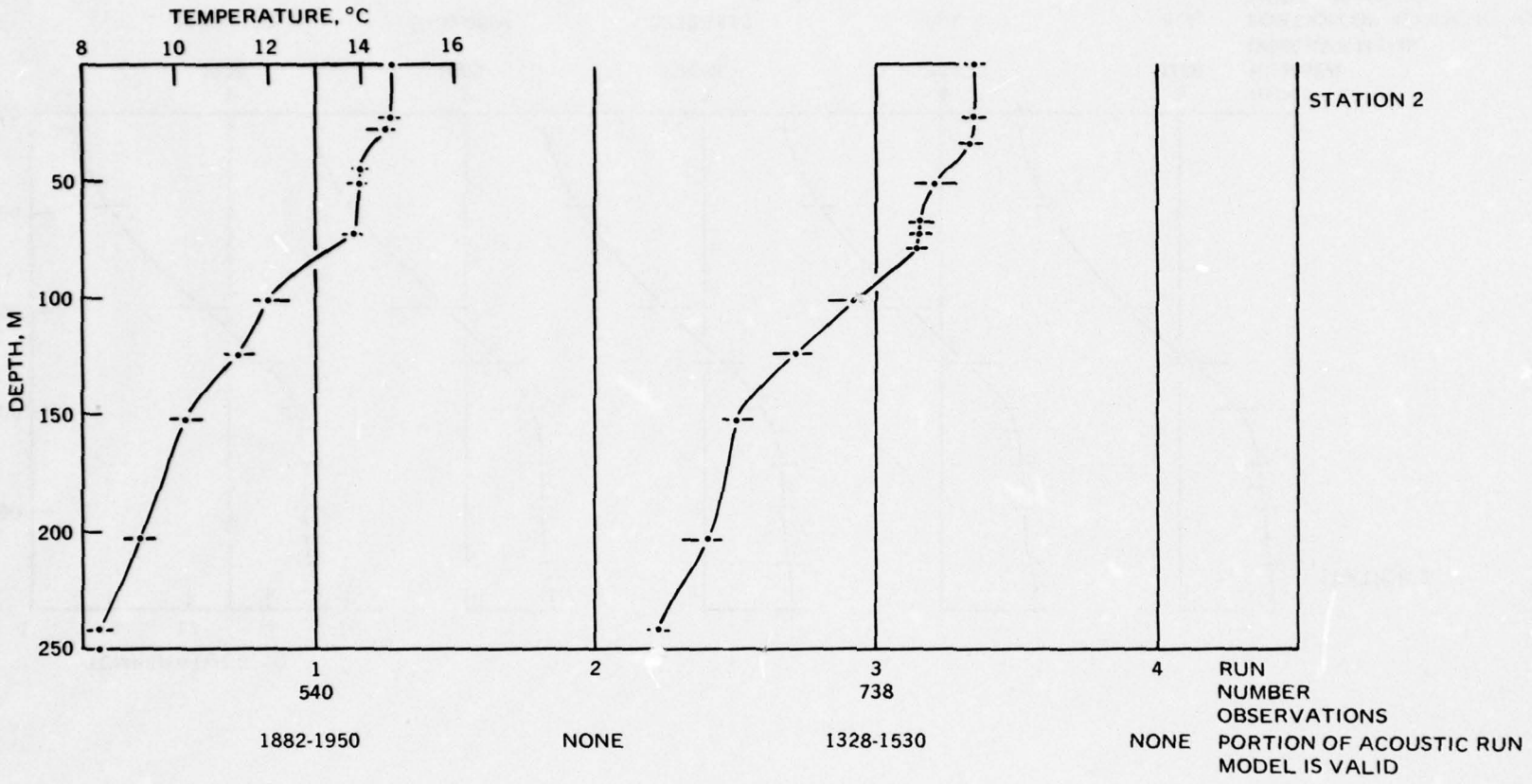

Figure 16. Continued.

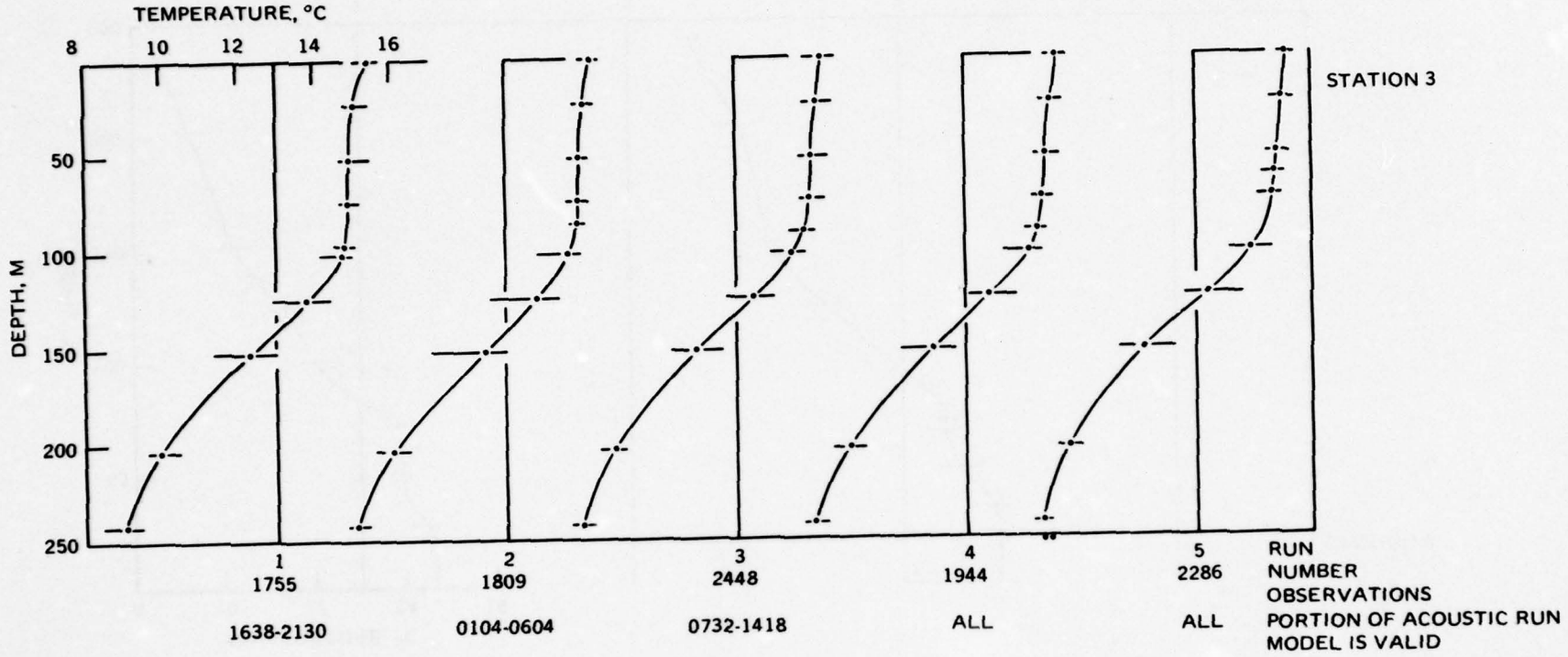

Figure 16. Continued.

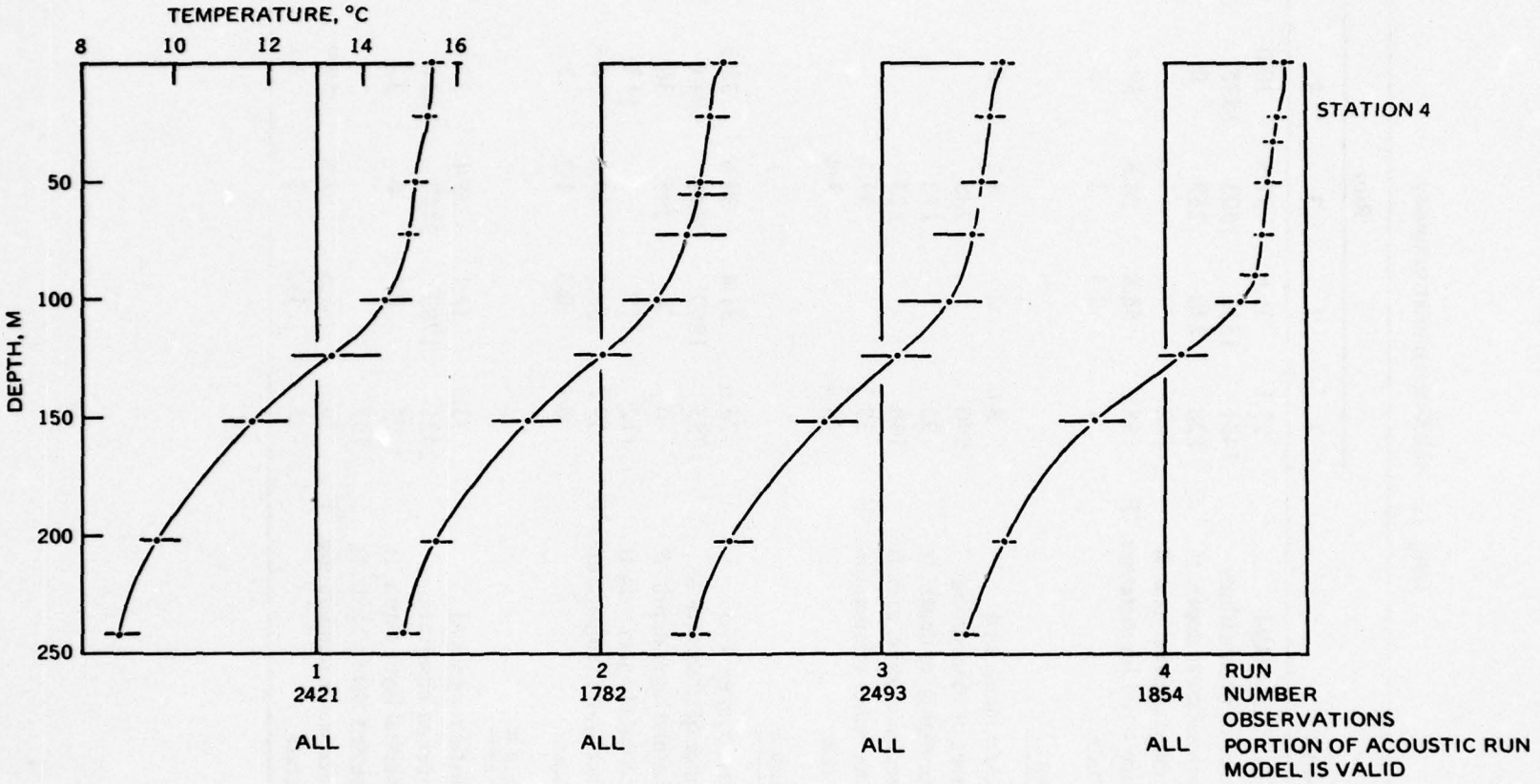

Figure 16. Continued.

Table 12. AMOS parameter summary.

	Run				
Station 1	1	2	3	4	5
Acoustic range, kyd	27.1	26.6	27.5	30.0	30.3
Number of observations	1431	1350	1503	1575	2421
Isothermal layer depth, ft	128	240	259	0	0
Depressed channel axis, ft	148				
Surface water temperature, °F	58.6	58.8	58.8	59.4	59.5
Sea state	1	2-3	2	3	2
Station 2					
Acoustic range, kyd	8.0	0	8.2	0	
Number of observations	540		738		
Isothermal layer depth, ft	92		112		
Depressed channel axis, ft	148		223		
Surface water temperature, °F	58.2		59.2		
Sea state	3→4		3→4		
Station 3					
Acoustic range, kyd	23.6	31.4	34.6	33.3	36.0
Number of observations	1755	1809	2448	1944	2286
Isothermal layer depth, ft	0	20	295	36	259
Depressed channel axis, ft	112	112		112	
Surface water temperature, °F	59.2	59.2	59.4	59.5	59.5
Sea state	0-1	0-3	1-3	2	2
Station 4					
Acoustic range, kyd	33.3	33.1	35.1	33.4	
Number of observations	2421	1782	2493	1854	
Isothermal layer depth, ft	92	0	0	36	
Depressed channel axis, ft	167				
Surface water temperature, °F	59.7	59.5	59.5	59.9	
Sea state	1	1→2	2	2	

PROPAGATION LOSS MEASUREMENTS

A detailed discussion of the instrumentation used to make the CW-pulse and explosive propagation loss measurements, the data reduction procedures, a summary of pertinent environmental measurements, plots of propagation loss versus range, and comments pertinent to specific propagation loss runs are contained in Ref. 1.* This section summarizes the information contained in Ref. 1. Table 13 summarizes information pertinent to the individual propagation loss runs.

CONTINUOUS WAVE (CW) MEASUREMENTS

CW-pulse propagation loss measurements were made on 15 of the propagation loss runs. Two frequencies were transmitted for each experimental run except for station 2 run 2, in which only one frequency was used. Three propagation loss runs were made using the 0.4- and 1.0-kHz sources, five the 1.5- and 2.5-kHz sources, six the 3.5- and 5.0-kHz sources, and one the 1.0-kHz only. Planned source depths were 0.7 of the measured surface layer depth or 15 m, whichever was the deeper, for 12 runs and 6 m for 3 runs. During each experiment a series of 500-msec pulses, at a 12-sec repetition rate for each frequency, were transmitted by the source ship as it opened or closed range at 3 knots from the receiver ship. Each minute, one pulse was omitted as an aid to later data reduction and processing. At one of the frequencies, four pulses were transmitted each minute. During the same minute, a second series of pulses, at the second frequency, were transmitted. The second group had the same structure as the first but was delayed 6 sec relative to the first. The resulting pulsing schedule was a series of eight pulses, alternating in frequency, 500 msec in length, sent each minute, with the first 12 sec silent. These transmissions were received on five receivers suspended from the receiver ship, which was hove to and drifting. Planned receiving depths were 6 m and 0.4, 0.8, 1.3, and 2.0 times the measured surface layer depth. The data were recorded on two six-channel Brush recorders and a magnetic tape recorder.

The Brush recorder record of the acoustic signal arrivals was used as the primary data source. Figure 17 is a 1-min sample of the recorded data. The hydrophone outputs were recorded on channels 1–5, with the shallowest hydrophone recorded on channel 1 and the deepest on channel 5. Generally, three arrivals were recorded for each 0.5-sec pulse. The first arrival traveled via the surface channel path and was the arrival of interest in these experiments. The second arrival traveled via one bottom reflection and the third via two bottom reflections. A radio pulse was transmitted with each acoustic pulse and its arrival was recorded on channel 6. Acoustic travel times were obtained from the difference in the time of arrival of the simultaneous radio and acoustic pulses. To obtain a travel time of the required accuracy, the Brush recorder speed was increased from the normal recording speed of 5 mm/sec to 125 mm/sec every 30 min. This permitted a travel-time determination accurate to ±0.01 sec. The acoustic range was obtained by multiplying the travel time by an appropriate average sound speed for near-surface propagation. During these experiments the sound speed varied from 1503.8 to 1507.0 m/sec. This results in a relative acoustic range accuracy of about 15 m, or 16 yd.

*N. J. Martini, T. E. Stixrud, and D. White wrote the section of the report concerned with the CW transmitting system, C. K. Lisle the section concerned with the CW receiving system, and R. W. Townsen the section concerned with the reduction of the CW-pulse records. D. L. Keir wrote the discussion of the explosive propagation loss measurements.

Table 13. Summary of propagation-loss experiments

Run	Date/time, LST	Range, kyd Minimum	Range, kyd Maximum	Frequency, kHz	Source depth, m	Receiver depth, m
STATION 1 (10–12 February 1972)						
1	10/0251-0647	0.5	27.1	1.5	41	6/24/59/98/148
				2.5	41	
2	11/0052-0515	2.2	26.6	0.4	45	4/17/43/72/112
				1.0	42	
3	11/0721-1330	0.1	38.9	3.5	45	4/17/43/72/112
				5.0	42	
4	11/1438-2119	0.1	43.7	3.5	7	5/19/47/77/120
				5.0	4	
5	12/1125-1400	1.2	30.3	explosive	18	6/23/57/95/145/38
STATION 2 (14–15 February 1972)						
1	14/1822-0024	0.2	32.4	1.5	38	5/19/47/77/120
				2.5	38	
2	15/0141-0508	10.7	29.5	1.0	39	4/17/43/72/112
				—	—	
3	15/1328-1940	0.2	25.0	3.5	38	4/17/43/72/112
				5.0	41	
4	15/2031-0052	1.7	28.1	0.4	8	4/17/43/72/112
				1.0	5	
STATION 3 (19–21 February 1972)						
1	19/1500-2130	5.2	31.1	explosive	18	6/34/69/112/173/38
2	20/0105-0630	3.9	33.6	1.5	42	6/37/73/119/182
				2.5	42	
3	20/0658/1418	0.1	37.5	0.4	42	6/34/69/112/173
				1.0	42	
4	20/1530-2052	0.1	33.3	3.5	44	6/36/72/117/180
				5.0	47	
5	20/2131-0400	2.9	36.0	3.5	6	6/35/71/115/177
				5.0	9	
STATION 4 (21–23 February 1972)						
1	21/2342-0646	0.1	33.3	3.5	43	6/36/73/118/181
				5.0	46	
2	22/1210-1705	0.1	33.1	explosive	18	6/36/72/117/181/38
3	22/1810-0104	2.3	35.1	1.5	43	6/36/72/117/180
				2.5	43	
4	23/0116-0632	2.6	33.4	1.5	43	6/36/72/117/180
				2.5	43	

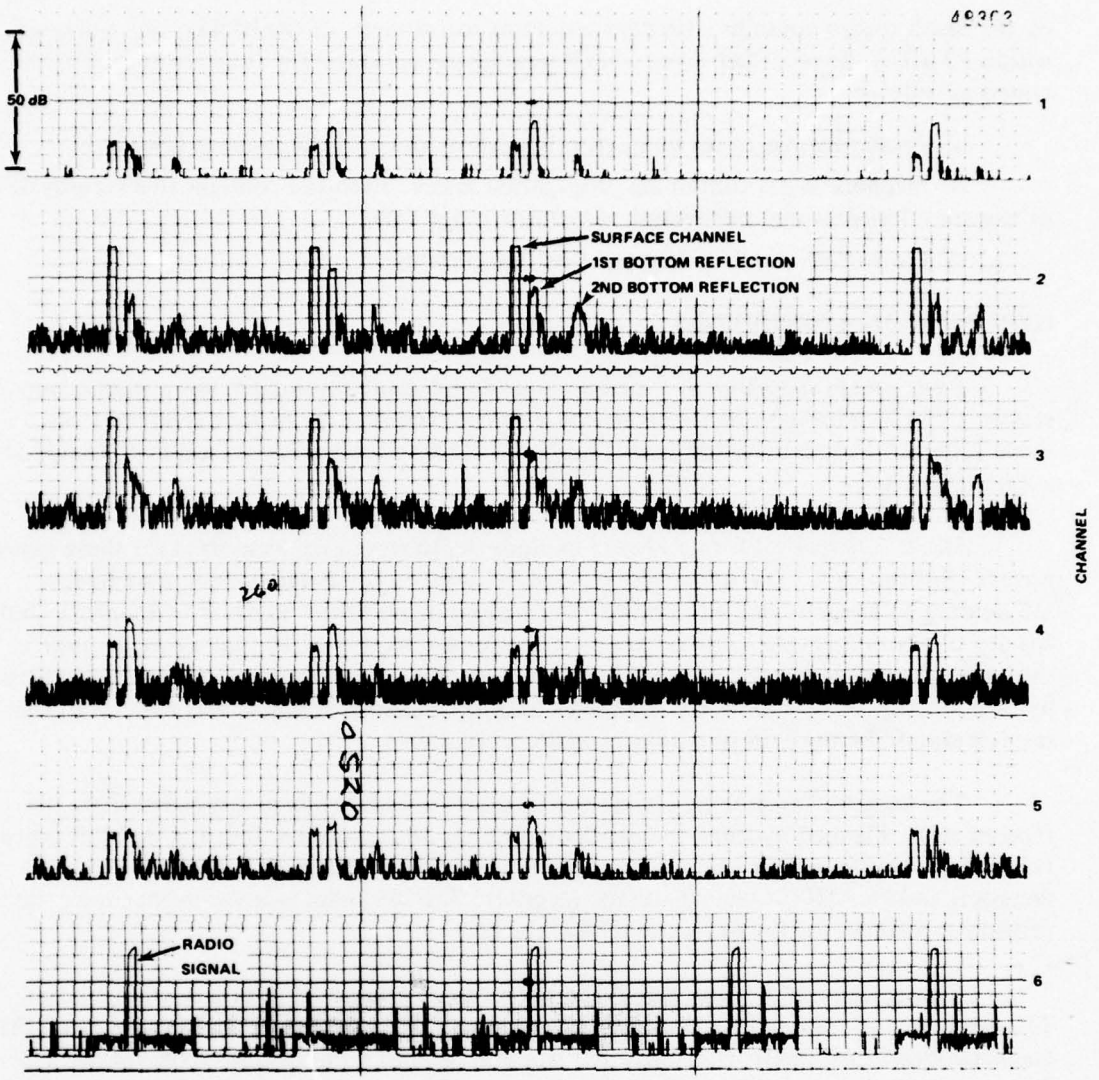

Figure 17. Sample Brush recorder record.

The level of the incoming signal and the accompanying background noise level was read from the Brush records and transcribed onto IBM keypunch work sheets. The data were then punched onto IBM cards. A UNIVAC 1110 computer with a capacity of 36-bit single precision was used in the data reduction procedure. The data reduction program handled all computations, storage, and plotting. The program consisted of a main routine and five subroutines, with all necessary data and transfer parameters being passed through a series of common statements. The main routine was designed to call the subroutines, compute the propagation loss for each received pulse, and output the propagation loss and range data. The subroutines handled reading of header cards, reading data cards, computing system loss levels for each pulse, computing acoustic ranges for each data set, and plotting propagation loss as a function of acoustic range for each hydrophone channel. The signal level recorded

on the Brush record contains a background noise component. If the background noise was within 10 dB of the recorded signal level it was subtracted out. The final results were presented as follows:

a. Printer listings of set number, propagation loss, and the range in kiloyards.

b. Magnetic tapes containing propagation losses. Each file contains five records of propagation loss data and one record of acoustic range data.

c. Plots of propagation loss as a function of range.

EXPLOSIVE MEASUREMENTS

Explosive propagation loss measurements were made on three of the acoustic runs: station 1 run 5, station 3 run 1, and station 4 run 2. The first explosive experiment was made using a 6-knot source-ship speed, while the other two experiments were conducted at a 3-knot speed.

Mk. 61 charges set for an 18.3-m explode depth were used as sources for these experiments. Prior to each experiment test shots were dropped to enable the operator to set attenuators on the receiving equipment. During each experiment, in order to achieve a shot spacing of approximately 1 kyd, charges were dropped every 5 or 10 min while the source ship opened or closed range at 6 or 3 knots, respectively. The charges were monitored by a hydrophone towed by the source ship. The output of this hydrophone was radioed to the receiver ship to be used for obtaining acoustic travel times.

The acoustic transmissions were received on six hydrophones suspended from the receiver ship. Planned hydrophone depths were 6 m, 38 m, and 0.4, 0.8, 1.3, and 2.0 times the measured surface layer depth. The data were recorded on two six-channel Brush recorders and an AMPEX wideband tape recorder. The magnetic tape recordings were the primary recordings for the explosive measurements.

Figure 18 is a block diagram of the explosive-measurement data reduction system. The magnetic tape record was fed into a scope and one channel of a Visicorder to check the magnetic tape signal level. The Visicorder was also used to monitor one of the frequencies before it was squared and integrated. The first amplifier was used at 0 dB gain setting as an impedance-matching device for the parallel output filter. The filter provided multiple outputs in one-third octave steps. The analog computer took four of the outputs and processed them by squaring and integrating. The received energy from the surface channel acoustic arrival was read off the Visicorder record as the height difference of the trace before and after the acoustic arrival. To improve signal-to-noise ratio on the playback records, the tape was played back at one-fourth the speed at which it was recorded. This procedure produced an increase of 6 dB in the apparent energy of the arrival and a 6-dB decrease in the tangent of the slope for the integrated noise. The filter outputs were set at one-fourth of the original frequencies to compensate for the reduction in playback tape speed.

Figure 19 is a facsimile of a Visicorder record. When the squarer–integrator is turned on, noise is integrated to form a line of more or less constant slope. The surface channel arrival results in a sharp increase in slope of the Visicorder trace. After the surface channel arrival has died out, the noise alone continues to be integrated. The energy of the surface

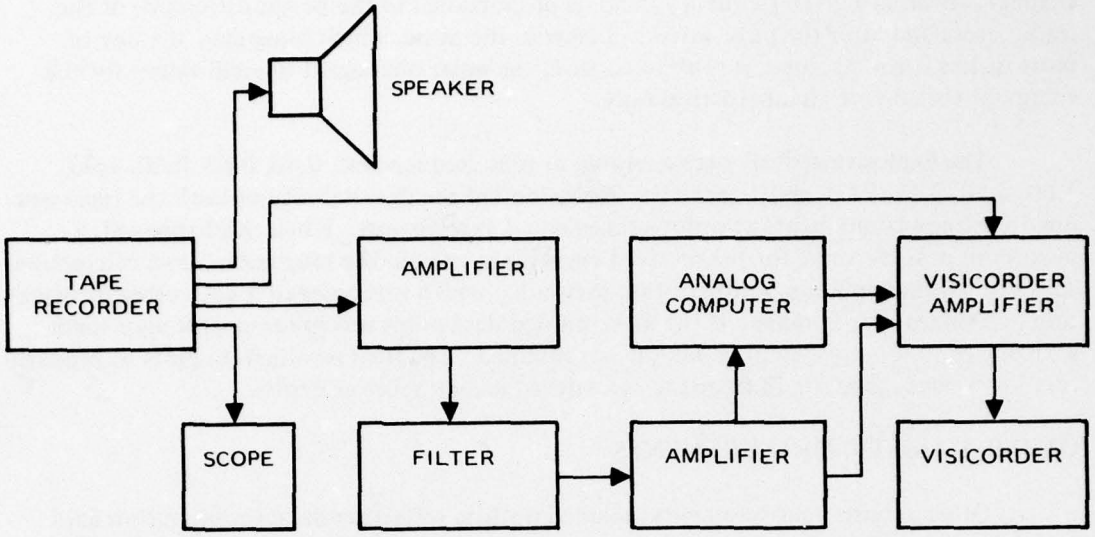

Figure 18. Block diagram of explosive data reduction system.

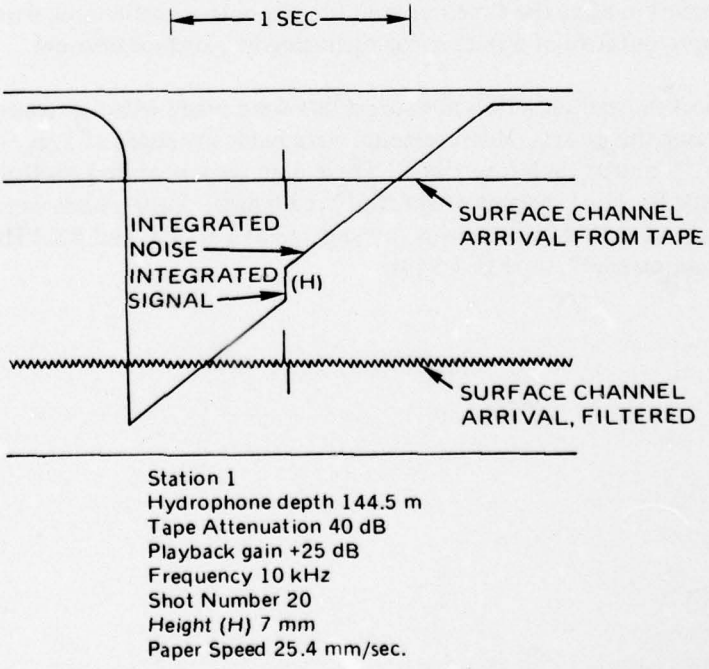

Figure 19. Sample Visicorder record of surface channel arrival.

channel arrival, in a given frequency band, is proportional to the height difference of the trace before and after the pulse arrival. Likewise the noise, which integrates to a line of more or less constant slope, is subtracted from the noise plus signal to yield values for the energy of the surface channel arrival only.

The explosive arrivals were analyzed at nine frequencies: 0.40, 0.63, 0.80, 1.00, 1.60, 2.50, 3.15, 5.00, and 10.00 kHz. Noise limited the detectability of both the high- and low-frequency components at various times on all experiments. When this happened, a maximum possible value for the received energy was used in the propagation loss calculation. This resulted in a minimum propagation loss value, which was compared with other propagation loss values near in range. If the noise-limited data point was in reasonable agreement with adjacent non-noise-limited data, it was retained. The final results were plots of propagation loss versus range for all frequencies analyzed and all receiver depths.

OTHER ACOUSTIC MEASUREMENTS

Other acoustic measurements included bottom reflection data, reverberation data, and short- and long-pulse fluctuation data as a function of range, receiver depth, and frequency. These data are not scheduled for analysis and reporting in the near future.

Bottom reflection data were collected on both CW pulse and explosive propagation loss experiments. As illustrated by Fig. 17 the quality of these data is excellent.

Reverberation data were recorded with the source ship and receiver ships approximately 1000 yd apart. Five-sec pulses at one-minute intervals were used. Since omnidirectional sources and receivers were used, the bottom reverberation obscured the surface channel reverberation after the time required for the bottom reflection arrival. Thus, these data are not representative of a fleet sonar operating in a surface channel.

The short-pulse fluctuation measurements were made with the source ship hove to while transmitting the pulses. Measurements were made at ranges of 3, 6, 9, 12, and 15 nm for a period of 10 min at each frequency. These data were recorded on Brush recorders and on magnetic tape for later analysis of spectral broadening. Long pulses were also recorded at the same ranges. A 10-min pulse was transmitted at 1.0, 3.5, and 5.0 kHz. The signals were recorded on magnetic tape at 7.5 ips.

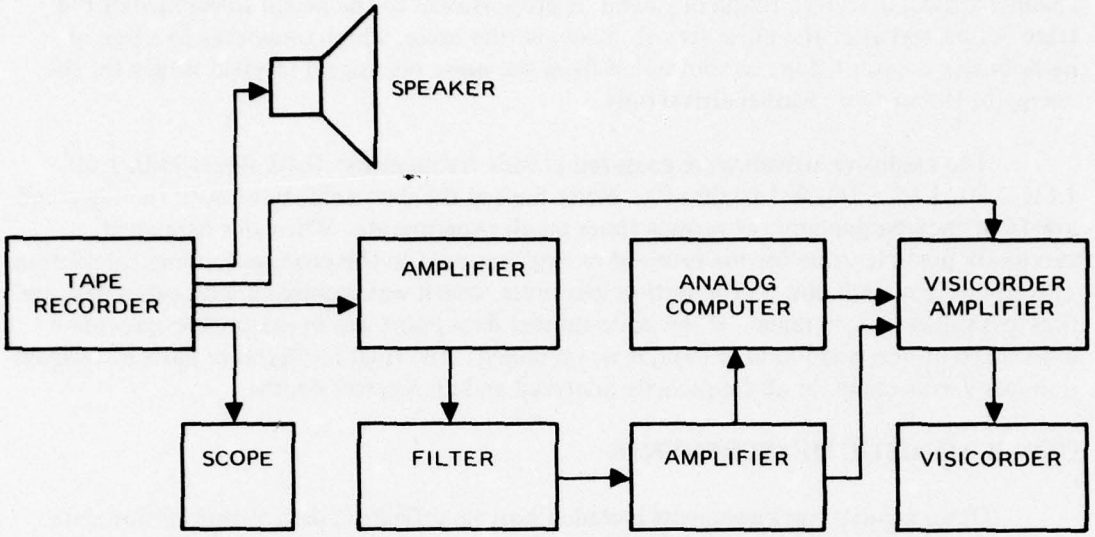

Figure 18. Block diagram of explosive data reduction system.

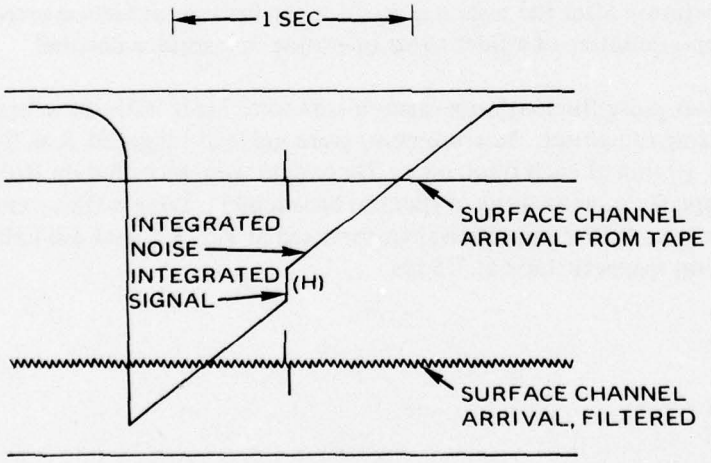

Station 1
Hydrophone depth 144.5 m
Tape Attenuation 40 dB
Playback gain +25 dB
Frequency 10 kHz
Shot Number 20
Height (H) 7 mm
Paper Speed 25.4 mm/sec.

Figure 19. Sample Visicorder record of surface channel arrival.

SUMMARY OF SOUND-SPEED PROFILE TYPES

This section categorizes and discusses the various types of sound-speed profiles which were observed during the SUDS I experiments.

Examination of the average sound-speed profiles presented in Ref. 2 indicates that they can be categorized into seven types. Table 14 presents a summary of the various profile types. Column 1 contains a description and column 2 a letter designator for each type. Column 3 is the total number of profiles of that type present during the propagation loss runs. Column 4 is the number of stations in which the profile type occurred. Column 5 is the relative prevalence of the profile type expressed as a percent. To obtain this value the range interval over which the particular profile occurred at the source was determined for each run. These range intervals were then summed for each type and divided by the sum for all types. The profile types are ordered in Table 14 on the basis of column 5. Column 6 designates the individual profiles of station 1 which were categorized as that type. When a pair of numbers separated by a slash occurs, the first number indicates the run number; the second number indicates the profile number as designated in Ref. 2. When a single number occurs, it is the run number. This represents those runs which were characterized by a single profile. Columns 7, 8, and 9 correspond to column 6 for stations 2, 3, and 4, respectively. The runs with the asterisks in columns 6 to 8 represent the profiles selected to illustrate the seven profile types. These profiles are plotted in Fig. 20.

Table 14 does not include all average profiles listed in Ref. 2. Transitional profiles were deleted. These are the profiles present between two sound-speed profile types representative of distinct water masses. Transitional profiles may take on the character of either water mass, depending on how the transition region is chosen. Since this choice is somewhat arbitrary, transitional profiles were deleted. Also deleted were profiles which were not measured, but predicted on the basis of water masses determined from previous propagation loss runs.

Individual profiles may differ considerably within each profile type. For example, many of the profiles in type A have a sound-speed maximum at the top of the thermocline (i.e., bottom of the depressed channel) rather than at the top of the depressed channel as shown in figure 20. As another example consider, in Ref. 2, profiles 1/3, 2/3, and 3/3 of station 2. These profile shapes lie between B and C. They consist of a surface layer over two linear layers. They are classified as type B, rather than C, because the surface channel extends almost to the top of the thermocline. Reasons for not combining types B and C into a single profile type will be presented later.

Figure 20 and Table 14 are not meant to be a definitive classification of near-surface sound-speed profiles. They are presented to illustrate the variety of profiles encountered during SUDS I. Many theoretical models of surface channel propagation are developed for the type B profile. However, type B was not as prevalent as type A and occurred over less than 20 percent of the range traversed by the source ship during the SUDS I propagation loss runs. Models based on type B profiles alone will have definite limitations. Exactly what these limitations are poses a large problem. For example, the presence or absence of a depressed channel may make little difference acoustically in many cases. However, for high frequencies and sources and receivers in the depressed channel, it could be the dominant feature of the profile.

Table 14. Summary of SUDS I sound-speed profile types

Profile Type	Profile Letter Designator	Number of Profiles	Number of Stations	Percent of Range	Station 1 Runs	Station 2 Runs	Station 3 Runs	Station 4 Runs
Surface channel over depressed channel	A	9	2	33.6		1/1* 2/1 3/2 3/2A	2/3 3/3 4 5	
Classical bilinear surface channel	B	5	2	17.6	2 3/1*	1/3 2/3 3/3		
Surface channel over two linear layers	C	3	2	16.5	1*			1 4
Negative gradients	D	4	2	15.7	3/2 4/2*			2 3
Simple depressed channel	E	3	2	15.1	4/1 5		1/3*	
Two depressed channels	F	1	1	1.1			1/1*	
Surface channel over two depressed channels	G	2	1	0.4			2/1 3/1*	

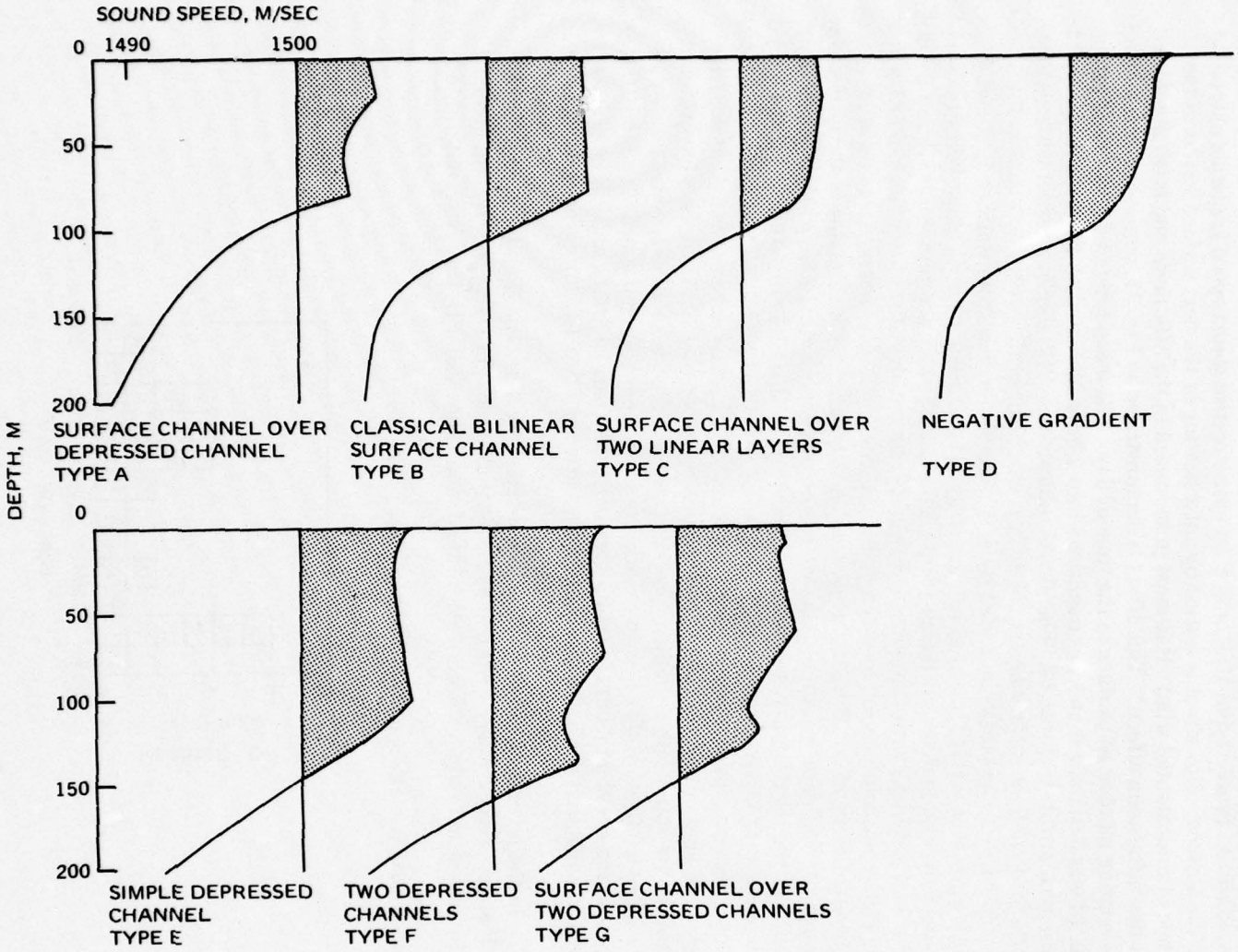

Figure 20. SUDS I sound-speed profile types.

Observe in Table 14 that no profile type occurred for more than two stations. This suggests a correlation between profile types and location. A temporal correlation can also be established. Profile types D, E, and F all have negative sound-speed gradients extending from the surface. This effect is caused by solar heating of the near-surface waters in the absence of a substantial wind. It is most pronounced in the afternoon and is often referred to as the "afternoon effect." This effect is demonstrated in Fig. 21, which presents a histogram relating number of profiles to the time of day. The mean time of day for each run in Table 14 was determined and was quantized into 2-hour increments. Each block in Fig. 21 represents a profile in Table 14. The blocks indicated by "N" signify profiles with negative sound-speed gradient surface layers. Note that all eight profiles with this characteristic occur after 1200 LST. The blocks indicated by a "P" signify profiles from stations 1, 3, and 4 with positive near-surface sound-speed gradients. Ten of these profiles occur before 1200 LST. The single exception occurs between 1800 LST and 2000 LST and represents station 3 run 4 profile 3. The blocks with the symbol (+) signify the profiles of station 2, all eight of which have positive near-surface sound-speed gradients. Station 2 was characterized by wind speeds which varied from 15 to 22 knots. High wind speeds cause vertical mixing in the near-surface layer and prevent negative surface gradients from developing due to afternoon solar heating. In contrast, the wind speeds observed during stations 1, 3, and 4 ranged from 4 to 14 knots. The wind speed for the exceptional "P" (between 1800 LST and 2000 LST) was 7 to 11 knots. This may provide a partial explanation for the exception, since seven of the eight negative sound-speed gradient profiles were accompanied by winds of 4 to 10 knots. However, one of the negative sound-speed gradient profiles was associated with wind speeds of 12 to 14 knots. A generalization that negative gradients are present for wind speeds less than 10 knots, positive sound-speed gradients for wind speeds greater than 15 knots, and either negative or positive sound-speed gradients for wind speeds between 11 to 14 knots is suggested.

In the presence of solar heating sound-speed profiles type G and C become profiles type F and D, respectively.* Note in Table 14 that these types were observed in pairs, i.e., types F and G were observed only at station 3, and types C and D were observed only at

*This is one of the reasons for treating type C as distinct from type B.

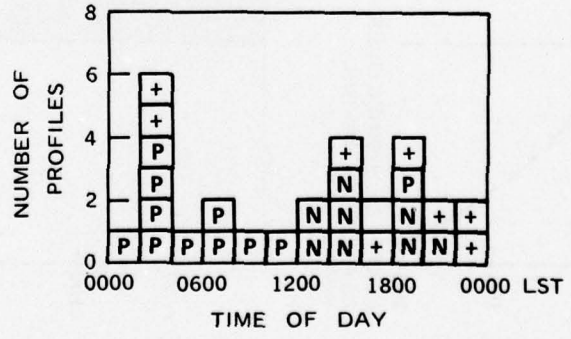

Figure 21. Number of profiles with positive (P) and negative (N) near-surface sound-speed gradients versus time-of-day for stations 1, 3, and 4. Station 2 positive profiles indicated by (+) symbol.

stations 1 and 4. With solar heating of the near-surface waters, types A and B can become type E. Types B and E were observed only at station 1, while types A and E were observed at station 3.

There were, in total, 18 propagation loss runs made at the 4 SUDS I acoustic stations. Nine of these runs were designated in Ref. 2 as being characterized by a single sound-speed profile. Thus, it would appear that spatial and temporal homogeneity occurred about 50 percent of the time. However, this observation is oversimplified. Initially, in determining the number of profiles necessary to describe the sound-speed distribution present during a propagation loss run, individual profiles were sampled every 30 min, using XBT measurements when available and thermistor chain measurements if the XBT measurement was missing. Propagation loss runs were considered to have multiple sound-speed profiles only if the 30-min-interval profiles showed consistent and systematic changes from one profile shape to another. The designation of multiple-profile propagation loss runs was made before the profiles were characterized by types. Moreover, the two procedures were carried out by different investigators. Nevertheless, all multiple profiles in Table 14 consist of at least two types. Progressive gradual changes within one profile type were treated as a single profile. This is the practical procedure, because the scatter in individual profiles can easily obscure trends.

In the process of reconciling the propagation loss measurements with the average profiles of Ref. 2, the thermistor chain measurements were examined in more detail. As will be shown later, averaged thermistor chain data exhibited an unexpected consistency, with even slight temperature trends with depth unobscured by the scatter in the measurements. A few runs were examined using 30-min averages of the thermistor chain measurements. These averages are based on 180 measurements. These 30-min averages showed not only progressive changes within one profile type, but also a change to a different profile type. These averages were obtained for a propagation loss run which was originally characterized by a single profile in Ref. 2. Thus, the profiles of Ref. 2 should not be regarded as closed cases. A wealth of thermistor chain data await further analysis. This may well indicate that none of the propagation loss runs should be regarded as homogeneous in range and time. Indeed, from an acoustic standpoint the changes occurring within a profile type could be more significant than the difference between profile types. From an oceanographic standpoint a compromise sample size of the thermistor chain measurements which averages out scatter but preserves trends should be determined. However, before embarking on such a study, the sensitivity of the acoustic models to sound-speed profile detail needs to be examined. There is little point in chasing down "ripples" in the profile if they have no acoustic significance.

DETAILED SOUND-SPEED PROFILES DERIVED FROM THERMISTOR CHAIN MEASUREMENTS

Sound speeds, at standard hydrographic cast depths, derived from average thermistor chain temperature measurements are given in Ref. 2. Other significant features, such as the depths of surface channels and/or depressed and refractive channels, are also given. The methods used to develop these average sound-speed profiles conform to the customary way of converting XBT, STD/SV, or hydrographic cast temperature and salinity measurements into sound-speed profiles. However, examination of the average thermistor chain measurements, prior to acoustic analyses, revealed that the average temperatures for the individual sensors could be used to much greater advantage than in just the determination of sound speeds at standard hydrographic cast depths. The data for individual thermistor beads represented a capability for greatly increased accuracy of critical input parameters to propagation loss models – in particular to the n-layer normal-mode model (Ref. 20). The sound-speed inputs to this model consist of n layers of the form

$$c^{-2} = a_n + b_n z, \tag{1}$$

where c is the sound speed, z is the depth, and a_n and b_n represent parameters for layer n.

The method of converting the thermistor chain measurements into model parameters is complicated and is the subject of this section. The method will be described for a specific set of thermistor chain measurements. The example chosen for exposition is the set of measurements made during station 4 run 4. This particular data set is an excellent example of the accuracies achievable when using the complete set of thermistor chain measurements. Average thermistor chain temperatures for each of the 44 thermistor beads spaced 5.63 m apart in depth are plotted in Fig. 22. These averages, rounded to the nearest 0.01°C, were obtained from 1854 scans of the thermistor chain's 44 sensors. These scans were made every 10 sec over the 5 hr 9 min duration of the propagation loss run. At a tow speed of 3 knots a complete temperature profile to 242 m was obtained every 17 yd along the track of the source ship. These averages, together with the maximum and minimum temperatures and the standard deviations for each sensor, are tabulated in Ref. 2.

The direct approach to obtaining sound speeds would be to convert each average temperature, plotted in Fig. 22, into sound speed. However, this cannot be done readily because there are no corresponding measurements of salinity. The method of directly converting temperature measurements into computed sound speeds was discussed in a previous section of this report. This method develops, for *each standard hydrographic cast depth*, relationships between temperature and computed sound speed. The effects of local salinity variations with temperature and depth are included implicitly in the computed sound speed. In using this method, the first step in converting temperature measurements into sound speeds is to obtain temperatures, at standard hydrographic cast depths, which are representative of the measurements plotted on Fig. 22. In deriving the sound-speed profiles presented in Ref. 2 the standard depth temperatures were obtained by interpolating between the average temperatures of the sensors just above and just below the standard depth. There are ten standard depths from the surface to 200 m. The interpolation procedure just described utilizes the temperature measurements from 21 thermistors and ignores the other 23 sensors. This procedure may be adequate at standard depths near the surface, where the spacing is only 10 m apart. However, it may fail to preserve the details of the vertical temperature

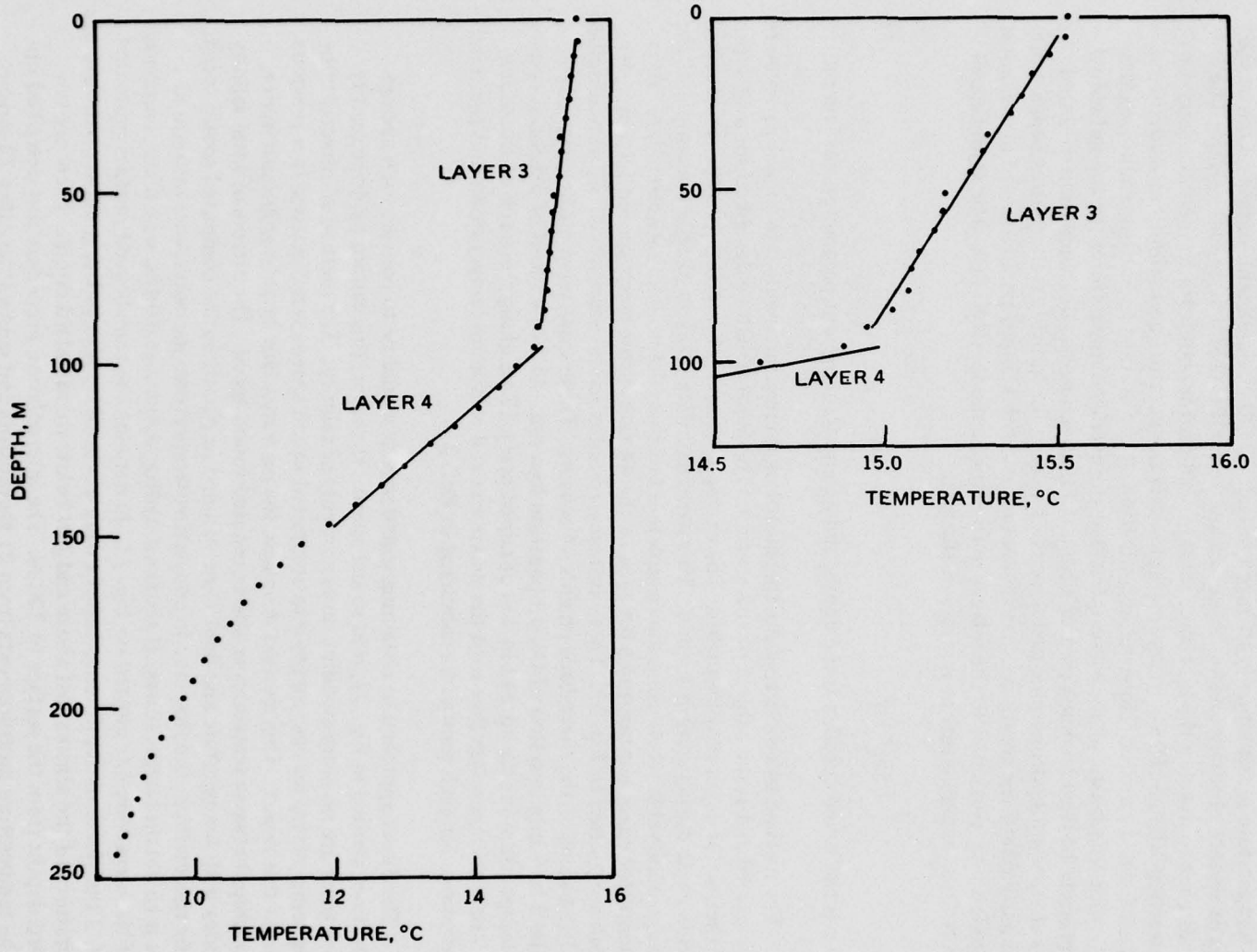

Figure 22. Station 4, run 4. Average temperatures derived from 1854 thermistor chain temperature scans. Lines are least-square fits to indicated temperatures.

distribution at deeper depths, where the sensor spacing increases. For example, in determining the temperatures at 50 and 75 m, the data from three of the thermistors between 50 and 75 m are ignored completely. Yet this is well above the thermocline and in a region where the propagation loss model is very sensitive to input parameters.

To obtain more accurate input parameters and to provide a better estimate of the accuracy of these parameters, a method was developed to utilize all of the thermistor measurements made in the layers where the acoustic input data are critical. Further discussion is facilitated by tables 15 and 16. Table 15 presents the profile parameters which are the inputs

Table 15. Sound-speed profile inputs for station 4 run 4 derived from thermistor chain measurements

Depth, m	Sound Speed, m/sec
0.0	1507.05
4.5	07.12
10.0	06.99
96.6	06.77
150.0	1497.25
200.0	90.71

Table 16. Station 4 run 4 temperatures and sound speeds derived from thermistor chain measurements

Depth, m	Temperature, °C	Sound Speed, m/sec		Difference, m/sec
		Derived	Estimated	
Layer 1				
0	15.54	1507.05	1507.05	0.00
10	(15.54)	(07.21)	(07.21)	0.00
Layer 3				
10	15.48	1507.02	1506.99	-0.03
20	15.41	06.95	06.96	0.01
30	15.35	06.94	06.94	0.00
50	15.22	06.87	06.89	0.02
75	15.06	06.77	06.82	0.05
100	(14.90)	(06.81)	(06.76)	-0.05
Layer 4				
75	(16.21)	(1510.55)	(1510.63)	0.08
100	14.73	06.24	06.17	-0.07
125	13.26	01.80	01.71	-0.09
150	(11.78)	(1497.16)	(1497.25)	0.09

to the computer program of the n-layer normal-mode propagation loss model. It presents the sound speed at various interfaces. The problem to be considered in the discussion to follow is how the data of Fig. 22 are converted into the data presented in Table 15. Table 16 contains data pertinent to an intermediate stage of the conversion process. The first column in Table 16 lists standard depths, the second temperatures, and the third sound speeds calculated using the relationships presented in Table 5. The fourth contains estimates of sound speed as obtained from a linear regression to the data in column 3, and the fifth contains the differences between columns 4 and 3. Various entries of Table 15 and 16 will be considered in more detail as the discussion progresses from Fig. 22 to Table 15.

The first step in this procedure is to group the data into layers in which the temperature appears to be a linear function of depth. This is accomplished by placing a transparent straight edge over the data and visually fitting contiguous data points. In the example of Fig. 22, three groups of data were determined. The first group is the surface observation, which in this case was taken to be a single point. The second group is the 16 consecutive measurements made from 5.63 to 90.08 m. This group is labeled as layer 3 in Fig. 22 consistent with its relation to layer 3 in Table 16. The third group consists of the 10 consecutive measurements made from 95.71 to 146.38 m and labeled layer 4 in Fig. 22. For this profile the measurements made at depths greater than 150 m were not used because the propagation loss model is rather insensitive to inputs in the thermocline.

In this example the near-surface layer poses a particular problem since a break in the temperature gradient probably occurs between the first and second thermistor. In most other profiles in which detailed thermistor measurements were examined, there are several, and in some cases many, sensors which can be grouped in with the surface sensor. This cannot be done in this example. Thus, some assumptions are necessary. An examination of the tabulated values for the second, third, and fourth sensor showed a linear temperature decrease with depth. Assuming that layer 1 was isothermal, having a temperature equal to the surface temperature, the intersection of the layer 1 temperature with the straight line connecting the second, third, and fourth temperatures was determined. The depth of this intersection, 4.5 m, was assumed to be the depth of the interface between layers 1 and 2. This is the depth of the second interface shown in Table 15. The sound speeds associated with layer 1 are given by the first two data lines in Table 16. The surface and 10-m temperatures are converted to sound speed using the relationships in Table 5, and the surface value, 1507.05 m/sec, is entered in Table 15. The sound speed at 4.5 m is determined from a linear fit to the surface and 10-m sound speeds. The resulting value of 1507.12 m/sec is entered in Table 15.

Next, least-square fits of straight lines were made to the layer 3 and layer 4 data sets. The regression equations are:

$$T = 15.543 - 0.00642Z \tag{2}$$

for layer 3 and

$$T = 20.646 - 0.0591Z \tag{3}$$

for layer 4. Equations (2) and (3) are plotted on Fig. 22. The data and equations are also plotted on an expanded scale on Fig. 22 to give a better impression of the goodness of fit in layer 3. The standard error of estimate for the fit of Eq. (2) is about 0.02°C. It is apparent

that the thermistor measurements present an extremely consistent set of values. Very accurate temperature gradients can be obtained from least-square fits, such as Eq. (2). The standard error of estimate for Eq. (3) is about 0.06°C. This is about three times the standard error of estimate for Eq. (2). This is not surprising since larger deviations are typical for measurements made in the thermocline. The propagation loss model is relatively insensitive to parameters in the thermocline, with the fortunate result that the accuracy of the temperature gradients, as determined by this method, is adequate.

The temperatures at standard hydrographic cast depths, shown in data lines 3 to 8 of Table 16, are obtained from Eq. (2). The remaining data lines of Table 16 are obtained from Eq. (3) at standard depths in a similar manner. Table 16 values in parentheses are extrapolations beyond the depth domains of the least-square fits. These are added to give more appropriate weights to the fitted data which lie outside the standard depths spanned by the data.

The sound speeds shown in column 3 of Table 16 were obtained from the relationships shown in Table 5. Linear regressions for layers 3 and 4 were made to the sound speeds listed in column 3. The resulting regressions are:

$$C = 1507.011 - 0.00250Z \tag{4}$$

for layer 3 and

$$C = 1524.012 - 0.17844Z \tag{5}$$

for layer 4. Sound speeds at standard hydrographic cast depths were calculated from Eqs. (4) and (5) and are shown in column 4 of Table 16. These equations are not plotted on Fig. 22. However, the residual errors are given in column 5 of Table 16. The corresponding standard error of estimate is about 0.04 m/sec for Eq. (4) and 0.12 m/sec for Eq. (5). There are two components of sound-speed error associated with the fitting procedures, one associated with Eq. (4) or (5) and the other associated with the temperature errors of Eqs. (2) and (3). In the temperature and depth regimes of interest, the 0.02°C standard error of estimate of Eq. (2) translates to 0.06 m/sec, while the 0.06°C standard error of estimate of Eq. (3) translates to 0.20 m/sec. Thus, the dominant component in both layers 3 and 4 is associated with the temperature fits of Eqs. (2) and (3).

The remaining entries of Table 15 can now be established. The sound speed at 10 m is obtained from Eq. (4). This 10-m depth was chosen for convenience but appears reasonable from the standpoint of Fig. 22. Thus, layer 2 in Table 15 is somewhat arbitrary in that it does not fit any basic data points but merely connects the 4.5- and 10.0-m points. The interface between layers 3 and 4 is determined by solving for the intersection of Eqs. (4) and (5). This yields a depth of 96.6 m and a sound speed of 1506.77 m/sec. The sound speed at 150 m is the value obtained from Eq. (5). This interface depth was chosen for convenience but appears reasonable from the standpoint of Fig. 22. The value at 200 m was obtained by converting the temperature, interpolated from the two temperatures bracketing 200 m, to sound speed. The procedure at this depth does not have to be too accurate because, as noted, the propagation loss model is very insensitive to profile parameters in the thermocline.

Using the depths and sound speeds tabulated in Table 15 as inputs, the normal-mode computer program evaluates the a_n and b_n of Eq. (1) for each layer. The fitting program

passes Eq. (1) through the sound speeds at the upper and lower interfaces of the layer. The last depth entry of Table 15, 200 m, is not really used as a layer interface. The sound speed at this depth is used to determine the parameters in the last layer with upper interface at the next-to-last depth, in this case 150 m. This last layer is an infinite half space with the sound speed approaching zero asymptotically as the depth goes to infinity. This is a standard method to model the surface channel region.

In summary, the general procedures for obtaining sound-speed profiles from the thermistor chain measurements have been given in detail for one example. Each thermistor chain data set poses its own problems and the method may differ slightly from that discussed. The method may seem somewhat arbitrary, but even the cruder aspects are superior to the methods currently in use. There is no doubt that with sufficient experience, standard curve fitting methods can be devised, perhaps with the entire procedure being computerized. The thermistor chain measurements would be the computer input and the fitted sound-speed profile would be the computer output. Such a computer program could also evaluate better statistical descriptions of the fits, such as standard errors of the gradients as well as the sound speeds. The accuracy of the fits could also be improved by increasing the number of layers. However, increasing the number of layers greatly increases the computation time of the propagation loss model. Before the fitting procedure could be standardized a study of sensitivity of the propagation loss model to sound-speed profile inputs should be made. There is little point to precisely fitting thermistor chain measurements to many layers if there is insignificant improvement in the acoustic result.

THEORETICAL AND EXPERIMENTAL PROPAGATION LOSS COMPARISONS

This section compares theoretical and experimental propagation losses for selected SUDS I runs. Five runs are discussed: station 4 runs 4 and 3, station 2 run 1, station 3 run 3, and station 1 run 2.

STATION 4 RUN 4

Morris (Ref. 4) compared the propagation losses measured during the SUDS I experiments with theoretical propagation losses calculated using two operational propagation loss prediction models and three laboratory models. The operational models were the Modified AMOS (NISSM) and the ASRAP II (FNWC) and the laboratory models were the Rough Surface Natural Mode (NSSC), Ray Mode II (NUSC), and Virtual Mode (BTL). Details of these models are presented in Ref. 4. The environmental inputs used by Morris were those presented by Cummins (Ref. 3). Comparisons were reported for five of the SUDS I propagation loss runs, including station 4 run 4. Concerning the station 4 run 4 results Morris says:

> This station was also selected because of unstable run conditions. For receivers in the duct, the agreement between the prediction models and acoustic data was not good. Good agreement, however, is shown below the duct at 117 meters at 1.5 kHz and at 180 meters at 2.5 kHz (figure 12).

Table 3 of Ref. 4 indicates that the ASRAP II propagation loss prediction model gave propagation losses which were 12 to 13 dB less than those measured on the shallowest receiver, and the Modified AMOS model gave losses that were 9 to 12 dB less. However, good agreement was shown between the Rough Surface Natural Model and the Modified AMOS model propagation losses and the experimental values measured by the 117-m receiver at 1.5 kHz and for the 180-m receiver at 2.5 kHz. In general, the run 4 theoretical propagation losses resulted in the poorest overall agreement with the experimentally measured losses for the in-layer receivers analyzed and reported in Ref. 4. Consequently, run 4 was selected for detailed analysis using a sound-speed profile derived from the thermistor chain temperature measurements.

Figure 23 shows the tracks of the source and receiver ships. Thermistor chain measurements were made along the source ship track. XBT profiles were measured at the locations indicated by the "dots" and the "circles." The "dots" show the locations of the XBT profiles accepted and the "circles" the locations of the profiles rejected as being inaccurate after a detailed accuracy analysis (Ref. 2).

SOUND-SPEED PROFILES DERIVED FROM THERMISTOR CHAIN AND XBT MEASUREMENTS

In this analysis three different sound-speed profiles derived from the thermistor chain and XBT temperature measurements will be used. Sound-speed profile I was derived from the thermistor chain measurements. The details of the derivation of this profile, presented in Table 15, were discussed in the previous section. Sound-speed profile II is presented in Table 17.

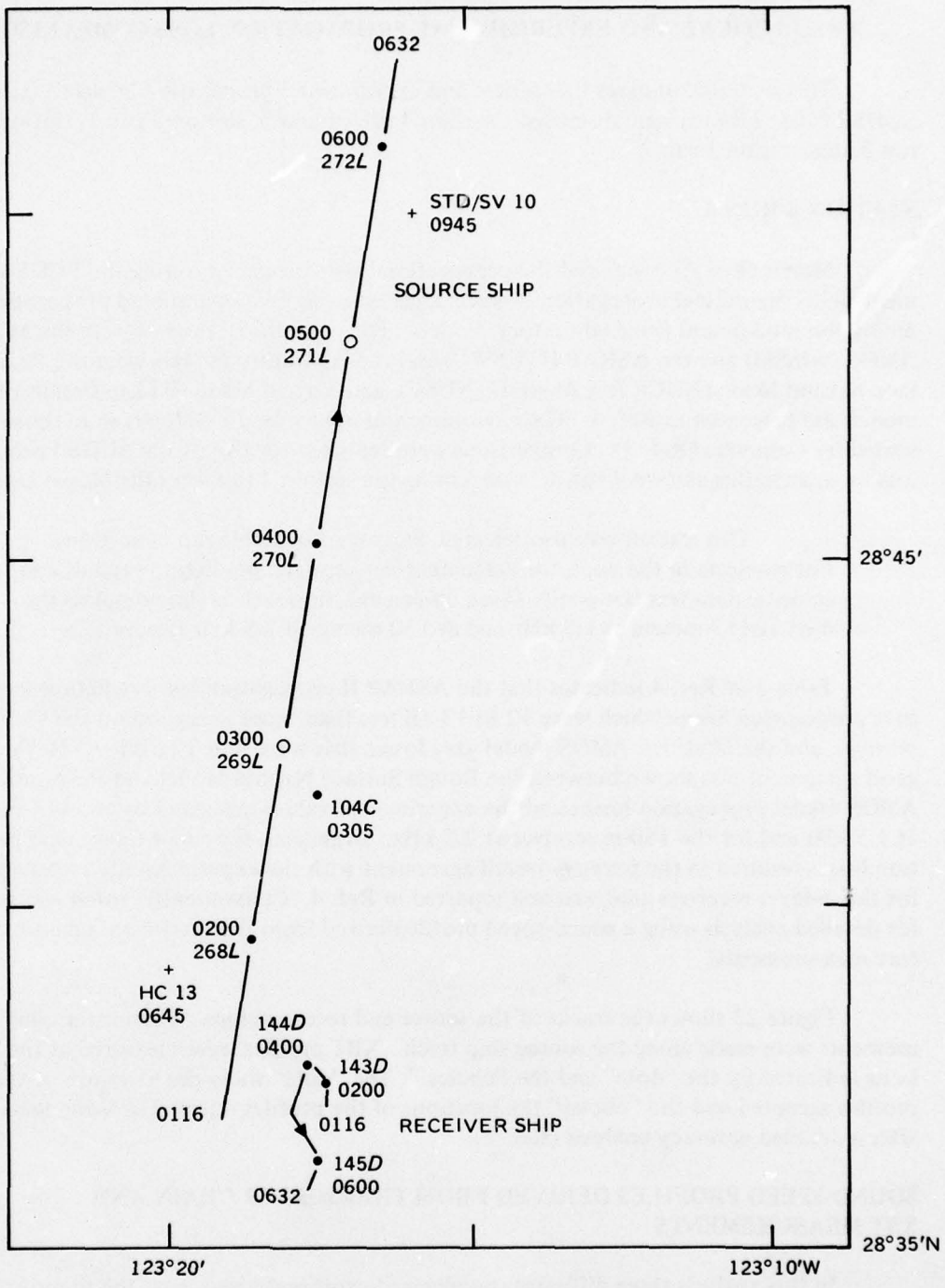

Figure 23. Location of station 4 run 4 thermistor chain, accurate XBT profiles (•), and rejected as inaccurate XBT profiles (○). The letter following the XBT number denotes the ship which took the measurement (*L: Lee, D: DeSteiguer, C: Cape*). Times shown are LST.

Table 17. Station 4 run 4 sound-speed profile presented in Ref. 3

Depth, m	Sound Speed, m/sec
0.0	1507.13
93.0	07.32
150.0	1497.62
200.0	90.51

This is the profile used by Morris (Ref. 4).* The details of the derivation of profile II are not known. According to Cummins:** "Sound-speed profiles presented in Ref. 3 were derived from a preliminary 'quick look' analysis using a qualitative average of selected XBT profiles."

Sound-speed profile III is presented in Table 18. This profile was derived using the seven reliable XBT profiles whose locations are shown by the "dots" in Fig. 23. Instead of visually reading the XBT profiles as is customary, the profiles were read at the standard hydrographic cast depths using a Hewlett-Packard 9864A Digitizer.† The depth and temperature of the surface layer were also read and recorded. The final temperature measurements were recorded to 0.01°C. Of the seven XBT profiles three were taken by the *Lee*, three by the *DeSteiguer*, and one by the *Cape*. The digitized temperature measurements were averaged and converted to sound speed using the relationships shown in Table 5. These data were then fit by straight lines to obtain the data presented in Table 18. The objective of preparing profile III was to obtain the best possible sound-speed profile derived from only reliable XBT profiles using improved digitizing methods.

*This profile was prepared about 5 years ago before the thermistor chain measurements were available and the XBT temperature profiles were subject to quality control. A total of 9 XBT profiles (Fig. 23) were made during run 4. Comparisons of the XBT temperatures with temperature measurements made using other instrumentation, subsequent to the preparation of profile II, showed that two of these XBT profiles were in error.

**Private communication from J. Cummins.

†The Hewlett-Packard 9864A Digitizer measures to the nearest 0.01 in. in x and y. Over an XBT temperature range from 6 to 19°C, this translates to a digitizing accuracy of 0.058°C. This is equal to about 0.15 m/sec in sound speed.

Table 18. Station 4 run 4 sound-speed profile derived from seven XBT profiles

Depth, m	Sound Speed, m/sec
0.0	1506.79
15.0	06.94
20.0	06.73
50.0	06.87
89.0	06.71
150.0	1498.08
200.0	90.39

To emphasize the differences between the near-surface regime of these three profiles, they are plotted in Fig. 24 using an expanded sound-speed scale. For these three profiles the depth of the top of the thermocline is quite consistent, varying from 89.0 to 96.6 m; however, the shapes of the profiles are significantly different from the surface to the top of the thermocline. Profile I, derived from the thermistor chain measurements, is characterized by a shallow surface channel underlain by negative sound-speed gradients at depths greater than about 4.5 m. The onset of modal trapping for this 4.5-m surface channel is estimated to occur at 19.3 kHz, well above the test frequencies of 1.5 and 2.5 kHz. Profile II is characterized by a 93.0-m surface channel. The onset of modal trapping for this surface channel is estimated to occur at 0.6 kHz. Thus, this profile contains an excellent surface channel for the test frequencies. The source depth of 43 m and receiver depths of 6, 36, and 72 m are all in this channel. These three receiver depths and source depths are indicated on Fig. 24. Profile III is characterized by a 15.0-m surface channel underlain by a 36-m depressed channel with axis of minimum sound speed at 20 m. The onset of modal trapping for the surface channel is estimated to occur at 4.1 kHz and the onset of trapping for the depressed channel is estimated to occur at 1.3 kHz. Only the depressed channel is effective at trapping the test frequencies. For this profile the sources are located in the depressed channel, the 6-m receiver in the surface channel, the 36-m receiver in the depressed channel, and the 72-m receiver in the negative sound-speed gradient layer below the depressed channel. Additionally, hydrographic cast 13 and STD/SV 10 were taken at the locations and times shown on Fig. 23. Hydrographic cast 13 exhibited a 30-m surface channel and STD/SV 10 exhibited a 20 m surface channel underlain by a depressed channel with axis of minimum sound speed at 30 m and a maximum sound speed at 50 m.

For most acoustic applications XBT profiles are read visually, without the assistance of a digitizer. Practice has shown that an experienced reader can visually read XBT analog records to an accuracy of about ±0.1°C. A temperature change of 0.1°C is equivalent to about 0.315 m/sec. For reference this difference in sound speed is indicated on Fig. 24 by the barbed line segment. A comparison of the three profiles at depths above the thermocline show that the differences between the XBT-derived profiles II and III and the thermistor chain-derived profile I are all within a ±0.1°C accuracy. A conclusion that there are no real differences between the three profiles is tempting. Such a conclusion, however, is probably premature since it is not clear how much of the difference between profiles is due to *instrument measuring error, the small XBT sample size, under sampling the XBT profiles by only using measured temperatures at standard hydrographic cast depths, and/or biasing of the XBT average profile since five of the XBT profiles were taken during the first half of the propagation run and only two during the last half.*

The sound-speed gradient for an isothermal, isohaline layer in the temperature and salinity regime of the SUDS I areas is 0.0165 sec^{-1}. This gradient is indicated on Fig. 24 by the dashed line. The surface channel sound-speed gradient for profile II is 0.0020 sec^{-1}, considerably less than the isothermal isohaline gradient. Assuming isohaline water, the difference between these two gradients can be accounted for by a 93-m temperature that is about 0.4°C less than the surface temperature. If profile II had been based on a 93-m temperature 0.6°C less than the surface temperature, profile II would have had a negative gradient greater than the thermistor chain-derived profile I. It is apparent that the acoustically important features of the sound-speed profile present during the station 4 run 4 propagation loss run represent a critical regime, requiring much more accuracy than can be obtained from a consideration of a few XBT measurements.

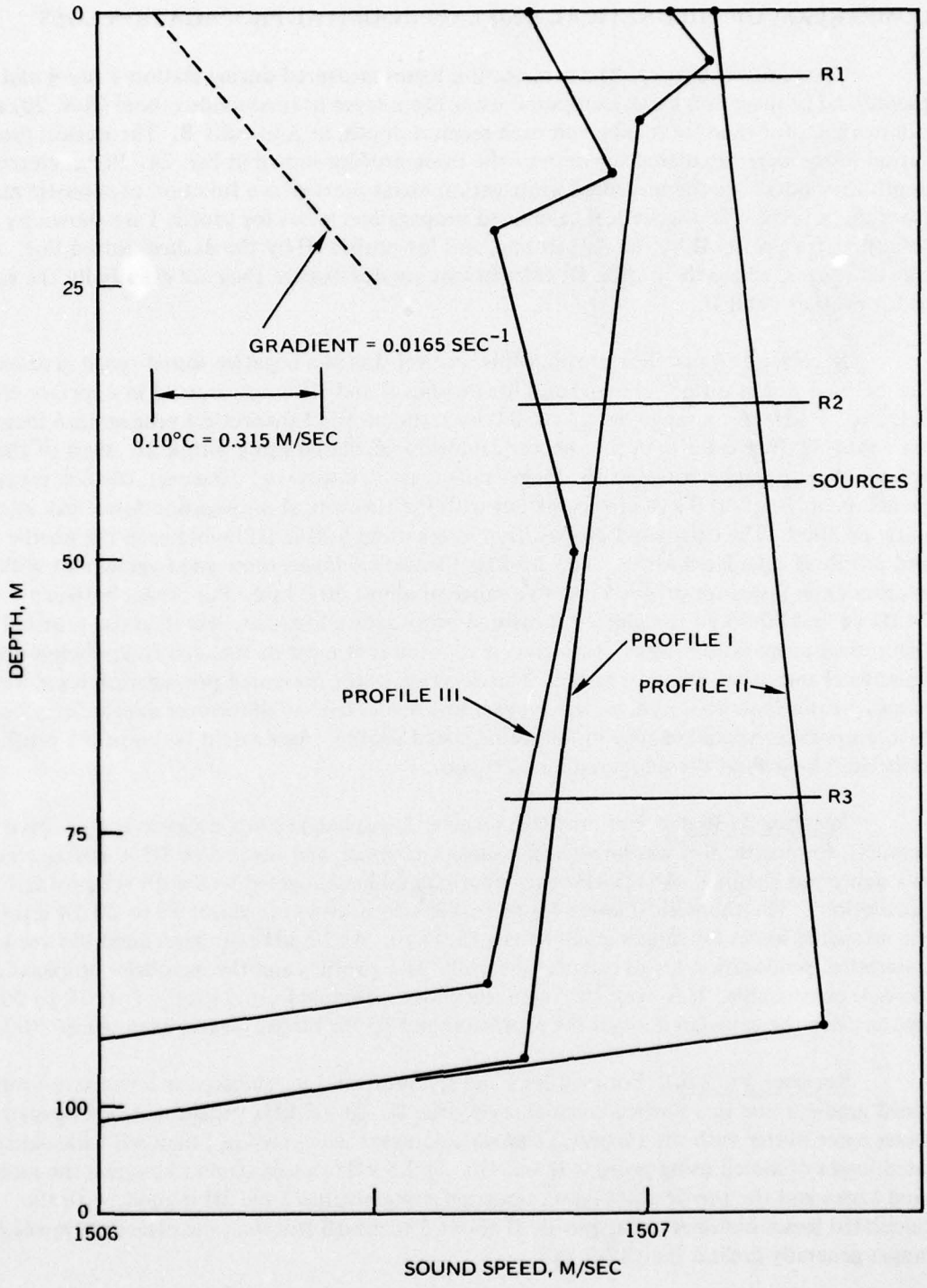

Figure 24. Station 4 run 4 near-surface sound-speed profiles. Dotted line is sound-speed gradient for isothermal (15.5°C), isohaline (33.61 ppt) layer.

COMPARISON OF THEORETICAL AND EXPERIMENTAL PROPAGATION LOSS

Comparisons between the propagation losses measured during station 4 run 4 and theoretical propagation losses computed using the n-layer normal-mode model (Ref. 20) are summarized, for each frequency and each receiver depth, in Appendix B. Theoretical propagation losses were calculated for each of the three profiles shown in Fig. 24. For each receiver depth the "dots" are the measured propagation losses plotted as a function of acoustic range from the source. The theoretical calculated propagation losses for profile I are shown by the solid line, for profile II by the dashed line, and for profile III by the dashed-dotted line. At shorter ranges, where the profile III calculations are not shown, they are essentially the same as for profiles I and II.

Receiver 1 (6 m). For profile I this receiver was in a negative sound-speed gradient just below a 4.5-m surface channel and for profiles II and III it was located in a surface channel. At 1.5 kHz, for a range of about 30.0 kyd, the profile I theoretical propagation losses are about 32 dB greater than the theoretical losses calculated using profile II. Most of the measured propagation losses at the longer ranges are below noise. However, the few measurements recorded at 30.0 kyd are consistent with the theoretical propagation losses calculated using profile I. The calculated propagation losses using profile III lie between the profile I and profile II calculated losses. The 2.5-kHz theoretical losses show good agreement with the experimental losses for profile I out to a range of about 30.0 kyd. For ranges between 24.0 kyd and 30.0 kyd the plotted measured propagation losses are less than the profile I theoretical propagation losses. However, it is noted that most of the arrivals are below the noise level and, thus, are not plotted. The decrease in the measured propagation losses for ranges greater than 30.0 kyd, which appears to some extent at all receiver depths, may be due to a temporal or spatial change in the sound-speed profile. Agreement between the profile II calculated losses and the measured losses is poor.

Receiver 2 (36 m). For profile I, receiver 2 was located in a negative sound-speed gradient, for profile II it was located in a surface channel, and for profile III it was located in a depressed channel. At 1.5 kHz the experimental losses agreed well with the profile I calculations. The theoretical losses for the other two profiles are about 10 to 20 dB less than the measured losses for ranges greater than 15.0 kyd. At 2.5 kHz the agreement between the theoretical propagation losses calculated for all three profiles and the measured propagation losses is comparable. However, the theoretical losses obtained using profile I are 10 to 20 dB greater than the calculated losses for profiles II and III for ranges greater than about 20.0 kyd.

Receiver 3 (72 m). For profiles I and III, receiver 3 was located in a negative sound-speed gradient and in a surface channel for profile II. At 1.5 kHz the measured propagation losses agree better with the theoretical losses calculated using profile I than with the calculated losses obtained using profiles II and III. At 2.5 kHz the agreement between the measured losses and the theoretical losses calculated using profiles I and III is good, with the calculated losses obtained using profile II about 5 to 10 dB less than the measured losses for ranges generally greater than 13.0 kyd.

Receiver 4 (117 m) and Receiver 5 (180 m). For all profiles, receivers 4 and 5 were in the strong negative sound-speed gradient associated with the main thermocline. At both frequencies the theoretical propagation losses obtained from all three profiles agree very well with the measured propagation losses. The 2.5-kHz propagation losses calculated using

profile III are not included on the receiver 5 plot since they are essentially the same as those obtained using the other two profiles.

Conclusions

- The poor agreement reported by Morris (Ref. 2) between theoretical and experimental propagation losses for receivers in the surface layer above the main thermocline is explained in terms of the near-surface sound-speed profile used as the input to the theoretical calculations. The propagation loss measurements, instead of being made in the presence of a slight positive sound-speed gradient representing a strong 93-m surface channel, were made with the receivers located in a predominantly negative sound-speed gradient.
- The good agreement reported by Morris (Ref. 3) between theoretical and experimental propagation losses for receivers in the main thermocline is also explained. The theoretical results appear to be independent, at least within the profile bounds shown in Fig. 24, of the sound-speed profile above the main thermocline.
- Theoretical propagation losses calculated using the n-layer normal-mode model are relatively insensitive to sound-speed profile inputs for receivers located in the main thermocline as compared to receivers above the thermocline.
- Acoustically important features of the sound-speed profile present during the station 4 run 4 propagation loss run represent a critical regime, requiring much more accuracy than can be obtained from a consideration of a few XBT measurements.

STATION 4 RUN 3

Figure 25 shows the tracks of the source and receiver ships for the station 4 run 3 propagation loss run. Also shown are the locations of the half-hourly XBT and thermistor chain temperature profiles used to determine the average sound-speed profile reported in Ref. 2. An examination of these profiles suggested that the propagation loss measurements were made in a single sound-speed profile volume. The individual profiles showed transient surface channels at depths varying from the surface to 67 m and intermittent small depressed channels at depths varying from 10 to 75 m. The average sound-speed profile was characterized by a negative sound-speed gradient from the surface to the depth of the deep sound-speed minimum. There were no surface or depressed channels retained in the average profile. A visual examination of the propagation loss plots showed that, although the average sound-speed profile did not have a surface channel, the propagation loss patterns exhibited a well-developed modal pattern. This observation is illustrated by Fig. 26. In addition, measurements were recorded for both frequencies on all receivers out to the 35.1 kyd maximum range of the run. These observations suggested that the propagation loss measurements were made in the presence of surface and/or depressed channels rather than in the presence of the negative sound-speed gradients characteristic of the Ref. 2 average sound-speed profile.

Sound-Speed Profiles Derived from Thermistor Chain Measurements

To examine the validity of the Ref. 2 conclusion that the water volume present during the run 3 propagation loss measurements was characterized by a single sound-speed profile, the thermistor chain data were subdivided into 30-min segments and average temperatures for these half-hour periods computed. These data are plotted on Fig. 27. The

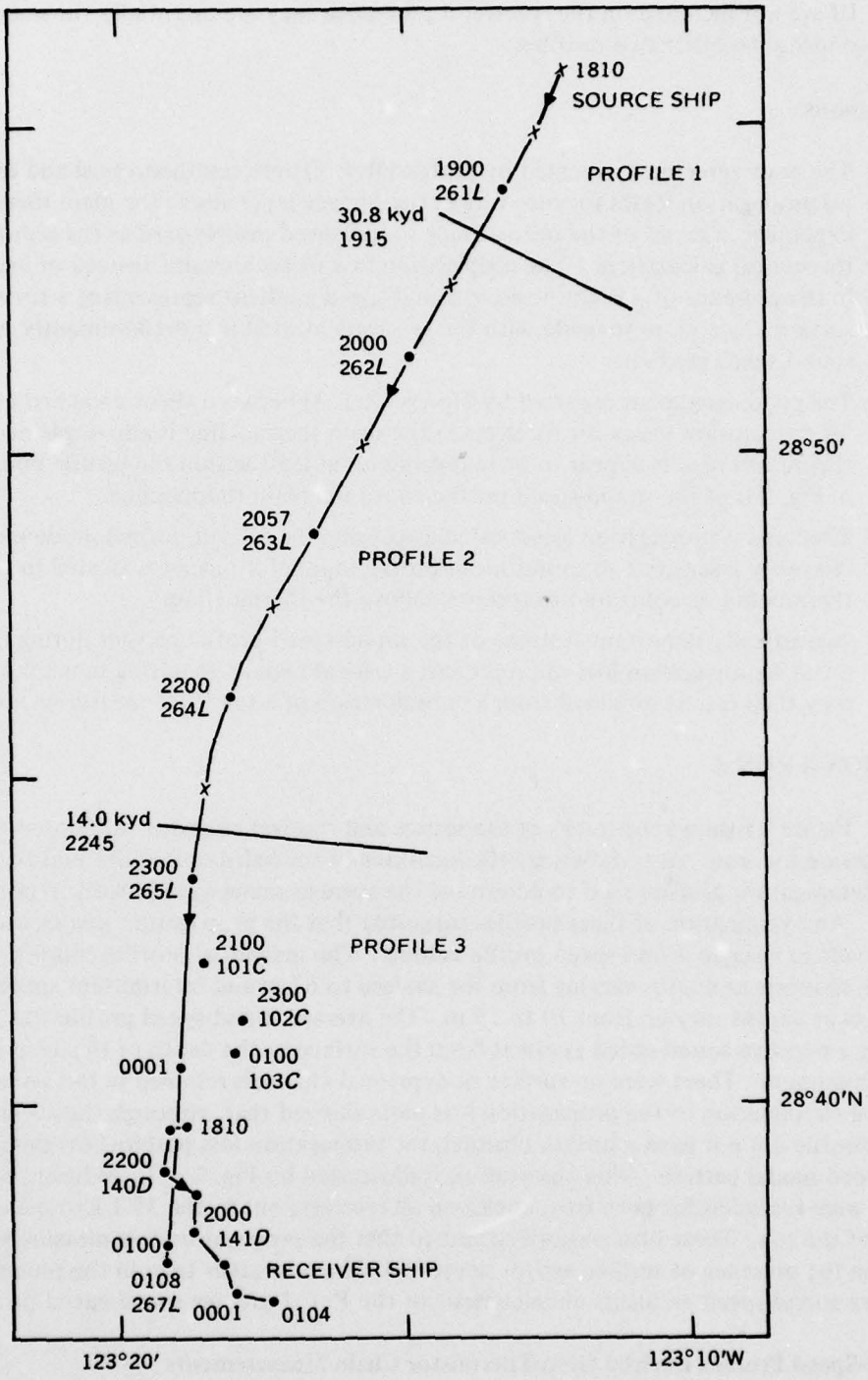

Figure 25. Station 4, run 3, 22-23 February 1972. Locations of XBT (•), thermistor chain profiles (X), source and receiver ships, and sound-speed profile boundaries. The letter following the XBT number denotes the ship which took the measurement (*L: Lee, D: DeSteiguer, C: Cape*). Times shown are LST.

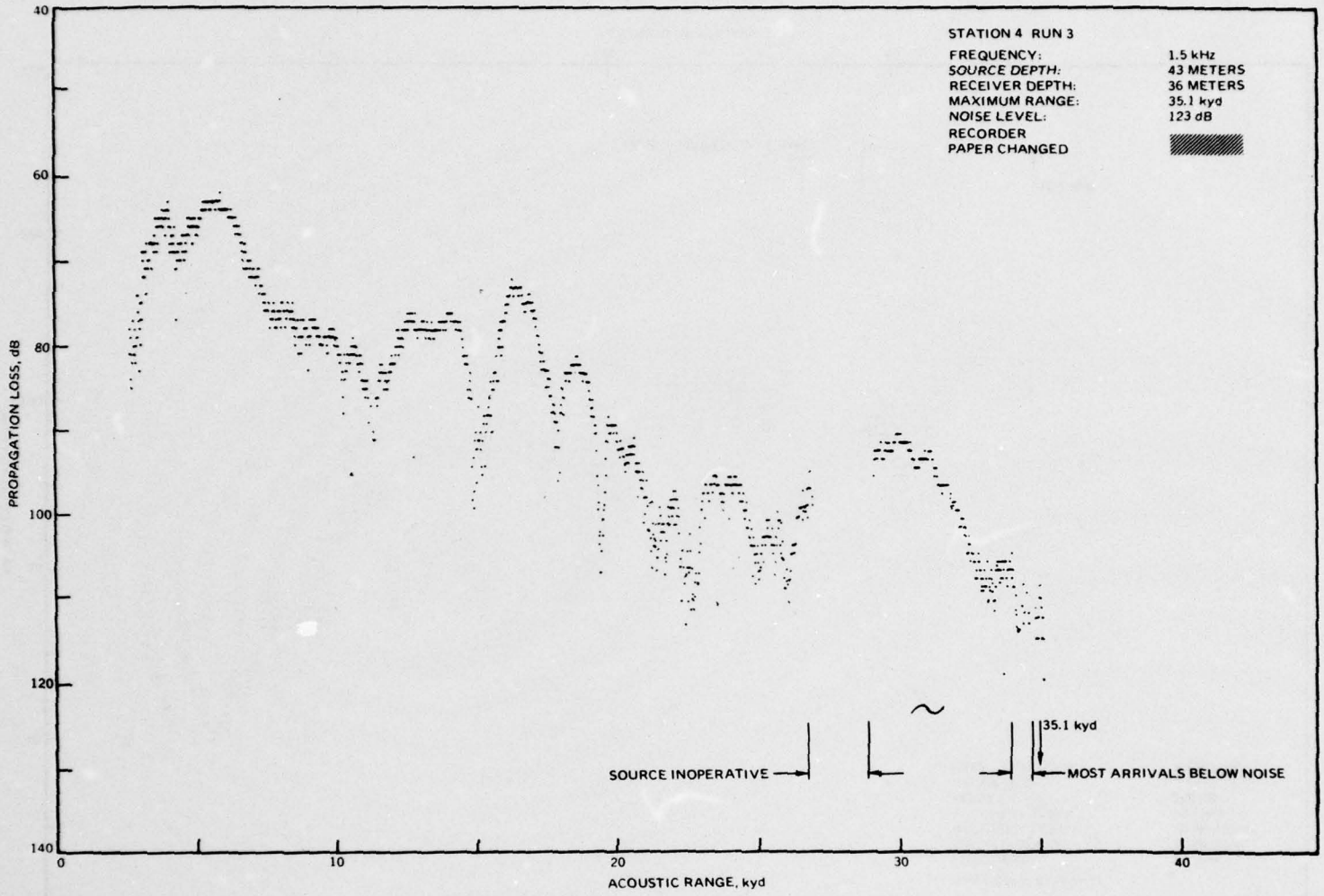

Figure 26. Propagation loss versus range.

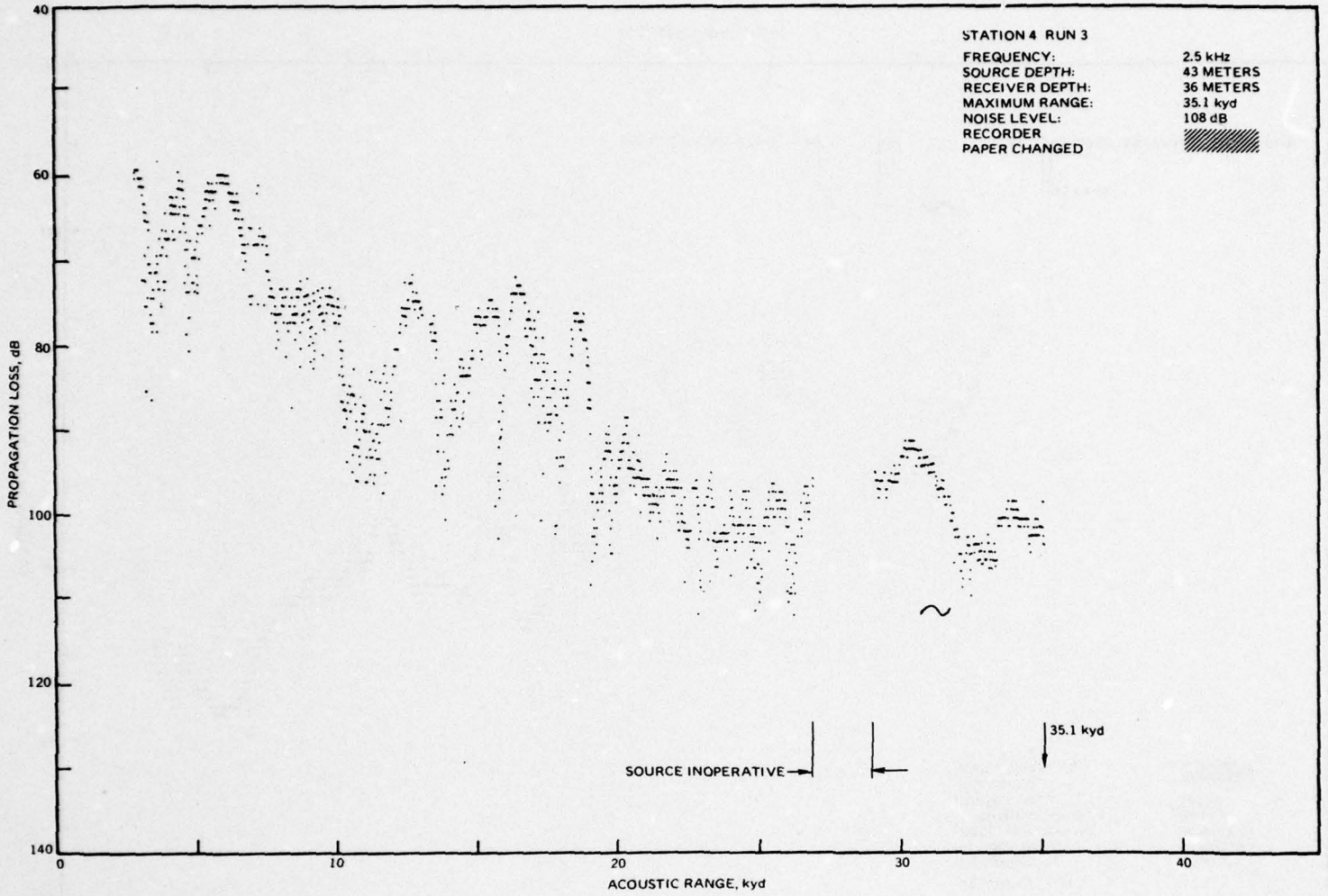

Figure 26. Continued.

"dots" show the average of 180 temperature measurements made by each of the 44 thermistor chain sensors positioned 5.6 m apart in depth. The left-hand profile is for the period 0815 to 0845 LST, the next for the period 0845 to 0915 LST, and so on to the last profile, which is for the period 0015 to 0045 LST. The profiles are numbered consecutively from left to right. Also shown to the right of the figure are the source (*) and receiver depths. An inspection of these data suggests that there was a systematic change in profile shape along the source track. Profiles 1 and 2 are quite different from profiles 6, 7, 8, and 9, and both of those sets are different from profiles 12 and 13. The boundaries between the three profile shapes were somewhat arbitrarily selected to be between profiles 2 and 3 and profiles 9 and 10. Figure 28 contains plots of the average temperature profiles derived from the thermistor chain measurements. The left-hand plot (labeled profile 4) is the average temperature profile for all 2493 scans of the thermistor chain made during run 3. The remaining plots are the average temperatures for the profile 1, 2, and 3 water volumes, respectively. The boundaries between these profile volumes are shown on Fig. 25. The boundary between profile 1 and 2 is at an acoustic range of 30.8 kyd, and the boundary between profiles 2 and 3 is at an acoustic range of 14.0 kyd.

The average temperature profiles were converted into n-layer linear-gradient sound-speed profiles by means of the method previously described. These data are shown in Table 19 and plotted on Fig. 29 for profile 4 and profile 2. The source and receiver depths are also shown on Fig. 29. For profile 4 the sources and receivers are all located in negative sound-speed gradients. For profile 2 the sources and receivers 2 and 3 are in the depressed channel, receiver 1 is in a negative gradient 13 m above the top boundary of the depressed channel, and receivers 4 and 5 are located below the surface layer in the main thermocline. The "dotted" lines on profile 2 indicate a modification of profile 2 that places receiver 1 at the top of the depressed channel (i.e., the sound speed at 78.6 m is adjusted to the sound speed at receiver 1).

Comparison of Theoretical and Experimental Propagation Loss

Theoretical propagation losses were calculated for profiles 4 and 2 by means of the same n-layer linear-gradient normal-mode model used in the analysis of the station 4 run 4 measurements. Profile 4 was selected since it was the profile recommended in Ref. 2 for any theoretical applications. Profile 2 was selected since it contains a depressed channel. The theoretical propagation losses should be smaller using profile 2 than using profiles 1 or 3. In selecting profiles 4 and 2 as inputs to the theoretical calculations, it was felt that the resulting calculated propagation losses would bracket the experimental propagation losses. Theoretical propagation losses were calculated for 1.5- and 2.5-kHz sources located at 43 m and receivers located at depths of 6, 36, 72, 117, and 180 m. These calculations are compared with the measured propagation losses in Appendix C. For each receiver depth the "dots" are the measured losses plotted as a function of acoustic range from the source. The theoretical calculations of propagation loss for profile 4 are indicated by the dashed line and for profile 2 by the solid line. The calculations for the modified profile 2 are shown for receivers 1, 2, and 3 by the dashed-dotted line. At the shorter ranges, where the modified profile 2 calculation are not shown, they are essentially the same as for the other two profiles. The modified profile 2 calculations for receivers 4 and 5 are not included on the plots for these receivers since they are virtually the same as those calculated using profile 2. The

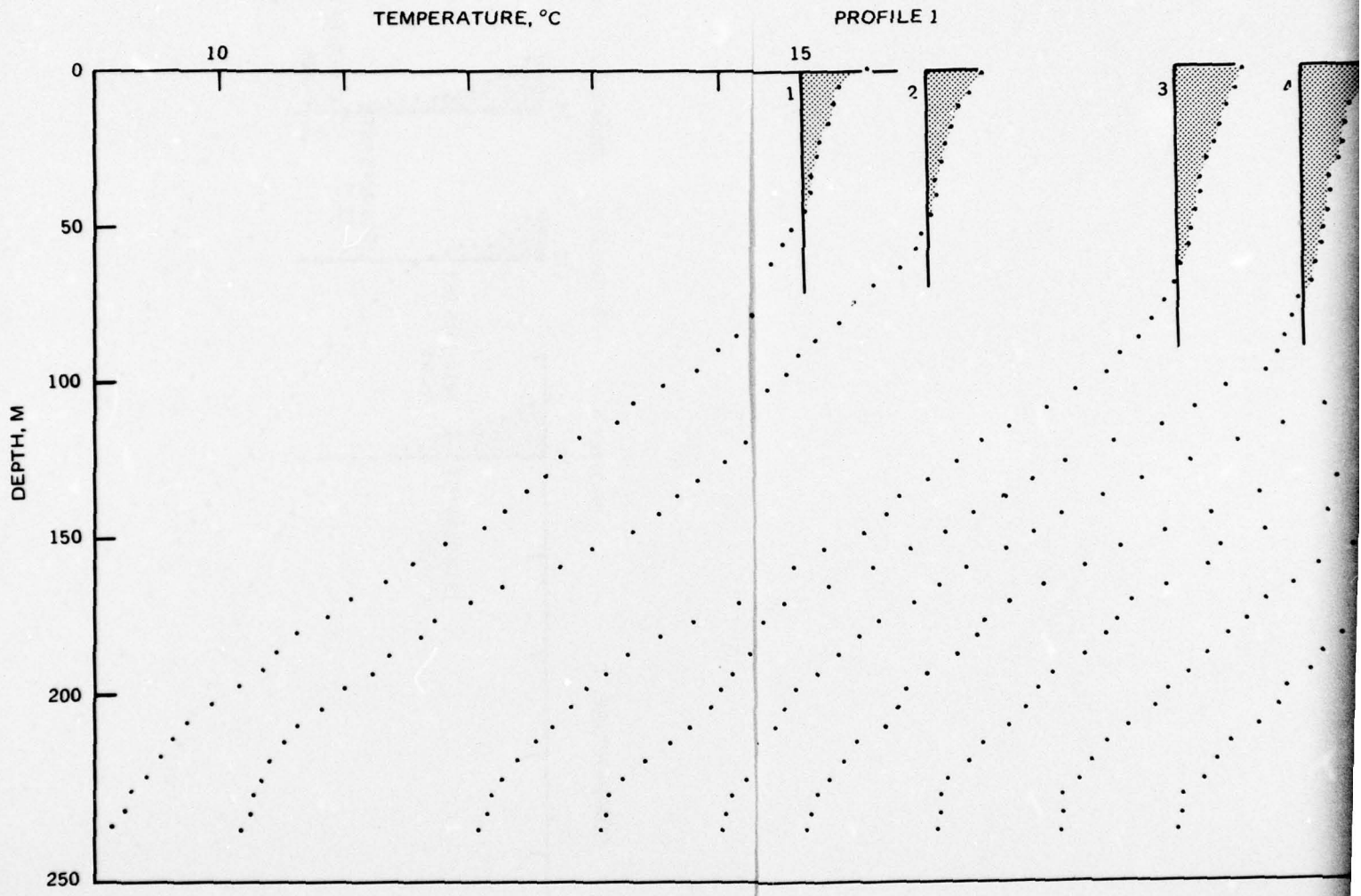

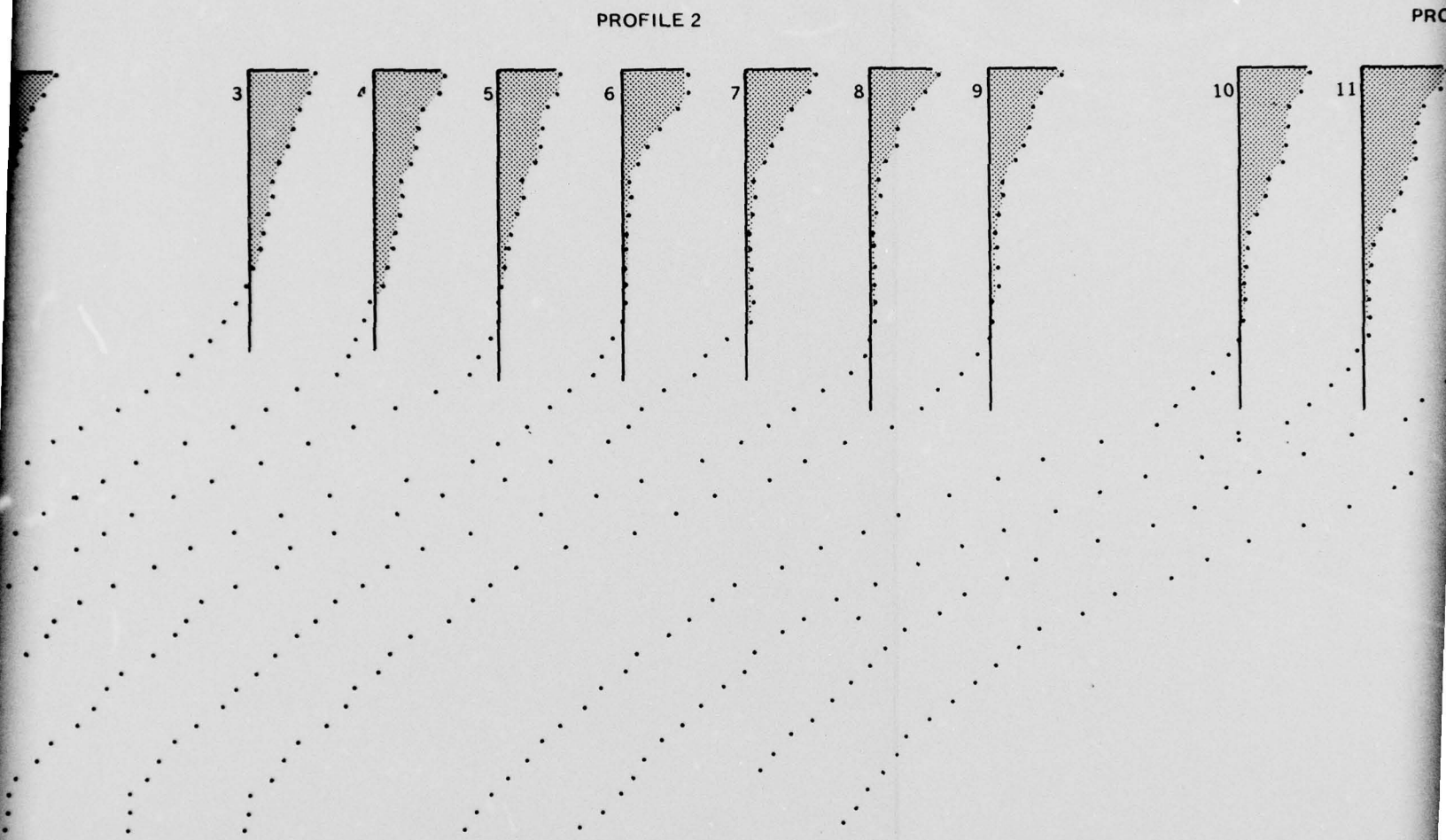

Figure 27. Station 4, run 3. Average temperatu
of the thermistor chain measurements.

12

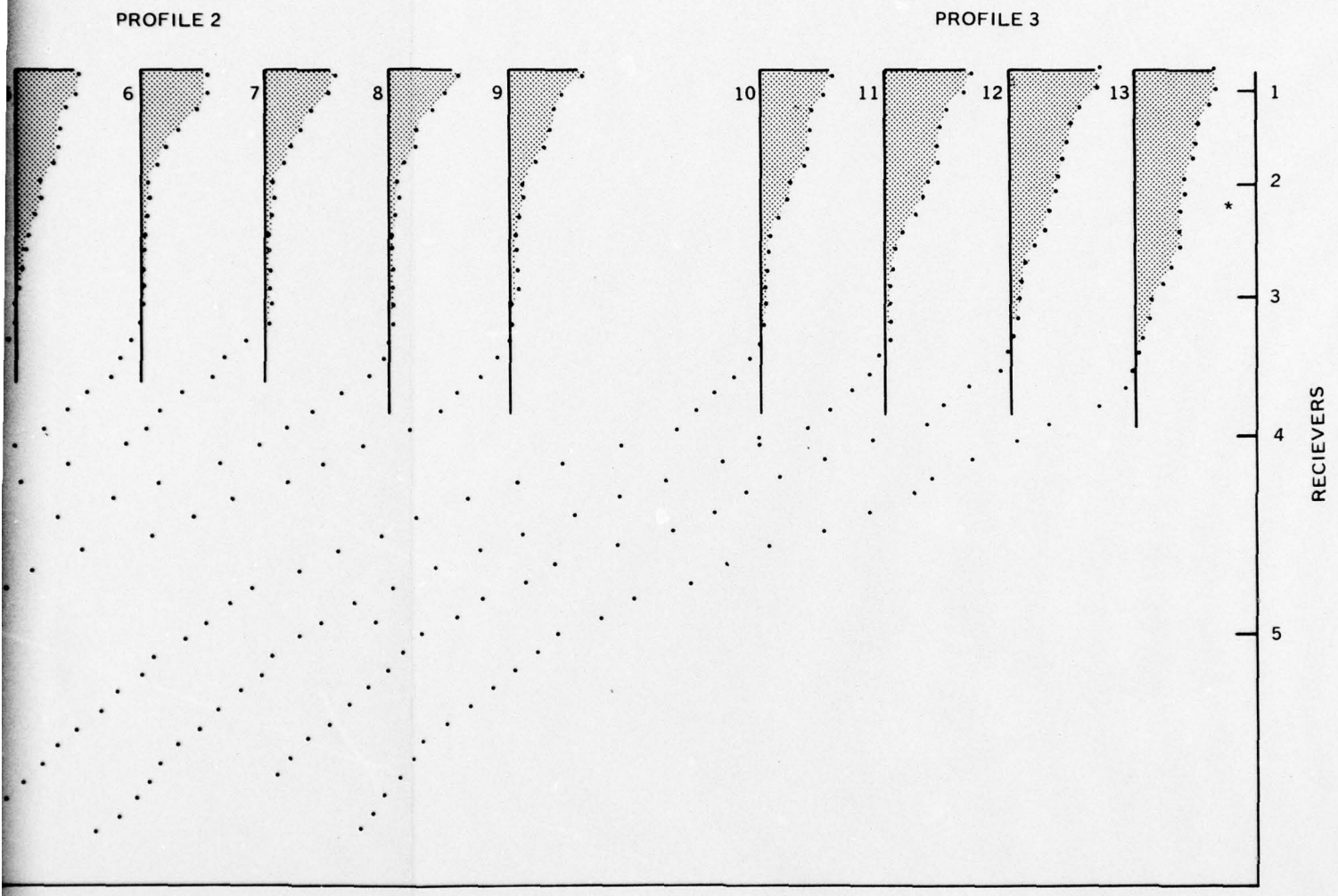

Figure 27. Station 4, run 3. Average temperatures for 30-min segments of the thermistor chain measurements.

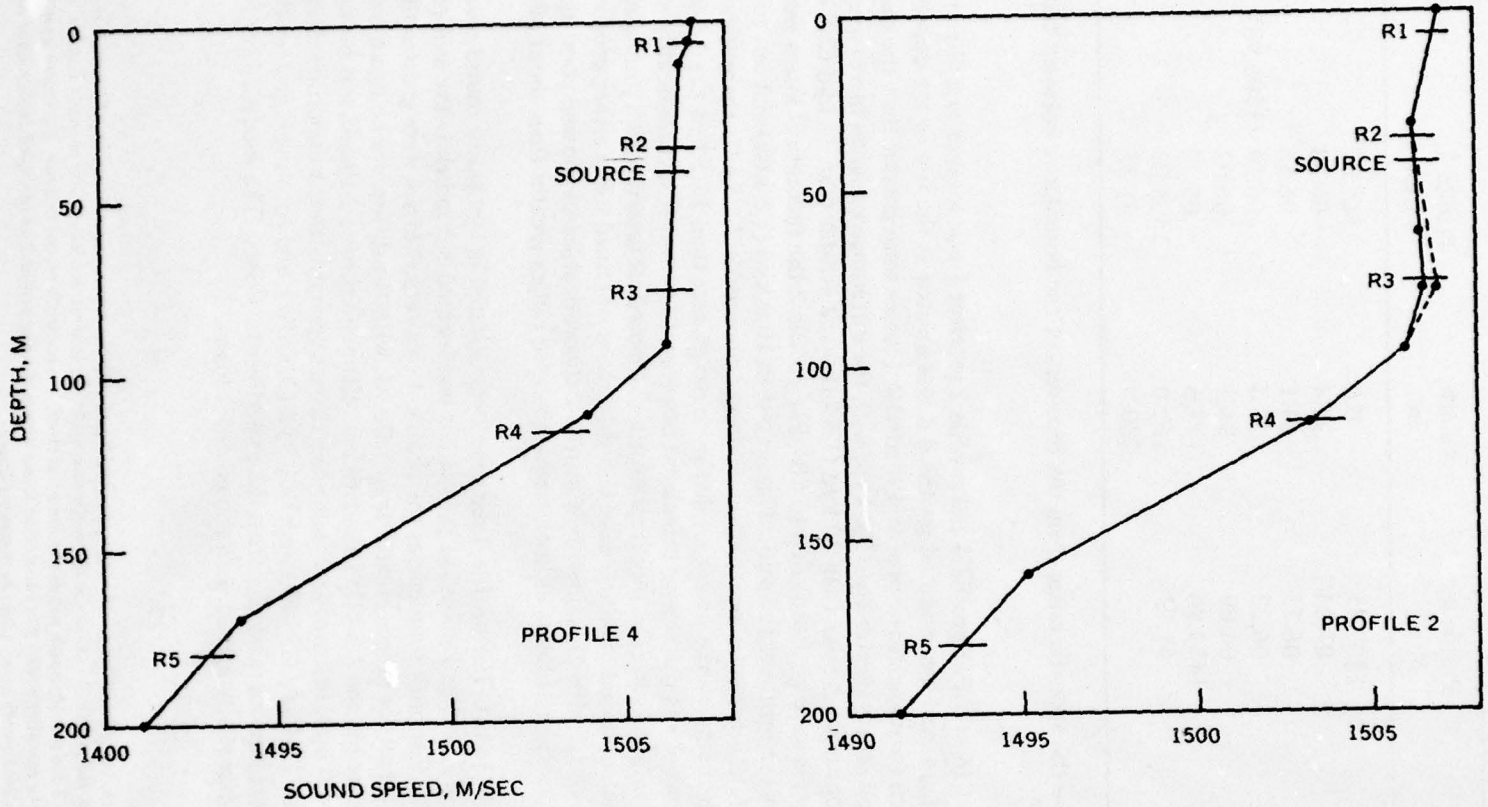

Figure 29. Station 4, run 3. Average sound-speed profiles derived from thermistor chain measurements.

AD-A049 077 NAVAL UNDERSEA CENTER SAN DIEGO CALIF F/G 17/1
SURFACE-DUCT SONAR MEASUREMENTS (SUDS I - 1972).(U)
NOV 76 E R ANDERSON
UNCLASSIFIED NUC-TP-463 NL

2 OF 3
AD A049077

Table 19. Station 4 run 3 linear-gradient sound-speed profiles

Depth, m	Profile 4, m/sec	Depth, m	Profile 2, m/sec
0.0	1507.15	0.0	1507.07
5.7	07.04	32.8	06.30
13.1	06.73	64.1	06.56
93.4	06.27	78.6	06.59 (1506.93)
112.5	04.09	96.3	06.02
170.3	1493.86	117.6	03.20
200.0	91.13	160.0	1495.09
		200.0	91.35

vertical lines show the acoustic range from the receivers of the boundaries between the three profile volumes.*

Receiver 1 (6 m). For profile 4 and profile 2 receiver 1 was located in a negative sound-speed gradient, and for modified profile 2 it was located at the top of the depressed channel. For both frequencies the profile 4 theoretical losses were greater than the experimental losses at all ranges greater than 3.0 kyd, with the difference being an increasing function of range. For ranges greater than 30 kyd (1.5 kHz) and greater than 25 kyd (2.5 kHz), the theoretical losses were greater than 140 dB. For profile 2 the theoretical losses were about the same as the profile 4 theoretical losses out to 10.0 kyd (1.5 kHz) and out to 17.5 kyd (2.5 kHz). For ranges greater than 10.0 kyd the profile 2 1.5-kHz theoretical losses agreed with the measured losses, while for ranges greater than 17.5 kyd the 2.5-kHz theoretical losses were less than those calculated using profile 4 but still considerably greater than the experimental losses. The modified profile 2 theoretical losses, which placed receiver 1 at the top of the depressed channel, were less than those obtained using either profiles 4 or 2, particularly at 2.5 kHz. The modified profile 2 theoretical losses showed good agreement with the experimental losses at both frequencies for ranges greater than about 10.0 kyd.

Receiver 2 (36 m). For profile 4 receiver 2 was located in a negative sound-speed gradient, and for profile 2 and modified profile 2 it was located 3.2 m below the axis of a depressed channel. For both frequencies the profile 4 theoretical losses were greater than the experimental losses for ranges greater than 5.0 kyd, with the difference being an increasing function of range for the 2.5-kHz calculations. Although profile 2 should not be valid at ranges less than 14.0 kyd, the profile 2 theoretical losses agreed with the experimental losses for ranges less than 7.0 kyd (1.5 kHz) and 18.0 kyd (2.5 kHz), and for ranges greater than the above they were considerably less than the experimental losses. The modified profile 2 theoretical losses essentially agreed with the profile 2 losses.

In comparing the profile 2 and modified profile 2 propagation losses with the experimentally measured losses, it is noted that the receivers are in the profile 3 volume for the entire run, while the sources, initially in the profile 1 volume, were towed into the profile 2 and profile 3 volumes as the run progressed. To correctly model this run, the source profile should be changed as the run progresses. The theoretical losses obtained using profile 2 or modified profile 2 for the entire run thus will not necessarily agree with the measured losses.

Receiver 3 (72 m). For profile 4 receiver 3 was located in the same negative sound-speed gradient as receiver 2, and for profile 2 and modified profile 2 it was located 1.6 m above the bottom of the depressed channel. The profile 4 theoretical losses agreed with the experimental propagation losses at both frequencies out to a range of 23.0 kyd. For ranges greater than 23.0 kyd the theoretical losses were greater than the experimental losses. Out to about 23.0 kyd the profile 2 and modified profile 2 theoretical losses differed little, except in detail, from the experimental losses. However, for ranges greater than 23.0 kyd the profile 2 theoretical losses were generally less than the measured losses. The effect of increasing the 78.6-m profile 2 sound speed by 0.34 m/sec (modified profile 2) on the theoretical losses was to increase the modal pattern. This latter pattern was more typical of the experimental loss pattern.

Receiver 4 (117 m) and Receiver 5 (180 m). For all profiles, receivers 4 and 5 were in a strong negative sound-speed gradient associated with the main thermocline. Out to about 25.0 kyd all theoretical propagation losses agreed well with the experimental losses. However, for ranges greater than 25.0 kyd the profile 4 theoretical losses were considerably greater than the experimental losses, and the profile 2 and modified profile 2 losses agreed with the experimental losses.

Conclusions

- The Ref. 2 conclusion that the run 3 sound-speed distribution could be represented by a single average sound-speed profile is probably incorrect.
- Half-hour-average profiles, derived from the thermistor chain temperature measurements, suggest that the temperature profile systematically changed during the propagation loss run. Further comparisons suggest the presence of three water volumes, each being characterized by a sound-speed profile. Comparisons of theoretical propagation losses computed using a sound-speed profile containing a depressed channel with the experimental propagation losses showed good general agreement. This supports the concept of a systematic sound-speed profile change during the run.
- A theoretical model permitting sound-speed profile changes as the run progressed would likely show better agreement with the experimental propagation losses than a theoretical model using a single sound-speed profile.
- Theoretical propagation losses computed for receivers located near the top or bottom of a depressed channel are quite sensitive to the depth of and sound speed at the channel boundaries.
- Out to ranges of about 25.0 kyd theoretical propagation losses are insensitive to the surface sound-speed profile for receivers located in the main thermocline.

STATION 2 RUN 1

One of the most interesting sets of propagation loss measurements, from an environmental point of view, was made during station 2 run 1. These measurements were made in the presence of a marked temperature frontal surface separating two water masses characterized by significantly different sound-speed profiles. Figure 30 is a temperature cross section along the track of the source ship. This section was generated using thermistor chain profiles taken at 5-min intervals. The heavy solid lines delineate the boundaries between three

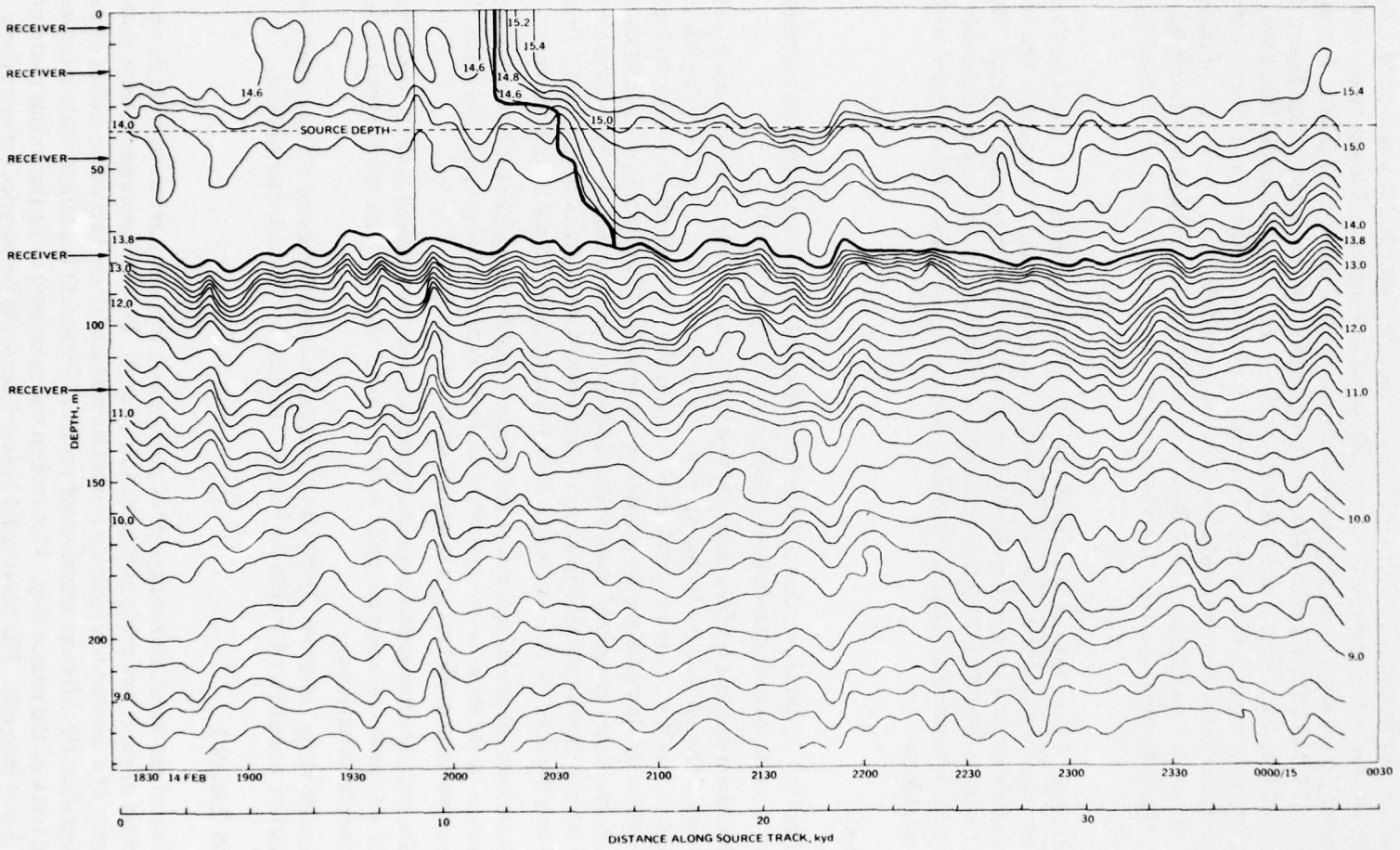

Figure 30. Station 2, run 1. Temperature section showing locations of temperature frontal surface.

distinct water masses. Two of the water masses extend from the ocean surface to a depth of about 79 m. These two water masses overlay a third water mass bounded by the 13.8°C isotherm. The temperature frontal surface is shown as a heavy solid line located at a range of 12.0 kyd at the surface and intersecting the 13.8°C isotherm at a range of 15.5 kyd. This temperature section shows that one water volume extended from the beginning of the section to 9.2 kyd and the second water volume began at 15.5 kyd and extended to the end of the run. Between 9.2 kyd and 15.5 kyd was a transition water volume, in which the temperature structure changed from the first into the second. The vertical lines on Fig. 30 show the position of these two boundaries. The dashed horizontal line indicates the source depth of 38 m and the arrows indicate the five receiver depths of 5, 19, 47, 77, and 120 m. At any depth the frontal surface is characterized by an exponential increase in temperature. In the first 700 yd from the frontal surface, the surface temperature increases about 0.6°C. This corresponds to an increase in sound speed of about 2 m/sec. The total change in surface temperature across the frontal surface was about 0.9°C. This corresponds to an increase in sound speed of about 2.8 m/sec. This total change took place over a distance of about 2300 yd. Note that the range of crossing the frontal surface varies with depth. There is a difference of 3900 yd between the crossing at the surface and the crossing at 79 m. Additional details concerning the characteristics of the frontal surface appear in Ref. 2.

Figure 31 presents a plan view of the experiment. The heavy dashed line shows the location of the frontal surface at the source depth of 38 m. The source was towed in a southeasterly direction, starting in one water mass and crossing over into the other water mass at a range of 13.5 kyd along the source ship's track. The receiver ship drifted in a southerly direction during the experiment. The light dashed lines show propagation paths at the indicated times during the run. The receivers remained in the first water mass, but their distance from the frontal surface generally decreased as the run progressed.

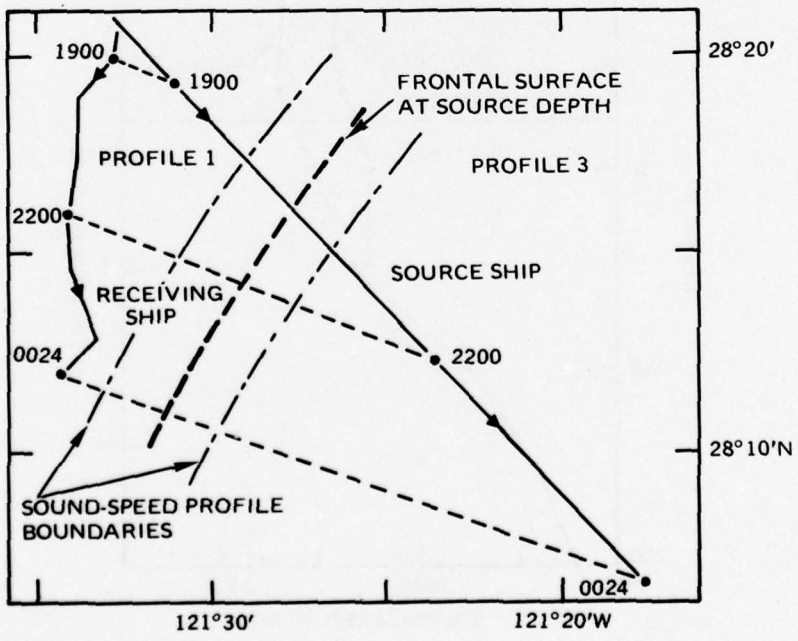

Figure 31. Plan view of station 2, run 1 experiment. Times shown are LST.

Sound-Speed Profiles Derived from Thermistor Chain Measurements

The dots in Fig. 32 are plots, at standard hydrographic cast depths, of the sound speeds derived from averaging the thermistor chain measurements made in the two water volumes. The straight lines represent an approximation to the sound-speed profiles by Gordon's n-layer propagation loss model (Ref. 20). In Gordon's model, the squared index of refraction is linear. The two profiles are identical for depths greater than 79 m. Profile 1 is modeled by six layers. It consists of a 23-m positive-gradient surface channel overlying a depressed channel with the axis of minimum sound speed at 50 m. There are negative-gradient layers for depths greater than 79 m. Profile 3 is modeled by five layers. It consists of a 30-m positive-gradient surface channel with negative-gradient layers below this depth. Receivers 1 and 2 are in the positive-gradient surface channel for both profiles. Receivers 3 and 4 are in the profile 1 depressed channel. The source is below the positive-gradient surface channel for both profiles. The source is not in the profile 1 depressed channel since the sound speed at the source exceeds the sound speed at the bottom of the depressed channel.

Comparison of Theoretical and Experimental Propagation Loss

Figure 33 presents some preliminary unpublished theoretical results obtained by D. F. Gordon. The dots are the 1.5-kHz propagation loss measurements for a source depth of 38 m and a receiver depth of 47 m.*

A maximum of four CW pulses were transmitted each minute. For simplification, all pulses received during each minute (i.e., 1, 2, 3, or 4) were averaged. These average values are plotted on Fig. 33.

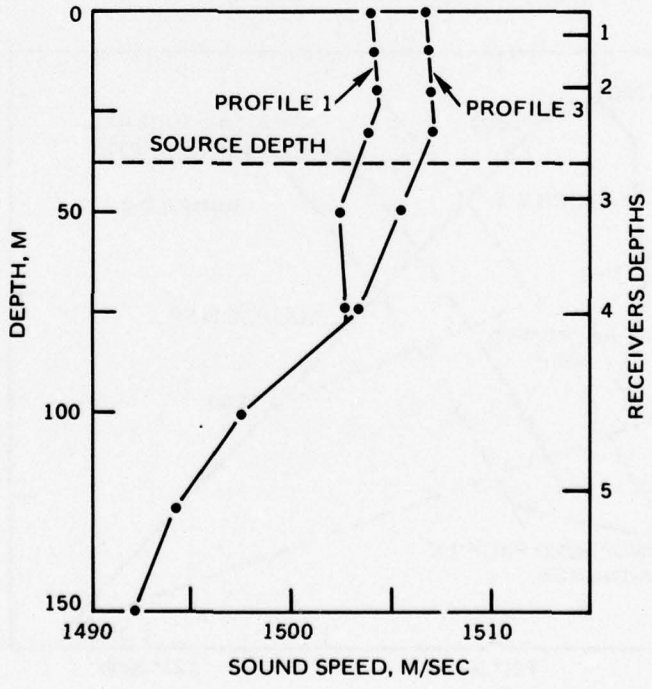

Figure 32. Station 2, run 1. Average sound-speed profiles.

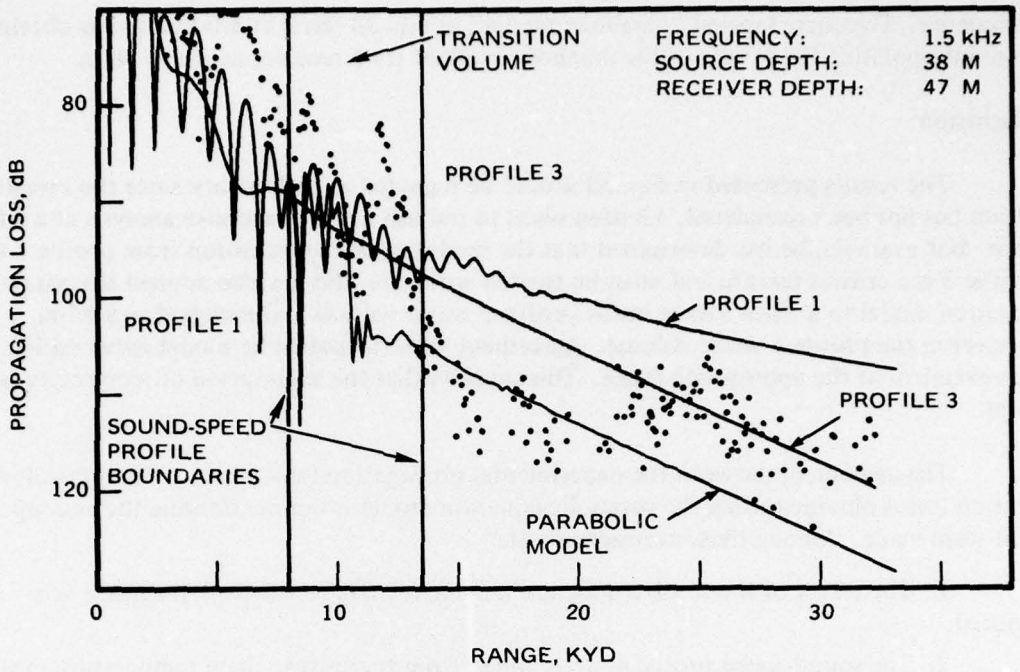

Figure 33. Comparison of theoretical and experimental propagation loss for station 2 run 1.

The solid curves labeled profile 1 and profile 3 are the theoretical propagation losses calculated using the n-layer normal-mode model (Ref. 20). The solid curve labeled parabolic model was obtained using the parabolic equation method. This method was originated by Tappert and Hardin (Ref. 21) for low-frequency propagation in deep water. A modified version of this method was developed at the Naval Undersea Center by Benthien and Gordon (Ref. 22). In order to examine propagation losses across a thermal frontal surface, such as encountered during station 2 run 1, Gordon subsequently adapted the Benthien and Gordon version to calculate high-frequency propagation losses in surface channels.

Since the source position is moving relative to the thermal frontal surface, it is not practical to make computations for the experimental configuration because the entire computation would have to be repeated for each range point. A simpler approach is to assume that the receiver position is fixed relative to the front and make a computation interchanging the role of source and receiver, i.e., apply the principle of reciprocity. Profile 1 was assumed to be valid from the receiver location to a range of 8.0 kyd from the receiver. This range is shown on Fig. 33 by a vertical line. From the beginning of the run to 8.0 kyd the propagation losses were computed using the n-layer normal-mode model with profile 1 as input. The normal-mode output was the complex acoustic pressure evaluated at 1-yd depth intervals from the surface to 210 yd. For depths greater than 210 yd the complex pressure was faired to zero at 255 yd, with faired values called out at 1-yd intervals. This set of complex pressure points was then used as inputs to the parabolic method, using a Fast Fourier Transform of 512 points. The parabolic method was then used to march through a transitional profile, based on the data presented in Fig. 30, and on into profile 3 of Fig. 32. The second vertical line, at a range of 14.2 kyd, indicates the range at which the transition to profile 3 has been

completed. The curve labeled "parabolic model" in Fig. 33 starts at 8.0 kyd and is obtained from interpolating the results of the parabolic method for a receiver depth of 38 m.

Discussion

The results presented in Fig. 33 should be regarded as preliminary since the investigation has not been completed. Gordon plans to publish a more extensive analysis at a later date. For example, he has determined that the modeling of the transition from profile 1 to profile 3 is a critical feature and must be treated with care. He has also applied the parabolic equation model to a 38-m source in the profile 3 water volume and matched to a 47-m receiver in the profile 1 water volume. Agreement with the parabolic model curve on Fig. 33 was excellent at the appropriate range. This suggests that the assumption of reciprocity is valid.

The agreement between the experimental propagation losses and the theoretical propagation losses obtained using the parabolic equation model is fair considering the assumptions that were made. Among these assumptions are:

1. The effect of the receiver location moving relative to the frontal surface was ignored.

2. The sound-speed profile as determined from thermistor chain temperature measurements made along the source ship track applies to the propagation loss paths.

3. The propagation loss paths cross the frontal surface at normal incidence (i.e., bending of the wave front out of the range-receiver depth plane in the azimuthal direction can be neglected).

The parabolic equation model propagation losses show an increase in propagation loss of about 10 dB at a range of about 10.0 kyd. For ranges greater than 10.0 kyd the parabolic equation model losses have a slope which is about the same as the n-layer normal-mode model results obtained using profile 3. The parabolic equation model shows higher losses than those computed for both profiles 1 and 3 using the n-layer normal-mode model. The increased experimental propagation loss shown in Fig. 33 for ranges greater than 13.0 kyd can reasonably be attributed to crossing the frontal surface. This is not always the case. Computations have also been made for the other receiver depths. These computations often show the parabolic equation model propagation losses lying between the n-layer normal-mode model losses for profiles 1 and 3. For these cases an increase in propagation loss cannot be attributed solely to crossing the frontal surface. In these cases the markedly increased propagation losses measured beyond the range of the frontal surface can be attributed to towing the source from a region of good acoustic propagation to a region of poor acoustic propagation.

These results emphasize the necessity for a thorough experimental probing of a frontal surface by "a series of propagation loss runs designed to separate effects due to crossing the frontal surface from differences in acoustic propagation in the two water volumes." Indeed, the design of experimental runs to investigate the propagation loss associated with a frontal surface needs to be done with much more care and precision than has been done in the past. "Some of the types of propagation loss runs that should be made are:

1. Runs parallel to the frontal surface confined to each of the two water volumes.

2. Runs normal to the frontal surface.
3. Runs at oblique angles to the frontal surface."

Runs made at a given angle to the frontal surface should be made twice: first with the fixed element (source or receiver) in one water volume and second with the fixed element in the other water volume. Runs in which both source and receiver move entail extremely complicated analysis. Thus, in designing future experimental runs, consideration should be given to keeping one element at a fixed position. Unless reciprocity is assumed, the analysis is much easier for the case of fixed source and moving receiver than vice versa. The validity of the principle of reciprocity should be examined for propagation across frontal surfaces with simultaneous acoustic transmission for both a source and receiver at each of two depths. Since many propagation loss runs appear to be required in order to study effects of a frontal surface on propagation loss, it may be desirable to use multiple receiver or source platforms so that concurrent propagation loss runs can be made under the same environmental conditions, rather than sequential runs which are subject to the problems of temporal environmental changes between runs. For adequate evaluation of the azimuthal bending of the wave front out of the range-depth plane, it may be necessary to use multiple elements spaced throughout the ocean volume.

Future Possibilities for the Parabolic Equation Model

In this study the parabolic equation model was applied to studying the propagation losses observed when crossing a thermal frontal surface. However, it could also be applied to any of the SUDS I propagation loss runs to account for changes in the sound-speed profile during the run. The basic method allows an unlimited number of profiles and could be applied with varying degrees of refinement, depending on the number of profiles treated. The simplest application would be to use the average sound-speed profiles published in Ref. 2. A more detailed application would be to use as inputs 30-min segments of averaged thermistor chain measurements as illustrated in Fig. 27. The most detailed application would be to use as inputs each individual scan of the thermistor chain. At a speed of 3 knots this corresponds to a profile every 17 yd in range. This would not be easy to implement, but the process is straightforward. For example, a method would have to be developed to convert each thermistor temperature measurement into sound speed. A rejection criterion for incorrect measurements would also have to be established, since the parabolic equation model has a tendency to magnify errors. Finally, there is the problem of converting the thermistor sampling grid in range and depth to the grid which the parabolic equation model uses to progress the acoustic wave. Once implemented, the entire process of converting thermistor chain temperature measurements to acoustic propagation loss could be done on a routine basis.

STATION 3 RUN 3

This run was also selected for analysis by Morris (Ref. 4) "because of the unstable run conditions." Table 3 (Ref. 4) indicates that at 0.4 kHz the agreement between the modified AMOS (NISSM) or ASRAP II prediction models and the experimental data was poor. The modified AMOS model gave propagation losses which were 6.8 to 10.8 dB less than those measured for the three shallowest receivers. Corresponding values for the ASRAP II model were 6.8 to 19.9 dB. In contrast, at 1.0 kHz the agreement between the modified AMOS or ASRAP II models and the experimental measurements was somewhat better than

the average agreement achieved on the five runs reported in Table 3 (Ref. 4). Figure 11A (Ref. 4) shows as much as a 20-dB difference between the Rough Surface Natural Mode (WAVE) model and experimental measurements for the 34-m receiver at a frequency of 0.4 kHz and a range of 12.0 kyd. This run was chosen for additional analysis to determine if the agreement with experiment could be improved by using a profile derived from thermistor chain measurements.

Sound-Speed Profiles

Based on the thermistor chain temperature measurements, this closing propagation loss run was characterized by three average sound-speed profiles (Ref. 2). However, two of the profiles applied only to the first 3.3 kyd of the run. The third profile characterized the remainder of the run from a range of 34.2 kyd to the end of the run at 0.1 kyd. Table 20 presents the average sound-speed profile corresponding to the profile presented in Ref. 2. However, the Table 20 average sound-speed profile was derived from the measurements made by all 44 thermistor sensors, using the techniques present earlier in this report to convert these measurements into sound-speed profiles. This profile will be referred to as profile I. Table 21 presents the corresponding average sound-speed profile presented in Ref. 3. This profile will be referred to as profile II. Profiles I and II are compared in Fig. 34. Profile I is characterized by a 6.8-m surface channel. Under the surface channel is a depressed channel

Table 20. Station 3 run 3 average sound-speed profile derived from thermistor chain measurements

Depth, m	Sound Speed, m/sec
0.0	1506.06
6.8	06.17
10.0	06.13
19.6	06.085
81.0	06.30
95.5	05.97
114.8	03.97
175.0	1493.81
200.0	91.45

Table 21. Station 3 run 3 average sound-speed profile presented in Ref. 3

Depth, m	Sound Speed, m/sec
0.0	1506.09
90.0	06.59
180.0	1492.34
200.0	91.38

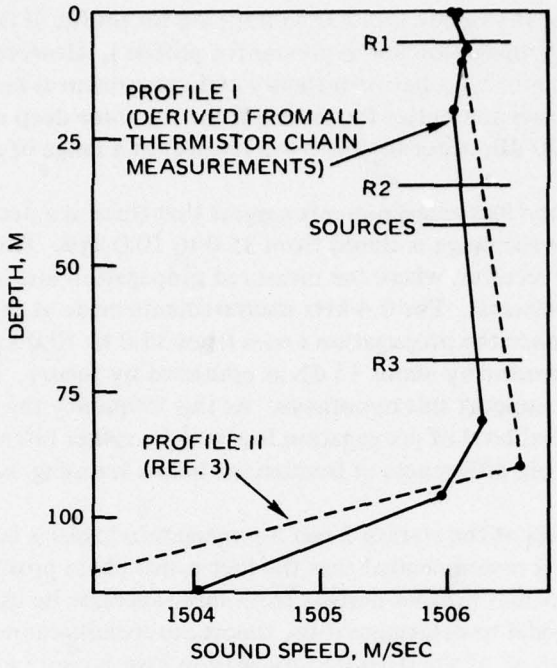

Figure 34. Station 3, run 3. Average sound-speed profiles.

with the axis of minimum sound speed at 19.6 m. The positive-gradient layer associated with the depressed channel extends to a depth of 81.0 m. Profile II is characterized by a surface channel extending from the surface to 90 m. Although the profiles differ in details, they are in good agreement from the standpoint of the absolute value of sound speed. At depths less than 81 m they differ by less than 0.24 m/sec. This is within a temperature difference of 0.1°C, which corresponds to a difference of about 0.3 m/sec in sound speed.

Comparison of Theoretical and Experimental Propagation Loss

Comparisons of the experimental propagation losses measured during the station 3 run 3 run with the propagation losses computed using the n-layer normal-mode model (Ref. 20) are summarized for each frequency and each receiver depth in Appendix D. The theoretical losses for profile I are shown by the solid line and for profile II by the dashed line.

First, consider the comparison at 1.0 kHz. In general, the theoretical results obtained from the two profiles agree with each other better than the results of either profile agree with the experimental measurements. For profile I, only one normal mode is trapped at 1.0 kHz, while two modes are trapped for profile II. In general the mean theoretical propagation loss is comparable for the two profiles. However, the use of profile II results in an interference structure between the two trapped modes which is not present in the results obtained using profile I.

Next, consider the comparison at 0.4 kHz. For 0.4 kHz there is little interference structure in the theoretical computations at long ranges since the first mode is not trapped

for either profile. The first mode is closer to trapping for profile II than for profile I. At the longer ranges the propagation loss is greater for profile I. However, for ranges greater than about 25.0 kyd agreement between theory and experiment is better for profile I for the two shallow receivers and better for profile II for the three deep receivers. The largest discrepancies, about 20 dB, occur for the 34-m receiver at a range of about 10.0 kyd.

The propagation loss measurements suggest that there is a decrease in the strength of the surface channel as the range is closed from 35.0 to 10.0 kyd. This is most evident at 0.4 kHz for the 69-m receiver, where the measured propagation loss increases by 10 dB over this decreasing range interval. The 0.4-kHz measurements made at the other receivers support this hypothesis since the propagation losses from 35.0 to 10.0 kyd remain almost constant rather than decreasing by about 15 dB as predicted by theory. In contrast, the 1.0-kHz measurements do not support this hypothesis. At this frequency the first mode is well trapped, and the general level of propagation loss may be rather insensitive to profile changes, which could result in big differences at frequencies below trapping, such as 0.4 kHz.

Further analysis of the station 3 run 3 propagation losses is beyond the scope of this report. However, "it is recommended that the thermistor chain profiles be averaged over half-hour intervals and that profiles derived from these averages be used as inputs to the parabolic equation model to determine if the theoretical results cannot be brought into closer agreement" with all of the 0.4-kHz propagation loss measurements, particularly for the 34-m receiver.

STATION 1 RUN 2

Initial comparisons of the propagation loss measurements preparatory to the analysis contained in this report showed that the station 1 run 2 and station 3 run 3 measurements were made in the presence of the following similar environmental and acoustic parameters:

	station 1 run 2		station 3 run 3	
frequency, kHz	0.4	1.0	0.4	1.0
source depth, m	45		42	
receiver depths, m	4		6	
	72		69	
	112		112	
maximum range, kyd	26.6		34.6	
surface channel, m	68		79	
wind wave, ft	1-2		1-2	
swell, ft	3-5		3-5	

Despite the above similarity, the propagation loss measurements for comparable receiver depths showed marked differences. Thus, it seemed appropriate to make theoretical propagation loss computations for station 1 run 2 to determine if the observed differences could be explained.

Sound-Speed Profiles Derived from Thermistor Chain Measurements

Reference 2 characterized this run by a single sound-speed profile. Table 22 presents the average sound-speed profile based on 1350 thermistor chain temperature profiles. This profile is compared to the corresponding profile for station 3 run 3 in Fig. 35. The profiles are quite similar. The station 3 run 3 sound speeds are about 0.7 m/sec higher than the station 1 run 2 sound speeds. However, this difference in the absolute value of sound speed has

Table 22. Station 1 run 2 sound-speed profile derived from thermistor chain measurements

Depth, m	Sound Speed, m/sec
0.0	1505.29
11.3	05.43
64.9	05.55
81.5	05.07
113.0	1497.72
134.6	94.31
163.3	92.67
200.0	92.48

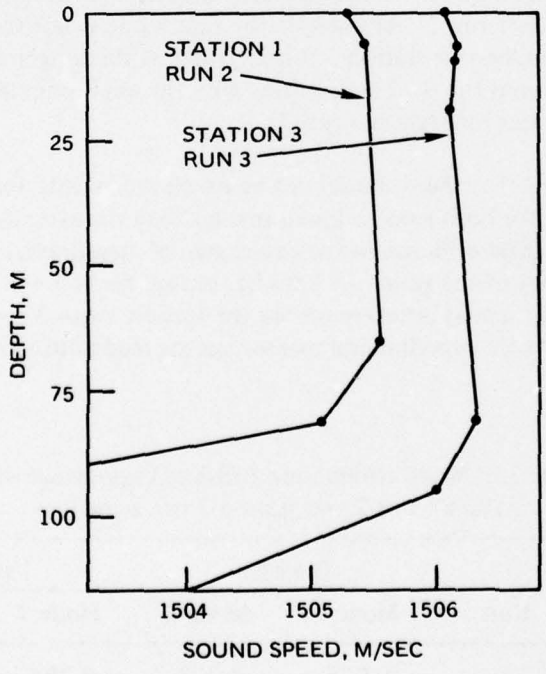

Figure 35. Station 1 run 2 and station 3 run 3 average sound-speed profiles.

little acoustic significance. The depth of the maximum sound speed was different, 81.0 m for station 3 run 3 versus 64.9 m for station 1 run 2. The differences between the maximum sound speed and the surface sound speed was 0.24 and 0.26 m/sec for the station 3 run 3 and station 1 run 2 profiles, respectively. Thus, on the basis of channel depths, the station 3 run 3 profile has a stronger channel, whereas on the basis of sound-speed gradient the station 1 run 2 profile has a stronger channel.

Comparison of Theoretical and Experimental Propagation Loss

Comparison of the propagation losses measured during station 1 run 2 with the theoretical propagation losses computed using the n-layer normal-mode model are summarized for each frequency and each receiver depth in Appendix E. The 0.4-kHz experimental losses are significantly less than the theoretical losses for the 4-, 17-, and 43-m receivers. For the 72- and 112-m receivers, located below the near-surface layer, agreement between the theoretical and experimental losses is excellent. The 1.0-kHz experimental losses are significantly less than the theoretical losses for the 4- and 17-m receivers. Agreement is fair for the 43-m receiver, while for ranges greater than about 10.0 kyd, the experimental losses are significantly greater than the theoretical losses for the 72- and 112-m receivers. This is somewhat surprising since, for comparisons presented in this report, theoretical and experimental propagation losses have agreed for most of the receivers located in the thermocline below the near-surface layer.

An explanation of the theoretical results is facilitated by Table 23. Table 23 lists the mode attenuation for the first two modes for both runs. Propagation is better for station 3 run 3 than for station 1 run 2. At 1.0 kHz the first mode is well trapped for station 3 run 3 but just barely for station 1 run 2. At 0.4 kHz the first mode is not trapped for either run, but the attenuation is smaller for station 3 run 3. Thus, at the longer ranges, the propagation loss will be less for station 3 run 3. This explains why the experimental propagation losses at the longer ranges are less for station 3 run 3.

Table 23 suggests that there should not be much modal interference since the attenuation of the first mode, for both runs, is much smaller than the attenuation of the second mode. Indeed, there is little evidence in the experimental measurements of modal interference at 0.4 kHz for either of the runs. At 1.0 kHz, except for the 4-m receiver, there is little experimental evidence of modal interference for the station 1 run 2 propagation loss measurements, while the 1.0 kHz experimental measurements made during station 3 run 3 exhibit modal interference.

Table 23. Mode attenuation (dB/kyd) associated with station 1 run 2 and station 3 run 3 profiles

		0.4 kHz		1.0 kHz	
Station	Run	Mode 1	Mode 2	Mode 1	Mode 2
1	2	0.976	4.203	0.296	2.000
3	3	0.615	3.618	0.037	0.753

There remain some marked differences between the station 1 run 2 and station 3 run 3 propagation loss measurements which the theoretical calculations do not support. One of these is the extremely low 0.4-kHz propagation losses measured during station 1 run 2 by the 4-m receiver. At a range of 10.0 kyd the propagation loss for this receiver is about 20 dB less than for the station 3 run 3 6-m receiver, with theory predicting values of –5 dB. Another marked difference is the very large 1.0-kHz propagation losses measured during station 1 run 2 by the 72- and 112-m receivers. For example, the 72-m propagation losses from 10.0 to 25.0 kyd are about 15 dB greater than for the station 3 run 3 69-m receiver. The corresponding theoretical value is only about 2 dB greater.

The combination of exceedingly small propagation losses measured by the shallow receivers at 0.4 kHz and the exceedingly large propagation losses measured by the deep receivers at 1.0 kHz is difficult to explain in terms of present understanding for non-range-dependent sound-speed profiles. Again it is recommended that the thermistor chain temperature profiles for station 1 run 2 be averaged over half-hour intervals and the associated sound-speed profiles be used as inputs to the parabolic equation model. Such studies of range-dependent profiles may well lead to unexpected results.

SOME ADDITIONAL COMMENTS

Before closing this section on comparison between theory and experiment, it should be noted that the experiments chosen for analysis represent a biased sample, i.e., the analyses were prompted by some abnormal feature associated with the propagation loss run. Station 4 run 4 and station 3 run 3 were chosen because of the poor agreement between experiment and theory obtained by Morris (Ref. 4); station 4 run 3 was chosen because the experimental acoustic propagation was good although the average sound-speed profile exhibited negative sound-speed gradients from the surface; station 2 run 1 was chosen because this run crossed a pronounced thermal frontal surface; and station 1 run 2 was chosen because of propagation loss differences from station 3 run 3 despite similar environmental and acoustic parameters.

The purpose of this section was to demonstrate that improved agreement could be achieved by using new approaches. These new approaches included such techniques as the n-layer normal-mode theory to treat complicated vertical structures in the sound-speed profiles, the parabolic equation method to treat horizontal structure in the sound-speed distribution, and the use of all of the measurements made by all of the thermistor chain sensors to determine the horizontal as well as vertical details of the sound-speed profiles. This purpose was accomplished in that these techniques in many cases explained the abnormalities which prompted the analysis.

Recall, however, that this is an abnormal sample drawn from the totality of the SUDS I propagation loss runs. It is not surprising then that the theoretical analysis in some cases did not fully explain the abnormal phenomenon, since only extreme cases were chosen for analysis. On the other hand, when there are large discrepancies to begin with, any new treatment is more likely to show greater improvement in agreement than would be the case were there only small discrepancies to start.

In order to adequately assess the utility of these new approaches, they should be applied consistently to all 18 of the SUDS I propagation loss runs, not to just the selected sample of 5 runs discussed in this section. Such a study is highly recommended and should

include an analysis using the simple models discussed by Morris (Ref. 4) and employing the best measured sound-speed profiles. A systematic and thorough analysis of all the data is necessary to answer the following questions:

a. Under what conditions are simple bilinear surface channel models adequate?

b. Can significant improvements be achieved by accounting for horizontal changes in the sound-speed profile by the parabolic equation model?

c. What is the sampling rate of the thermistor chain data necessary to provide accurate profiles, i.e., profiles accurate enough from the standpoint of their acoustic response?

In future investigations the comparison between experiment and theory should be placed on a more quantitative basis than the simple visual comparisons of Appendices B to E. Morris (Ref. 4) presents statistical measures of comparison with simple models. However, Morris notes that "the natural mode models with their beat patterns do not lend themselves to statistical tests based on differences." Such tests would show poor agreement between theory and experiment, even though the only difference between them was a displacement between the beat patterns. Some quantitative method needs to be devised for comparing theoretical and experimental data to adequately account for a displacement between experimental and theoretical beats.

Preparation of this section pointed up another problem related to the difficulty of finding normal-mode eigenvalues for the n-layer normal mode model. This model has been used extensively in deep-water propagation. However, this study represents the first application to complicated surface channels. Locating the eigenvalues for these complicated sound-speed structures is never routine and can be extremely difficult, depending upon the structure and the frequency. Of particular difficulty were profile III, shown in Fig. 24, and the profile for station 1 run 2, shown in Fig. 35. Indeed, the eigenvalues of profile III, shown in Fig. 24, had to be established by calculating eigenvalues for a variety of frequencies and making use of the fact that the eigenvalues are continuous functions of frequency. A theoretical study discussing this problem and illustrating the various techniques used for finding and identifying modes is recommended. Such a study should also consider techniques which can be implemented in a computer to automate the process as completely as possible.

A thorough theoretical study of propagation for profiles with negative gradients only is recommended. Indeed, very little is known about the propagation characteristics of the negative bilinear profile, i.e., a slightly negative gradient surface layer overlying a strong negative gradient thermocline, to say nothing of multi-layer negative gradient profiles such as illustrated by profile 4 of Fig. 29.

COMPARISON OF THERMISTOR CHAIN AND XBT DERIVED SOUND-SPEED PROFILES

In most experimental and operational situations, only XBT temperature profiles, many times limited in number, are available for deriving the sound-speed profiles necessary as inputs to the various propagation loss prediction models currently in use. It is instructive to examine the sound-speed profiles that result from a consideration of only the available XBT profiles taken during station 4 runs 3 and 4.

In most applications the XBT profiles are visually read and recorded with a maximum accuracy of ±0.1°C. A temperature change of 0.1°C is equivalent to about 0.315 m/sec. Various techniques are used to convert these temperature measurements into sound speeds. In the discussions to follow the XBT profiles were read, using a Hewlett-Packard 9864A Digitizer, to an accuracy of about 0.058°C, equivalent to about 0.15 m/sec in sound speed. These temperatures were converted to sound speed by means of the relationships presented in Table 5.

STATION 4 RUN 4

A comparison of sound-speed profiles derived from the thermistor chain and XBT temperature measurements made during the station 4 run 4 propagation loss run showed that the differences above the main thermocline could be accounted for by a temperature difference of ±0.1°C. Although the differences were small, they were acoustically important, and it was not apparent how much of the difference could be attributed to instrument measuring error, small XBT sample size, and/or undersampling the XBT profiles by only using measured temperatures at standard hydrographic cast depths. Some insight into these options might be obtained by examining the individual XBT profiles taken during this run.

Table 24 compares simultaneous XBT and thermistor chain measurements at standard hydrographic cast depths. The locations of the XBT profiles are shown in Fig. 23. The thermistor chain data are derived from the profile starting at the time the XBT probe was released. For example, XBT 268L was released at 0200:00 LST. The chain temperatures shown in Table 20 were linearly interpolated from the thermistor profile beginning at 0200:00 LST. A thermistor chain scan takes 8.6 sec. For comparison it takes the XBT probe 47.3 sec to drop from the surface to 242 m. In the upper 75 m, where temperature gradients are small, the differences varied from –0.12°C to +0.11°C, with an average difference of +0.009°C. Measurements made for depths greater than 75 m were made in the thermocline, where small differences in depth may result in relatively large differences in temperature. These differences varied from –0.27°C to +0.27°C. The average of all 30 differences was –0.02°C, with only 3 differences exceeding the manufacturer's specified accuracy of ±0.2°C. In the present discussion, depths less than 100 m are the most important. Can the differences between the station 4 run 4 profile I and profiles II and III be attributed to XBT measuring accuracy? The answer, based on these data, is inconclusive.

The upper portion of Fig. 36 shows sound-speed profiles derived from the seven individual XBT profiles made during run 4. The three profiles plotted to the left were taken by the *Lee* along the source ship track, the next three were taken by the *DeSteiguer* at the southern end of the propagation loss run, and the right-hand profile was taken by the *Cape*

Table 24. Comparison of XBT and thermistor chain temperature measurements (°C) read at standard hydrographic cast depths

Depth, m	0200 LST			0402 LST			0600 LST		
	268L	Chain	Diff.	270L	Chain	Diff.	272L	Chain	Diff.
0	15.64	15.57	0.07	15.43	15.55	-0.12	15.39	15.47	-0.08
10	15.64	15.56	0.08	15.38	15.48	-0.10	15.38	15.48	-0.10
20	15.59	15.48	0.11	15.28	15.37	-0.09	15.33	15.39	-0.06
30	15.54	15.43	0.11	15.22	15.30	-0.08	15.28	15.32	-0.04
50	15.44	15.39	0.05	15.17	15.11	0.06	15.12	15.08	0.04
75	15.18	15.15	0.03	15.16	15.06	0.10	15.12	15.03	0.09
100	14.68	14.92	-0.24	14.65	14.76	-0.11	14.53	14.48	0.05
125	13.25	13.42	-0.17	13.22	13.38	-0.16	13.23	13.14	0.09
150	11.88	12.05	-0.17	11.48	11.75	-0.27	11.88	11.61	0.27
200	9.55	9.72	-0.17	9.65	9.71	-0.06	9.77	9.61	0.16

about 10.0 kyd north of the southern end of the run. At the bottom of the figure are plots of average XBT profiles derived from the *Lee* profiles, the *DeSteiguer* profiles, all seven profiles, and of five profiles omitting XBT 143D and 144D, respectively. The third profile is profile III in Fig. 24. Of interest is the large difference between individual profiles, with the extremes being represented by XBT 144D and 104C. Additionally, none of the individual profiles exhibit the negative sound-speed gradient characteristic of the average thermistor chain profile I (Fig. 24). Comparison of the *Lee* and *DeSteiguer* average profiles with profile III suggests that the presence of the depressed channel in profile III is the result of including XBT 143D and 144D in the averages used to determine profile III. The right-hand average profile results from omitting these two profiles. This profile results in a 50-m surface channel largely because of the inclusion of XBT 104C in the average. Thus, it is concluded that profile III is largely an artifact resulting from an inadequate XBT sample size.

Figure 37 compares simultaneous XBT temperature profiles derived from XBT records read at standard hydrographic cast depths and thermistor chain scans starting at the same time the XBT probe was released. These are the same data used in preparing Table 24. The thermistor chain measurements are 5.6 m apart in depth. The 0200 LST thermistor chain profile shows two near-isothermal layers from 28 to 56 m and 68 to 79 m, while the XBT-derived profile shows negative gradients at all depths greater than 10 m. These differences are probably related to undersampling the XBT record. The 0402 LST and 0600 LST thermistor chain scans show near-isothermal layers from 51 to 85 m and 51 to 90 m, respectively. XBT 270L and 272L both show isothermal layers from 50 to 75 m. These comparisons suggest that the accurate definition of acoustically important sound-speed profile features is affected by undersampling the XBT record. Additional information on the effect of the sampling interval is contained in Fig. 38. In this figure the XBT profiles were sampled at 5-m intervals, roughly equivalent to the thermistor chain sampling interval. These measurements are plotted together with the thermistor chain measurements in the same format used in Fig. 37. The agreement between the XBT and thermistor chain measurements, as far as defining acoustically important profile gradient features, is remarkable.

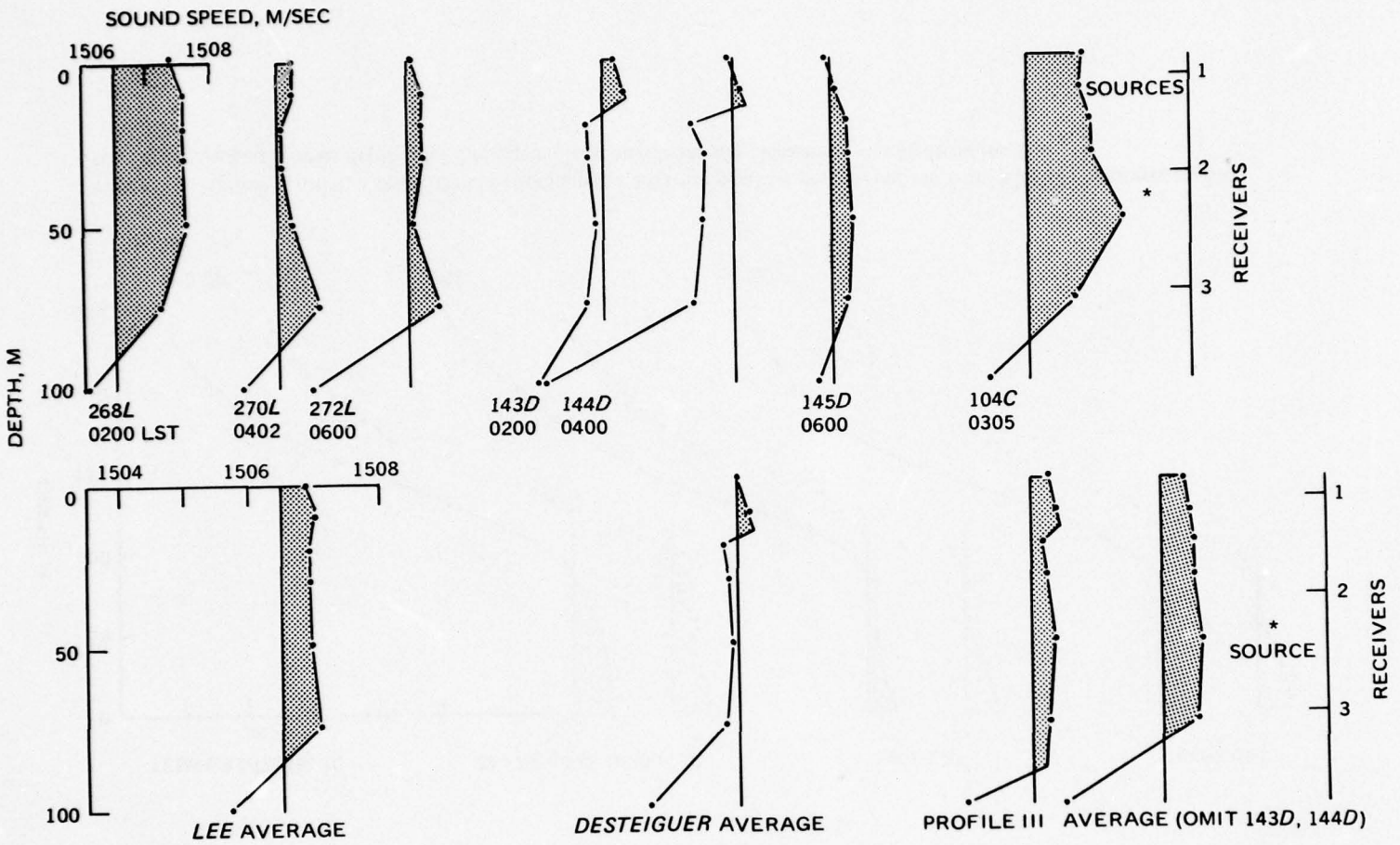

Figure 36. Station 4 run 4 sound-speed profiles derived from XBT temperatures read at standard hydrographic cast depths. The letter following the XBT number denotes the ship which took the measurement (*L: Lee, D: DeSteiguer, C: Cape*).

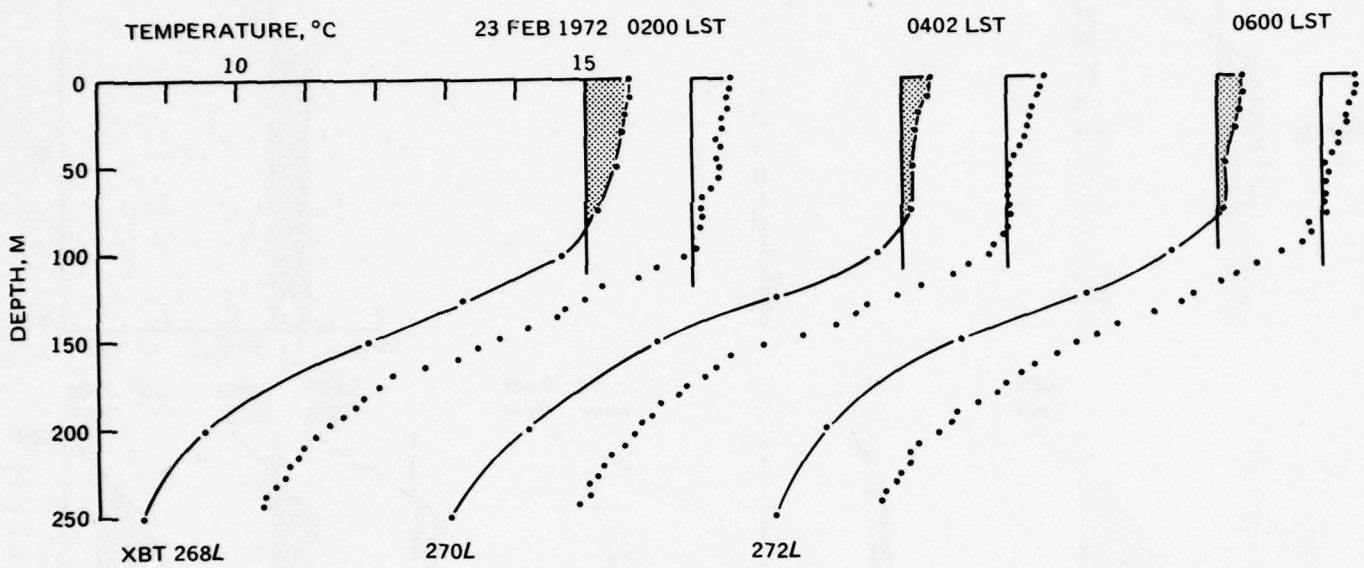

Figure 37. Station 4, run 4. Comparison of simultaneous XBT temperature profiles derived from XBT temperatures read at standard hydrographic cast depths and thermistor chain measurements. Measurements made by the *Lee*;

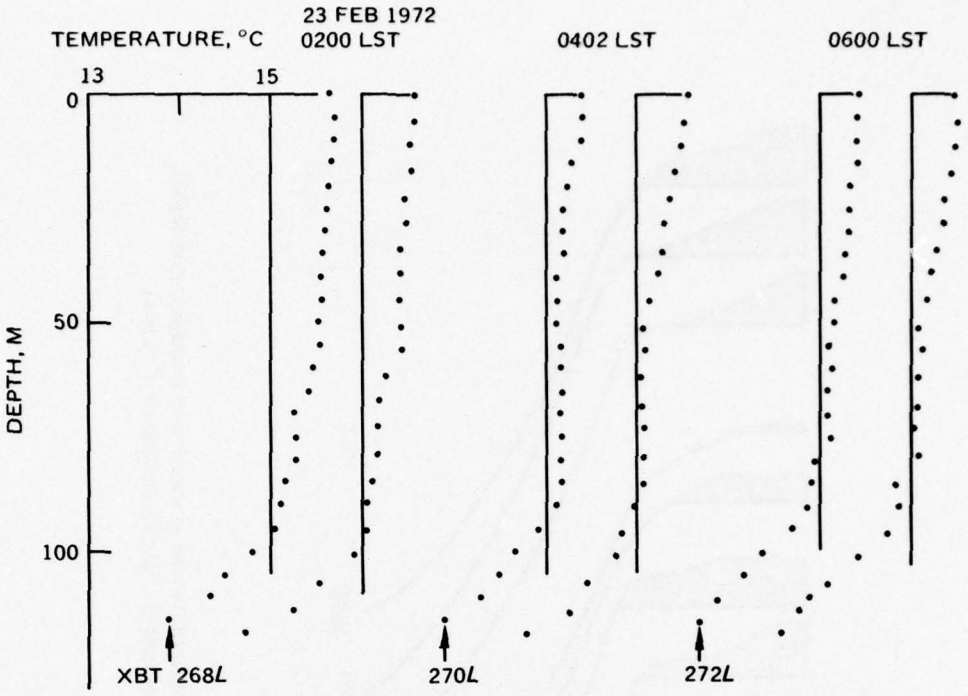

Figure 38. Station 4, run 4. Comparison of simultaneous XBT temperature records digitized at 5-m intervals using an HP 9864A digitizer and thermistor chain measurements. Measurements made by the *Lee*.

STATION 4 RUN 3

Eleven XBT profiles were obtained during the propagation loss measurements made during run 3 – six from the *Lee*, two from the *DeSteiguer*, and three from the *Cape*. The locations of these measurements are shown on Fig. 25. The temperatures were read from the XBT analog recording at standard hydrographic cast depths. Figure 39 is a plot of the resulting XBT temperature profiles. In the absence of the information previously developed from a consideration of the 30-min-average thermistor chain temperature measurements (Fig. 27), these plots show little evidence of a systematic change in profile shape during the progress of the run. Using the guidance provided by the previous analysis of the 30-min-average thermistor chain measurements, the average temperatures were computed for the following sets of XBT profiles: all eleven XBT profiles, 261L, 262L to 265L, and 267L, 140D, 141D, 101C to 103C. These data are plotted in Fig. 40. The major differences between these plots and those of Fig. 28 are the slight positive temperature gradient from the surface to 10 m for XBT profile 1 and the 10-m isothermal layer for XBT profile 3.

The average temperatures for the four profiles of Fig. 40 were converted to sound speed using the relationships presented in Table 5. The sound speeds for profiles 4 and 2 are presented in Fig. 41. The format for Fig. 41 is the same as that used in Fig. 29. The major difference between XBT profile 4 and thermistor chain profile 4 is the XBT profile 4 10-m surface channel. This places receiver 1 in a positive sound-speed gradient rather than in a negative sound-speed gradient. Otherwise the two profiles are similar, at least with

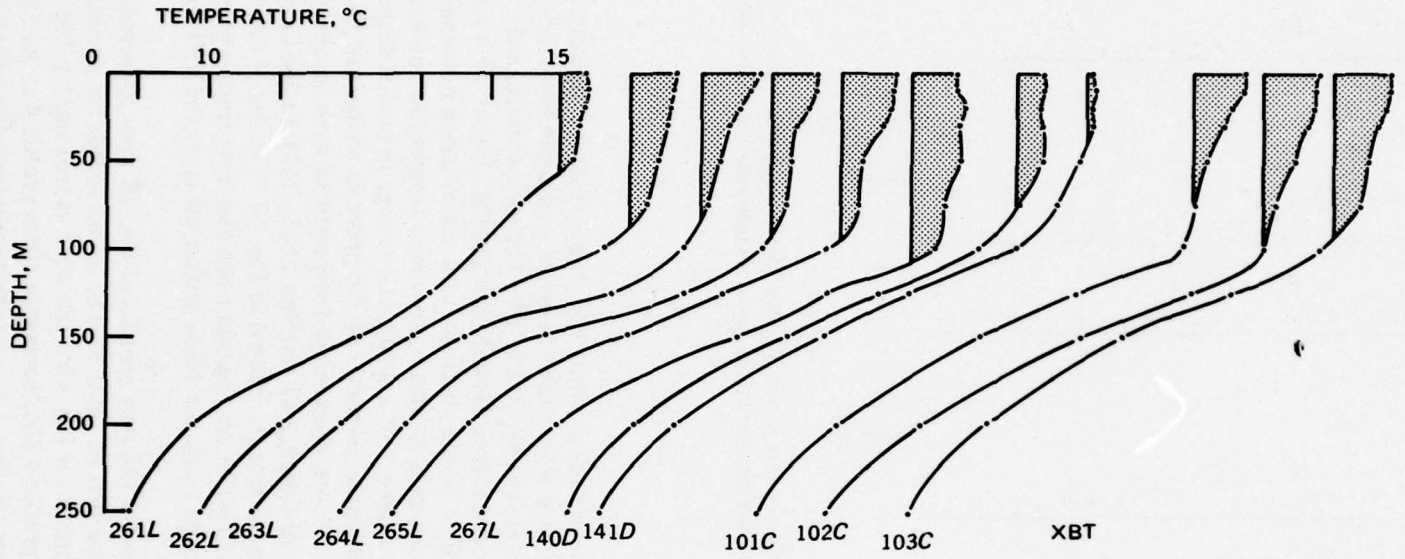

Figure 39. Station 4, run 3. XBT temperature profiles derived from XBT temperatures read at standard hydrographic cast depths. The letter following the XBT number denotes the ship which took the measurement (*L: Lee, D: DeSteiguer, C: Cape*).

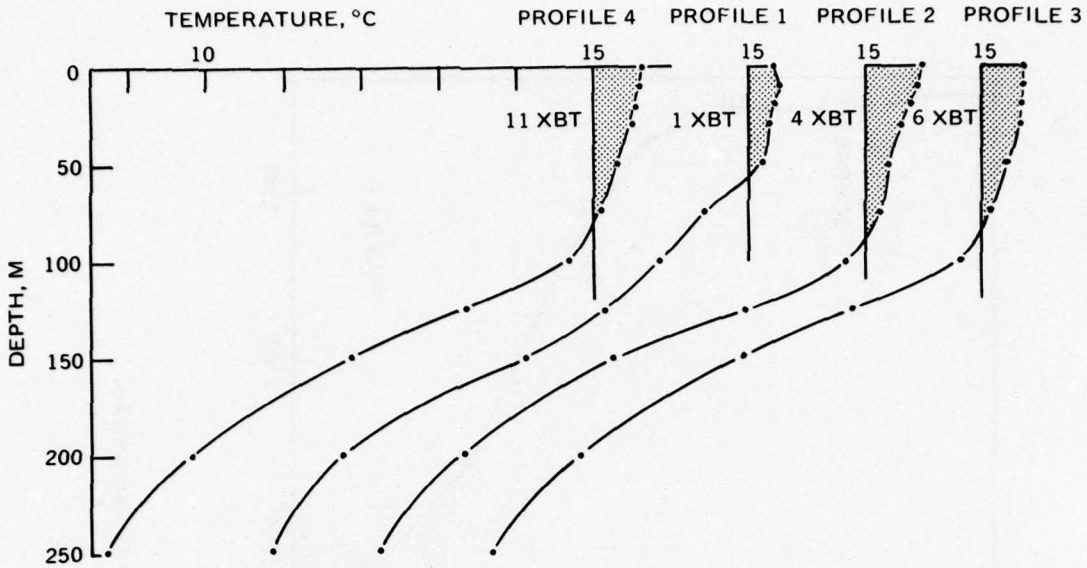

Figure 40. Station 4, run 3. Average temperature profiles derived from XBT measurements.

respect to the sound-speed gradients at source and receiver depths. XBT profile 2 has a depressed channel with the axis of minimum sound speed at 50 m. The more accurate thermistor chain measurements placed the axis at 32.8 m. Additionally, the difference in the depressed channel minimum and maximum sound speed is only 0.07 m/sec for the XBT profile 2, in contrast with 0.29 m/sec for the thermistor chain profile 2. The bottom of the depressed channel is at 75 m for XBT profile 2 and at 78.6 m for the thermistor chain profile 2. This places receiver 3 just out of the depressed channel rather than in the channel. XBT profile 1 has a 20-m surface channel and a depressed channel with minimum sound speed at 30 m, and XBT profile 3 has a 30-m surface channel. In contrast the thermistor chain profiles 1 and 3 both have negative sound-speed gradients from the surface to the depth of the deep sound-speed minimum.

CONCLUSIONS

a. In the data sets examined, the effect of XBT temperature measuring errors on acoustically important sound-speed parameters was inconclusive.

b. Average sound-speed profiles derived from XBT profiles may contain artifacts due to an inadequate XBT sample size.

c. Sound-speed profiles derived from XBT temperature profiles read at standard hydrographic cast depths by means of a digitizer contain surface and depressed channels not present in sound-speed profiles derived from the more accurate, and numerous, thermistor chain temperature profiles. These results suggest that XBT profiles read at standard hydrographic cast depths do not provide adequate sound-speed inputs to presently used propagation loss models. Better agreement between thermistor chain and XBT-derived sound-speed profiles is obtained by digitizing the XBT profiles at 5-m depth intervals from the surface to the top of the main thermocline rather than at standard hydrographic cast depths.

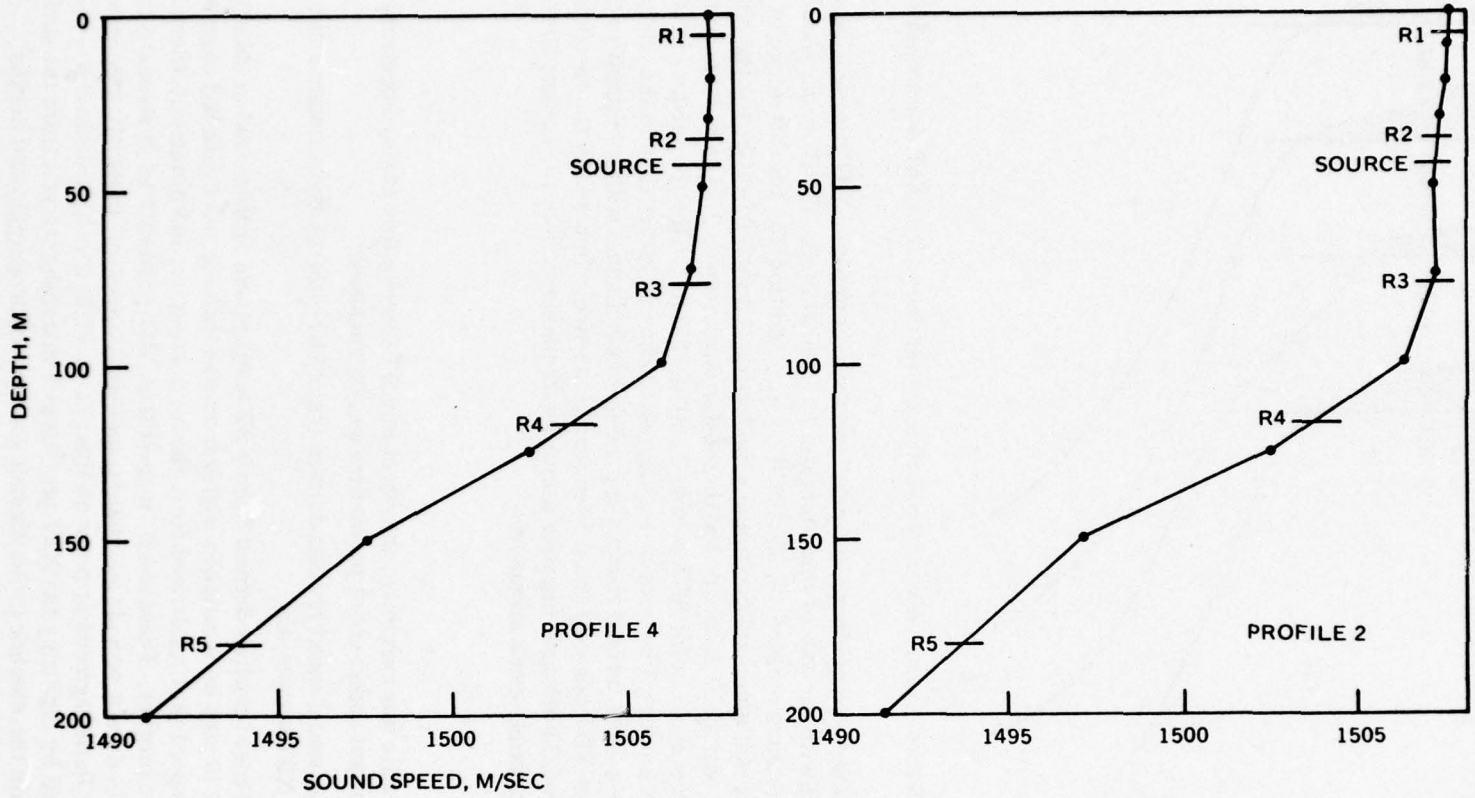

Figure 41. Station 4, run 3. Average sound-speed profiles derived from XBT measurements.

EXAMINATION OF GENERAL CHARACTERISTICS IN THE EXPERIMENTAL PROPAGATION LOSS DATA SETS

A previous section discussed comparisons of theoretical and experimental propagation losses for specific propagation loss runs. This section compares pairs of experimental propagation loss data sets for significant differences. Corresponding pairs of propagation loss measurements taken from all of the SUDS I propagation loss runs are examined for consistency of effect. Theory serves as a guide as to which effects to examine, and this then dictates the pairs of measurements to be compared. For the purposes of this report the comparisons between data sets are divided into three broad categories: greater than, comparable, and less than. In practice this classification was made by overlaying propagation loss plots and making a visual comparison. This classification is adequate to define the general characteristics of interest. Once the propagation loss measurements have been entered into NAVDAB, a more quantitative and rigorous assessment should be made utilizing computer techniques.

COMPARISON OF PROPAGATION LOSSES MEASURED BY THE TWO SHALLOWEST RECEIVERS

The two shallowest receiver depths were planned to be 6 m and 40 percent of the measured surface-layer depth. In practice, the shallowest receiver depth varied from 4 to 6 m, and the next shallowest receiver depth varied from 17 to 37 m, depending on the layer depth present during the experimental run.

Reference 23 discusses the phenomenon known as the surface-decoupling effect. This effect results in increased propagation losses for near-surface receivers. The phenomenon is described in terms of the surface-decoupling depth,which is defined as the depth of the maximum near-surface response of the last trapped normal mode. The propagation loss monotonically increases with decreasing depth in the region shallower than the surface-decoupling depth. This increased loss is referred to as the surface-decoupling loss. Below the surface-decoupling depth, the propagation loss is likely to be less than that observed in the decoupling region. The effect is greatest at the lower frequencies. For example, for a 58-m isothermal surface channel, the surface-decoupling depth for a frequency of 0.4 kHz is 33 m. For an isothermal surface channel of 11 m, the surface-decoupling depth for a frequency of 5.0 kHz is 6 m. As the channel depth is increased, the surface-decoupling depth decreases. At a frequency of 0.4 kHz there is a high probability that a 6-m receiver will be in the surface-decoupling region. However, it is not likely that this will occur for a frequency of 5.0 kHz.

On the basis of these generalities, it is predicted that the 0.4-kHz propagation loss for the shallowest receiver located at 4 to 6 m would be greater than that at the next shallowest depth of 17 to 37 m. On the other hand, the 5.0-kHz propagation loss would be comparable for the two receiver depths. The validity of this general prediction was examined by comparing measured propagation losses for the two shallowest receivers on all of the SUDS I propagation loss runs for pulsed sources.* For each run at each frequency, range intervals were determined for three categories:

1. $H_S > H_D$ – propagation loss definitely greater for the shallowest receiver

*For clarity in the remainder of the discussion, the shallowest and deepest receivers are designated as H_S and H_D, respectively.

2. $H_S \simeq H_D$ – propagation loss about the same for both receivers

3. $H_S < H_D$ – propagation loss definitely less for the shallowest receiver

The range intervals for all runs for a given frequency and given category were combined and normalized to the total range interval covered by all propagation loss runs. These results are summarized in Table 25. Column 1 gives the frequency. Column 2 indicates the number of SUDS I propagation loss runs at the indicated frequency. Columns 3 to 5 present the range intervals for each of the three categories. The range intervals are expressed as a percent of the total range. For example, at 3.5 kHz the measured losses were higher on the shallowest receiver for 29 percent of the total range covered on all 3.5 kHz SUDS I propagation loss runs, comparable on the two receivers for 58 percent of the total range, and smaller on the shallowest receiver for 13 percent of the total range.

Although the range intervals for individual runs were variable, the combined data presented in Table 25 suggest some significant trends. The category $H_S > H_D$ is a monotonic decreasing function of frequency, and the category $H_S < H_D$ is a monotonic increasing function of frequency. The general increase of the category $H_S \simeq H_D$ signifies that the losses show better agreement with increasing frequency. The data shown in Table 25 are in good agreement with general predictions based on the theory of surface decoupling.

Some important operational conclusions may be drawn from these results. The shallowest receiver, at 4 to 6 m, corresponds to the depth of surface ship hull-mounted sonars. At 5.0 kHz this depth appears to be as good as greater depths in the surface layer. However, there appears to be some performance degradation, even at 3.5 kHz, with the degradation becoming progressively greater at lower frequencies. In the case of active sonars the surface-decoupling effect is compounded, since the results apply equally well to both source and receiver. Thus, there is increased propagation loss to the target because of a shallow source and also increased propagation loss from the target because of a shallow receiver.

The penalty which is paid for a shallow source or receiver can be further investigated in two ways – experimentally or theoretically. The following are recommended for future investigation:

1. The experimental data summarized in Table 25 can be subjected to a detailed comparison on a pulse-by-pulse basis by utilizing a computer. The data should be partitioned

Table 25. Comparison of propagation losses measured by the two shallowest receivers

Frequency, kHz	Number of Runs	Percent of Total Range Interval		
		$H_S > H_D$	$H_S \approx H_D$	$H_S < H_D$
0.4	3	100	0	0
1.0	4	96	4	0
1.5	5	56	39	5
2.5	5	30	58	12
3.5	6	29	58	13
5.0	6	15	72	13

into more quantitative categories than were used to prepare the data presented in Table 25. One possible choice is 3-dB increments. In this case the categories would be $0 < H_S - H_D < 3$ dB, $0 \leq H_D - H_S < 3$ dB, $3 \leq H_S - H_D < 6$ dB, $3 \leq H_D - H_S < 6$ dB, etc. This would provide a better quantitative measure for the given experimental depth.

2. From the theoretical standpoint, normal-mode calculations could be made to determine the optimum receiver or source depth for each of the SUDS I propagation loss run sound-speed profiles and for each frequency. Comparison of the theoretical losses at this optimum depth with the theoretical losses for 4- to 6-m receiver depth would establish the penalty for a hull-mounted sonar.

DEPENDENCE OF PROPAGATION LOSS ON FREQUENCY

The theoretical rationale for appropriate experimental comparisons of propagation loss for various frequencies is facilitated by some results presented by Cummins (Ref. 24). This unpublished paper contains theoretical normal-mode calculations for a sound-speed profile considered to be representative of station 3 runs 2, 3, and 4. The parameters for this profile are presented in Table 26. Computed propagation losses, based on the Table 26 profile, are summarized in Fig. 42. Figure 42 shows the minimum theoretical propagation losses as a function of frequency for three ranges – 18.0, 30.0, 42.0 kyd. A 44-m source depth was used for the computation. The data presented in Fig. 42 were obtained by calculating the propagation loss at the indicated range for a given frequency as a function of receiver depth and then recording the propagation loss of the receiver having the minimum propagation loss. This procedure smooths out the interactions between frequency and receiver depth. This results in a smooth function which shows, for a given range, the surface-channel response as a function of frequency.

At long ranges, such as illustrated in Fig. 42, the propagation loss is dominated by the total attenuation. The total attenuation consists of the sum of the mode attenuation and the absorption. The mode attenuation decreases with increasing frequency, while the absorption increases with increasing frequency. The mode attenuation, which results from leakage out of the surface-channel, dominates at the lower frequencies near the cutoff frequency. For the sound-speed profile used in this analysis, the onset of trapping for the first mode is at a frequency of 0.337 kHz, labeled f_{CO} in Fig. 42. The high-frequency rolloff, shown in Fig. 42, results from the absorption loss.*

Thorpe's absorption loss values were used in this computation (Ref. 25).

Table 26. Station 3 runs 2, 3, and 4 sound-speed profiles (after Cummins, Ref. 24)

Depth, m	Sound Speed, m/sec
0	1505.65
93	06.20
200	1494.00

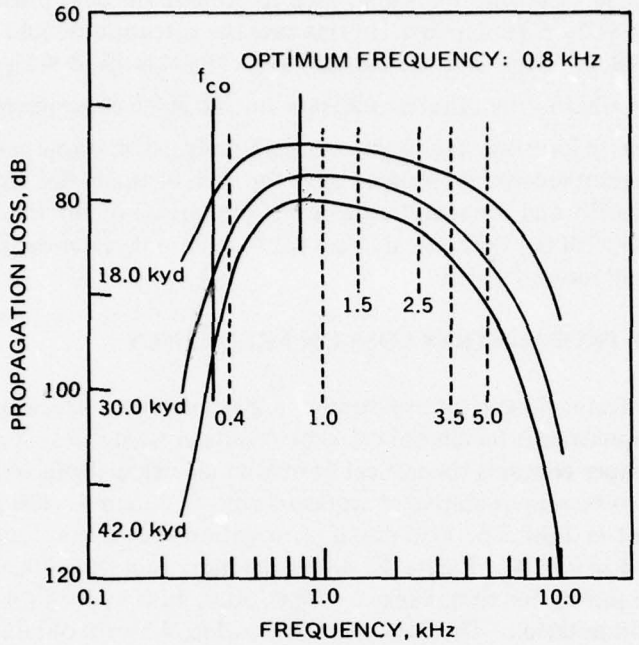

Figure 42. Propagation loss at depth of minimum loss as a function of frequency.

As shown in Fig. 42 the optimum frequency is about 0.8 kHz. This frequency is well above the onset of trapping for the first mode. For the profile presented in Table 26 this corresponds to a mode strength parameter M = 4.13 (see Ref. 23), which is near the onset of trapping for the second mode.

For the SUDS I experiments three pairs of frequencies were used: 0.4 and 1.0 kHz, 1.5 and 2.5 kHz, and 3.5 and 5.0 kHz. These pairs of frequencies are identified on Fig. 42 by the vertical dashed lines. It is noted that these calculations show little difference in propagation loss between frequencies of 1.5 and 2.5 kHz. In contrast, the theoretical propagation losses at 0.4 and 5.0 kHz are considerably larger than those calculated for 1.0 and 3.5 kHz.

In order to obtain a feeling for the response of other surface channels, the assumption is made that M = 4.13 is invariant, i.e., that the optimum frequency at long range is associated with this channel strength. Based on this assumption, Table 27 was prepared for an isothermal isohaline surface channel with a sound-speed gradient equal to 0.018 sec^{-1}. Table 27 shows estimated values of surface channel depth that are optimum for the SUDS I experimental frequencies. On the basis of the data presented in Table 27, some useful predictions can be made. For example, the 1.0-kHz propagation loss will be less than the 0.4-kHz propagation loss for surface channel depths less than 55 m, and the 3.5-kHz propagation loss will be less than the 5.0-kHz propagation loss for channel depths deeper than 24 m. Another way of stating this result is that, except for very deep surface channels, the propagation loss at 1.0 kHz will be less than the 0.4-kHz propagation loss and, except for very shallow layers, the propagation loss at 3.5 kHz will be less than the 5.0-kHz propagation loss. These predictions may be tested by comparing the experimental propagation losses

Table 27. Values of surface channel depth corresponding to M = 4.13 for an isothermal, isohaline surface channel

Frequency, kHz	Surface-Channel Depth, m
0.4	102
1.0	55
3.5	24
5.0	19

measured on all five receivers during all of the SUDS I propagation loss runs made at these two pairs of frequencies.

Comparison of Experimental 3.5- and 5.0-kHz Propagation Loss

The most conclusive results are for the six 3.5- and 5.0-kHz propagation loss runs. For all receiver depths for station 1 runs 3 and 4, station 2 run 3, and station 3 run 5, the propagation losses were visually less at 3.5 kHz than at 5.0 kHz. The same was true for station 3 run 4, with the exception of the 6-m receiver. For this receiver the propagation losses were comparable for ranges less than 8.0 kyd, but again the 3.5-kHz propagation losses were less for ranges greater than 8.0 kyd. The major exception was observed during station 4 run 1. On all five receiver depths the propagation loss was visually less at 5.0 kHz out to range of 15.0 to 20.0 kyd. For ranges greater than these the propagation loss for these two frequencies was comparable.

The experimentally observed channel depths associated with the station 1, 2, and 3 runs were between 37 and 95 m. However, the channel depth observed during station 4 run 1 was only 16 m. Comparison of these depths with those listed in Table 27 indicates that one would indeed expect the propagation loss at 3.5 kHz to be less than that at 5.0 kHz for the station 1, 2, and 3 runs, but the opposite to hold for station 4 run 1. Thus, the SUDS I 3.5- and 5.0-kHz experimental propagation losses are in substantial agreement with the theoretical predictions.

Comparison of Experimental 0.4- and 1.0-kHz Propagation Loss

Three propagation loss runs were made using the 0.4- and 1.0-kHz sources. Comparison of the experimental measurements are presented in Fig. 43. The comparisons are grouped into three categories:

$H_1 < H_2$ 

$H_1 \approx H_2$ 

$H_1 > H_2$ 

where H_1 and H_2 are the 0.4- and 1.0-kHz propagation losses, respectively. The range intervals corresponding to these categories are shown for each of the five receiver depths for each of the three runs. The maximum range of the propagation loss run is indicated by a vertical

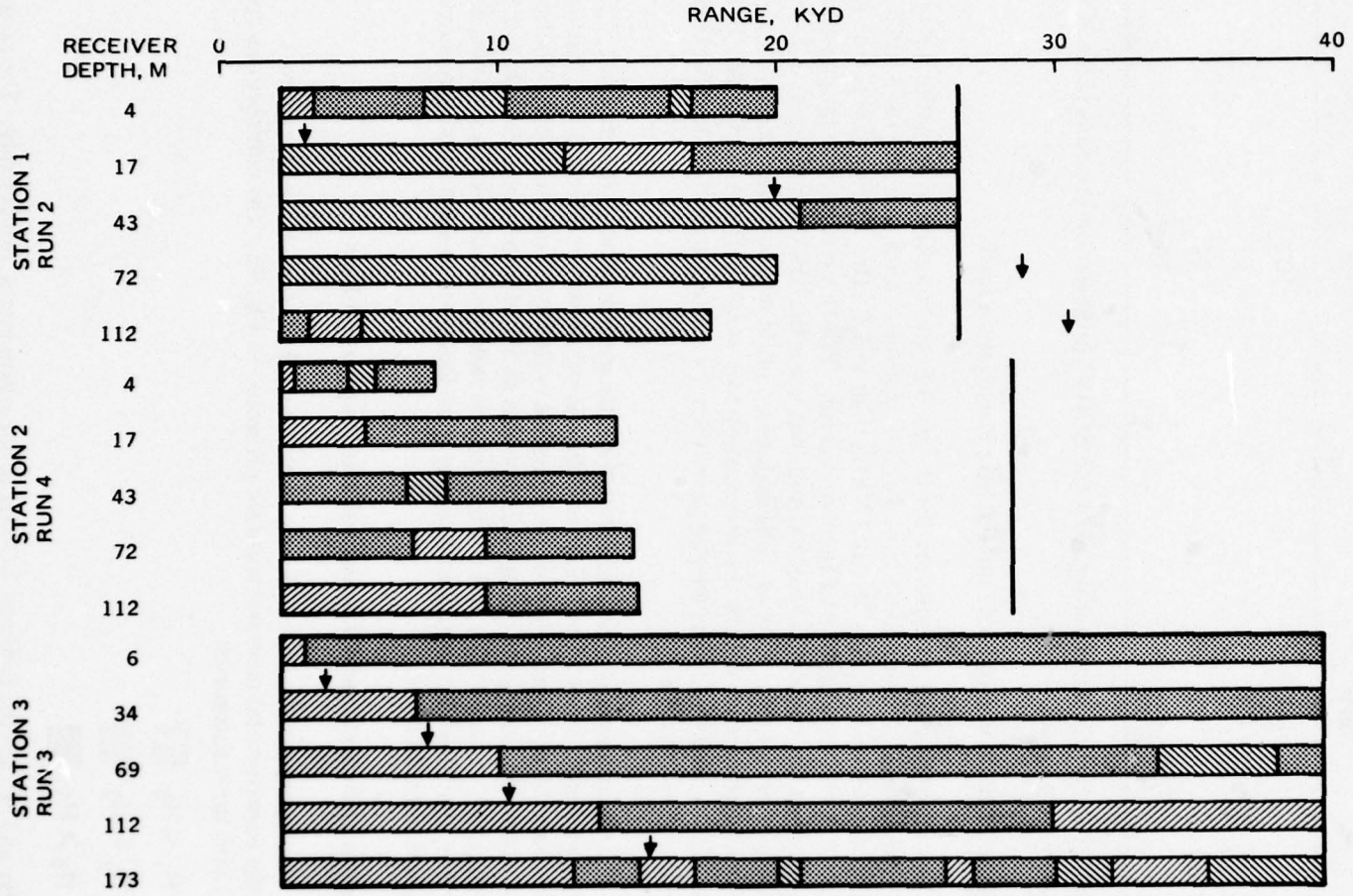

Figure 43. Comparison of 0.4-kHz and 1.0-kHz propagation losses.

bar crossing the data for all five receivers. For some receivers on station 1 run 2 and all receivers on station 2 run 4, no comparisons are shown for the longer ranges since the 0.4-kHz arrivals were below the noise level and no comparison could be made.

The surface channel depth for station 2 run 4 was 30 m. Comparison of this depth with those shown in Table 27 indicates that propagation losses should be less at 1.0 kHz than at 0.4 kHz. The data of Fig. 43 are in general agreement with this prediction. The surface channel depths for station 1 run 2 and station 3 run 3 were 68 m and 80 m, respectively. Unfortunately these channel depths are between the depths listed in Table 27 for 0.4 and 1.0 kHz. Thus, Tabie 27 is of little help in estimating which frequency should have the larger propagation loss. However, theoretical computations for these two runs were made, and discussed, earlier in this report. These theoretical computations predicted that the total attenuation was greater at 0.4 kHz than at 1.0 kHz for both of these runs. Thus, it would be expected that in Fig. 43 the ▩ intervals would be more prevalent than the ▧ intervals. This is the case for station 3 run 3, but certainly not for station 1 run 2.

In order to analyze these comparisons in more detail, Table 28 was prepared from the theoretical calculations. The table lists the crossover range, defined as the range beyond which the theoretical propagation loss at 0.4 kHz exceeds that at 1.0 kHz. For ranges greater than the crossover range, the attenuation term dominates. At ranges shorter than the crossover range, the theoretical loss is generally smaller at 0.4 kHz than at 1.0 kHz. This characteristic cannot be tested into very small ranges because of the necessity of summing very large numbers of modes in order to obtain reliable results. The problem of summing modes is greatest for the shallowest receivers. In Table 28 the crossover ranges cannot be established for the two shallowest receivers, but upper bounds can be determined. These upper bounds represent the shortest range at which the theoretical calculations are reliable. Indeed, for the shallowest receivers there may not be a crossover range, since the propagation loss at 0.4 kHz may always be larger than the 1.0-kHz propagation loss. This is because the

Table 28. Theoretical crossover range for station 1 run 2 and station 3 run 3*

	Receiver Depth, m	Crossover Range, kyd
Station 1 Run 2	4	< 1.5
	17	2.9
	43	19.8
	72	28.9
	112	30.5
Station 3 Run 3	6	< 2.5
	34	1.7
	69	5.3
	112	8.2
	173	13.9

*The propagation loss at 0.4 kHz is larger than that at 1.0 kHz beyond the crossover range.

surface decoupling loss, which was discussed earlier in a comparison of losses between the two shallowest receivers, is much greater at the lower frequencies for a receiver 4 to 6 m below the surface. The experimental results shown in Fig. 43 confirm this. The ▩ regions predominate the ▧ regions for the shallowest receiver.

The data presented in Table 28 show that the crossover range increases with increasing receiver depth. This trend can be explained from a theoretical standpoint. The increased mode attenuation at 0.4 kHz results in less energy at long ranges as compared to 1.0 kHz. However, this is not a dissipative mechanism (loss of acoustic energy), it is a leakage mechanism. The smaller amount of acoustic energy at long range must be accounted for by a greater amount of energy at closer ranges. The leakage energy manifests itself by smaller propagation loss at the closer ranges to an increased degree for deeper receivers, i.e., the deep receivers at closer ranges receive the leakage energy which does not travel to greater ranges.

Note also in Table 28 that the crossover ranges for station 1 run 2 are much greater than for station 3 run 3. Long-range propagation conditions are better for station 3 run 3 as compared to station 1 run 2. However, the results of Table 28 cannot be rationalized on this basis since the better propagation conditions apply to both frequencies. Without further analysis, beyond the scope of this report, the larger crossover ranges cannot be associated with poorer long-range propagation.

The crossover ranges of Table 28 are designated in Fig. 43 by the arrows. The experimental data are in substantial agreement with the trends discussed in connection with Table 28, i.e., the crossover ranges increase with increasing depth, and the crossover ranges are larger for station 1 run 2 as compared to station 3 run 3. Indeed for station 3 run 3, agreement between the crossover range and the onset of the ▩ intervals is excellent considering the visual approach used to obtain the experimental data of Fig. 43. The theoretical computations also explain why the propagation losses for station 1 run 2 are generally less at 0.4 kHz for the three deepest receivers. The only large discrepancy between experimental data and the theoretical crossover ranges is for the 17-m receiver for station 1 run 2. However, this problem has already been considered in the previous discussion of this run. The measured propagation losses for the shallow receivers at 0.4 kHz was exceedingly small compared to the theoretical calculations.

It is evident from the results presented in Fig. 43 that the comparison of propagation losses at various frequencies, based on total attenuation, is too simplistic. Although this analysis worked well at 3.5 and 5.0 kHz, it only applies to long ranges for 0.4 and 1.0 kHz. Unfortunately, the term "long range" is too variable to be of much practical use. Depending upon receiver depth and propagation conditions, this long range varied from as low as 1.7 kyd to as high as 30.5 kyd.

The experimental and theoretical results suggest further investigation of propagation at frequencies below the onset of trapping in surface channels. It may very well be that increased leakage at these frequencies results in lower propagation loss for below-layer targets at close range.

There is another aspect of making a theoretical investigation of frequencies below the onset of trapping in surface channels. E. Murphy and F. Jensen (private communication) of the SACLANT ASW Research Centre have concluded that the properties of the

sound-speed profile for the entire water column in deep water, including the bottom, are of increasing importance for a proper description of the behavior of a near-surface sound field as a function of frequency below cutoff. D. White (private communication) of the Naval Undersea Center has also observed in a shallow-water study that the mode eigenvalues are different when only a positive-gradient surface layer and a negative thermocline are modeled as compared to modeling the entire water column with a structured bottom. These studies suggest that the approaches used in this report, i.e., modeling only the region from the surface to about 200 m depth, are suspect at frequencies below the onset of trapping in the surface channel. A thorough theoretical study of this problem, comparing results of a surface-channel model with those of a corresponding model of the entire ocean column, is recommended. This study may help explain why the agreement reported here between theory and experiment at 0.4 kHz has, on the whole, been rather poor.

COMPARISON OF PROPAGATION LOSS FLUCTUATION FOR HIGH AND LOW WIND SPEEDS

This section examines the effect of wind speed, or sea-surface roughness, on the fluctuation of propagation loss.* One effect of a high wind speed (high-wind-generated waves) is to increase the fluctuation of propagation loss. In this analysis the fluctuation for pairs of similar propagation loss runs under different wind conditions was visually compared by observing the relative amount of scatter in the pairs of propagation loss plots. Any contributions to the scatter resulting from obvious modal interference patterns were ignored.

The first analysis was made by comparing similar data sets from runs made during stations 1, 3, and 4. In this analysis the measurements made during station 2 runs were not used because of the temperature frontal surface present during these runs. The effect of crossing a frontal surface on propagation loss fluctuation is not known and could possibly obscure, or mask, the effect of wind speed. Comparisons were made for 20 pairs of data sets having similar sound-speed profiles. Of these comparisons 10 showed no difference between runs, 7 showed the greater fluctuation associated with the run having the higher wind speed, and 3 showed the greater fluctuations associated with the run having the lower wind speed. Although these results were somewhat encouraging, they can hardly be regarded as conclusive evidence of a correlation between wind speed and propagation loss fluctuation. Unfortunately, the wind speeds were not radically different for the runs compared. The maximum wind speed was 12 knots. In most cases the lowest wind speed reported for the run with the higher wind speeds overlapped the highest wind speed on the run with the lower wind speeds. Thus effects caused by slight differences in wind speed could easily be obscured by the relatively insensitive visual comparison technique used in the analysis.

Since the wind speeds observed during the station 2 runs were radically different from those observed during the runs made at the other three stations, the next step was to reconsider the use of the station 2 data. Comparisons made in the second analysis were limited to using only those portions of the station 2 measurements which did not cross the thermal front. The data available for comparison were the station 2 run 1 measurements made over the range interval from 0.2 to 8.6 kyd, and the station 2 run 3 measurements made over the range interval from 0.2 to 8.3 kyd.

For each of these two data sets, three sets of propagation loss measurements made at other stations at the same frequencies and source depths were available for comparison. Table 29 identifies these eight data sets. In addition, the wind speeds, wave and swell heights, and source depths are listed. The upper four sets of measurements were made using 1.5- and 2.5-kHz sources, and the lower four sets were made using 3.5- and 5.0-kHz sources. The wind speeds for the station 2 runs are much higher than those observed during the stations 3 and 4 measurements. For station 2 run 1 the ratios of the wind speeds range from a minimum

In the discussion to follow it is assumed that the local wind speed is an index of sea-surface roughness. This is not strictly true since the total sea-surface roughness is composed of a wave component and a swell component and the wave component is also a function of the duration of the local wind. The wave component is generated by the local wind, while the swell component is a wave generated in some other location and decaying into the local area. Thus, it is possible to have a large sea-surface roughness associated with a large swell in the presence of a low wind speed. In other words, there is no correlation between local wind speed and swell.

Table 29. Wind speed, wave and swell height, and source depth for runs used in propagation loss fluctuation comparisons

	Station 2 Run 1	Station 3 Run 2	Station 4 Run 3	Station 4 Run 4
Wind Speed, knots	16-20	< 5	4-8	8-10
Wave, ft	3-8	< 1	1	1
Swell, ft	6-10	3-6	3-8	3-8
Source Depth, m	38	42	43	43
	Station 2 Run 3	**Station 4 Run 1**	**Station 3 Run 4**	**Station 1 Run 3**
Wind Speed, knots	17-22	1-6	8-12	4-8
Wave, ft	3-7	< 1	1-2	1
Swell, ft	8-12	8-10	3-5	3
Source Depth, m	38-41	43-46	44-47	45-42

of 1.6 to a maximum of 5.0. Corresponding values for station 2 run 3 are 1.4 to 22.0. It should be pointed out that the sound-speed profile shapes for the runs to be compared are not similar in any sense. The assumption is made that the effect of large differences in wind speed will prevail over any effect on fluctuation due to variations in sound-speed profile shapes.

Table 30 presents the 1.5- and 2.5-kHz propagation loss fluctuation comparisons. The station 2 run 1 measurements are compared with those made at station 3 run 2, station 4 run 3, and station 4 run 4. The entry P means that the fluctuation was significantly higher for station 2 run 1, the entry N means that the fluctuation was significantly lower for station 2 run 1, and the entry I means that there was no visual difference in the fluctuation. The receiver depths are not identical for the data sets to be compared but are about the same.

Table 30. Comparison of station 2 run 1 propagation loss fluctuation with station 3 run 2, station 4 run 3, and station 4 run 4 propagation loss fluctuation

Receiver Depth, m	Frequency, kHz	Station 3 Run 2	Station 4 Run 3	Station 4 Run 4
5-6	1.5	P	P	I
72-77		P	I	P
117-120		P	N	I
5-6	2.5	P	P	P
72-73		P	I	I
117-120		P	N	I

Out of the 18 comparisons listed in Table 30, 10 are P, 2 are N, and 6 are I. These comparisons certainly suggest a positive correlation between wind speed and fluctuation. Note that all entries listed under station 3 run 2 are P. As shown in Table 29 the largest wind-speed differences are between station 2 run 1 and station 3 run 2. The entries for station 4 run 4 indicate some positive correlation with wind speed, whereas the entries for station 4 run 3 indicate no correlation. This is somewhat unexpected because the wind speed difference between station 2 run 1 and station 4 run 3 are greater than the wind speed differences between station 2 run 1 and station 4 run 4. Consideration of wave and swell heights does not help in the analysis since they are the same for station 4 run 3 and station 4 run 4. No reason can be suggested at this time to explain the station 4 run 3 N entries. The I entries in Table 30 could be eliminated by a detailed quantitative statistical analysis. However, until this is done it is not known whether these would fall into the P or N categories.

Table 31 presents the comparison of the station 2 run 3 propagation loss fluctuations with each of the three comparable sets from stations 1, 3, and 4. Out of the 22 entries in Table 31, 8 are P, 1 is N, and 13 are I. These 3.5- and 5.0-kHz comparisons again indicate a positive correlation between wind speed and fluctuation. However, the results are not as conclusive as the 1.5- and 2.5-kHz results presented in Table 30. As shown in Table 29 significantly greater wind speeds were recorded during station 3 run 4 as compared to station 4 run 1. However, the comparisons in Table 31 between station 2 run 3 and station 3 run 4 and station 4 run 1 each contain three positive and three indeterminate correlations. Moreover, the comparisons of station 2 run 3 with station 1 run 3 appear to be less correlated with wind speed than do the station 2 run 3 comparisons with station 4 run 1, even though the wind speeds recorded during station 1 run 3 are higher than those recorded during station 4 run 1.

In conclusion, it appears that there is, in general, a positive correlation of fluctuation with wind speed, although there are unexplained exceptions. The correlation appears to be greater at 1.5 and 2.5 kHz as compared to 3.5 and 5.0 kHz. There is no question that a more

Table 31. Comparison of station 2 run 3 propagation loss fluctuation with station 4 run 1, station 3 run 4, and station 1 run 3 propagation loss fluctuation

Receiver Depth, m	Frequency, kHz	Station 4 Run 1	Station 3 Run 4	Station 1 Run 3
4-6	3.5	P	P	I
17				P
43				I
72-77		I	P	N
112-118		I	I	I
4-6	5.0	P	P	I
17				P
43				I
72-77		P	I	I
112-118		I	I	I

detailed analysis will be necessary before the effect of wind speed (sea-surface roughness) on propagation loss fluctuation can be adequately assessed.

Even more important than the effect of surface roughness on fluctuation is its effect on the mean level of propagation loss. The effect of scattering is to enhance propagation for receivers below the surface channel at the expense of somewhat increased losses for receivers in the surface channel. Gordon (Ref. 26) has shown that the experimental signal levels for below-layer receivers are higher than can be accounted for by diffraction alone and that the differences between experiment and diffraction theory could be correlated with wind speed – the higher the wind speed the larger the difference. The SUDS I data represent a good large data set that can assist in the determination of the relative importance of diffraction and scattering contributions to the acoustic field of below-layer receivers. A first step in this determination would be to incorporate the rough surface corrections contained in the Rough Surface Natural Mode Model (NUC WAVE) into the n-layer normal-mode model.

One rather difficult problem is the development of a propagation loss model which includes both range-dependent sound-speed profiles and surface scattering. The parabolic equation method or modified normal-mode approaches can be used to treat range-dependent sound-speed profiles. However, the introduction of scattering effects into such models appears to be very difficult. Thus, it will be difficult to develop models which adequately assess the effects of surface scattering on the mean propagation loss, to say nothing of models which would address the fluctuation.

Before concluding this discussion of propagation loss fluctuation, it should be noted that thermal microstructure may play an important role. One possible approach to assess its importance would be to correlate propagation loss fluctuation with some measure of the variability of the sound-speed profiles as determined from the thermistor chain temperature measurements. Exactly what this measure of variability should be cannot be specified until the thermistor chain data are examined in much greater detail.

CONCLUSIONS

The following summarizes the primary conclusions. Other conclusions concerning details of the observations and analyses may be found in the text.

ACOUSTIC

1. Because of surface-decoupling effects, theory predicts that the 0.4-kHz propagation loss for the shallowest receiver (4 to 6 m) is greater than at the next shallowest receiver (17 to 34 m) and at 5.0 kHz the propagation loss is comparable for the two receiver depths. A comparison of the propagation losses measured by the two shallowest receivers suggests that at 5.0 kHz the propagation loss at the shallowest receiver, corresponding to the depth of a surface ship hull-mounted sonar, was comparable to the propagation loss measured at the next deepest receiver. However, there appears to be some performance degradation at the shallowest receiver, even at 3.5 kHz, with the degradation becoming progressively greater at lower frequencies.

2. Two of the 0.4-kHz and 1.0-kHz propagation loss runs were made in the presence of similar oceanographic and acoustic parameters. Despite the similarity, the propagation loss measurements for comparable receiver depths showed marked differences. Some of the differences were explained in terms of the number of modes trapped in the near-surface channels. However, there still remained some marked differences which the theoretical calculations did not support. For example, the combination of exceedingly small propagation losses measured by the shallow receivers at 0.4 kHz and the exceedingly large propagation losses measured by the deep receivers at 1.0 kHz is difficult to explain in terms of present understanding for non-range-dependent sound-speed profiles.

3. Theoretical propagation losses calculated using the n-layer normal-mode model are relatively insensitive to sound-speed profile inputs for receivers located in the main thermocline as compared to receivers located above the thermocline.

4. Comparison of theoretical and measured propagation losses suggests that acoustically important features of the sound-speed profiles present during some propagation loss runs represent critical regimes, requiring much greater accuracy than can be obtained from a consideration of a few XBT measurements.

5. Theory predicts that, except for deep surface channels, 1.0-kHz propagation loss is less than 0.4-kHz propagation loss and, except for shallow surface channels, 3.5-kHz propagation loss is less than that at 5.0 kHz. Visual comparisons showed that the 3.5- and 5.0-kHz experimental propagation losses were in substantial agreement with theory. However, at 0.4 and 1.0 kHz the agreement was good only at long range, where long range varied from 1.7 kyd to 30.5 kyd, depending upon receiver depth and propagation conditions.

6. Visual comparison of propagation loss fluctuation for propagation loss runs made during high wind speeds with those made during low wind speeds showed a positive correlation of propagation loss fluctuations with wind speed, although there were some unexplained exceptions. The correlation was better at 1.5 and 2.5 kHz than at 3.5 and 5.0 kHz.

7. Theoretical propagation losses computed for receivers located near the top or bottom of a depressed channel were quite sensitive to the depths of the channel boundaries and the sound speeds at those depths.

8. Agreement between preliminary theoretical propagation losses calculated using the parabolic equation model and propagation losses measured when towing the sources across a marked temperature frontal surface with a measured change in surface temperature of 0.6°C (equivalent to about 2.0 m/sec) in 700 yd was encouraging, considering the assumptions that were made.

OCEANOGRAPHIC

1. Examination of the average sound-speed profiles derived from thermistor chain measurements at standard hydrographic cast depths indicates that they can be categorized into seven general types. The most prevalent average profile was a surface channel over a depressed channel and the least prevalent a surface channel over two depressed channels. The classical bilinear surface channel, used by most propagation loss models, was the second most prevalent type.

2. A comparison of sound-speed profiles derived from XBT profiles read with a digitizer and thermistor chain measurements suggests that XBT profiles read at standard hydrographic cast depths do not provide adequate sound-speed inputs to presently used propagation loss models. Better agreement between thermistor chain and XBT-derived sound-speed profiles was obtained by digitizing the XBT profiles at 5-m depth intervals from the surface to the top of the main thermocline.

3. Initial analysis indicated that nine of the propagation loss runs were characterized by single sound-speed profiles, suggesting spatial and temporal homogeneity in sound speed. A few of these runs were reanalyzed using half-hour averages of the thermistor chain measurements. These half-hour average sound-speed profiles, based on 180 thermistor chain temperature profiles, showed progressive changes within one profile type and, in some cases, a change to a different profile type. This suggests that perhaps none of the sound-speed profiles for the propagation loss runs is spatially or temporally homogeneous.

4. Customary methods of converting temperature and salinity measurements into sound-speed profiles utilize measurements at standard hydrographic cast depths and certain special depths, such as the depth of surface channels and depressed channels. Detailed examination of the thermistor chain measurements indicates that the average temperatures for the individual thermistor chain sensors represent a capability for greatly increasing the accuracy of critical input parameters to propagation loss models.

5. Comparison of STD/SV measured sound speeds with sound speeds computed from the STD/SV measurements of temperature, salinity, and depth shows that the measured sound speeds are consistently and systematically lower than the computed sound speeds. At 250 m the average difference is small, 0.02 m/sec. The difference systematically increases to 0.21 m/sec at 1000 m and to 0.26 m/sec at 3000 m.

6. Between 1200 LST and 2200 LST negative sound-speed gradients starting at the surface were present when wind speeds were less than 10 knots, positive when wind speeds were greater than 15 knots, and either negative or positive for wind speeds between 11 and 14 knots.

7. Because of problems caused by strong winds, heavy seas, unfamiliarity of personnel with a new complex temperature measuring system, the lack of a station-keeping capability, and the lack of a depth sensor on the Teletherm buoys, only the temperature

measurements made during stations 3 and 4 in the surface layer, where vertical gradients are small or nonexistent, are valid. The primary value of these measurements is as an indicator of temporal temperature stability in the surface layer.

RECOMMENDATIONS

The following summarizes the primary recommendations. Other recommendations concerning details of the analyses may be found in the text.

1. Reduce, analyze, and report the bottom-reflected measurements made during all propagation loss runs, the short-pulse fluctuation measurements made for 10-min samples at various fixed ranges, and the bistatic reverberation measurements made with source and receiver 1.0 kyd apart.

2. Apply the new approaches of this report, as well as the simple models presently in general use, to all of the SUDS I propagation loss runs.

3. Study the sensitivity of propagation loss models to the details of the sound-speed profile inputs. Once the sensitivity is established, determine an optimum sample size of the thermistor chain measurements that averages out scatter but preserves trends, and utilizing average thermistor chain temperatures, develop a computerized technique for statistically fitting functions appropriate to the propagation loss model being employed.

4. Study the application of the parabolic equation model to complex environmental situations, such as those present during station 2 run 1. Since the basic method allows the introduction of an unlimited number of sound-speed profiles, it could be applied with varying degrees of refinement.

5. Plan and conduct an experiment to investigate the effect of a temperature frontal surface on propagation loss.

6. Determine whether or not theoretical propagation loss calculations can be brought into closer agreement with the station 3 run 3 and station 1 run 2 experimental propagation losses by using sound-speed profiles derived from half-hour averages of thermistor chain temperature measurements as inputs to the parabolic equation model.

7. Investigate the penalty paid for a shallow source, or receiver, by subjecting the experimental data to a detailed comparison on a pulse-to-pulse basis by utilizing a computer and making normal-mode calculations to determine the optimum receiver or source depth for each of the SUDS I propagation loss run sound-speed profiles and for each frequency. Comparison of the theoretical losses at the optimum depth with the theoretical losses for the 4- to 6-m receiver depths would establish the penalty for a hull-mounted sonar.

8. Develop techniques for the quantitative comparison between experiment and theory that will adequately account for a displacement between experimental and theoretical beats.

9. Study the problem of finding mode eigenvalues for multiple-channel profiles and for negative-gradient profiles, such as were encountered during the SUDS I propagation loss runs.

10. Investigate propagation at frequencies below the onset of trapping in surface channels. The theoretical analysis should compare the results of a surface channel model with those of a corresponding model of the entire ocean column.

11. Study the effect of wind speed on propagation loss by incorporating the rough surface correction contained in the rough surface natural-mode model (NUC WAVE) into the n-layer normal-mode model.

12. Assess the importance of thermal microstructure on propagation loss fluctuation by correlating propagation loss fluctuation with some measure of the variability of the sound-speed profile as determined from the thermistor chain temperature measurements.

13. Utilize the average values of the AMOS parameters listed in Table 12 in any application of the AMOS model to the SUDS I propagation loss measurements.

14. During SUDS I only a few XBT profiles were recorded by the receiver ship. In future experiments it is recommended that a greater number of XBT records be obtained.

REFERENCES

1. Naval Undersea Center, NUC TP 464, vols. I–V, Surface-Duct Sonar Measurements (SUDS I – 1972): Propagation Loss Measurements, E. R. Anderson, editor, April 1976.

2. Naval Undersea Center, NUC TP 465, vol. I–V, Surface-Duct Sonar Measurements (SUDS I – 1972): Oceanographic Measurements, by E. R. Anderson, January 1976.

3. Naval Undersea Center, NUC TN 883, vol. 1–5, Preliminary Data Report for Surface-Duct Sonar Measurements, Cruise I (SUDS I 1972), J. Cummins, editor, November 1972.

4. Naval Undersea Center, NUC TP 377, Comparison of Propagation Prediction Models with SUDS I Acoustic Data, by H. E. Morris, April 1974.

5. U. S. Naval Underwater Sound Laboratory, USL Report 255A, Report on the Status of Project AMOS (Acoustic, Meteorological, and Oceanographic Survey), by H. W. Marsh and M. Schulkin, March 1955 (revised May 1967).

6. Navy Electronics Laboratory, NEL R&D Report 559, Results of a Long-Range 530-cps Underwater Sound Transmission Experiment, by M. A. Pedersen, E. R. Anderson, J. F. Kidd, and R. M. Lesser, 17 January 1955.

7. Navy Electronics Laboratory, NEL RP 1407, A Normal Mode Approach to Underwater Sound Propagation, by M. A. Pedersen and D. F. Gordon, 27 September 1966.

8. M. A. Pedersen and D. F. Gordon, "Normal Mode Theory Applied to Short-Range Propagation in an Underwater Acoustic Surface Duct," *J. Acoust. Soc. Am.*, vol. 37, pp. 105–118, 1965.

9. Reference available to qualified requesters.

10. Arthur D. Little, Inc., Report No. 4171166, Acoustic Transmission in an Ocean Surface Duct, November 1966.

11. Lockheed-California Company, Report No. 20556, Normal Mode Propagation Study, May 1967.

12. Naval Undersea Research and Development Center, NUC TP 243, Sound Speed in Seawater as a Function of Realistic Temperature-Salinity-Pressure Domains, by E. R. Anderson, August 1971.

13. Reference available to qualified requesters.

14. Naval Undersea Center, NUC TR 301, vol. II, Gulf of Alaska Sonar Tests: April-August 1971: STD/SV, SVTP, and XBT Data Report, by E. R. Anderson and J. R. Lovett, August 1972.

15. Reference available to qualified requesters.

16. Lockheed-California Company, LR 25432, Teletherm Buoy Data Report: Support for Acoustic Model Validation, by D. P. Hamm and L. D. Coates.

17. J. W. Cooley and J. W. Tukey, "An Algorithm for the Machine Calculation of Complex Fourier Series," *Mathematical Computation*, vol. 19, pp. 297–301, 1965.

18. Naval Undersea Center, NUC TR 301, vol. III, Gulf of Alaska Sonar Test Results: April-August 1971: Comparison of Measured and Computed Sound Speeds, by E. R. Anderson, December 1972.

19. Reference available to qualified requesters.

20. Reference available to qualified requesters.

21. Tappert, F. D. and R. H. Hardin, A Synopsis of the AESD Workshop in Acoustic Modeling by Non Ray Techniques, 22–25 May 1973, Washington, D.C., AESD TN-73-05, ONR, Arlington, VA., November 1973.

22. Benthien, G. W. and D. F. Gordon, "Comparison of the Parabolic Equation Method with Other Propagation Loss Models," *J. Acoust. Soc. Am.*, vol. 55: S45(A), 1974.

23. Naval Undersea Center NUC TP 488, Low-Frequency Propagation Effects for Sources or Receivers Near the Ocean Surface, by M. A. Pedersen, D. F. Gordon, and D. White, September 1975.

24. Cummins, J., "Surface Duct Propagation Loss Measurements," *J. Acoust. Soc. Am.*, vol. 55: S56(A) (abstract), 1974.

25. Thorp, W. H., "Analytic Description of the Low-Frequency Attenuation Coefficient," *J. Acoust. Soc. Am.*, vol. 42: 270, July 1967.

26. Reference available to qualified requesters.

APPENDIX A

SEASONAL VARIATION IN TEMPERATURE, SALINITY, AND COMPUTED SOUND SPEED OBSERVED IN 1949

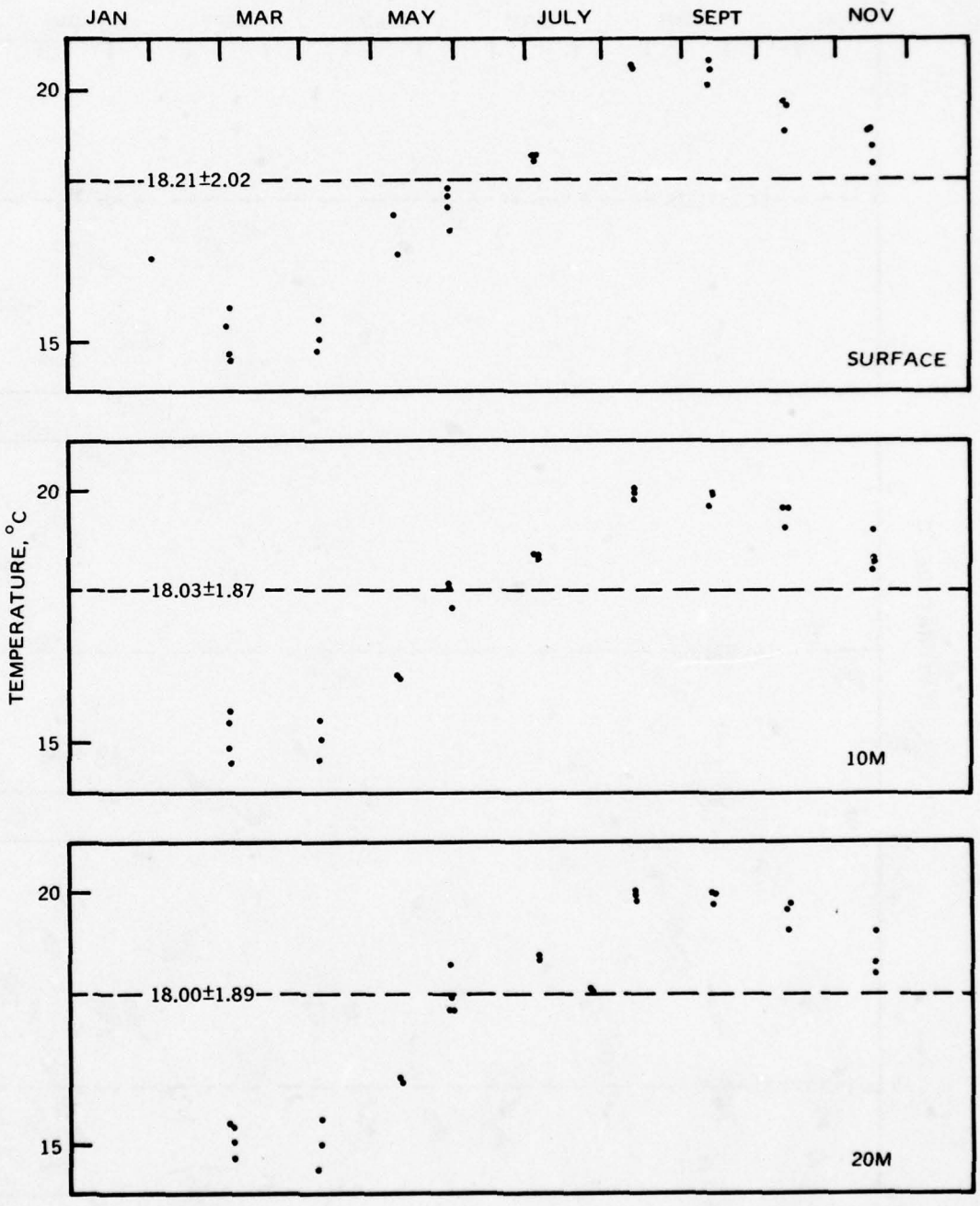
JAN
MAR
MAY
JULY
SEPT
NOV
20
15
18.21±2.02
SURFACE
TEMPERATURE, °C
18.03±1.87
10M
18.00±1.89
20M

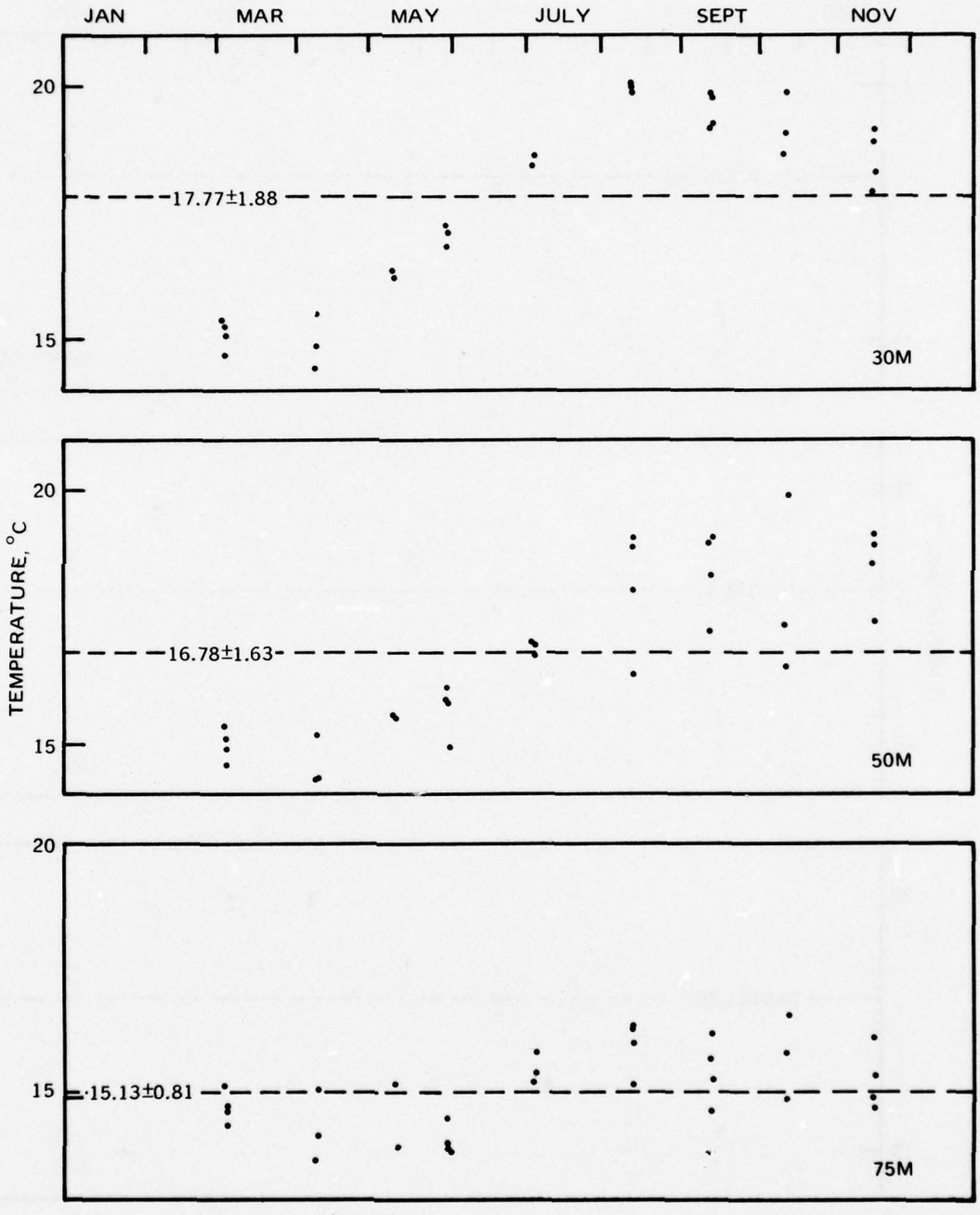
JAN
MAR
MAY
JULY
SEPT
NOV
20
15
17.77±1.88
30M
20
15
16.78±1.63
50M
TEMPERATURE, °C
20
15
15.13±0.81
75M

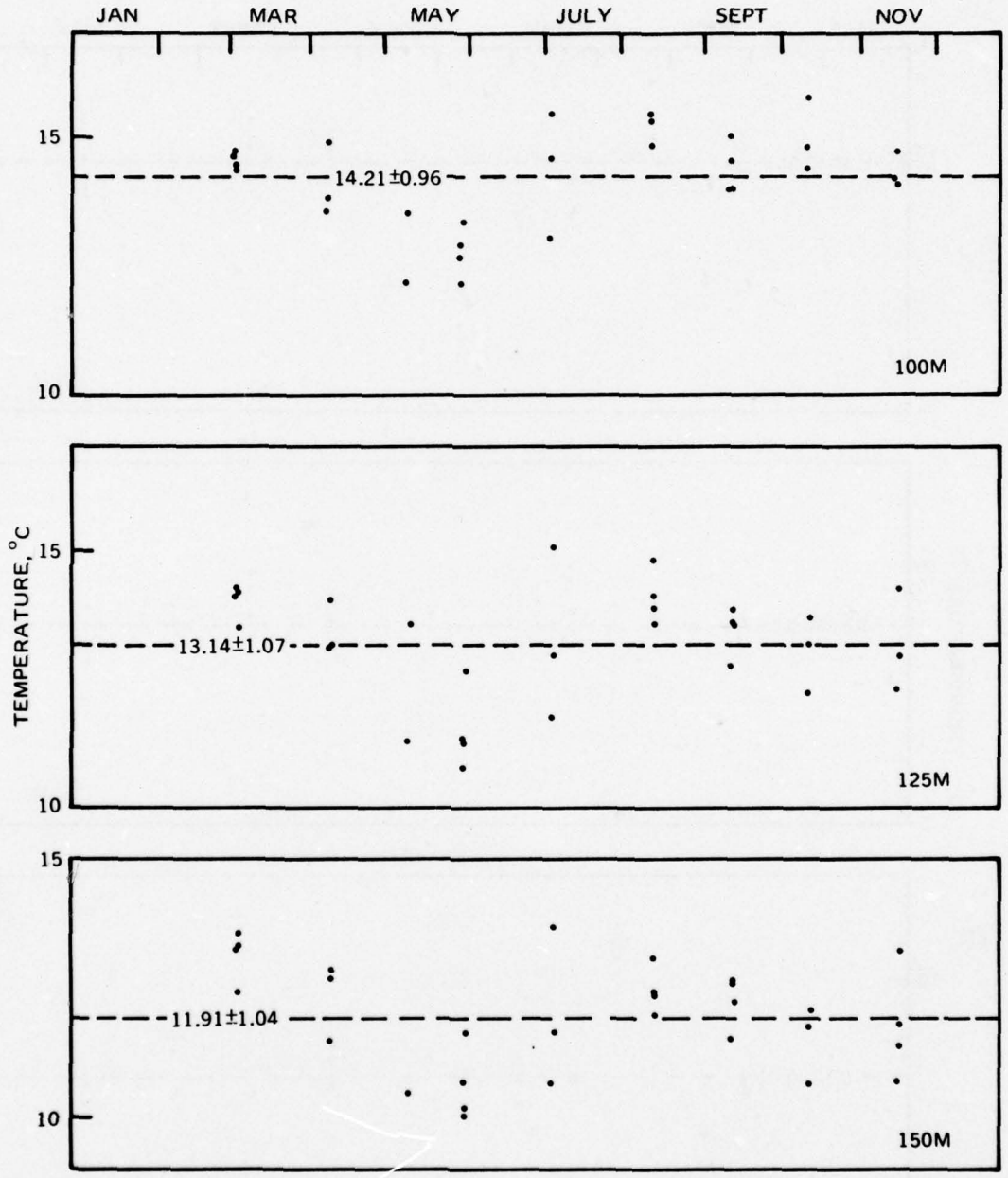
JAN
MAR
MAY
JULY
SEPT
NOV
15
14.21±0.96
10
100M
TEMPERATURE, °C
15
13.14±1.07
10
125M
15
11.91±1.04
10
150M

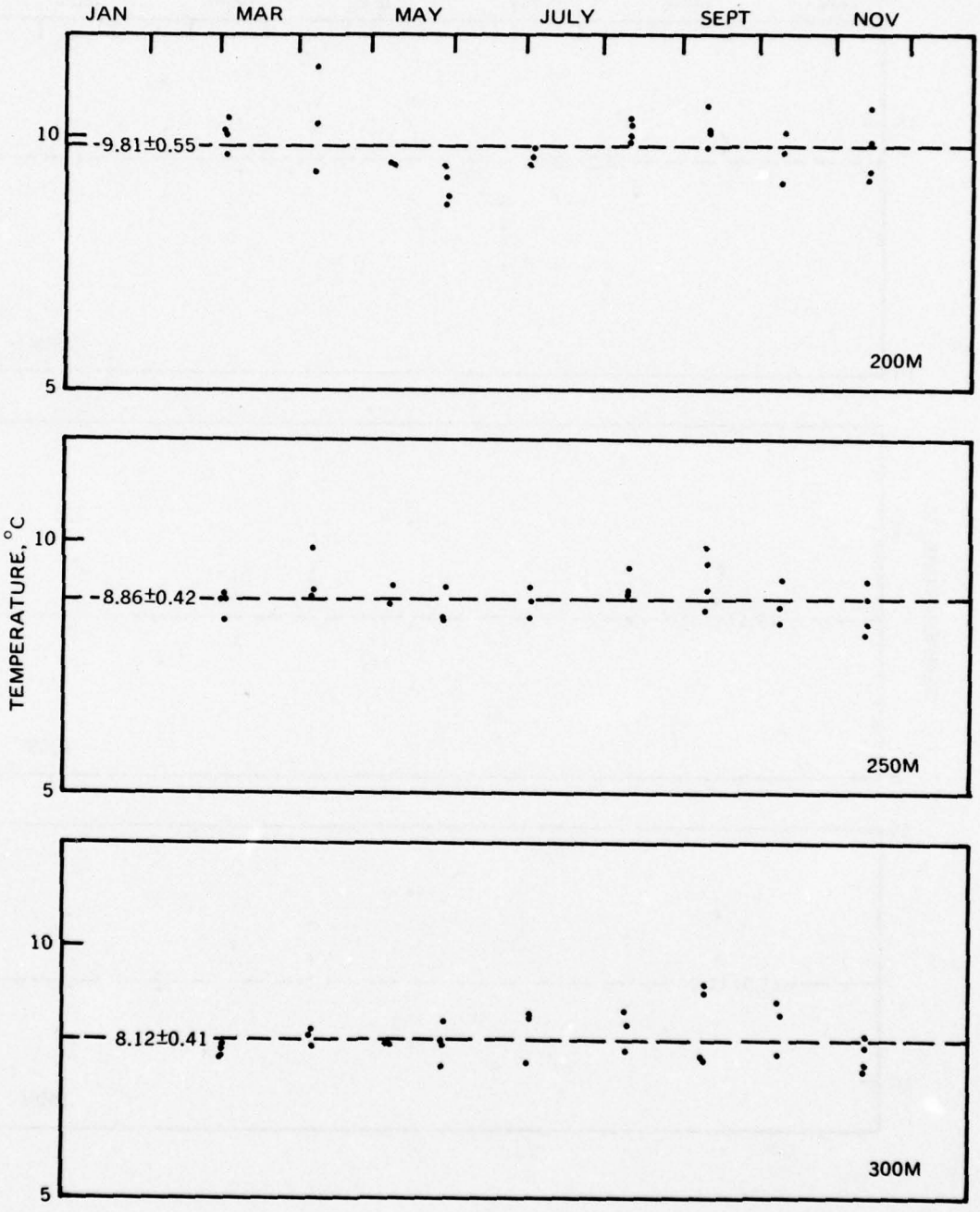
JAN
MAR
MAY
JULY
SEPT
NOV
10
-9.81±0.55
5
200M
TEMPERATURE, °C
10
-8.86±0.42
5
250M
10
8.12±0.41
5
300M

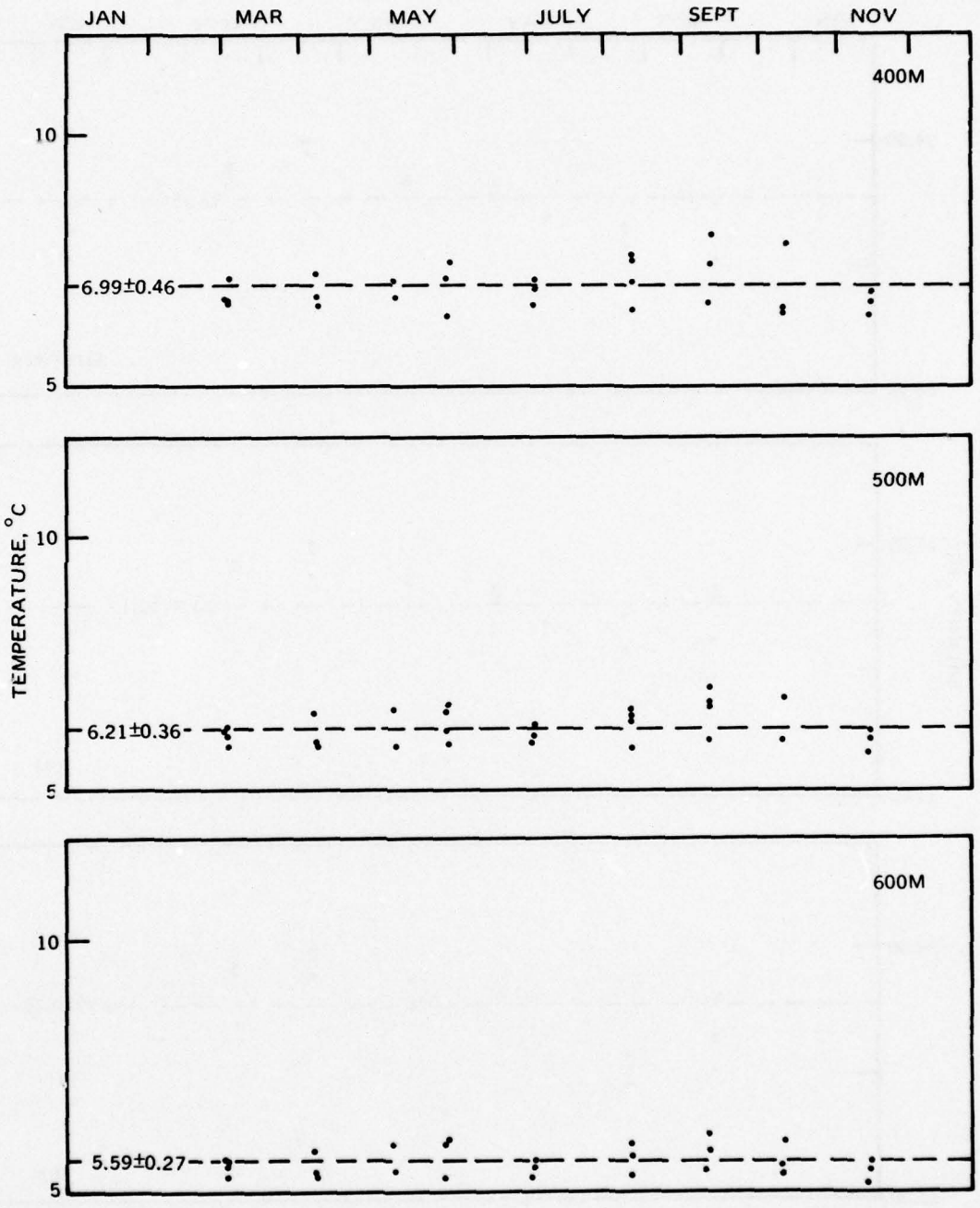
JAN
MAR
MAY
JULY
SEPT
NOV
400M
10
6.99±0.46
5
500M
TEMPERATURE, °C
10
6.21±0.36
5
600M
10
5.59±0.27
5

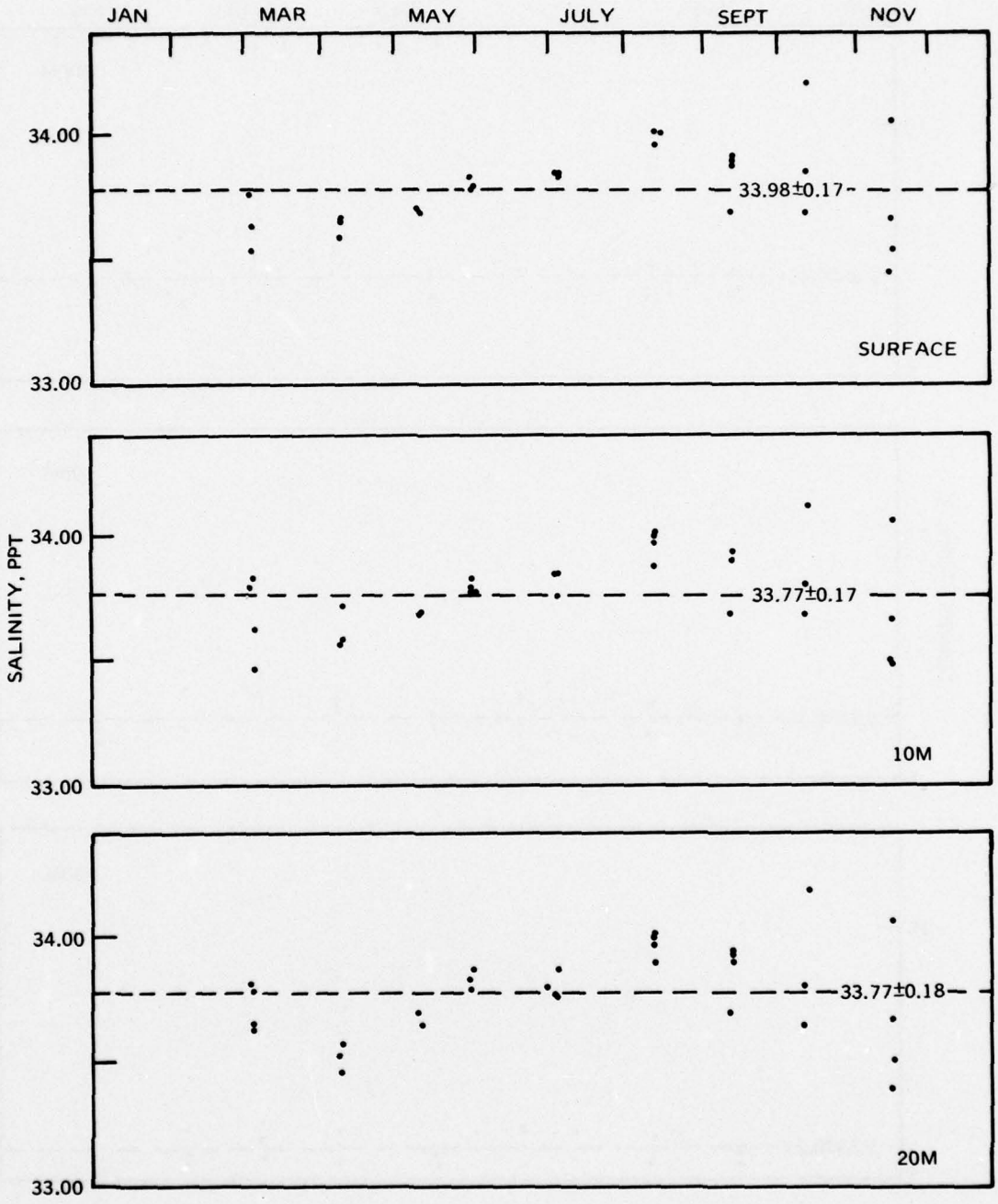
JAN
MAR
MAY
JULY
SEPT
NOV
34.00
33.00
33.98±0.17
SURFACE
SALINITY, PPT
34.00
33.00
33.77±0.17
10M
34.00
33.00
33.77±0.18
20M

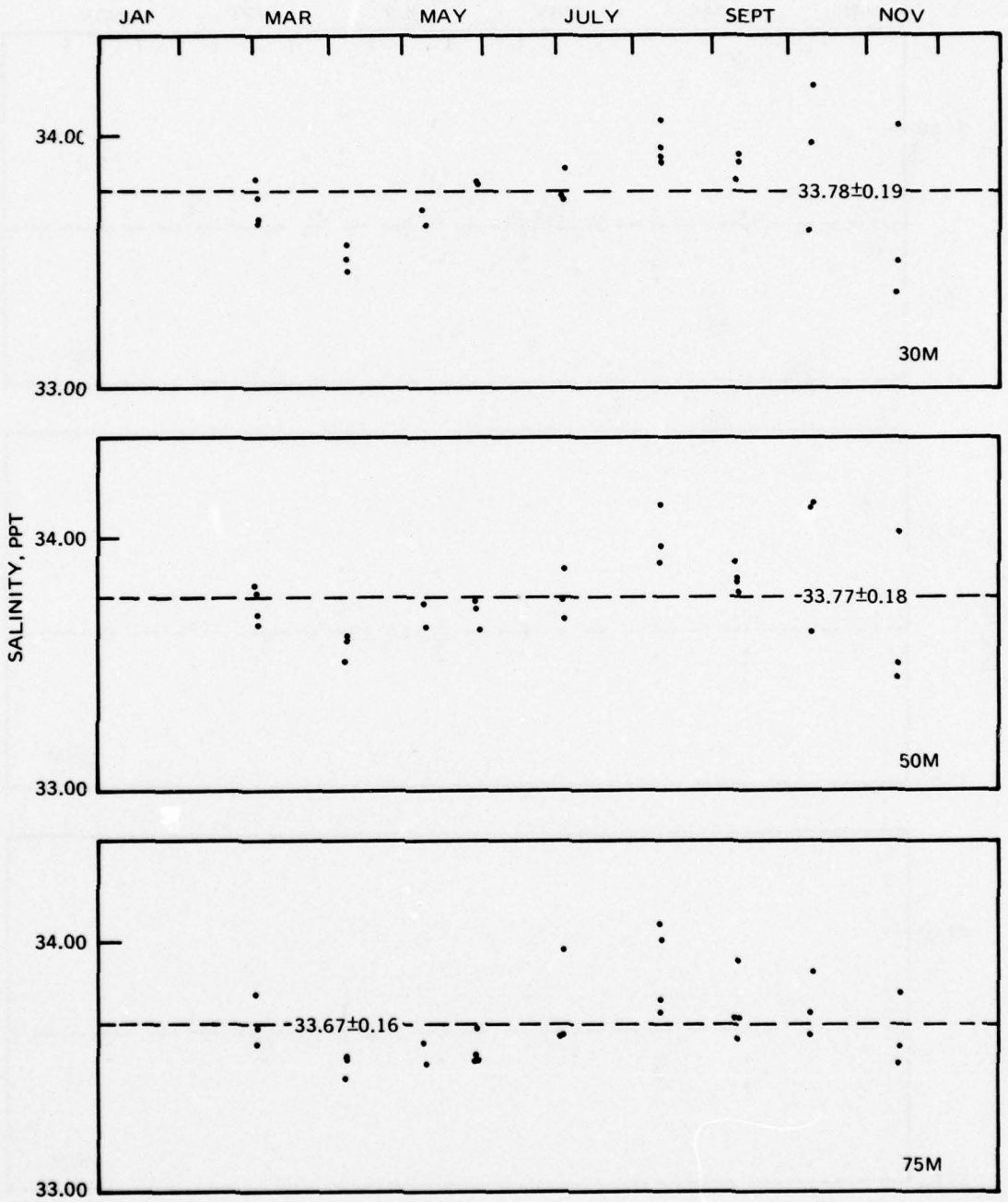
JAN
MAR
MAY
JULY
SEPT
NOV
34.00
33.78±0.19
30M
33.00
SALINITY, PPT
34.00
33.77±0.18
50M
33.00
34.00
33.67±0.16
75M
33.00

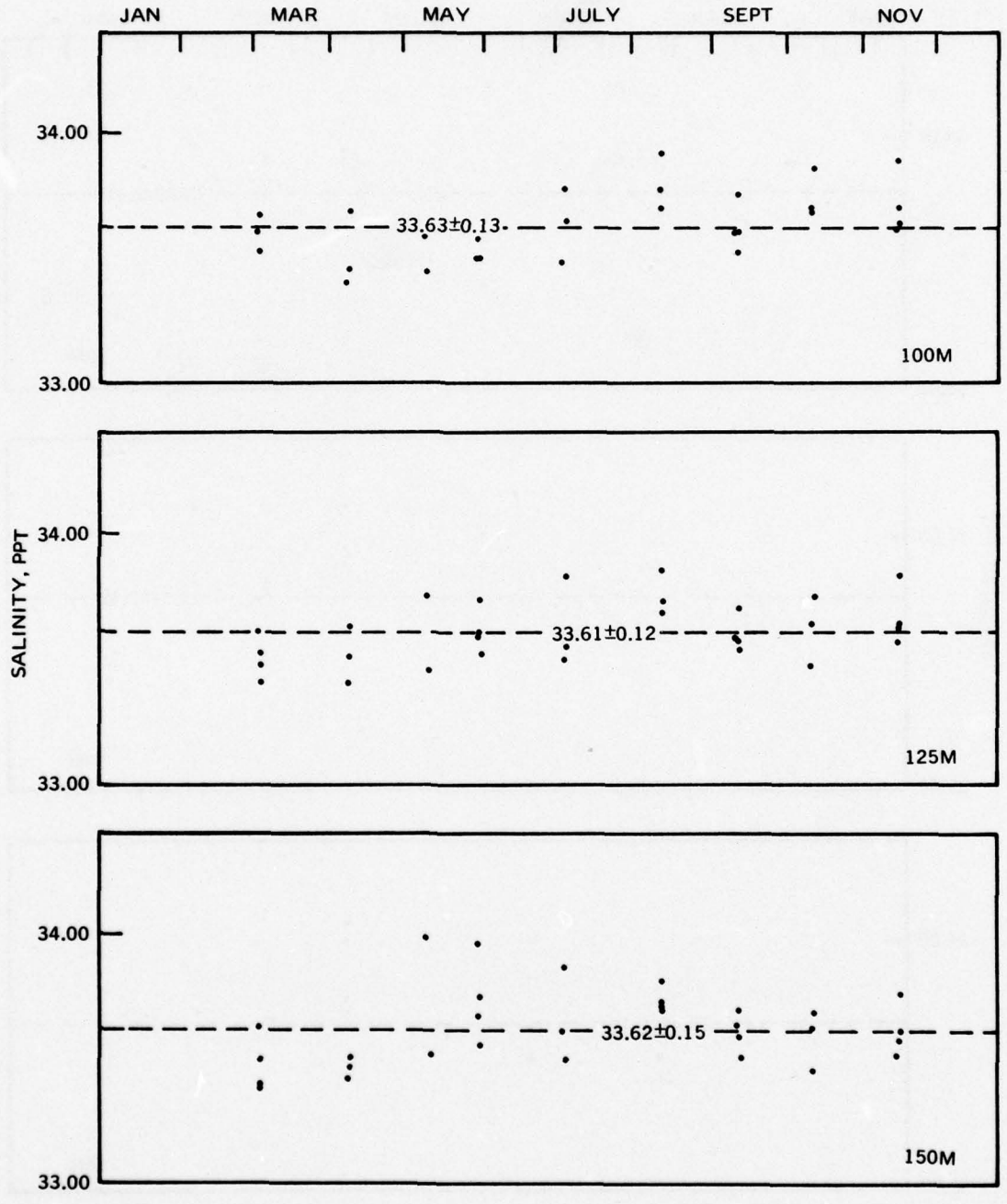
JAN
MAR
MAY
JULY
SEPT
NOV
34.00
33.63±0.13
33.00
100M
SALINITY, PPT
34.00
33.61±0.12
33.00
125M
34.00
33.62±0.15
33.00
150M

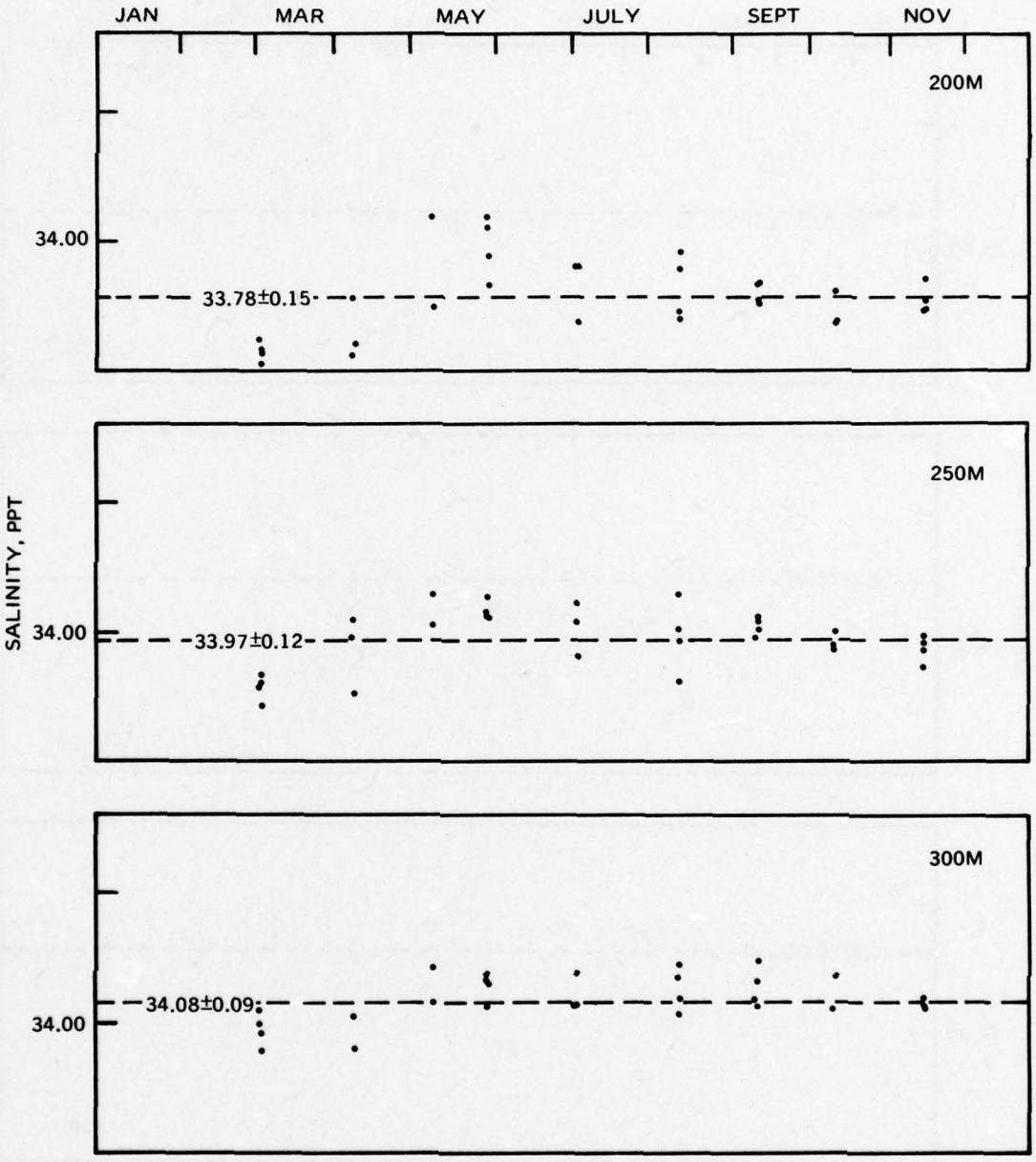
JAN
MAR
MAY
JULY
SEPT
NOV
200M
34.00
33.78±0.15
250M
SALINITY, PPT
34.00
33.97±0.12
300M
34.00
34.08±0.09

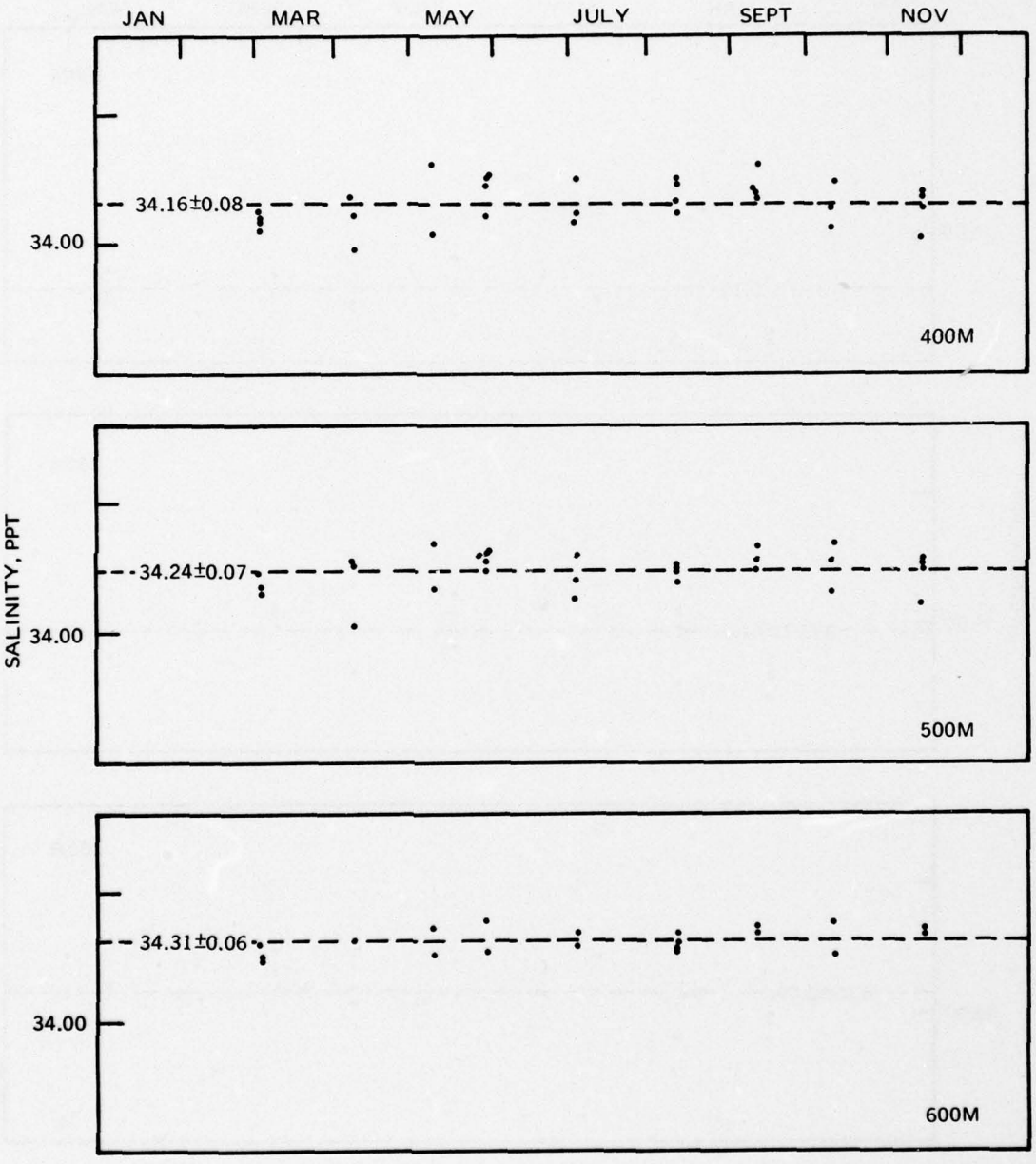
JAN
MAR
MAY
JULY
SEPT
NOV
34.16±0.08
34.00
400M
SALINITY, PPT
34.24±0.07
34.00
500M
34.31±0.06
34.00
600M

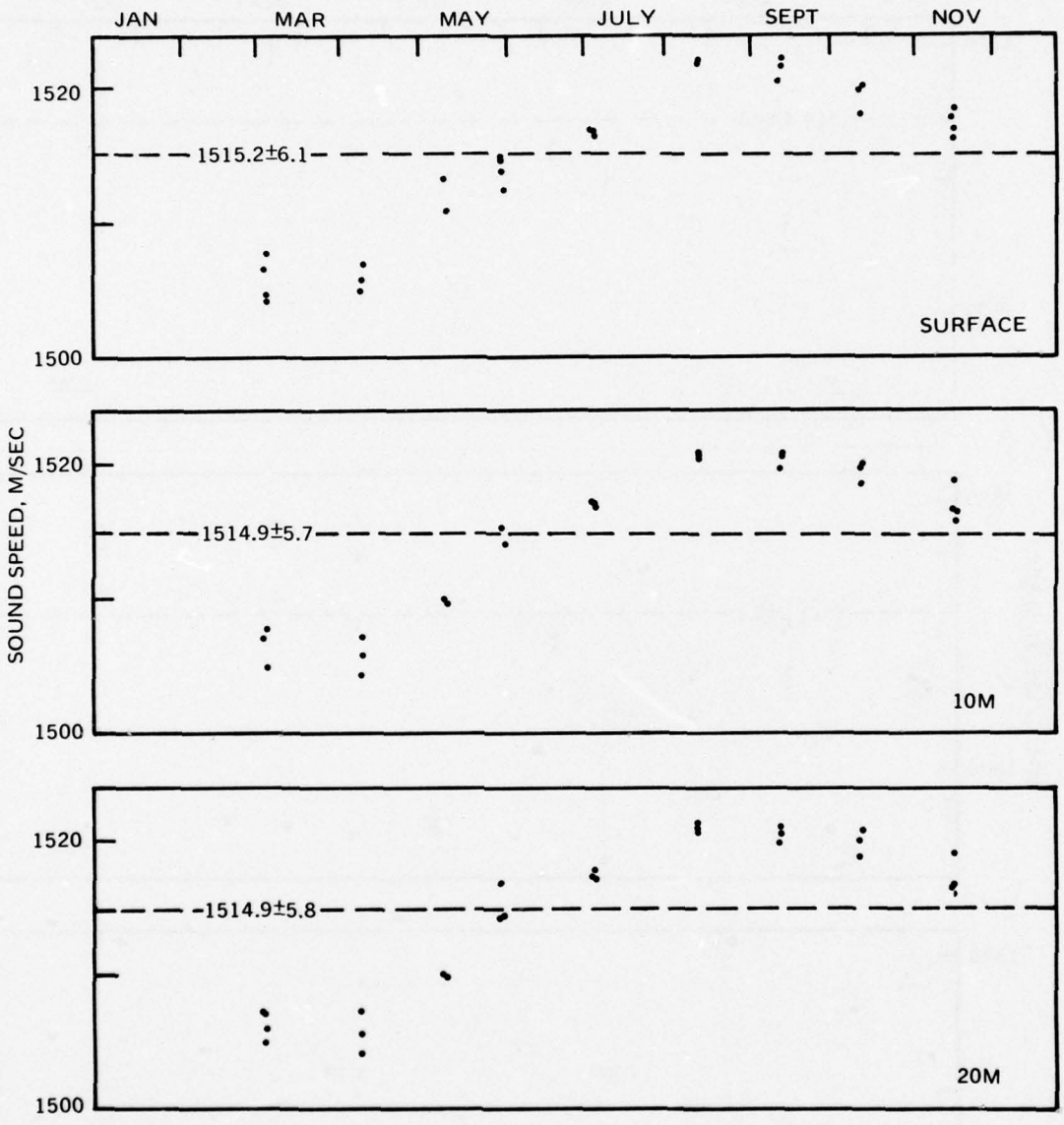
JAN
MAR
MAY
JULY
SEPT
NOV
1520
1515.2±6.1
1500
SURFACE
SOUND SPEED, M/SEC
1520
1514.9±5.7
1500
10M
1520
1514.9±5.8
1500
20M

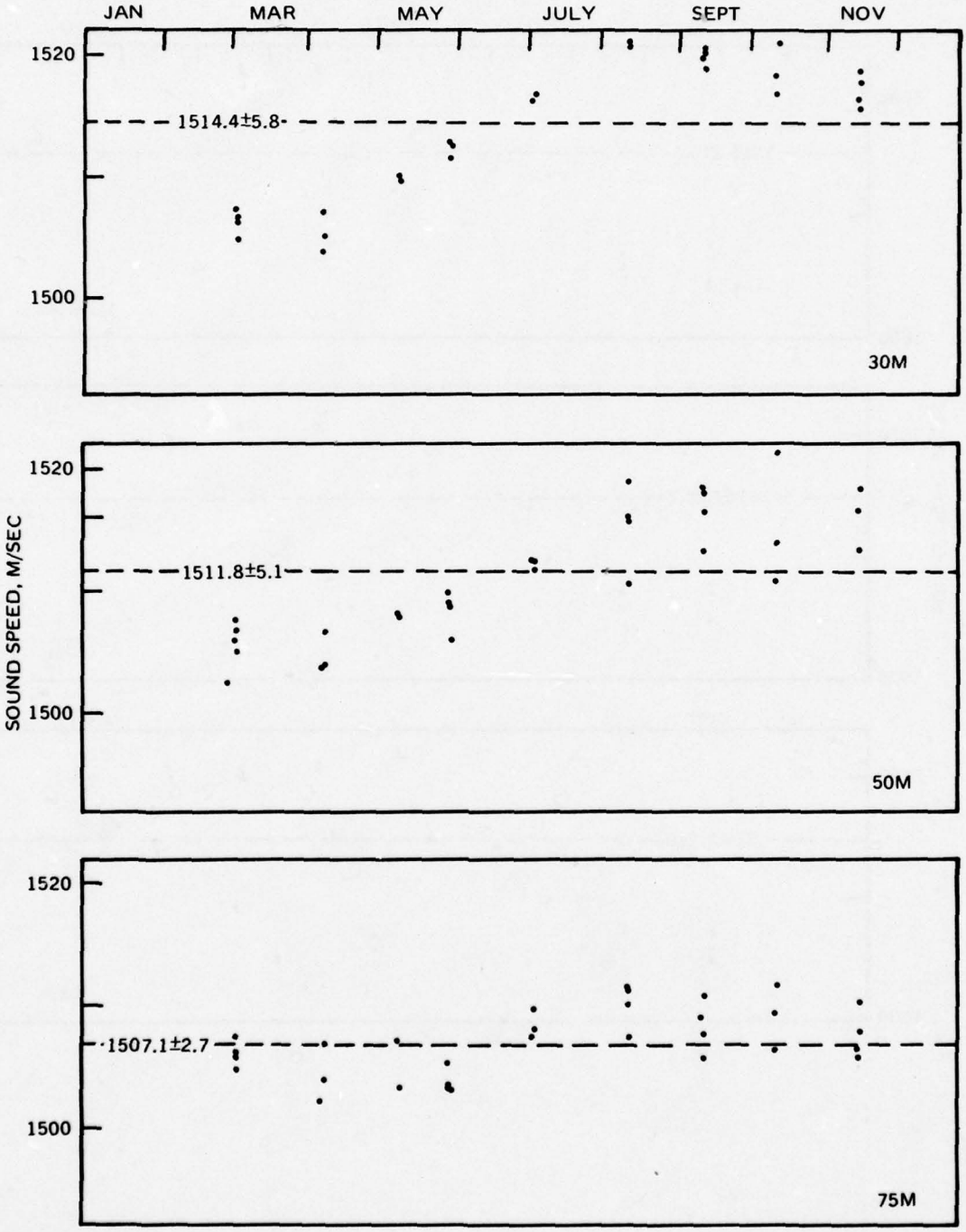
JAN
MAR
MAY
JULY
SEPT
NOV
1520
1514.4±5.8
1500
30M
SOUND SPEED, M/SEC
1520
1511.8±5.1
1500
50M
1520
1507.1±2.7
1500
75M

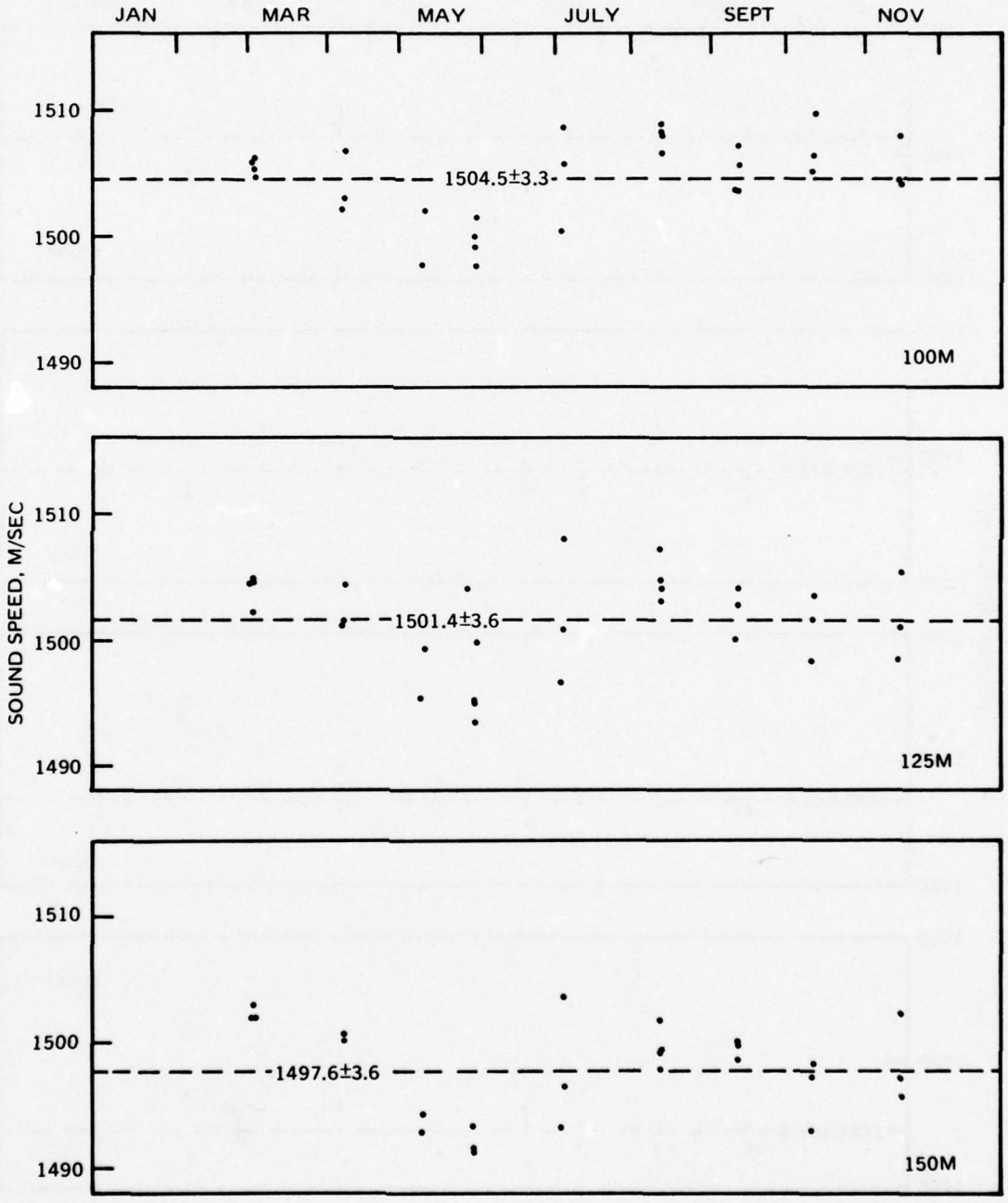
JAN
MAR
MAY
JULY
SEPT
NOV
1510
1500
1490
1504.5±3.3
100M
SOUND SPEED, M/SEC
1510
1500
1490
1501.4±3.6
125M
1510
1500
1490
1497.6±3.6
150M

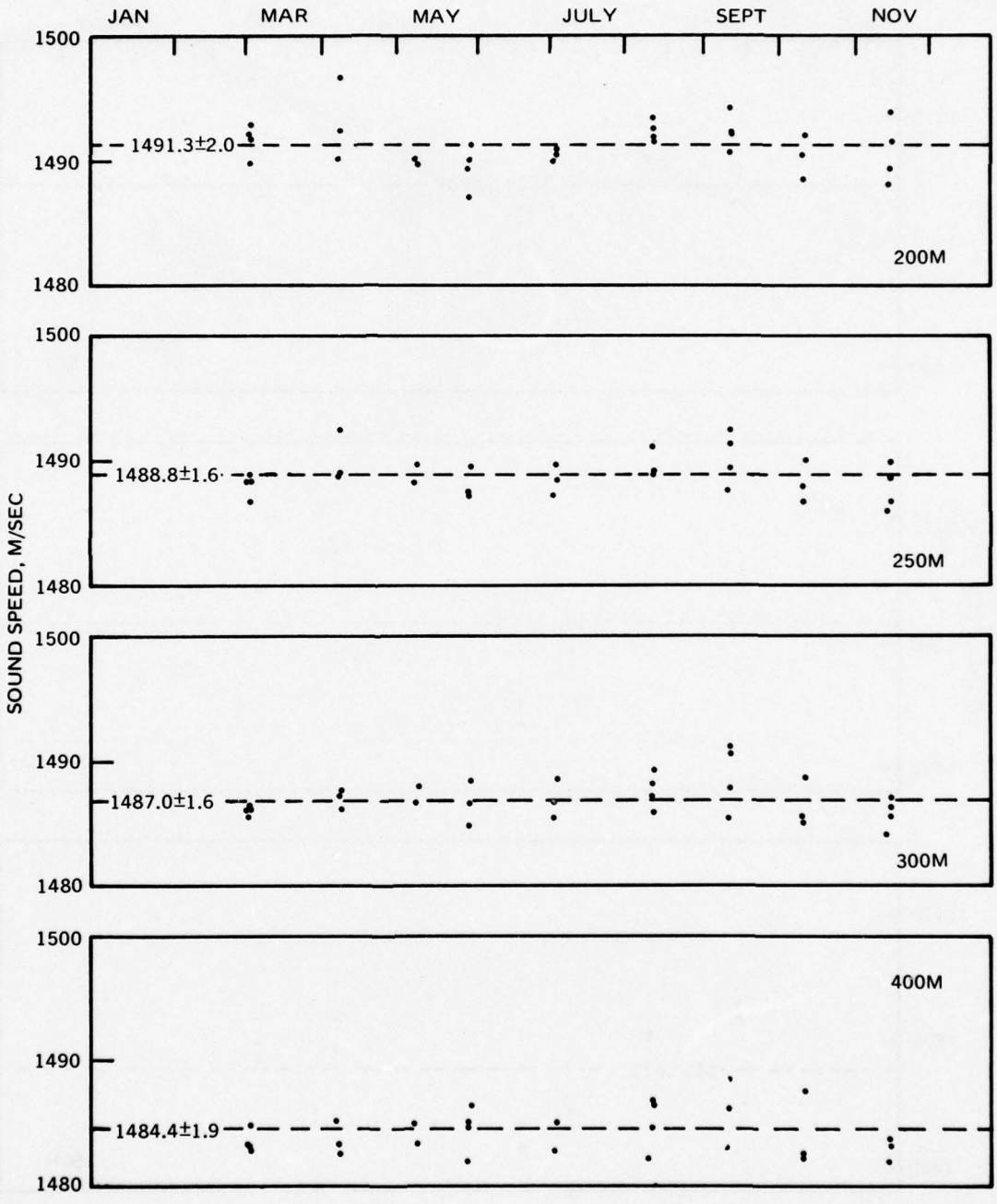
JAN
MAR
MAY
JULY
SEPT
NOV
SOUND SPEED, M/SEC
1500
1490
1480
1491.3±2.0
200M
1488.8±1.6
250M
1487.0±1.6
300M
1484.4±1.9
400M

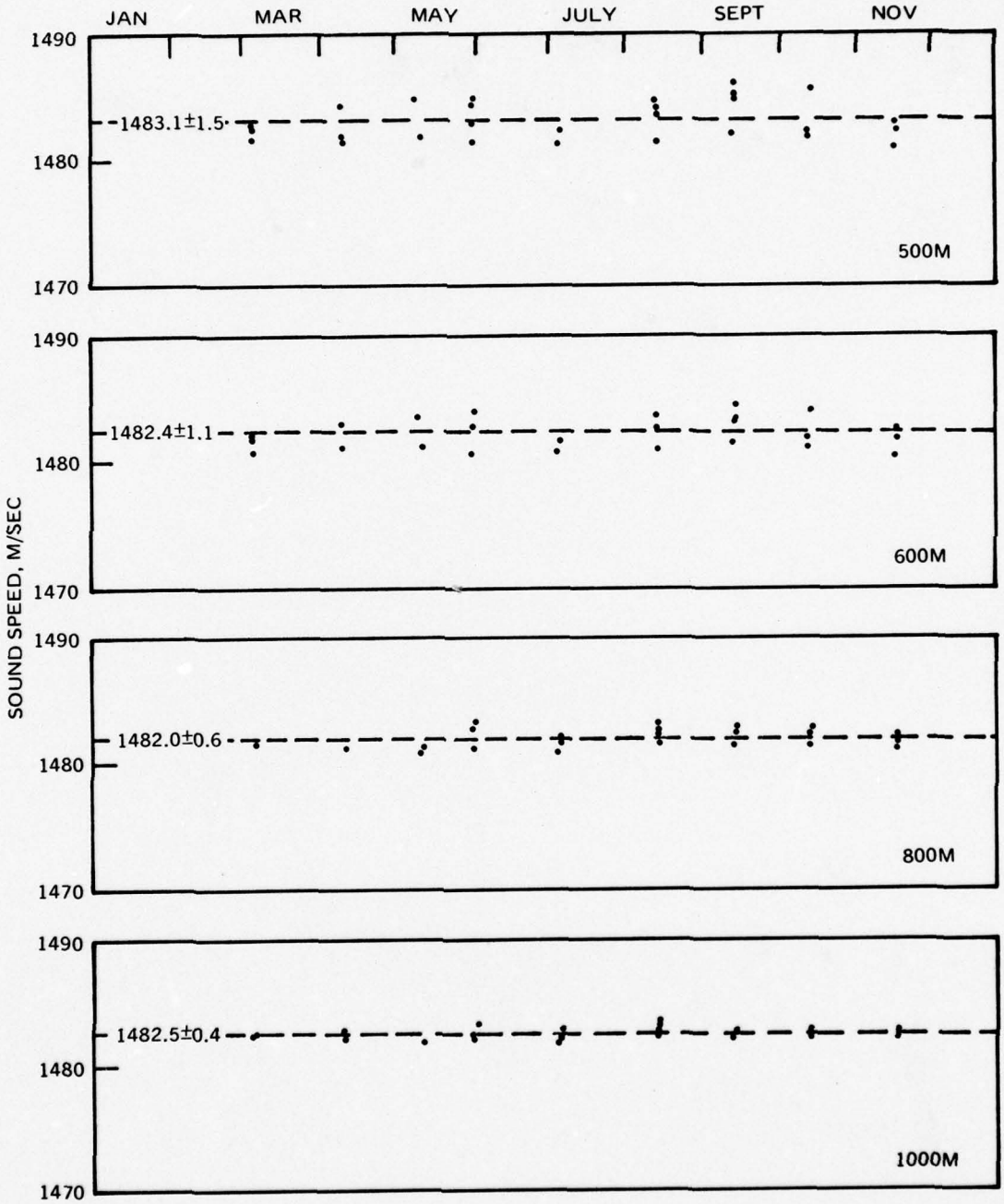
JAN
MAR
MAY
JULY
SEPT
NOV
SOUND SPEED, M/SEC
1490
1480
1470
1483.1±1.5
500M
1482.4±1.1
600M
1482.0±0.6
800M
1482.5±0.4
1000M

APPENDIX B

EXPERIMENTAL AND THEORETICAL PROPAGATION LOSSES FOR STATION 4 RUN 4

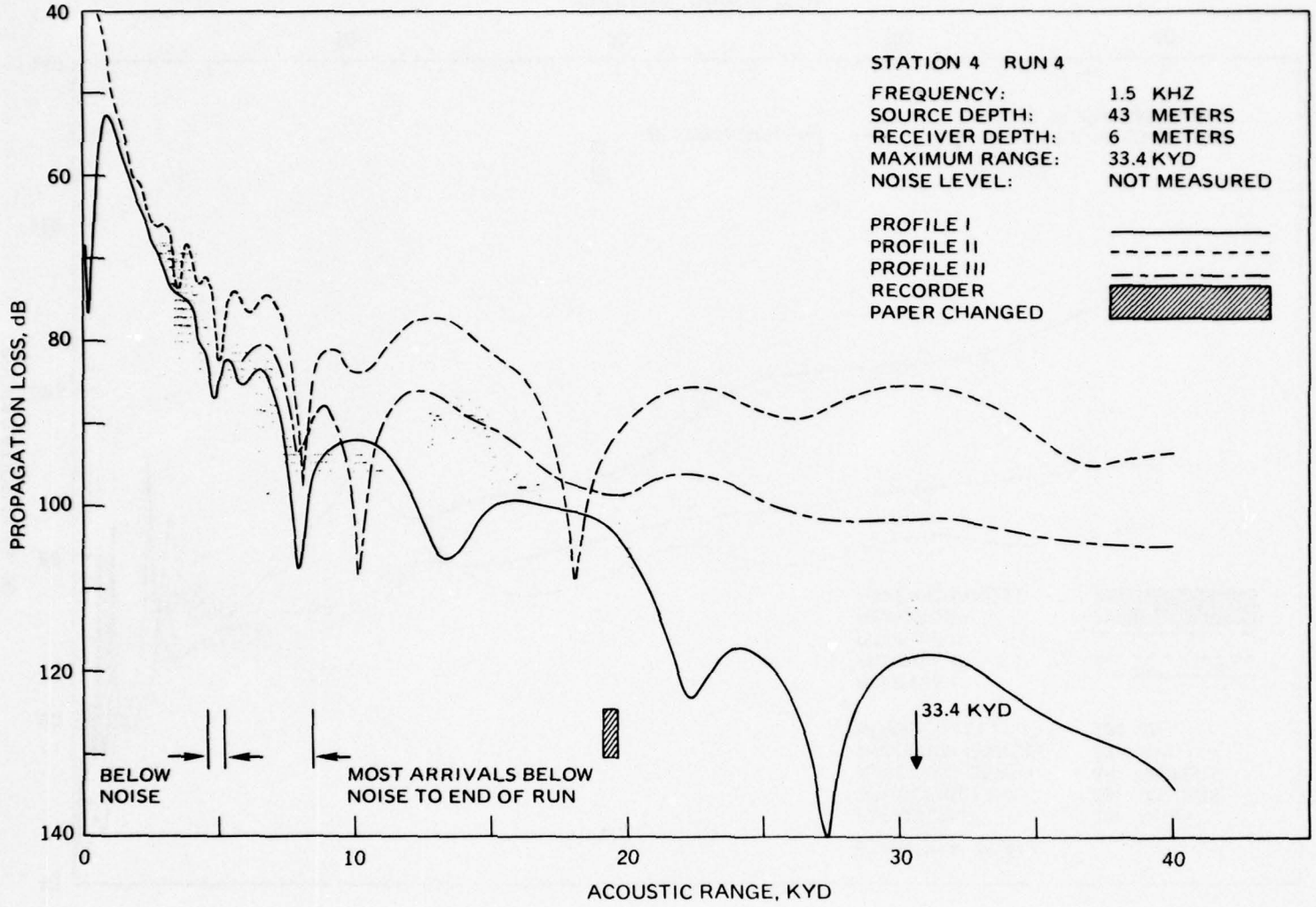
STATION 4 RUN 4
FREQUENCY: 1.5 KHZ
SOURCE DEPTH: 43 METERS
RECEIVER DEPTH: 6 METERS
MAXIMUM RANGE: 33.4 KYD
NOISE LEVEL: NOT MEASURED
PROFILE I
PROFILE II
PROFILE III
RECORDER PAPER CHANGED
PROPAGATION LOSS, dB
40
60
80
100
120
140
0
10
20
30
40
ACOUSTIC RANGE, KYD
33.4 KYD
BELOW NOISE
MOST ARRIVALS BELOW NOISE TO END OF RUN

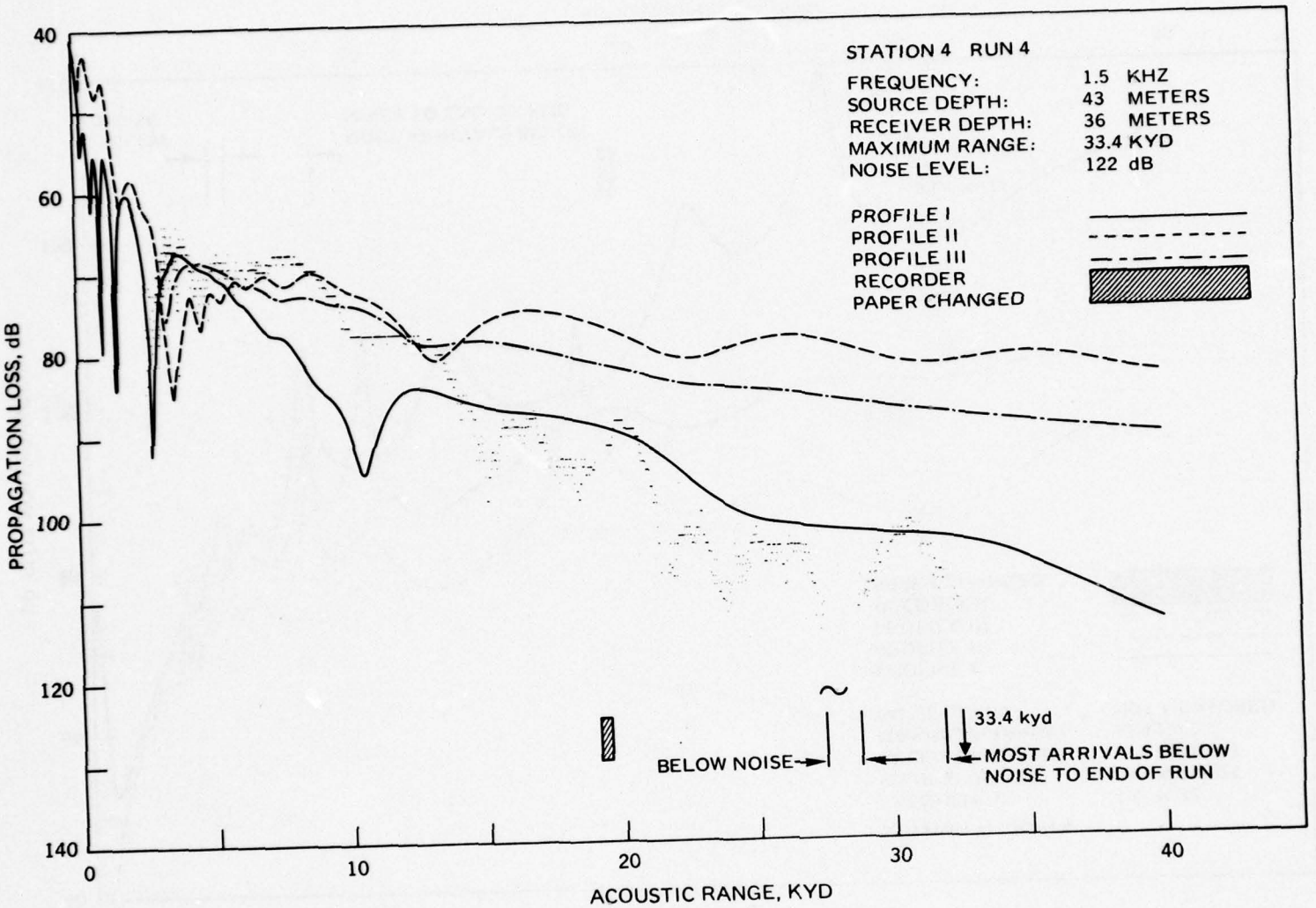
STATION 4 RUN 4
FREQUENCY: 1.5 KHZ
SOURCE DEPTH: 43 METERS
RECEIVER DEPTH: 36 METERS
MAXIMUM RANGE: 33.4 KYD
NOISE LEVEL: 122 dB
PROFILE I
PROFILE II
PROFILE III
RECORDER PAPER CHANGED
PROPAGATION LOSS, dB
40
60
80
100
120
140
0
10
20
30
40
ACOUSTIC RANGE, KYD
33.4 kyd
BELOW NOISE
MOST ARRIVALS BELOW NOISE TO END OF RUN

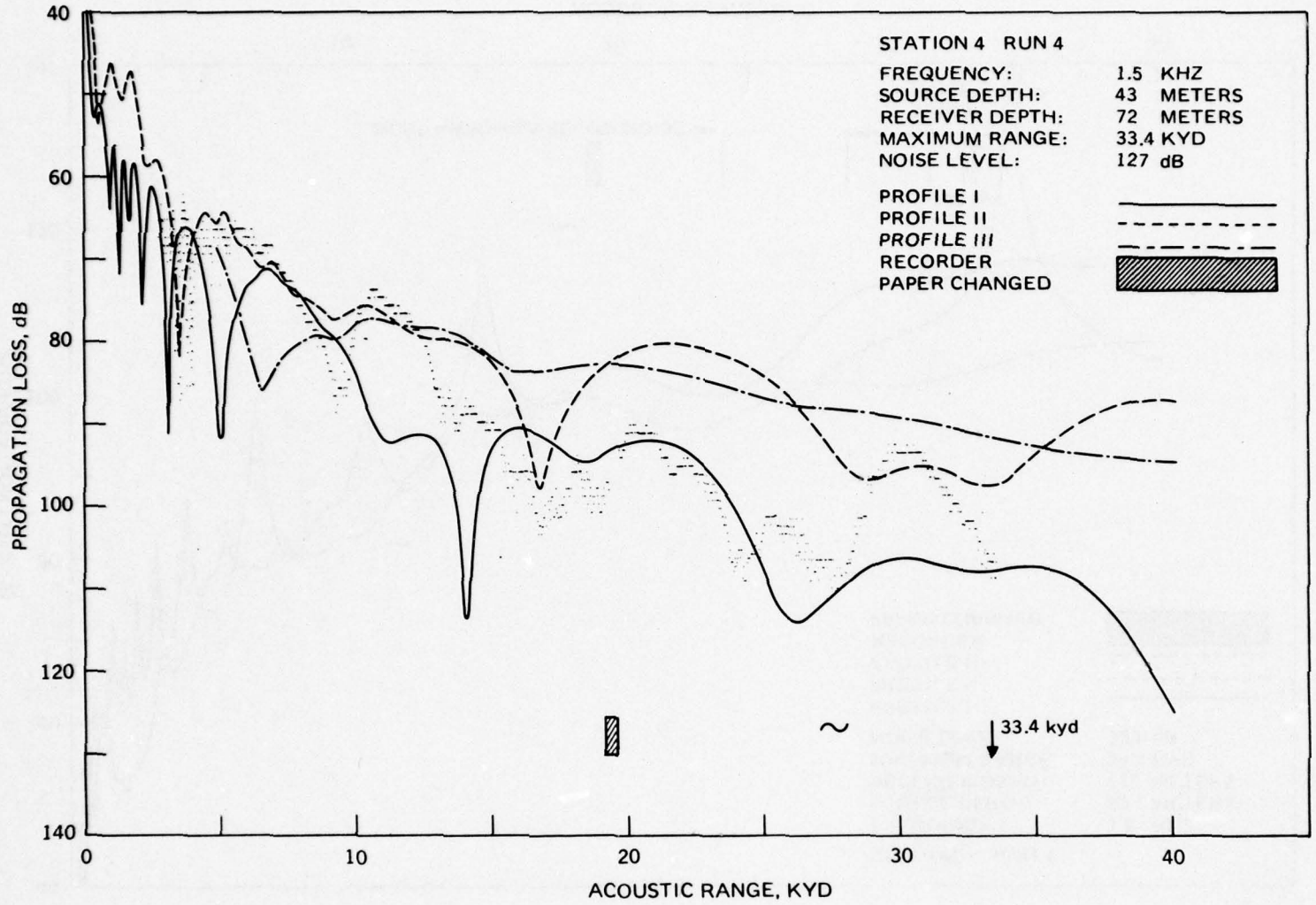
STATION 4 RUN 4
FREQUENCY: 1.5 KHZ
SOURCE DEPTH: 43 METERS
RECEIVER DEPTH: 72 METERS
MAXIMUM RANGE: 33.4 KYD
NOISE LEVEL: 127 dB
PROFILE I
PROFILE II
PROFILE III
RECORDER PAPER CHANGED
33.4 kyd
PROPAGATION LOSS, dB
ACOUSTIC RANGE, KYD
40
60
80
100
120
140
0
10
20
30
40

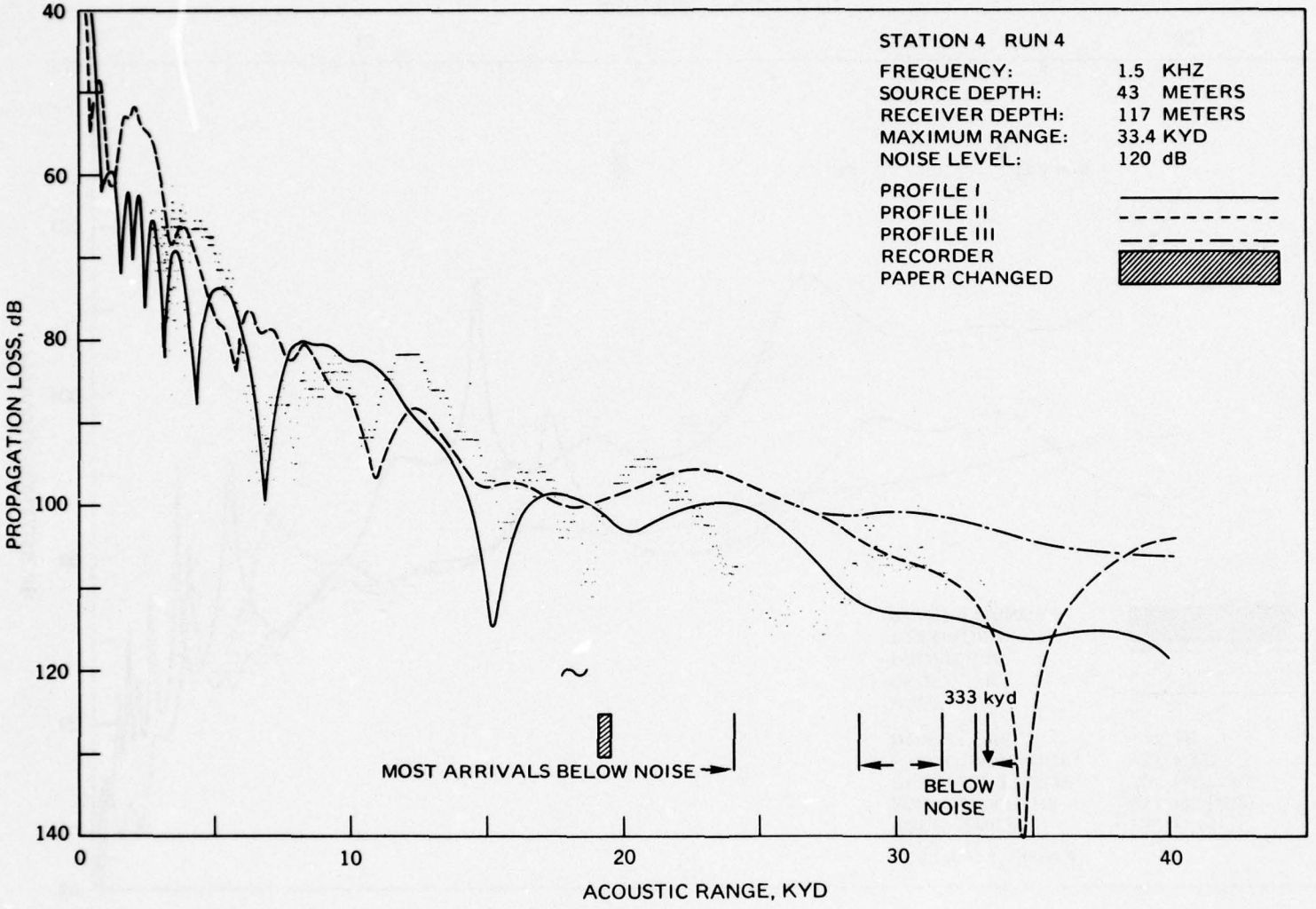
STATION 4 RUN 4
FREQUENCY: 1.5 KHZ
SOURCE DEPTH: 43 METERS
RECEIVER DEPTH: 117 METERS
MAXIMUM RANGE: 33.4 KYD
NOISE LEVEL: 120 dB
PROFILE I
PROFILE II
PROFILE III
RECORDER PAPER CHANGED
PROPAGATION LOSS, dB
40
60
80
100
120
140
0
10
20
30
40
ACOUSTIC RANGE, KYD
MOST ARRIVALS BELOW NOISE
333 kyd
BELOW NOISE

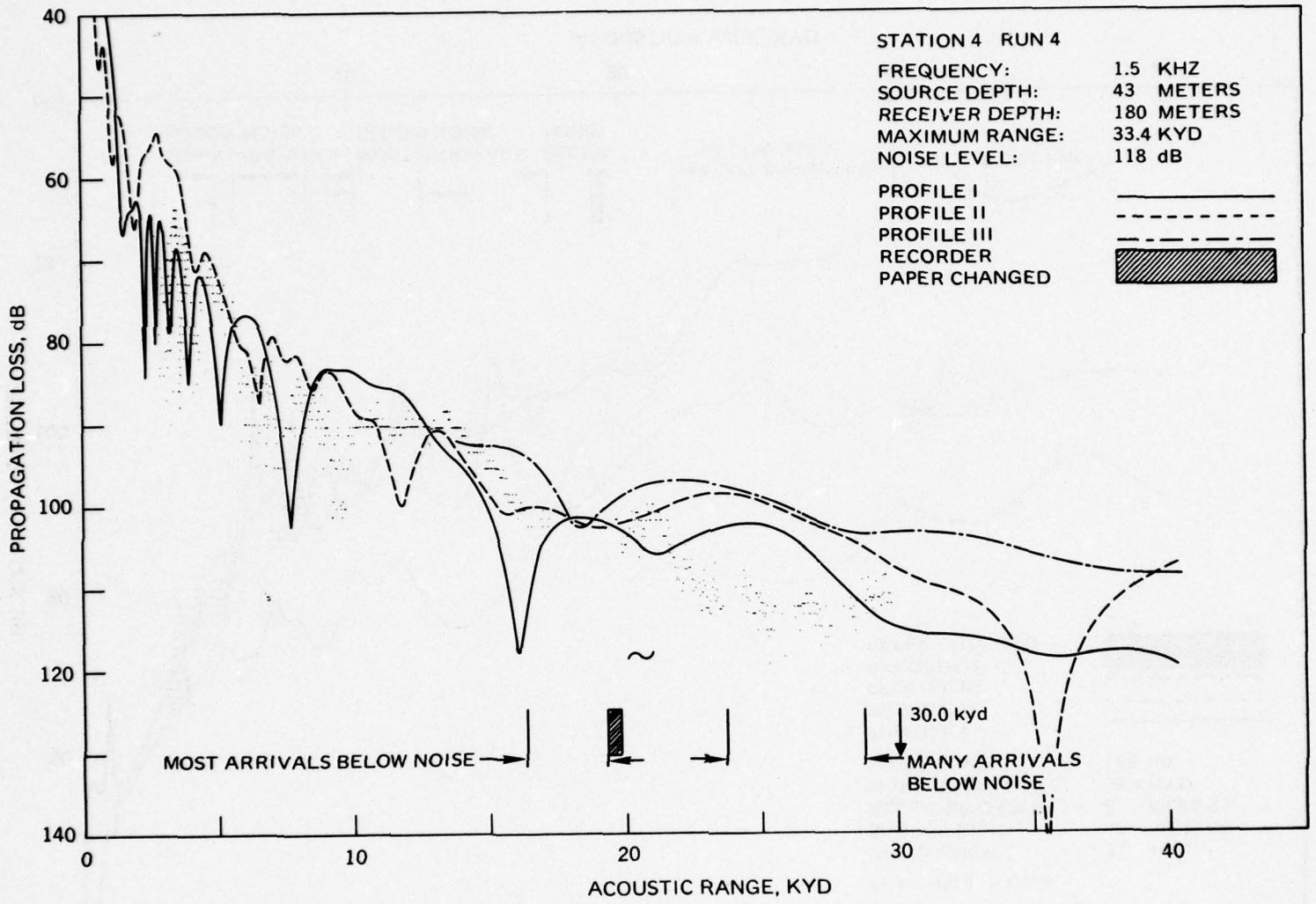
STATION 4 RUN 4
FREQUENCY: 1.5 KHZ
SOURCE DEPTH: 43 METERS
RECEIVER DEPTH: 180 METERS
MAXIMUM RANGE: 33.4 KYD
NOISE LEVEL: 118 dB
PROFILE I
PROFILE II
PROFILE III
RECORDER PAPER CHANGED
PROPAGATION LOSS, dB
40
60
80
100
120
140
0
10
20
30
40
ACOUSTIC RANGE, KYD
MOST ARRIVALS BELOW NOISE
30.0 kyd
MANY ARRIVALS BELOW NOISE

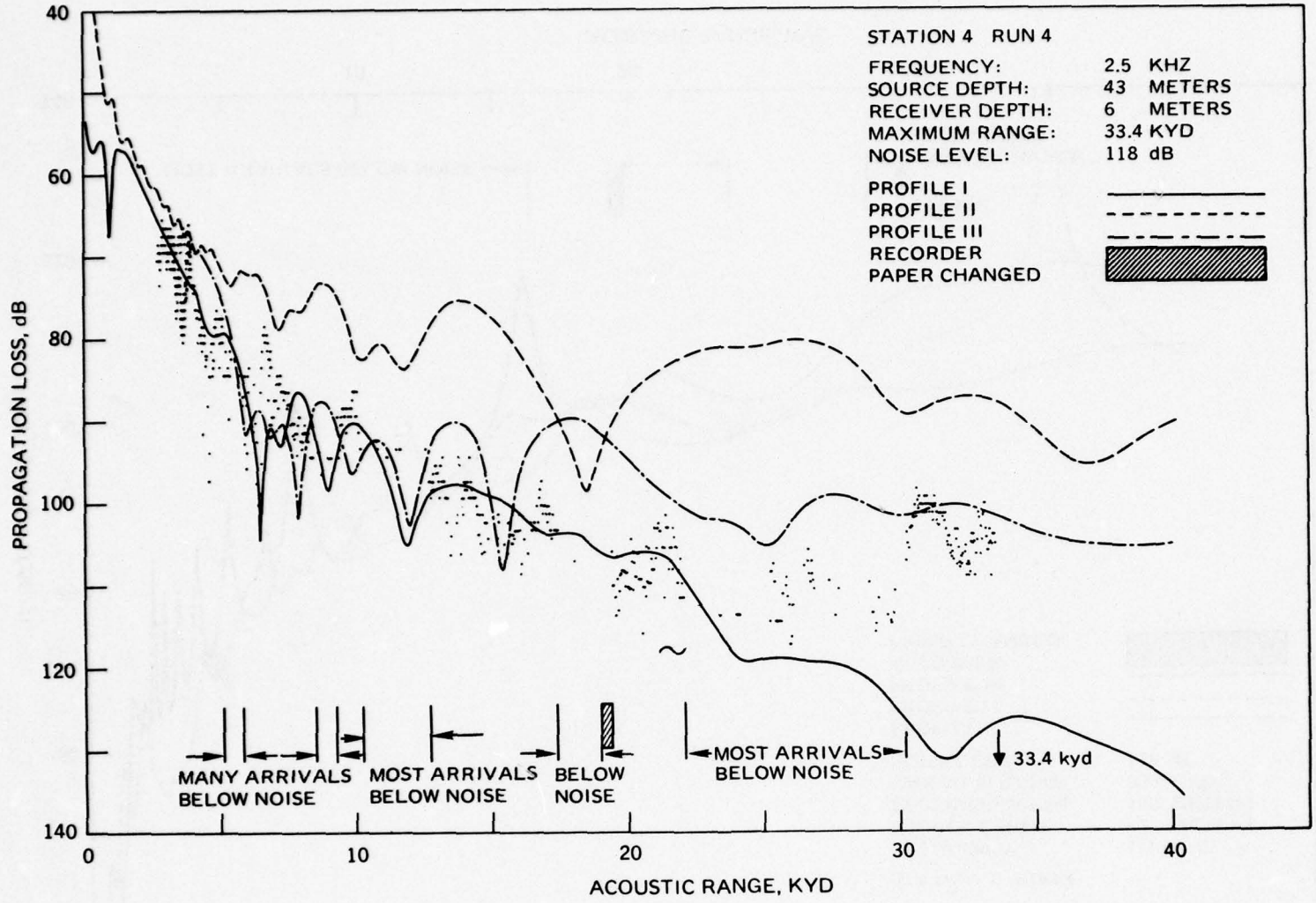
STATION 4 RUN 4
FREQUENCY: 2.5 KHZ
SOURCE DEPTH: 43 METERS
RECEIVER DEPTH: 6 METERS
MAXIMUM RANGE: 33.4 KYD
NOISE LEVEL: 118 dB
PROFILE I
PROFILE II
PROFILE III
RECORDER PAPER CHANGED
PROPAGATION LOSS, dB
40
60
80
100
120
140
0
10
20
30
40
ACOUSTIC RANGE, KYD
MANY ARRIVALS BELOW NOISE
MOST ARRIVALS BELOW NOISE
BELOW NOISE
MOST ARRIVALS BELOW NOISE
33.4 kyd

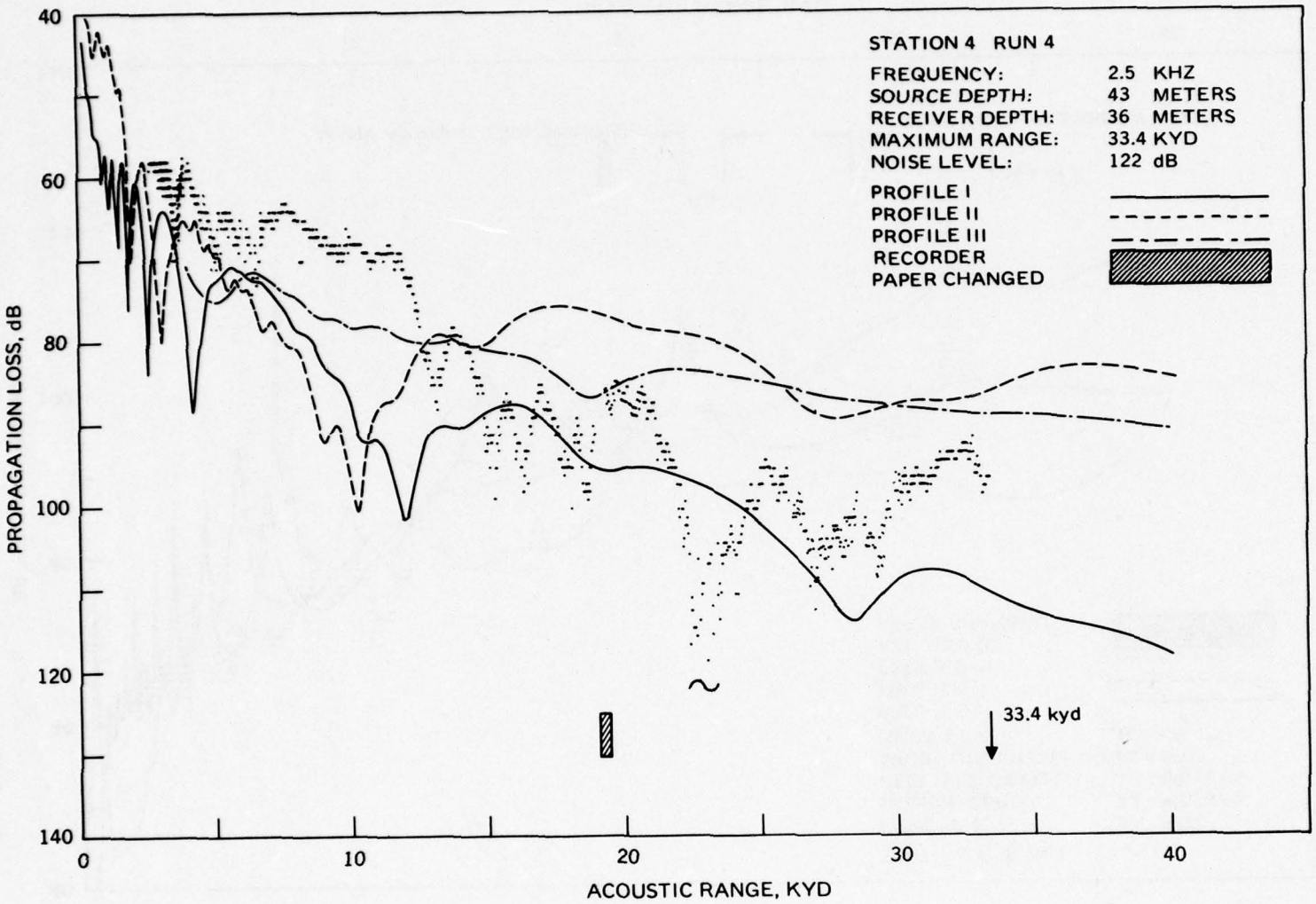
STATION 4 RUN 4
FREQUENCY: 2.5 KHZ
SOURCE DEPTH: 43 METERS
RECEIVER DEPTH: 36 METERS
MAXIMUM RANGE: 33.4 KYD
NOISE LEVEL: 122 dB
PROFILE I
PROFILE II
PROFILE III
RECORDER PAPER CHANGED
33.4 kyd
PROPAGATION LOSS, dB
ACOUSTIC RANGE, KYD
40
60
80
100
120
140
0
10
20
30
40

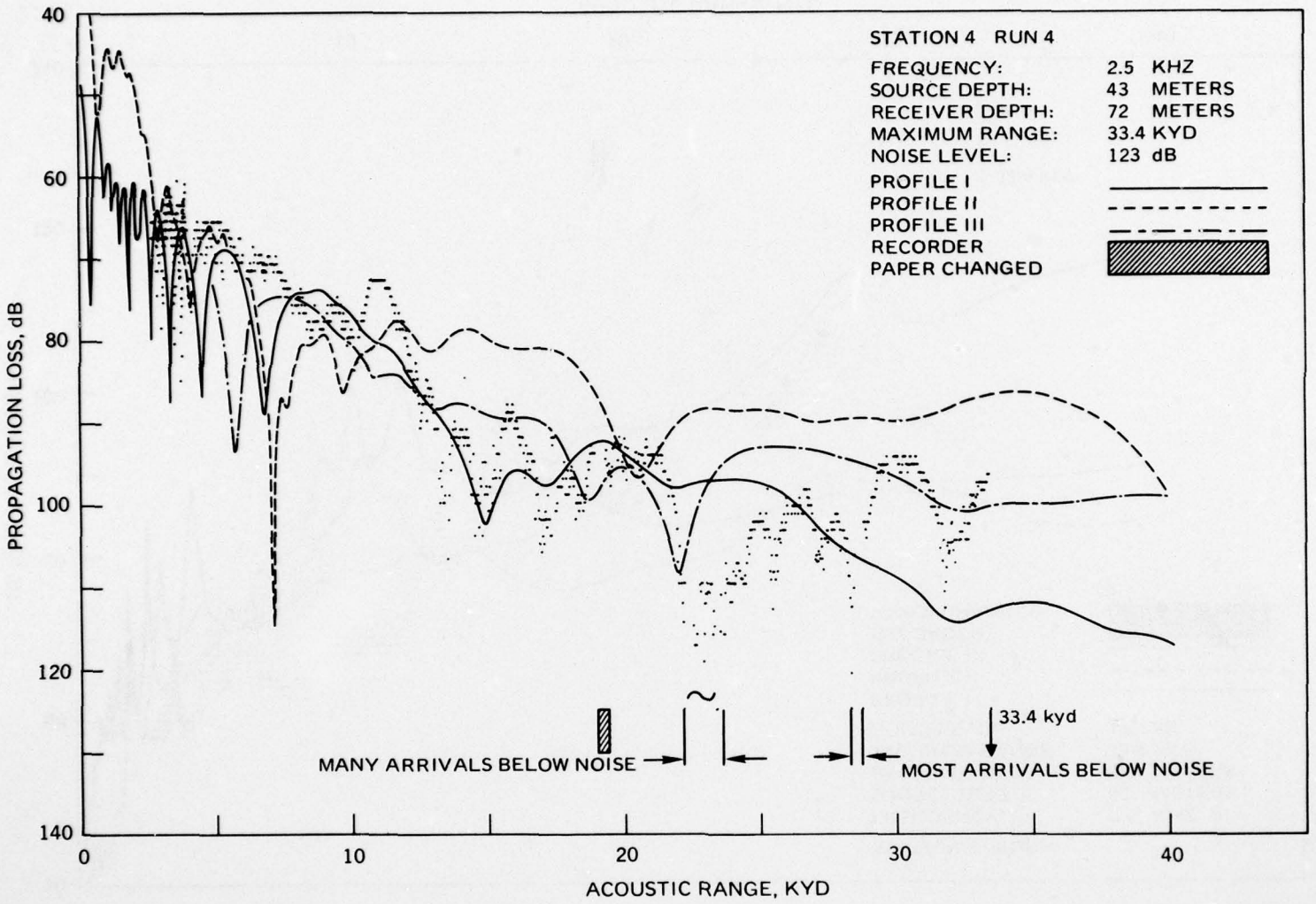
STATION 4 RUN 4
FREQUENCY: 2.5 KHZ
SOURCE DEPTH: 43 METERS
RECEIVER DEPTH: 72 METERS
MAXIMUM RANGE: 33.4 KYD
NOISE LEVEL: 123 dB
PROFILE I
PROFILE II
PROFILE III
RECORDER PAPER CHANGED
PROPAGATION LOSS, dB
40
60
80
100
120
140
0
10
20
30
40
ACOUSTIC RANGE, KYD
MANY ARRIVALS BELOW NOISE
33.4 kyd
MOST ARRIVALS BELOW NOISE

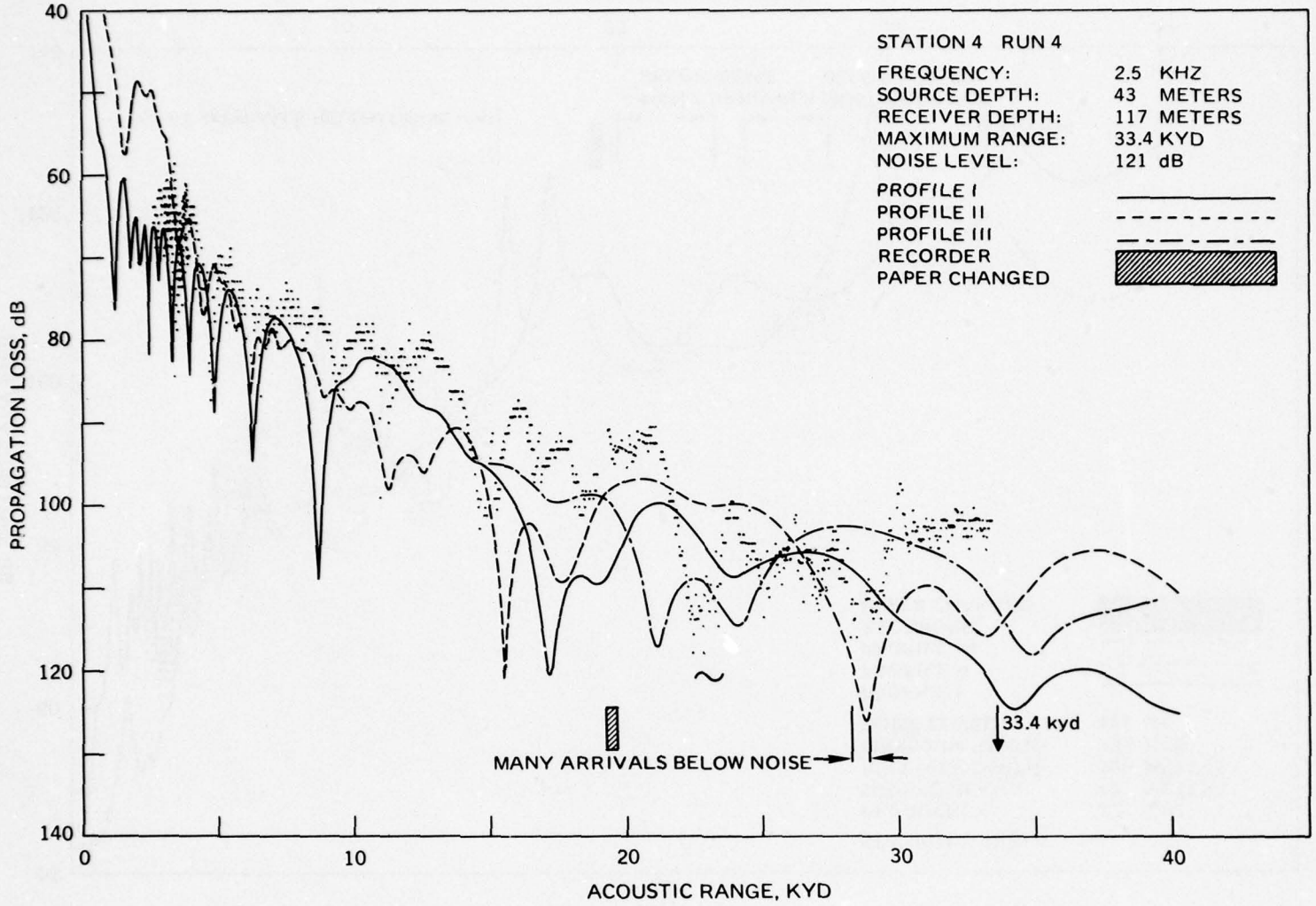
STATION 4 RUN 4
FREQUENCY: 2.5 KHZ
SOURCE DEPTH: 43 METERS
RECEIVER DEPTH: 117 METERS
MAXIMUM RANGE: 33.4 KYD
NOISE LEVEL: 121 dB
PROFILE I
PROFILE II
PROFILE III
RECORDER PAPER CHANGED
MANY ARRIVALS BELOW NOISE
33.4 kyd
PROPAGATION LOSS, dB
ACOUSTIC RANGE, KYD
40
60
80
100
120
140
0
10
20
30
40

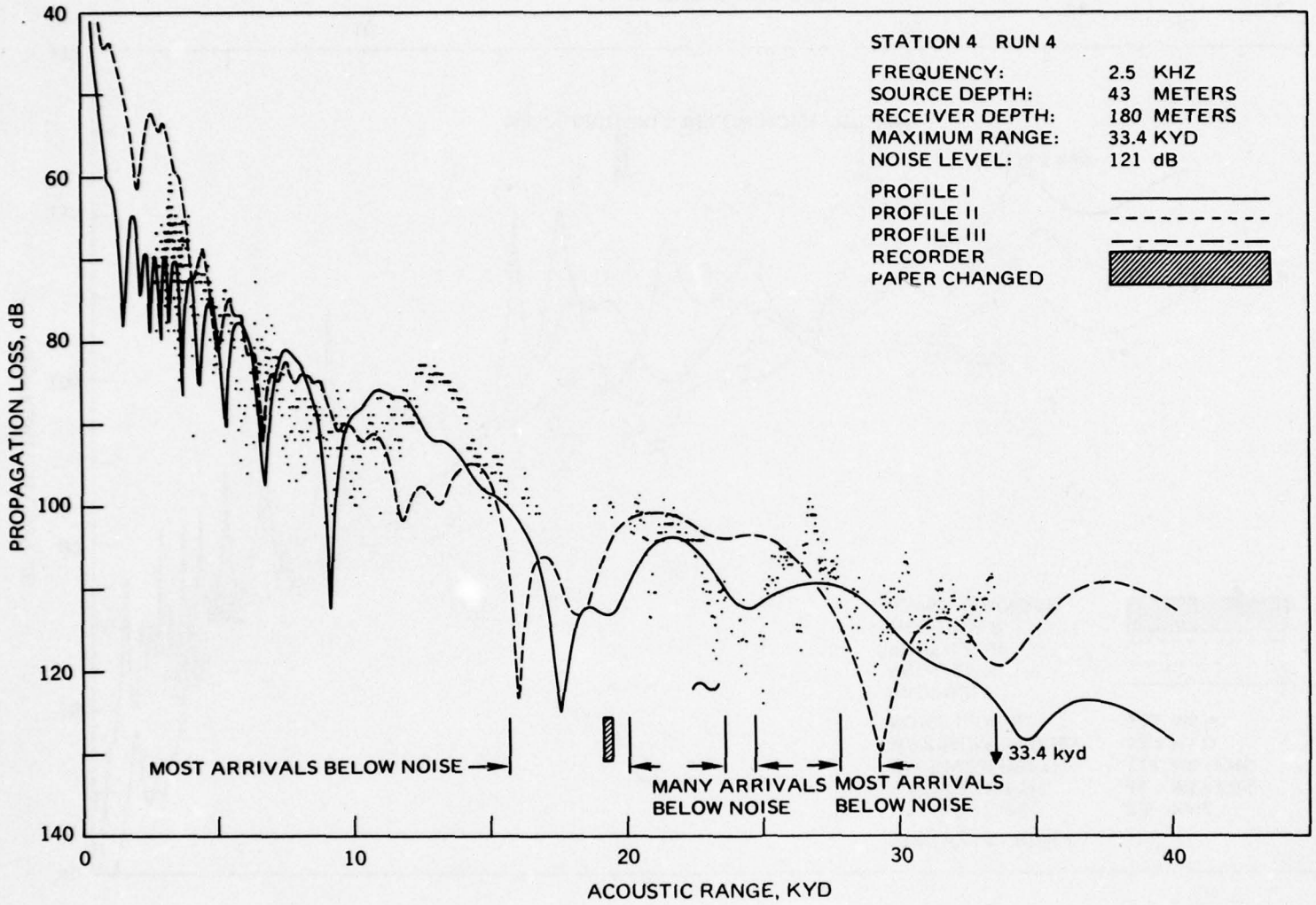
STATION 4 RUN 4
FREQUENCY: 2.5 KHZ
SOURCE DEPTH: 43 METERS
RECEIVER DEPTH: 180 METERS
MAXIMUM RANGE: 33.4 KYD
NOISE LEVEL: 121 dB
PROFILE I
PROFILE II
PROFILE III
RECORDER PAPER CHANGED
PROPAGATION LOSS, dB
40
60
80
100
120
140
0
10
20
30
40
ACOUSTIC RANGE, KYD
MOST ARRIVALS BELOW NOISE
MANY ARRIVALS BELOW NOISE
MOST ARRIVALS BELOW NOISE
33.4 kyd

APPENDIX C

EXPERIMENTAL AND THEORETICAL PROPAGATION LOSSES FOR STATION 4 RUN 3

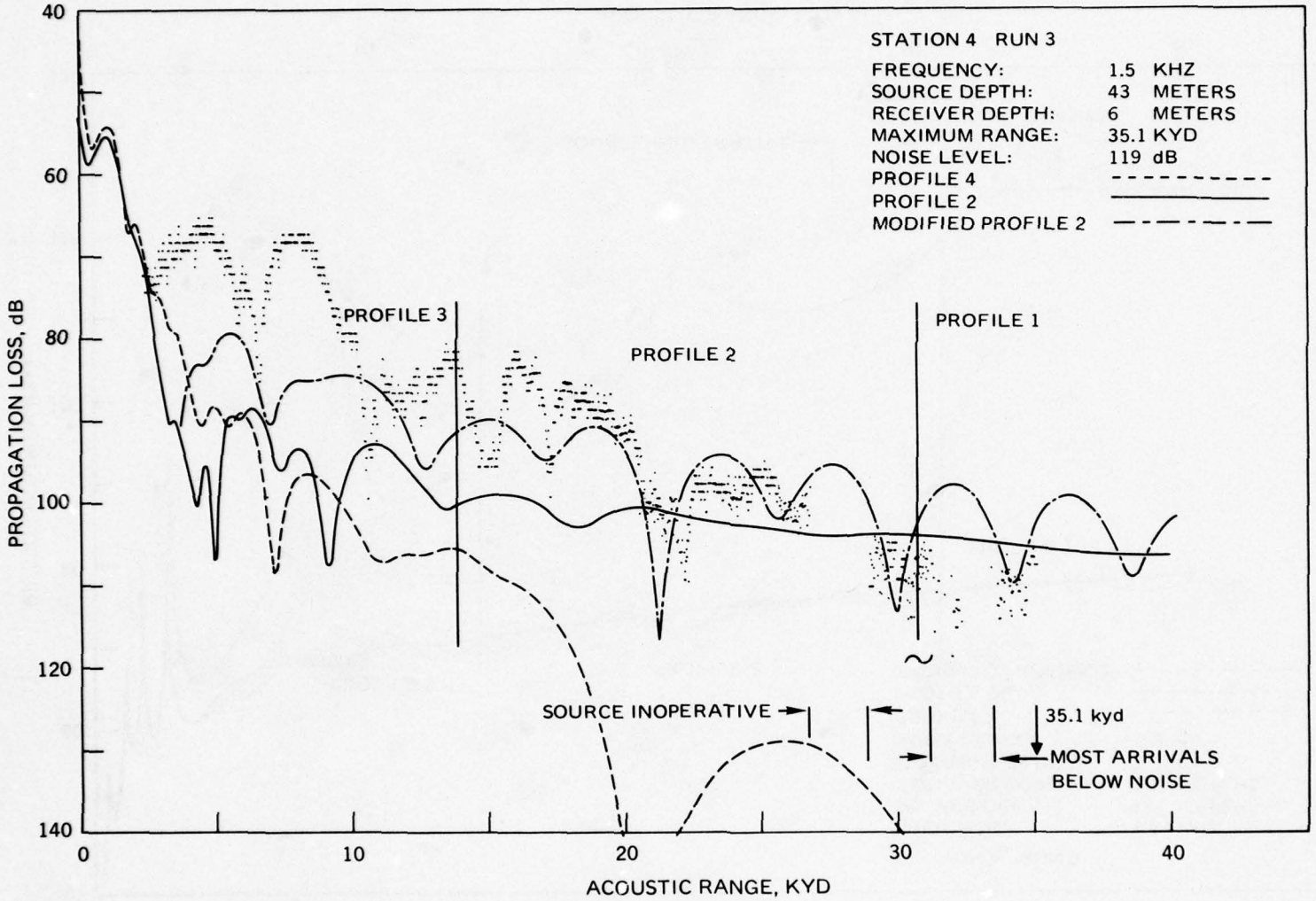
STATION 4 RUN 3
FREQUENCY: 1.5 KHZ
SOURCE DEPTH: 43 METERS
RECEIVER DEPTH: 6 METERS
MAXIMUM RANGE: 35.1 KYD
NOISE LEVEL: 119 dB
PROFILE 4
PROFILE 2
MODIFIED PROFILE 2
PROFILE 3
PROFILE 2
PROFILE 1
SOURCE INOPERATIVE
35.1 kyd
MOST ARRIVALS BELOW NOISE
PROPAGATION LOSS, dB
ACOUSTIC RANGE, KYD
40
60
80
100
120
140
0
10
20
30
40

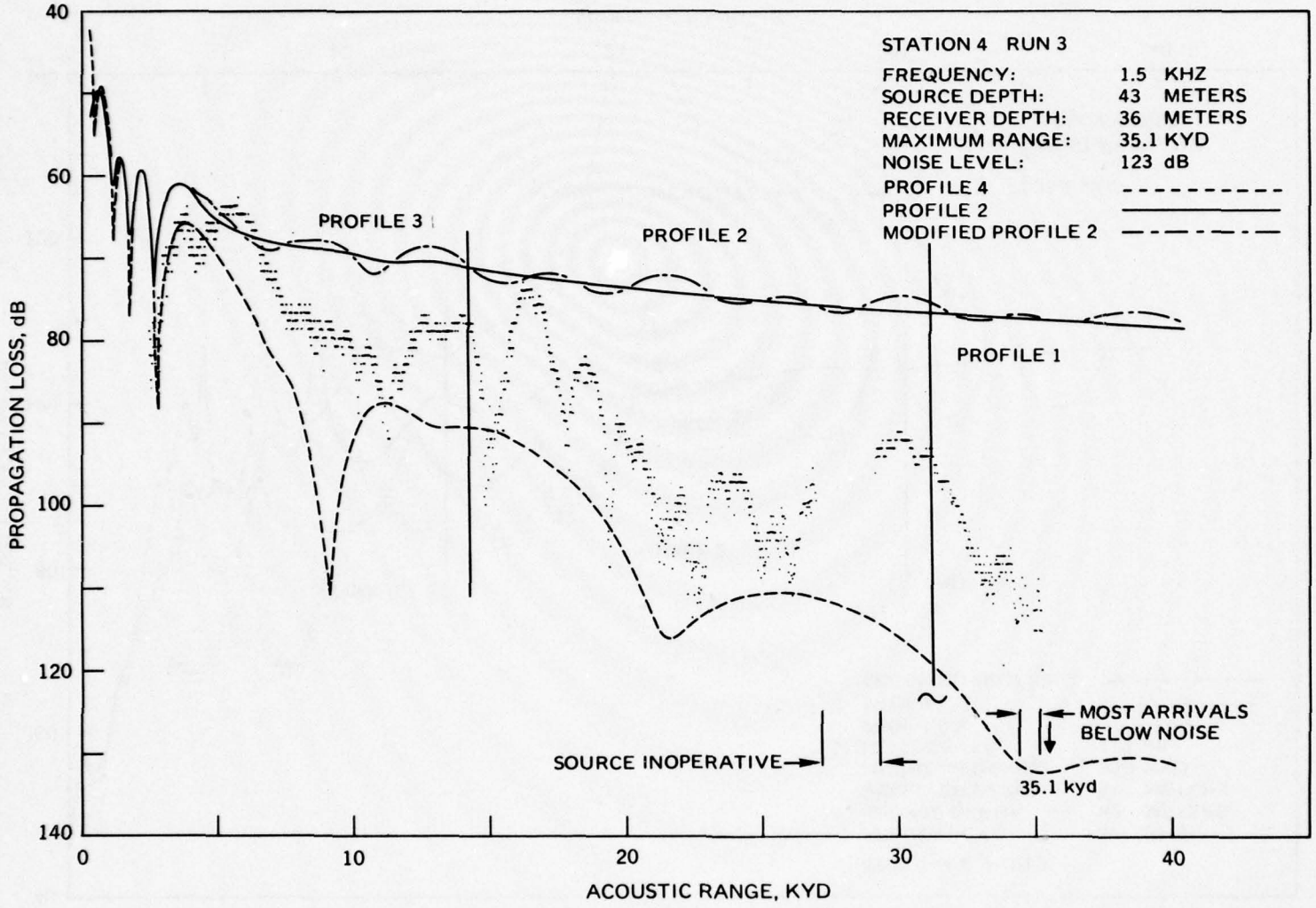
STATION 4 RUN 3
FREQUENCY: 1.5 KHZ
SOURCE DEPTH: 43 METERS
RECEIVER DEPTH: 36 METERS
MAXIMUM RANGE: 35.1 KYD
NOISE LEVEL: 123 dB
PROFILE 4
PROFILE 2
MODIFIED PROFILE 2
PROFILE 3
PROFILE 2
PROFILE 1
MOST ARRIVALS BELOW NOISE
SOURCE INOPERATIVE
35.1 kyd
PROPAGATION LOSS, dB
ACOUSTIC RANGE, KYD
40
60
80
100
120
140
0
10
20
30
40

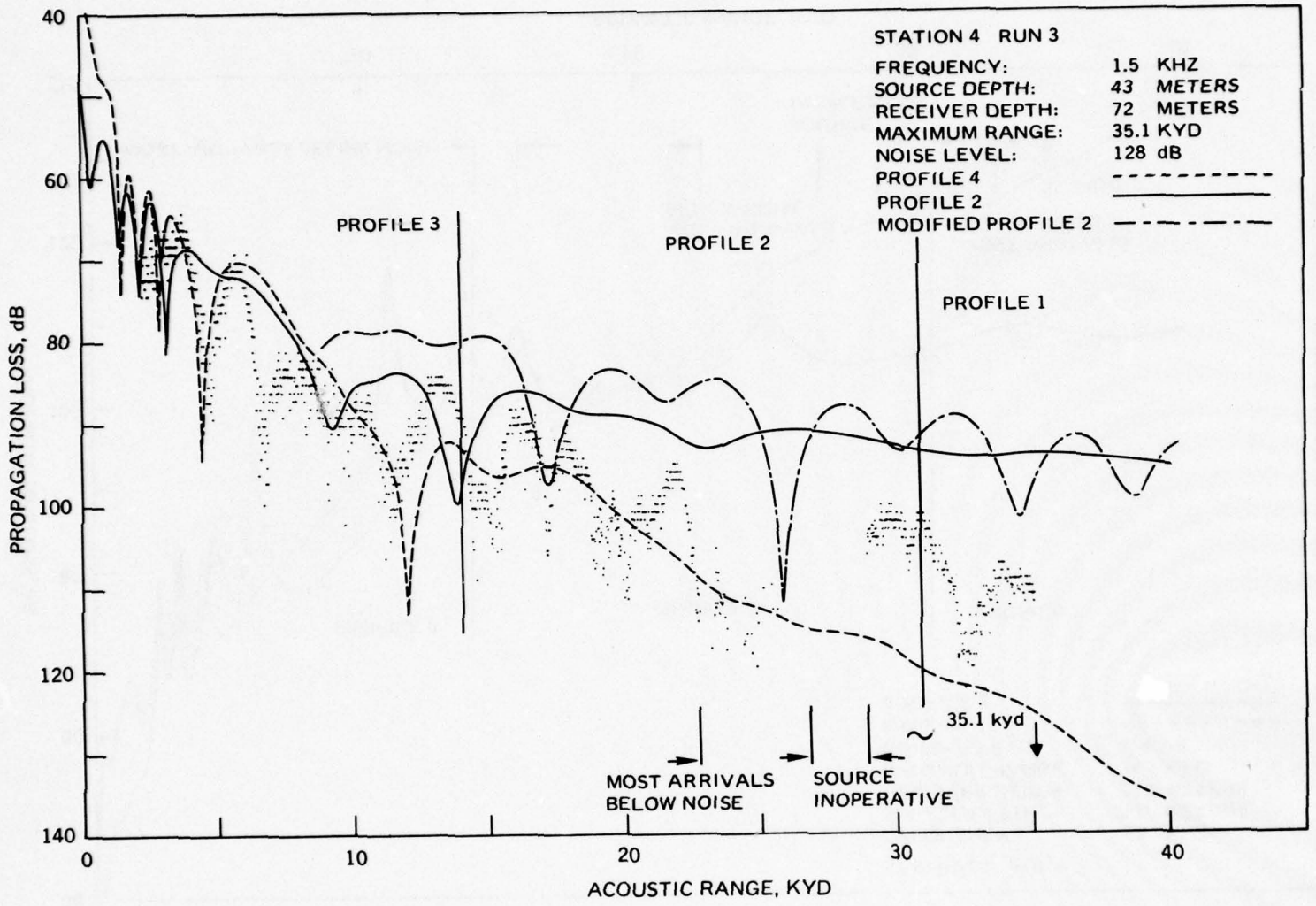
STATION 4 RUN 3
FREQUENCY: 1.5 KHZ
SOURCE DEPTH: 43 METERS
RECEIVER DEPTH: 72 METERS
MAXIMUM RANGE: 35.1 KYD
NOISE LEVEL: 128 dB
PROFILE 4
PROFILE 2
MODIFIED PROFILE 2
PROFILE 3
PROFILE 2
PROFILE 1
35.1 kyd
MOST ARRIVALS BELOW NOISE
SOURCE INOPERATIVE
PROPAGATION LOSS, dB
ACOUSTIC RANGE, KYD
40
60
80
100
120
140
0
10
20
30
40

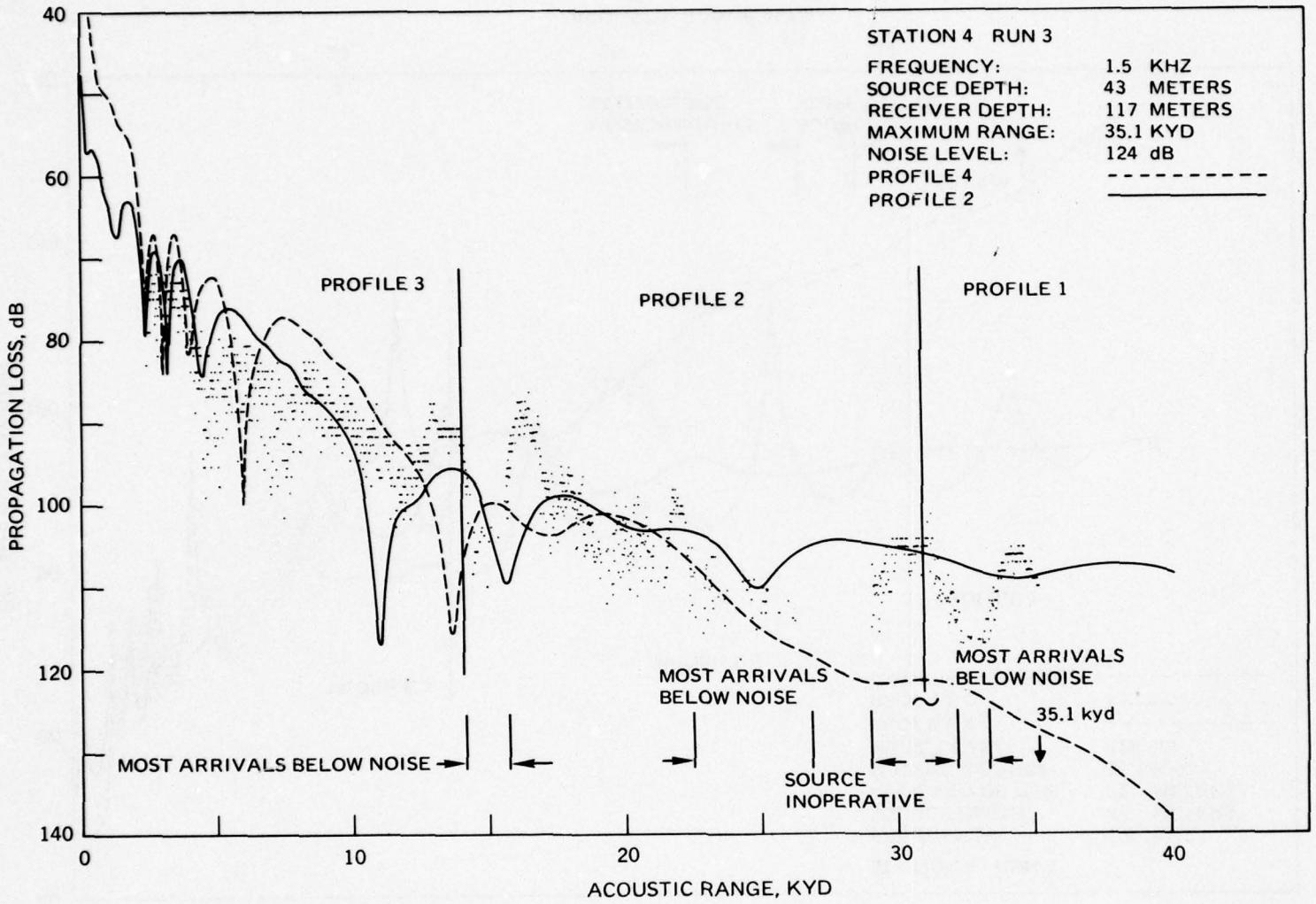
STATION 4 RUN 3
FREQUENCY: 1.5 KHZ
SOURCE DEPTH: 43 METERS
RECEIVER DEPTH: 117 METERS
MAXIMUM RANGE: 35.1 KYD
NOISE LEVEL: 124 dB
PROFILE 4
PROFILE 2
PROFILE 3
PROFILE 2
PROFILE 1
MOST ARRIVALS BELOW NOISE
MOST ARRIVALS BELOW NOISE
MOST ARRIVALS BELOW NOISE
35.1 kyd
SOURCE INOPERATIVE
PROPAGATION LOSS, dB
ACOUSTIC RANGE, KYD
40
60
80
100
120
140
0
10
20
30
40

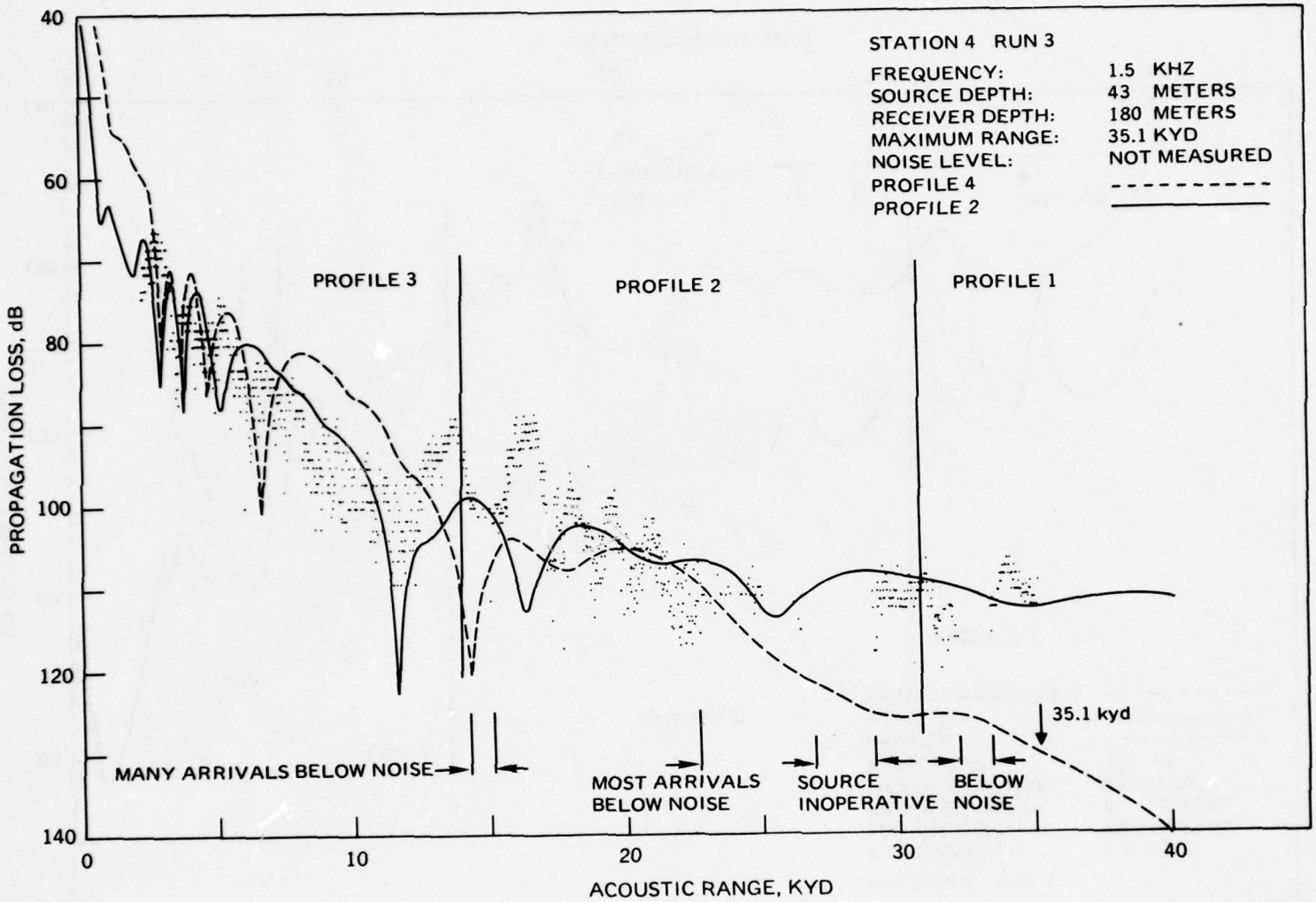
STATION 4 RUN 3
FREQUENCY: 1.5 KHZ
SOURCE DEPTH: 43 METERS
RECEIVER DEPTH: 180 METERS
MAXIMUM RANGE: 35.1 KYD
NOISE LEVEL: NOT MEASURED
PROFILE 4
PROFILE 2
PROFILE 3
PROFILE 2
PROFILE 1
35.1 kyd
MANY ARRIVALS BELOW NOISE
MOST ARRIVALS BELOW NOISE
SOURCE INOPERATIVE
BELOW NOISE
PROPAGATION LOSS, dB
ACOUSTIC RANGE, KYD
40
60
80
100
120
140
0
10
20
30
40

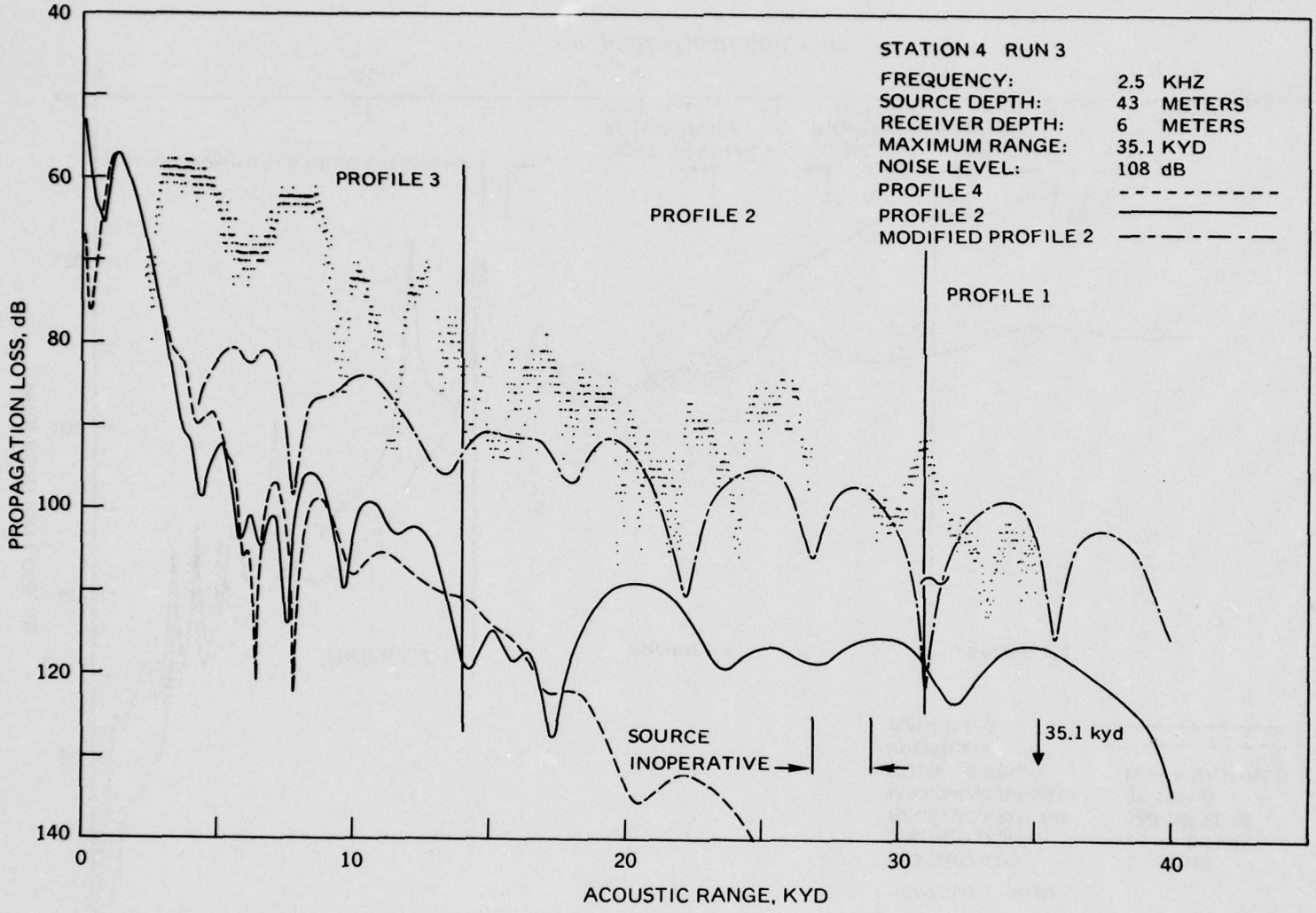
STATION 4 RUN 3
FREQUENCY: 2.5 KHZ
SOURCE DEPTH: 43 METERS
RECEIVER DEPTH: 6 METERS
MAXIMUM RANGE: 35.1 KYD
NOISE LEVEL: 108 dB
PROFILE 4
PROFILE 2
MODIFIED PROFILE 2
PROFILE 3
PROFILE 2
PROFILE 1
SOURCE INOPERATIVE
35.1 kyd
PROPAGATION LOSS, dB
ACOUSTIC RANGE, KYD
40
60
80
100
120
140
0
10
20
30
40

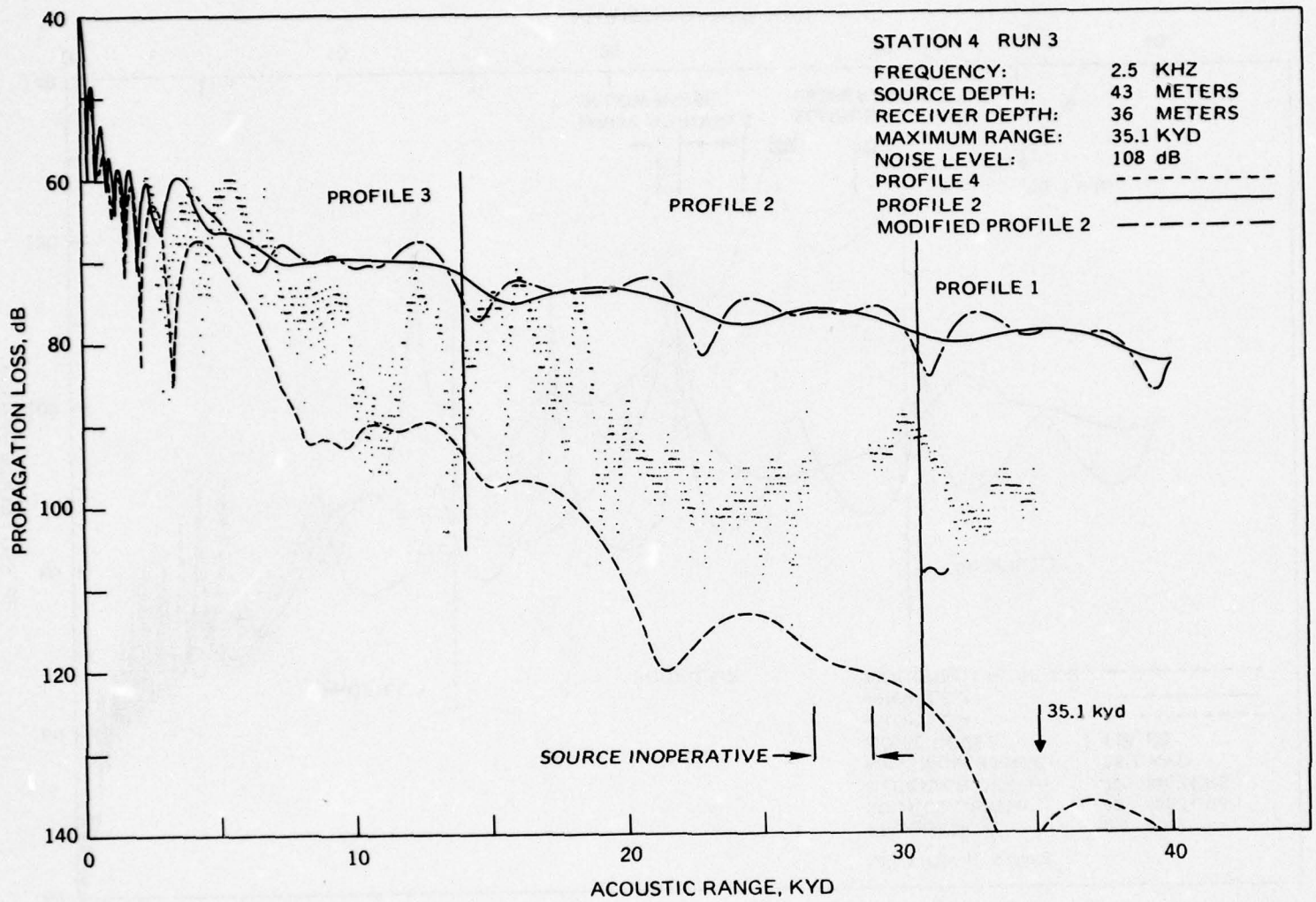
STATION 4 RUN 3
FREQUENCY: 2.5 KHZ
SOURCE DEPTH: 43 METERS
RECEIVER DEPTH: 36 METERS
MAXIMUM RANGE: 35.1 KYD
NOISE LEVEL: 108 dB
PROFILE 4
PROFILE 2
MODIFIED PROFILE 2
PROFILE 3
PROFILE 2
PROFILE 1
35.1 kyd
SOURCE INOPERATIVE
PROPAGATION LOSS, dB
ACOUSTIC RANGE, KYD
40
60
80
100
120
140
0
10
20
30
40

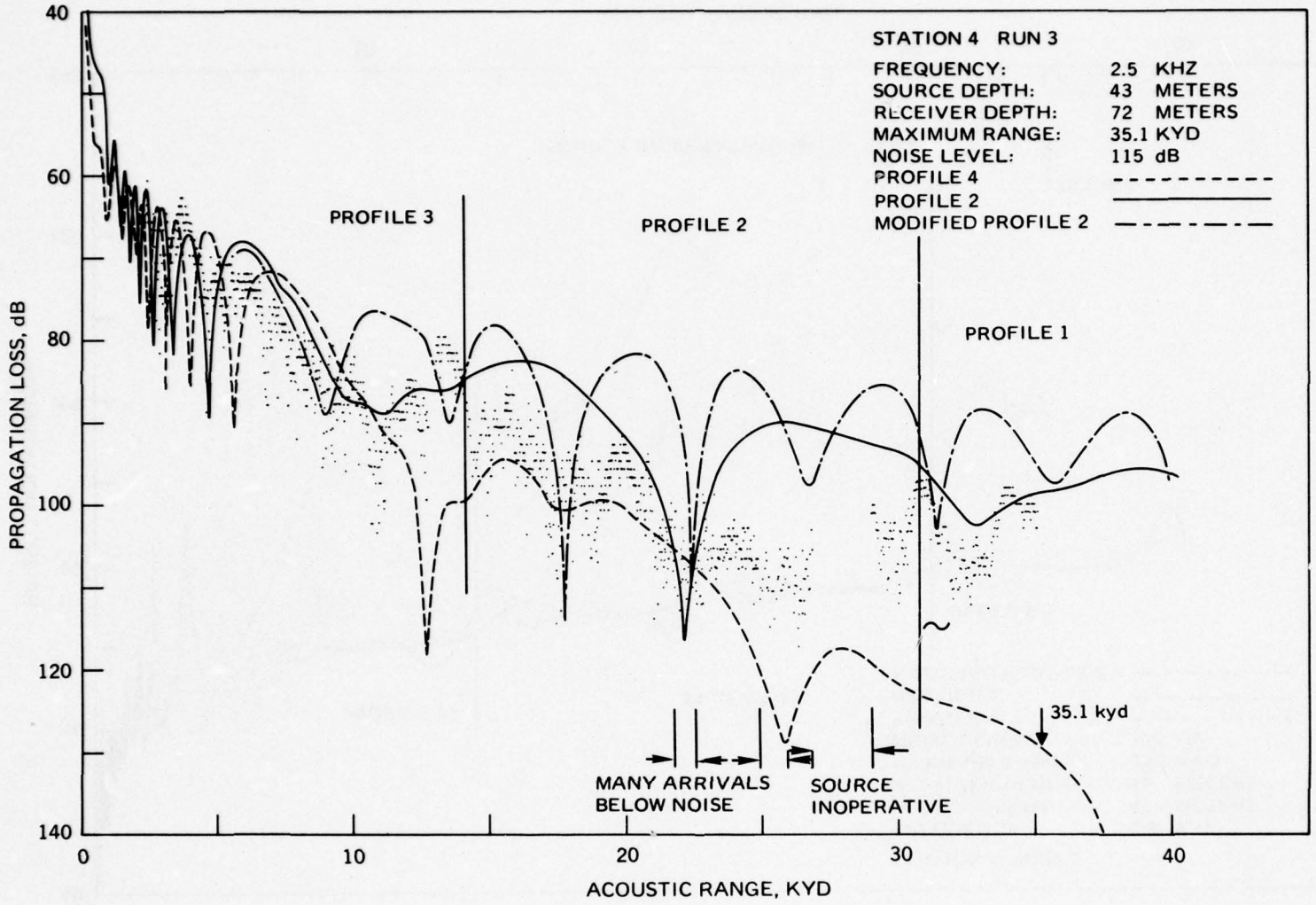
STATION 4 RUN 3
FREQUENCY: 2.5 KHZ
SOURCE DEPTH: 43 METERS
RECEIVER DEPTH: 72 METERS
MAXIMUM RANGE: 35.1 KYD
NOISE LEVEL: 115 dB
PROFILE 4
PROFILE 2
MODIFIED PROFILE 2
PROFILE 3
PROFILE 2
PROFILE 1
35.1 kyd
MANY ARRIVALS BELOW NOISE
SOURCE INOPERATIVE
PROPAGATION LOSS, dB
ACOUSTIC RANGE, KYD
40
60
80
100
120
140
0
10
20
30
40

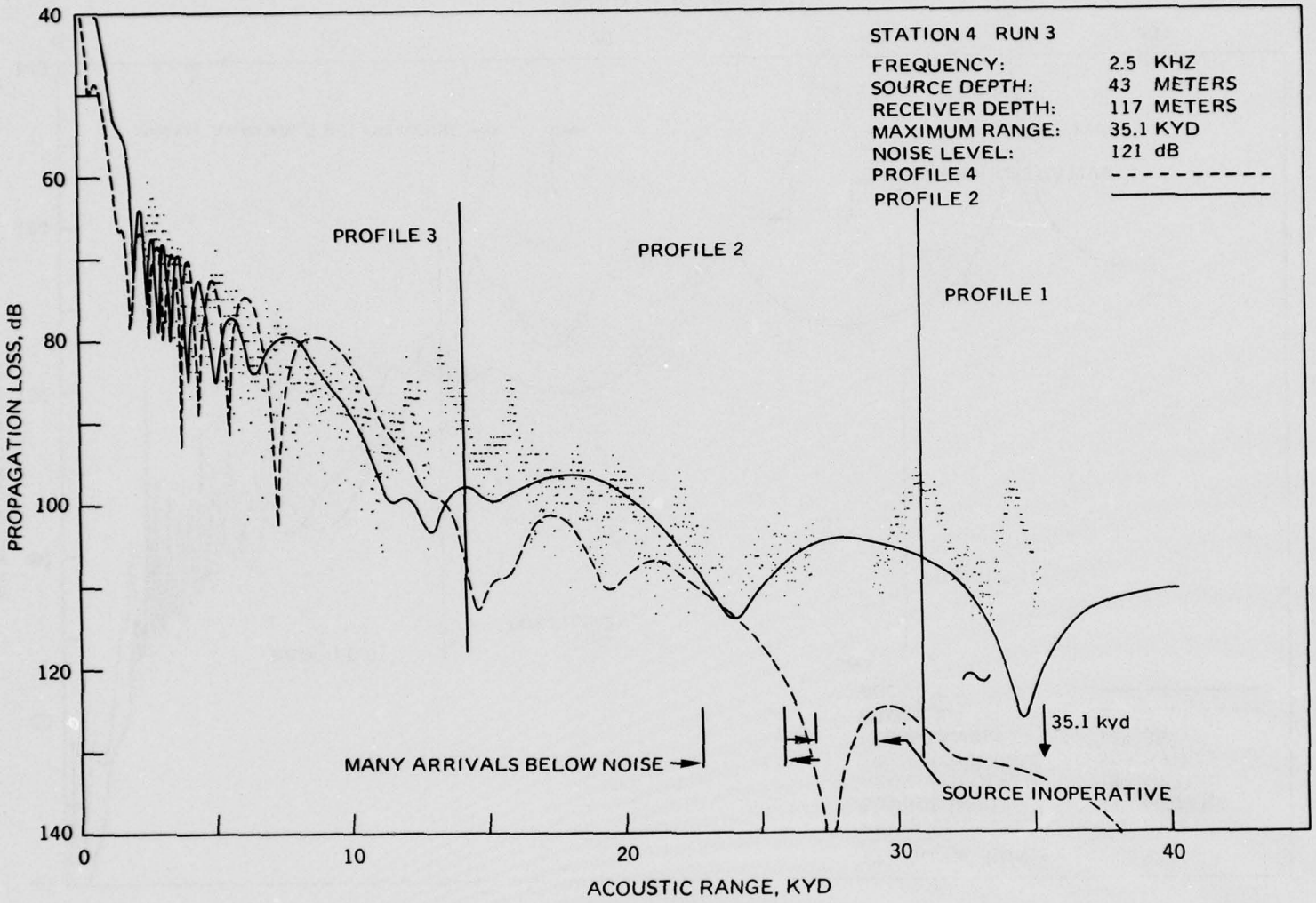
STATION 4 RUN 3
FREQUENCY: 2.5 KHZ
SOURCE DEPTH: 43 METERS
RECEIVER DEPTH: 117 METERS
MAXIMUM RANGE: 35.1 KYD
NOISE LEVEL: 121 dB
PROFILE 4
PROFILE 2
PROFILE 3
PROFILE 2
PROFILE 1
35.1 kyd
MANY ARRIVALS BELOW NOISE
SOURCE INOPERATIVE
PROPAGATION LOSS, dB
ACOUSTIC RANGE, KYD
40
60
80
100
120
140
0
10
20
30
40

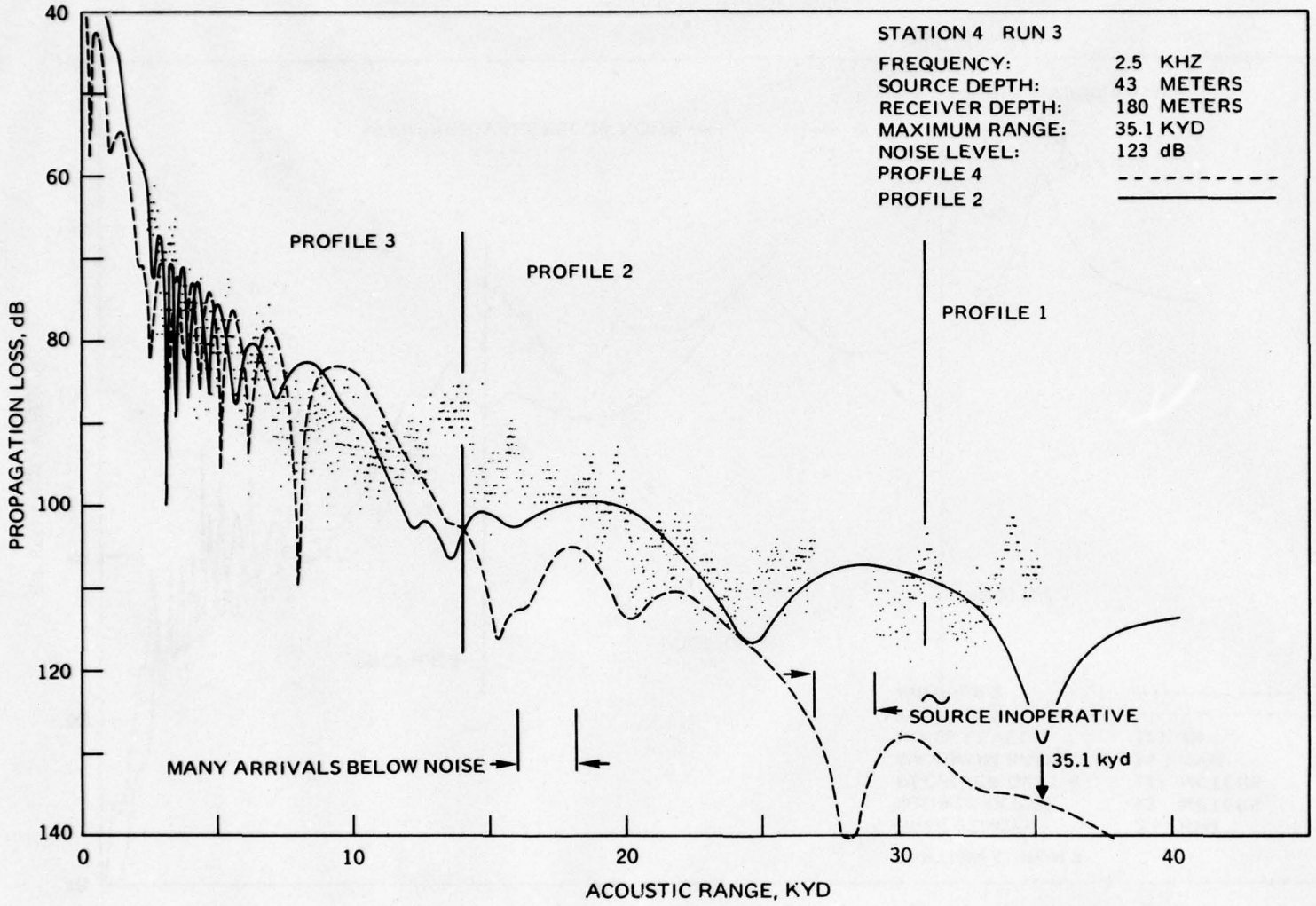
STATION 4 RUN 3
FREQUENCY: 2.5 KHZ
SOURCE DEPTH: 43 METERS
RECEIVER DEPTH: 180 METERS
MAXIMUM RANGE: 35.1 KYD
NOISE LEVEL: 123 dB
PROFILE 4
PROFILE 2
PROFILE 3
PROFILE 2
PROFILE 1
SOURCE INOPERATIVE
35.1 kyd
MANY ARRIVALS BELOW NOISE
PROPAGATION LOSS, dB
ACOUSTIC RANGE, KYD
40
60
80
100
120
140
0
10
20
30
40

APPENDIX D

EXPERIMENTAL AND THEORETICAL PROPAGATION LOSSES FOR STATION 3 RUN 3

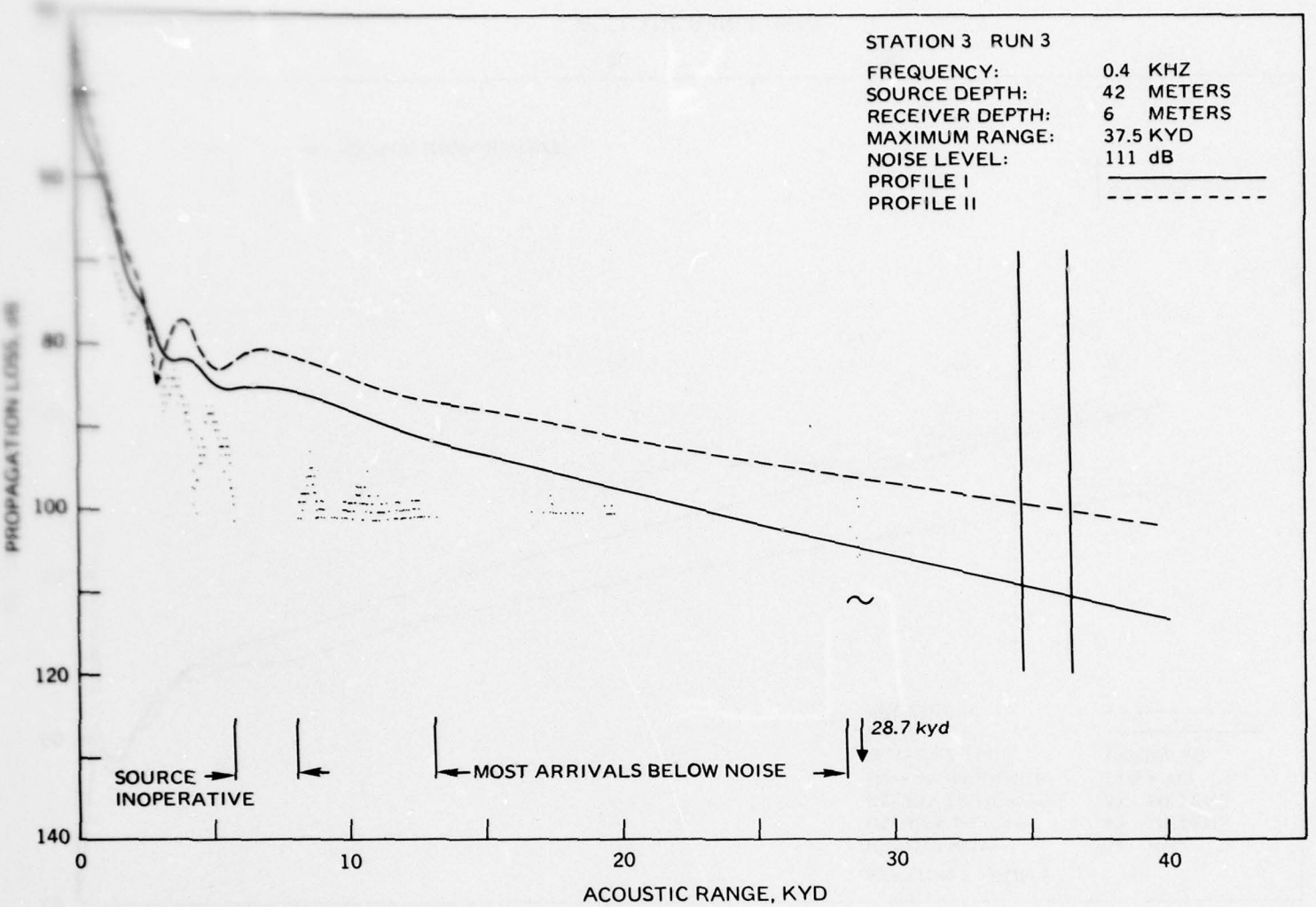
STATION 3 RUN 3
FREQUENCY: 0.4 KHZ
SOURCE DEPTH: 42 METERS
RECEIVER DEPTH: 6 METERS
MAXIMUM RANGE: 37.5 KYD
NOISE LEVEL: 111 dB
PROFILE I
PROFILE II
PROPAGATION LOSS, dB
80
100
120
140
28.7 kyd
SOURCE INOPERATIVE
MOST ARRIVALS BELOW NOISE
0
10
20
30
40
ACOUSTIC RANGE, KYD

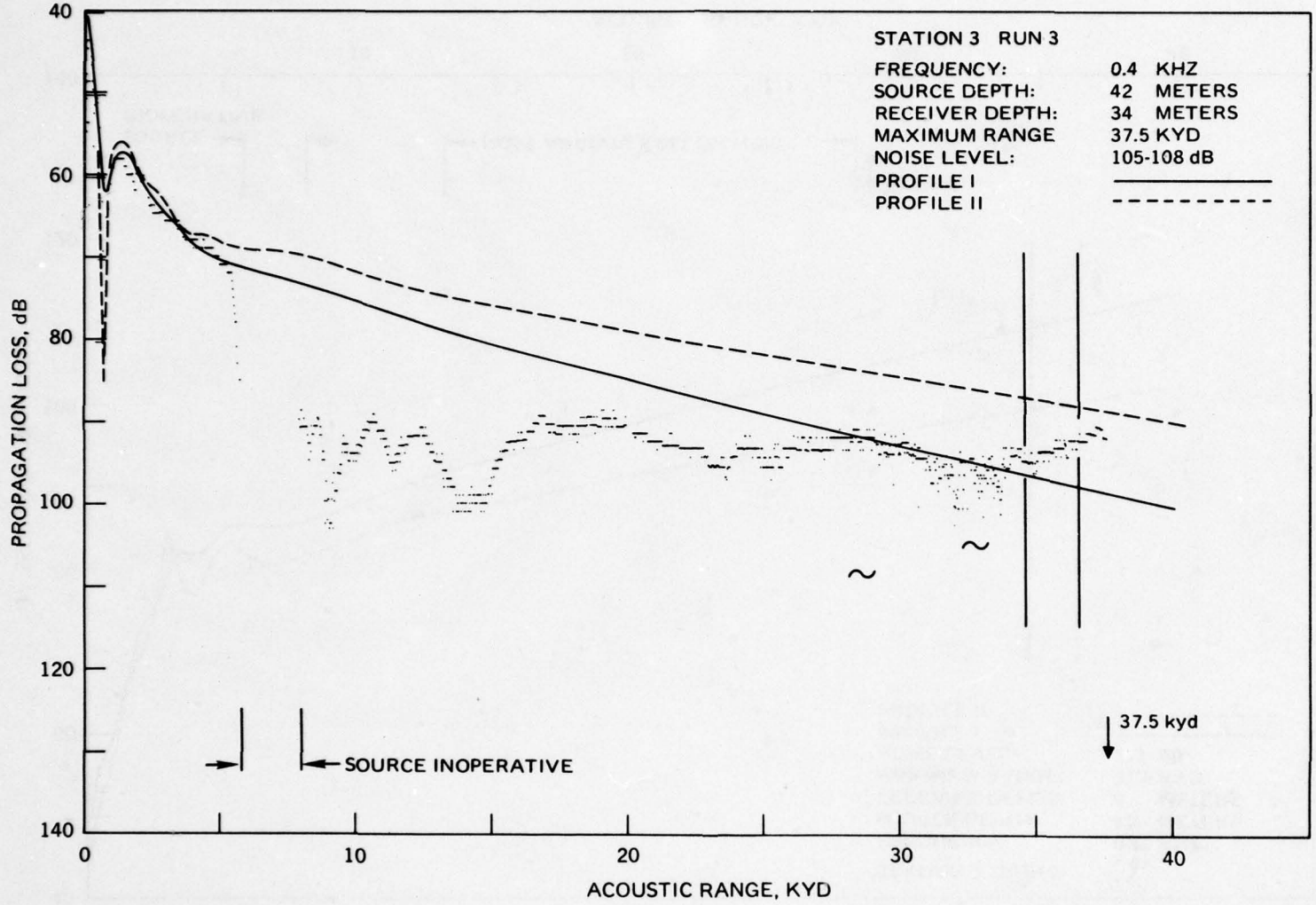
STATION 3 RUN 3
FREQUENCY: 0.4 KHZ
SOURCE DEPTH: 42 METERS
RECEIVER DEPTH: 34 METERS
MAXIMUM RANGE 37.5 KYD
NOISE LEVEL: 105-108 dB
PROFILE I
PROFILE II
SOURCE INOPERATIVE
37.5 kyd
PROPAGATION LOSS, dB
ACOUSTIC RANGE, KYD
40
60
80
100
120
140
0
10
20
30
40

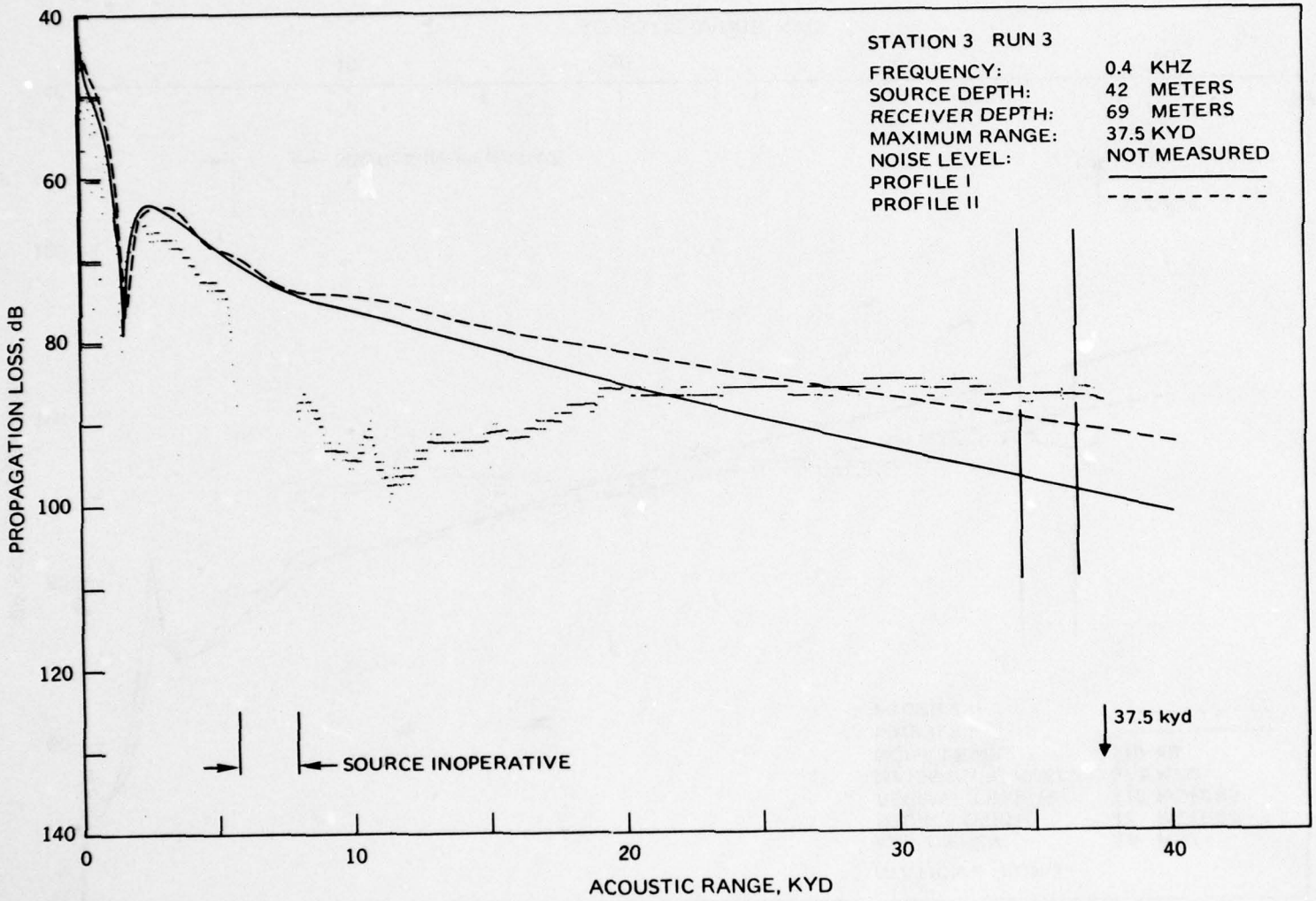
STATION 3 RUN 3
FREQUENCY: 0.4 KHZ
SOURCE DEPTH: 42 METERS
RECEIVER DEPTH: 69 METERS
MAXIMUM RANGE: 37.5 KYD
NOISE LEVEL: NOT MEASURED
PROFILE I
PROFILE II
SOURCE INOPERATIVE
37.5 kyd
PROPAGATION LOSS, dB
ACOUSTIC RANGE, KYD
40
60
80
100
120
140
0
10
20
30
40

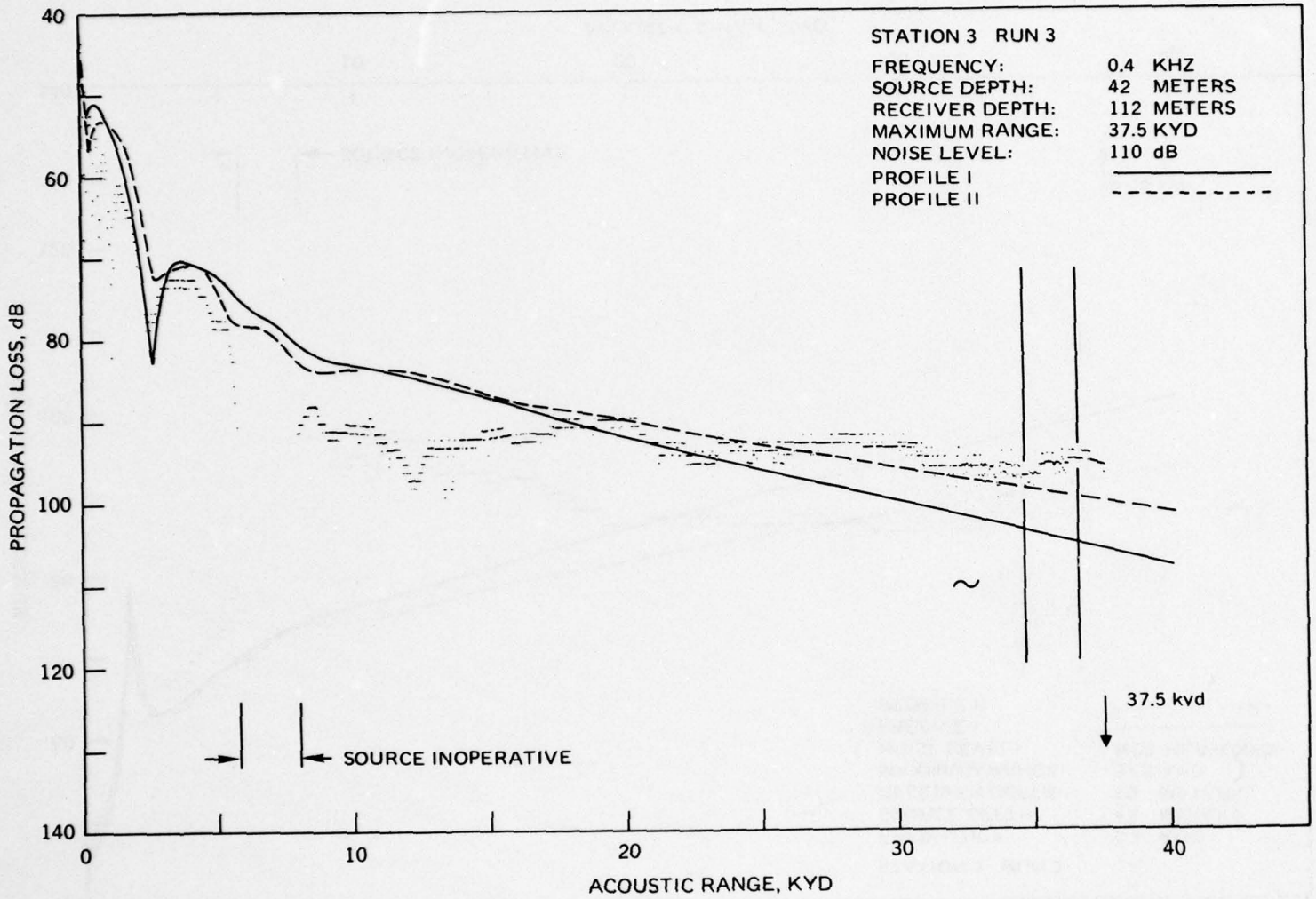
STATION 3 RUN 3
FREQUENCY: 0.4 KHZ
SOURCE DEPTH: 42 METERS
RECEIVER DEPTH: 112 METERS
MAXIMUM RANGE: 37.5 KYD
NOISE LEVEL: 110 dB
PROFILE I
PROFILE II
PROPAGATION LOSS, dB
40
60
80
100
120
140
0
10
20
30
40
ACOUSTIC RANGE, KYD
37.5 kyd
SOURCE INOPERATIVE

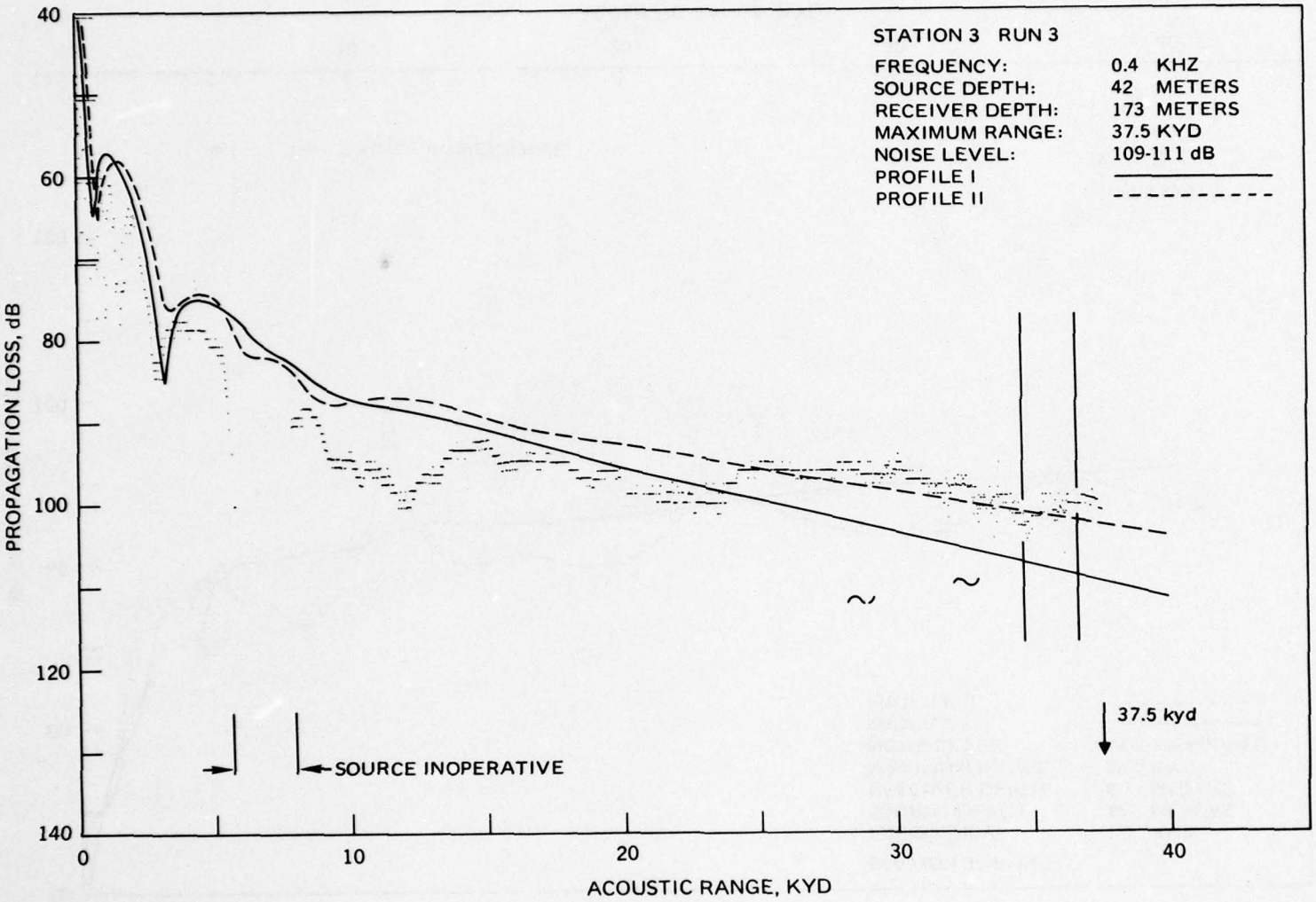
STATION 3 RUN 3
FREQUENCY: 0.4 KHZ
SOURCE DEPTH: 42 METERS
RECEIVER DEPTH: 173 METERS
MAXIMUM RANGE: 37.5 KYD
NOISE LEVEL: 109-111 dB
PROFILE I
PROFILE II
PROPAGATION LOSS, dB
40
60
80
100
120
140
0
10
20
30
40
ACOUSTIC RANGE, KYD
37.5 kyd
SOURCE INOPERATIVE

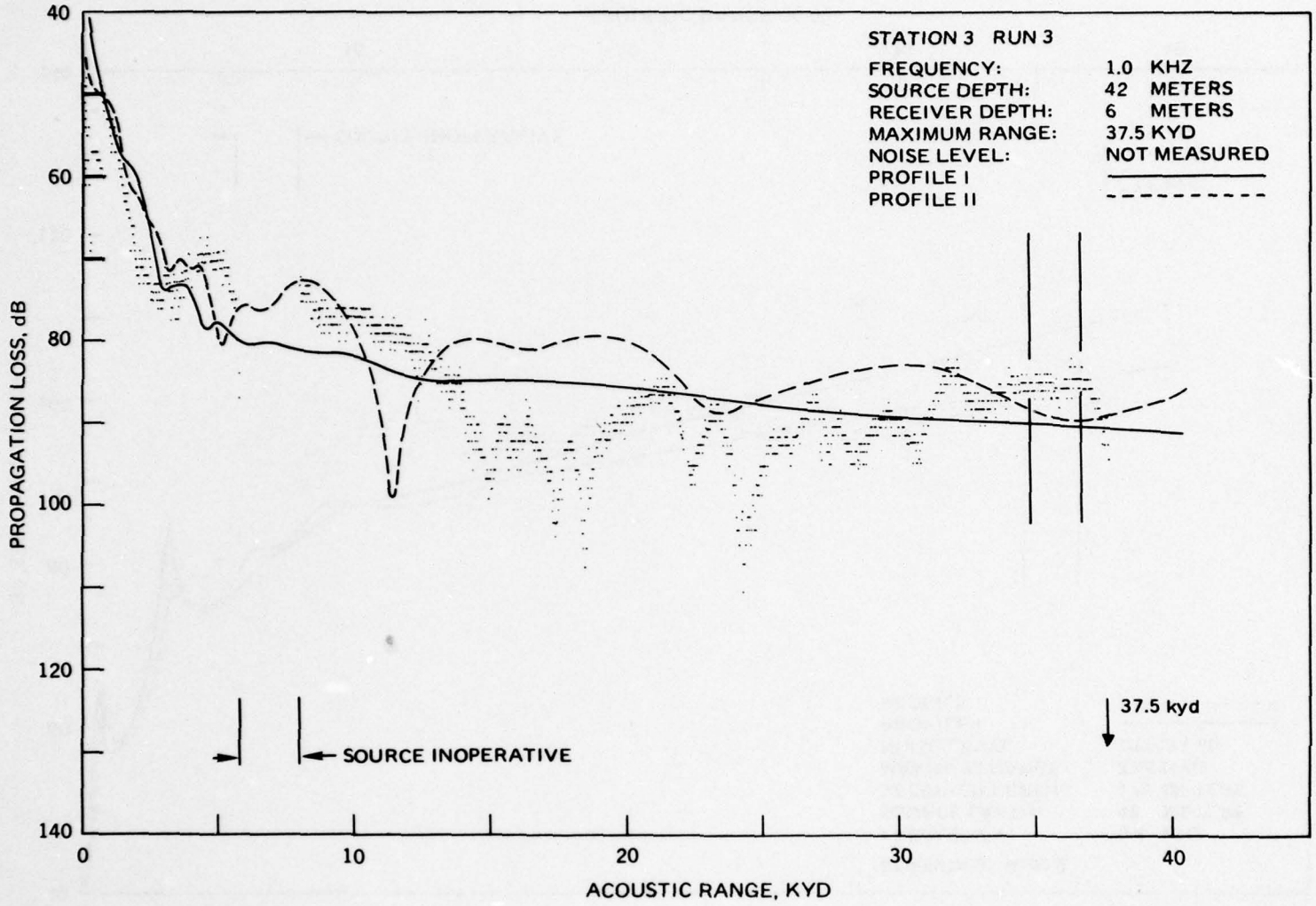
STATION 3 RUN 3
FREQUENCY: 1.0 KHZ
SOURCE DEPTH: 42 METERS
RECEIVER DEPTH: 6 METERS
MAXIMUM RANGE: 37.5 KYD
NOISE LEVEL: NOT MEASURED
PROFILE I
PROFILE II
SOURCE INOPERATIVE
37.5 kyd
PROPAGATION LOSS, dB
ACOUSTIC RANGE, KYD
40
60
80
100
120
140
0
10
20
30
40

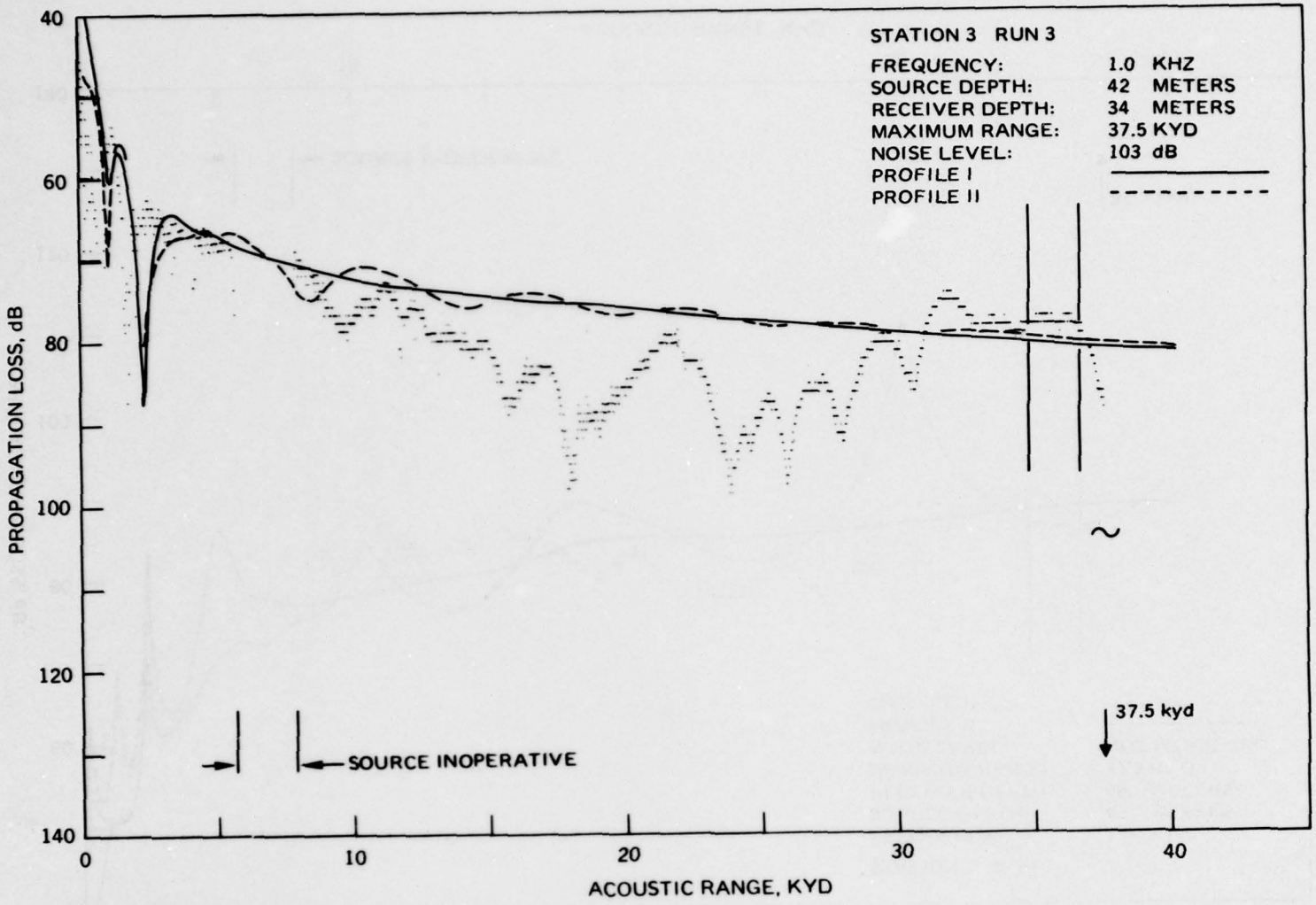
STATION 3 RUN 3
FREQUENCY: 1.0 KHZ
SOURCE DEPTH: 42 METERS
RECEIVER DEPTH: 34 METERS
MAXIMUM RANGE: 37.5 KYD
NOISE LEVEL: 103 dB
PROFILE I
PROFILE II
PROPAGATION LOSS, dB
40
60
80
100
120
140
0
10
20
30
40
ACOUSTIC RANGE, KYD
SOURCE INOPERATIVE
37.5 kyd

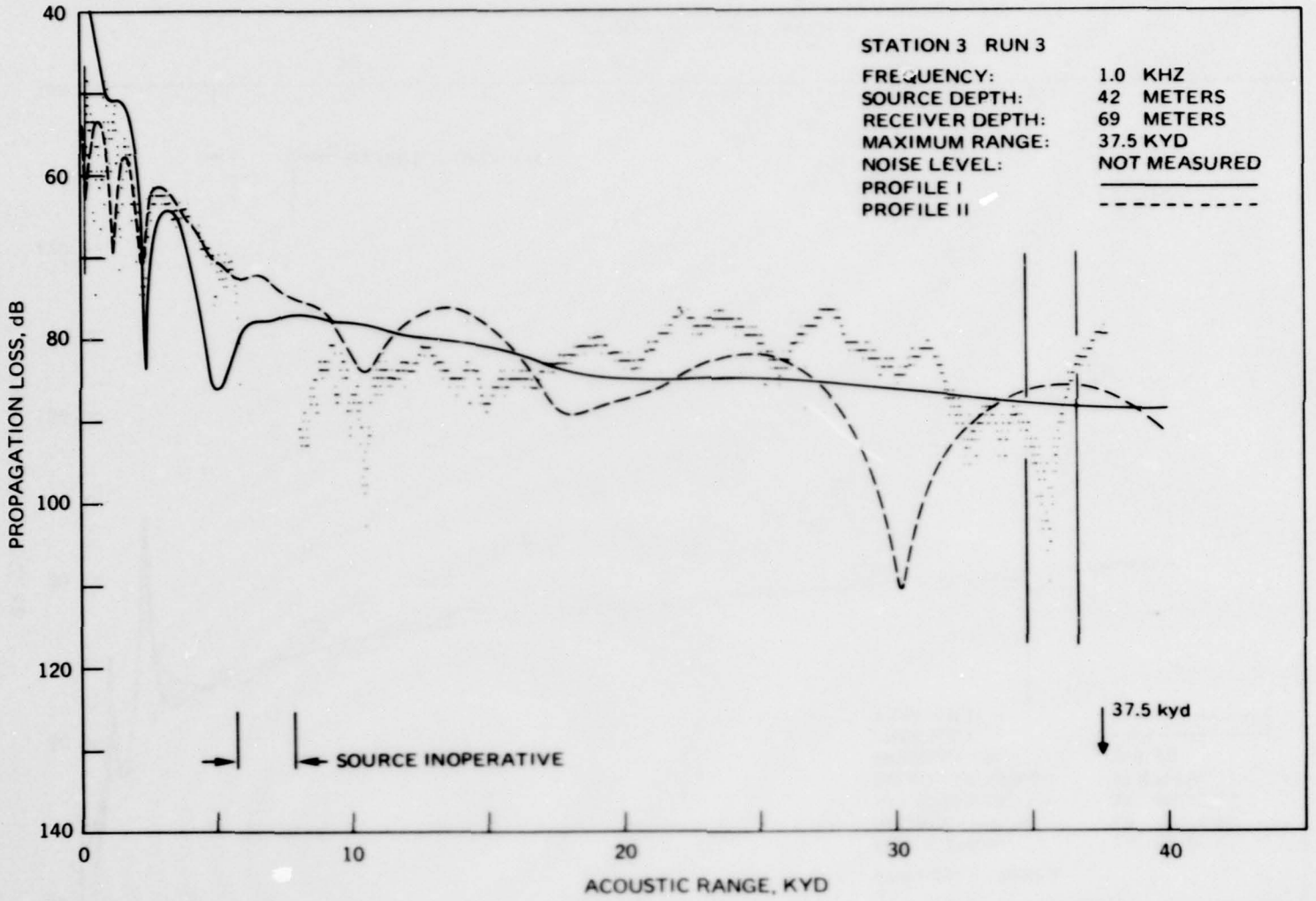
STATION 3 RUN 3
FREQUENCY: 1.0 KHZ
SOURCE DEPTH: 42 METERS
RECEIVER DEPTH: 69 METERS
MAXIMUM RANGE: 37.5 KYD
NOISE LEVEL: NOT MEASURED
PROFILE I
PROFILE II
SOURCE INOPERATIVE
37.5 kyd
PROPAGATION LOSS, dB
ACOUSTIC RANGE, KYD
40
60
80
100
120
140
0
10
20
30
40

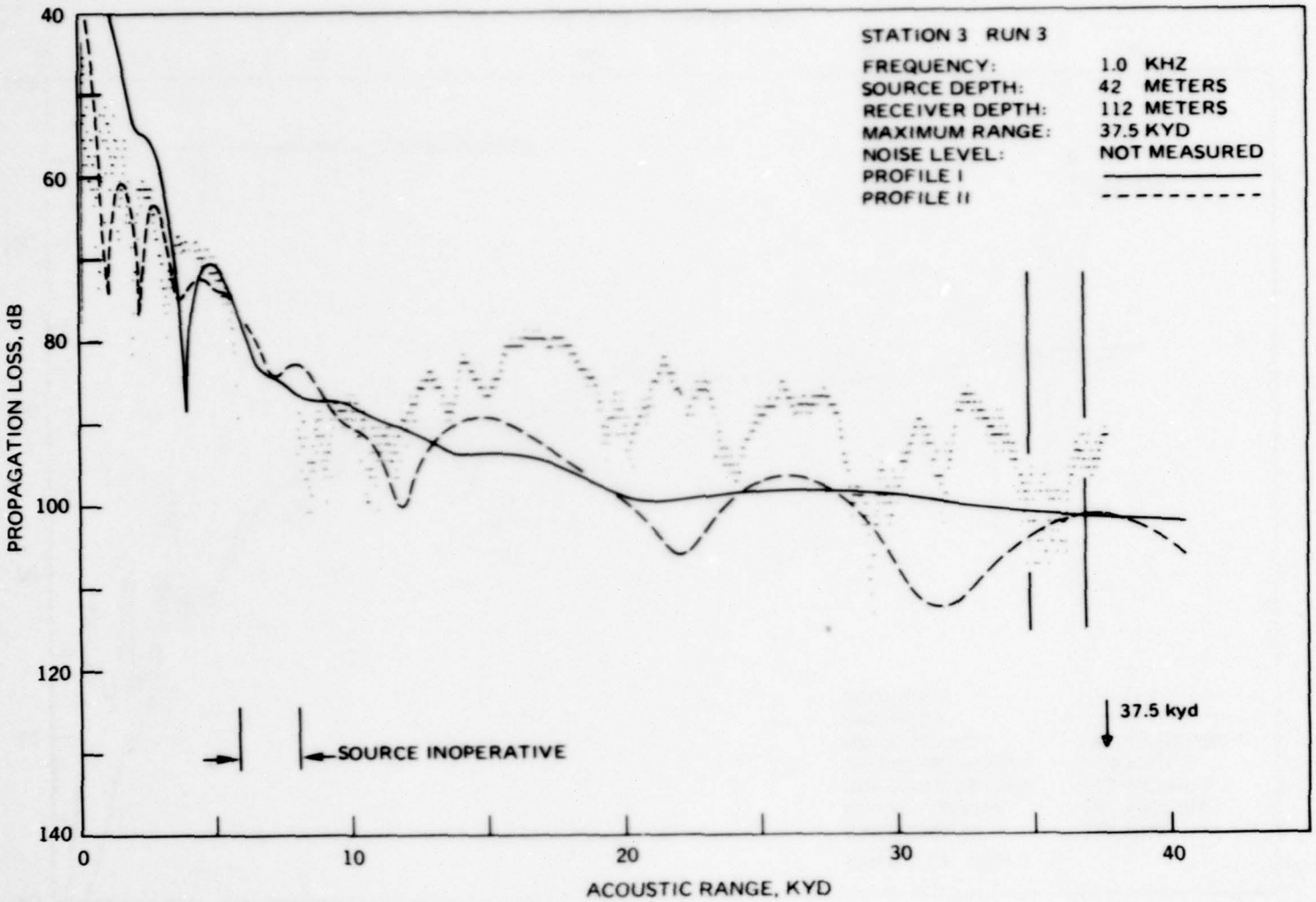
STATION 3 RUN 3
FREQUENCY: 1.0 KHZ
SOURCE DEPTH: 42 METERS
RECEIVER DEPTH: 112 METERS
MAXIMUM RANGE: 37.5 KYD
NOISE LEVEL: NOT MEASURED
PROFILE I
PROFILE II
PROPAGATION LOSS, dB
40
60
80
100
120
140
0
10
20
30
40
ACOUSTIC RANGE, KYD
SOURCE INOPERATIVE
37.5 kyd

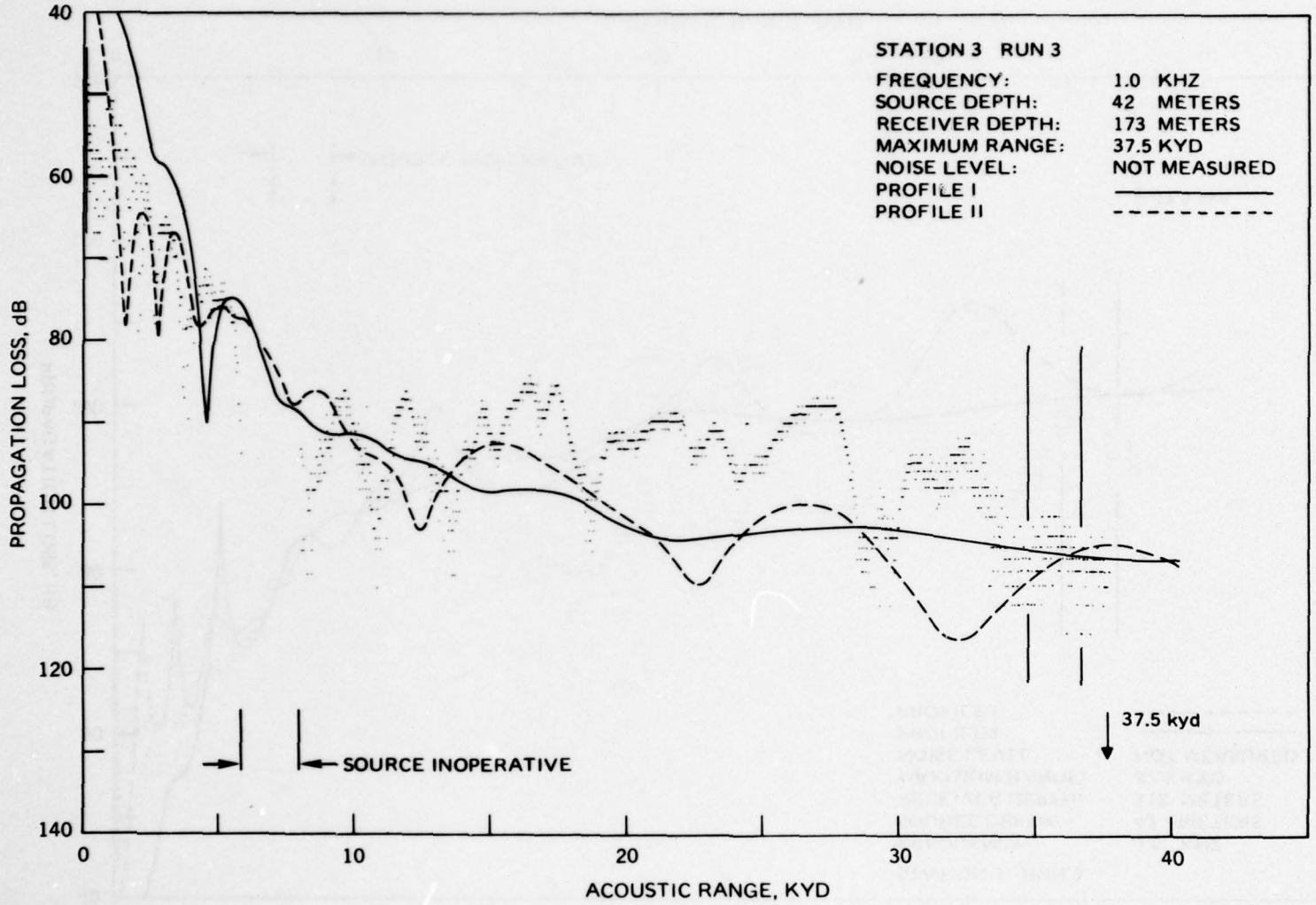
STATION 3 RUN 3
FREQUENCY: 1.0 KHZ
SOURCE DEPTH: 42 METERS
RECEIVER DEPTH: 173 METERS
MAXIMUM RANGE: 37.5 KYD
NOISE LEVEL: NOT MEASURED
PROFILE I
PROFILE II
PROPAGATION LOSS, dB
40
60
80
100
120
140
0
10
20
30
40
ACOUSTIC RANGE, KYD
37.5 kyd
SOURCE INOPERATIVE

APPENDIX E

EXPERIMENTAL AND THEORETICAL PROPAGATION LOSSES FOR STATION 1 RUN 2

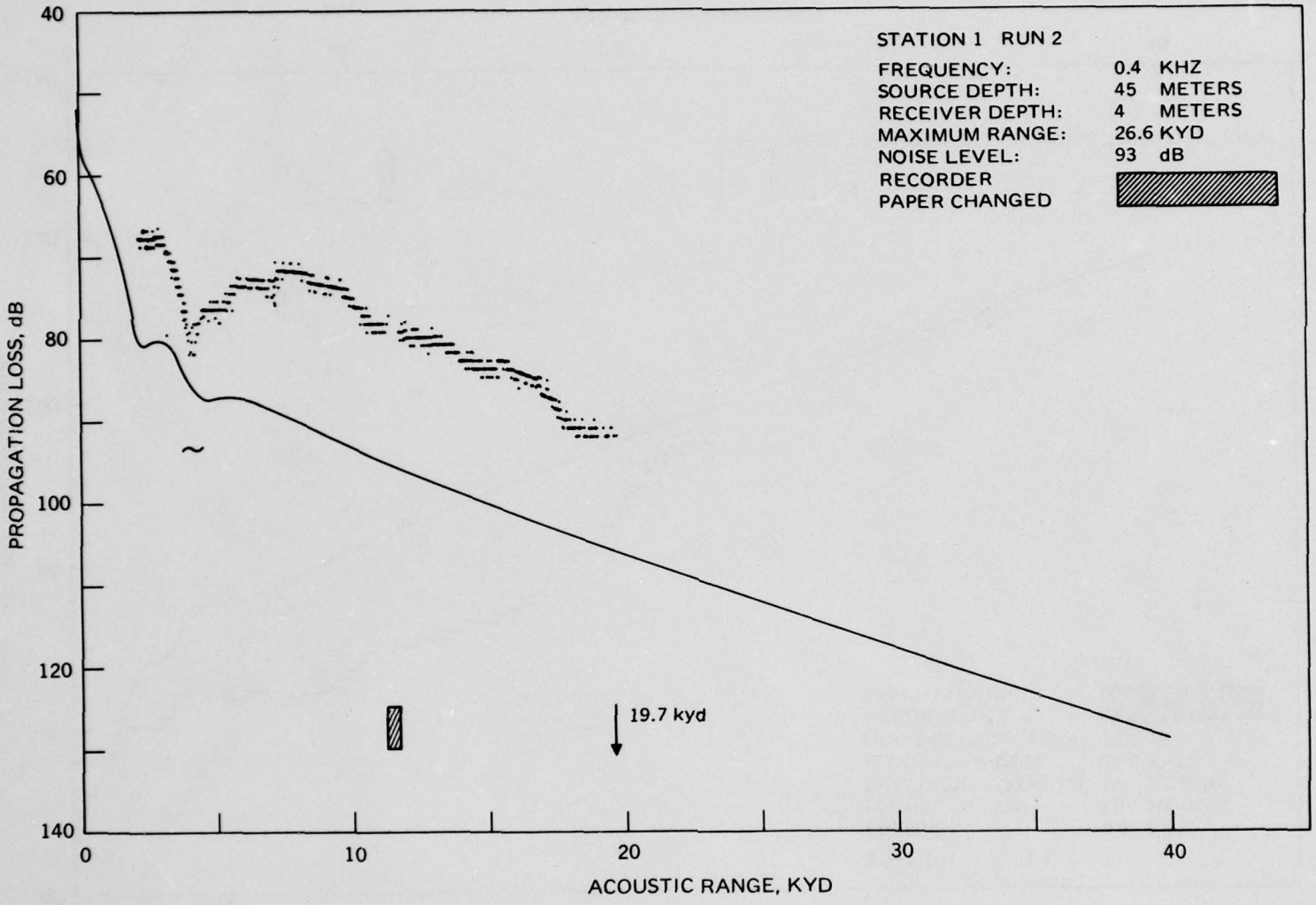
STATION 1 RUN 2
FREQUENCY: 0.4 KHZ
SOURCE DEPTH: 45 METERS
RECEIVER DEPTH: 4 METERS
MAXIMUM RANGE: 26.6 KYD
NOISE LEVEL: 93 dB
RECORDER PAPER CHANGED
19.7 kyd
PROPAGATION LOSS, dB
ACOUSTIC RANGE, KYD
40
60
80
100
120
140
0
10
20
30
40

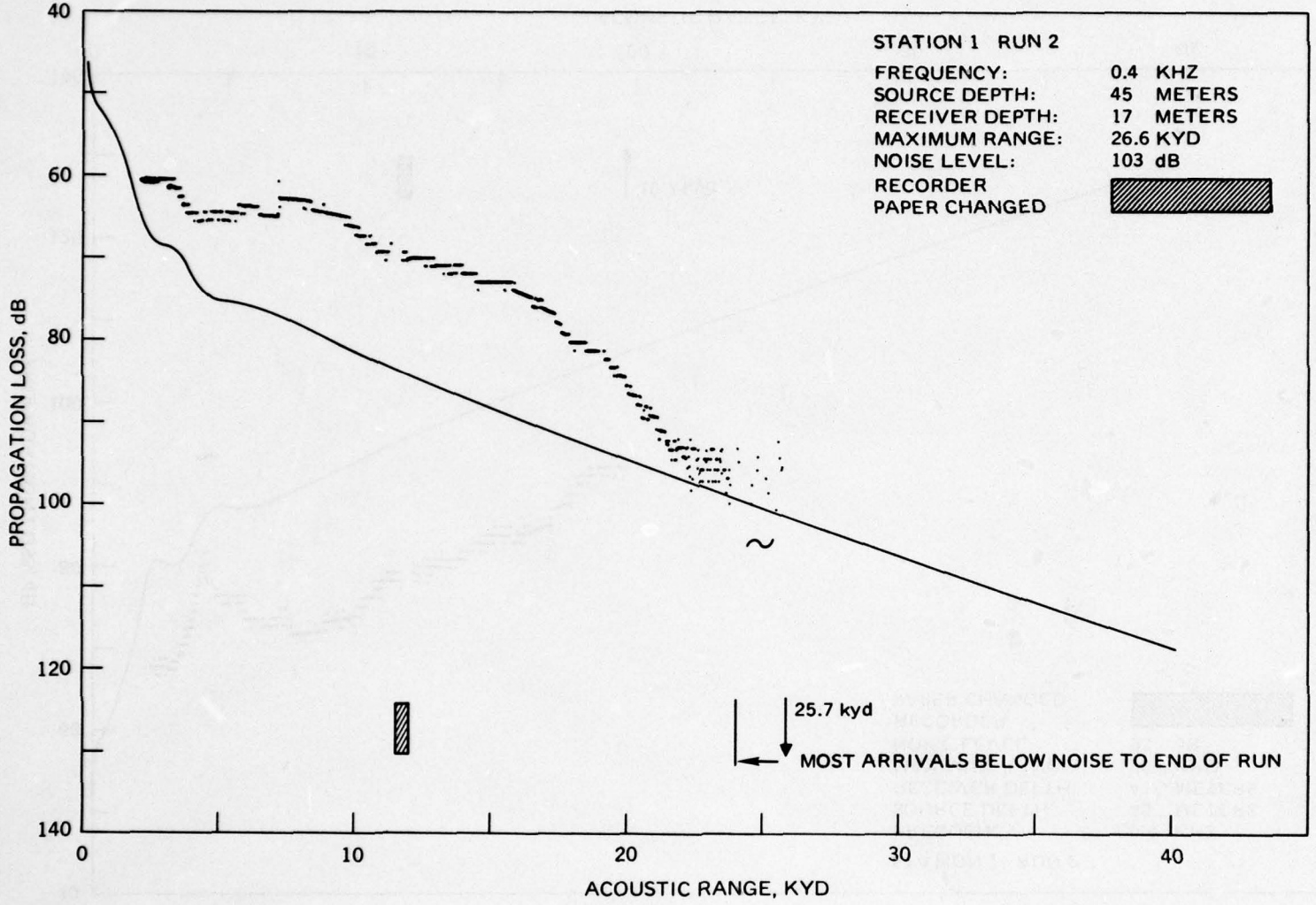
STATION 1 RUN 2
FREQUENCY: 0.4 KHZ
SOURCE DEPTH: 45 METERS
RECEIVER DEPTH: 17 METERS
MAXIMUM RANGE: 26.6 KYD
NOISE LEVEL: 103 dB
RECORDER PAPER CHANGED
25.7 kyd
MOST ARRIVALS BELOW NOISE TO END OF RUN
PROPAGATION LOSS, dB
40
60
80
100
120
140
0
10
20
30
40
ACOUSTIC RANGE, KYD

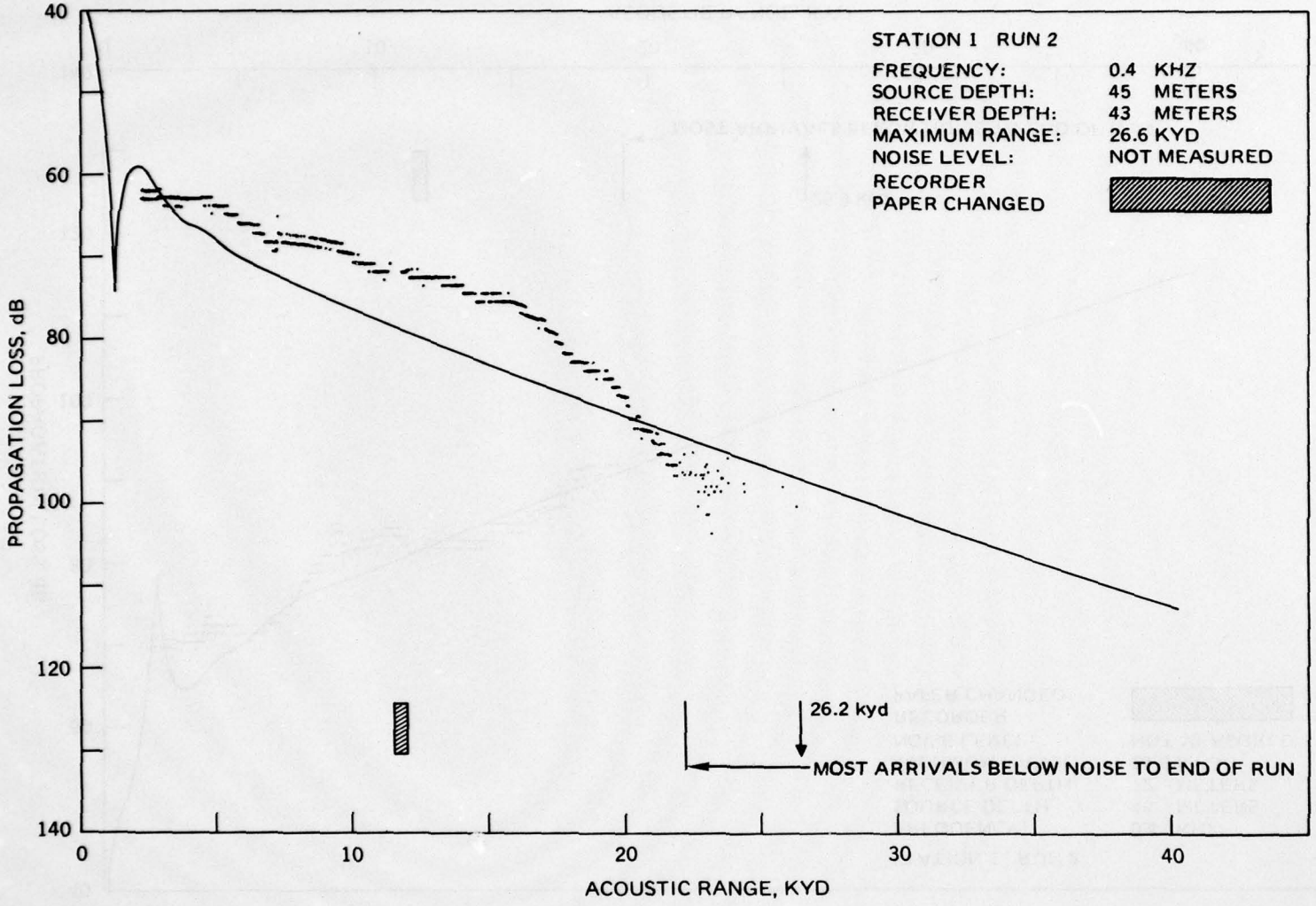
STATION 1 RUN 2
FREQUENCY: 0.4 KHZ
SOURCE DEPTH: 45 METERS
RECEIVER DEPTH: 43 METERS
MAXIMUM RANGE: 26.6 KYD
NOISE LEVEL: NOT MEASURED
RECORDER PAPER CHANGED
26.2 kyd
MOST ARRIVALS BELOW NOISE TO END OF RUN
PROPAGATION LOSS, dB
40
60
80
100
120
140
0
10
20
30
40
ACOUSTIC RANGE, KYD

AD-A049 077 NAVAL UNDERSEA CENTER SAN DIEGO CALIF F/G 17/1
SURFACE-DUCT SONAR MEASUREMENTS (SUDS I - 1972).(U)
NOV 76 E R ANDERSON
NUC-TP-463

UNCLASSIFIED NL

3 OF 3
AD
A049077

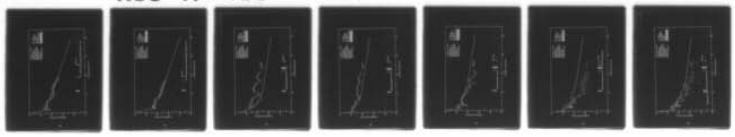

END
DATE
FILMED
3-78
DDC

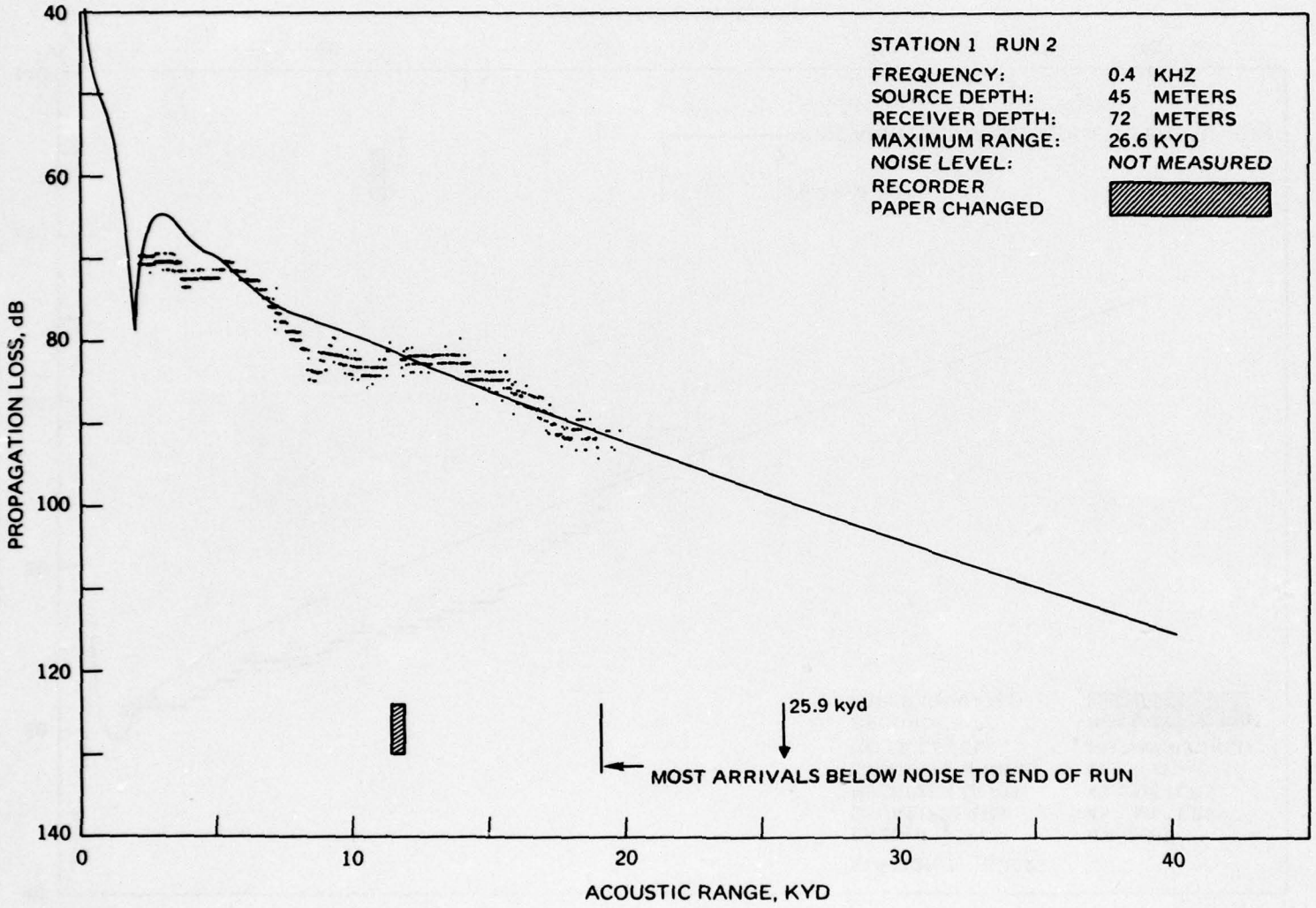
STATION 1 RUN 2
FREQUENCY: 0.4 KHZ
SOURCE DEPTH: 45 METERS
RECEIVER DEPTH: 72 METERS
MAXIMUM RANGE: 26.6 KYD
NOISE LEVEL: NOT MEASURED
RECORDER PAPER CHANGED
25.9 kyd
MOST ARRIVALS BELOW NOISE TO END OF RUN
PROPAGATION LOSS, dB
40
60
80
100
120
140
0
10
20
30
40
ACOUSTIC RANGE, KYD

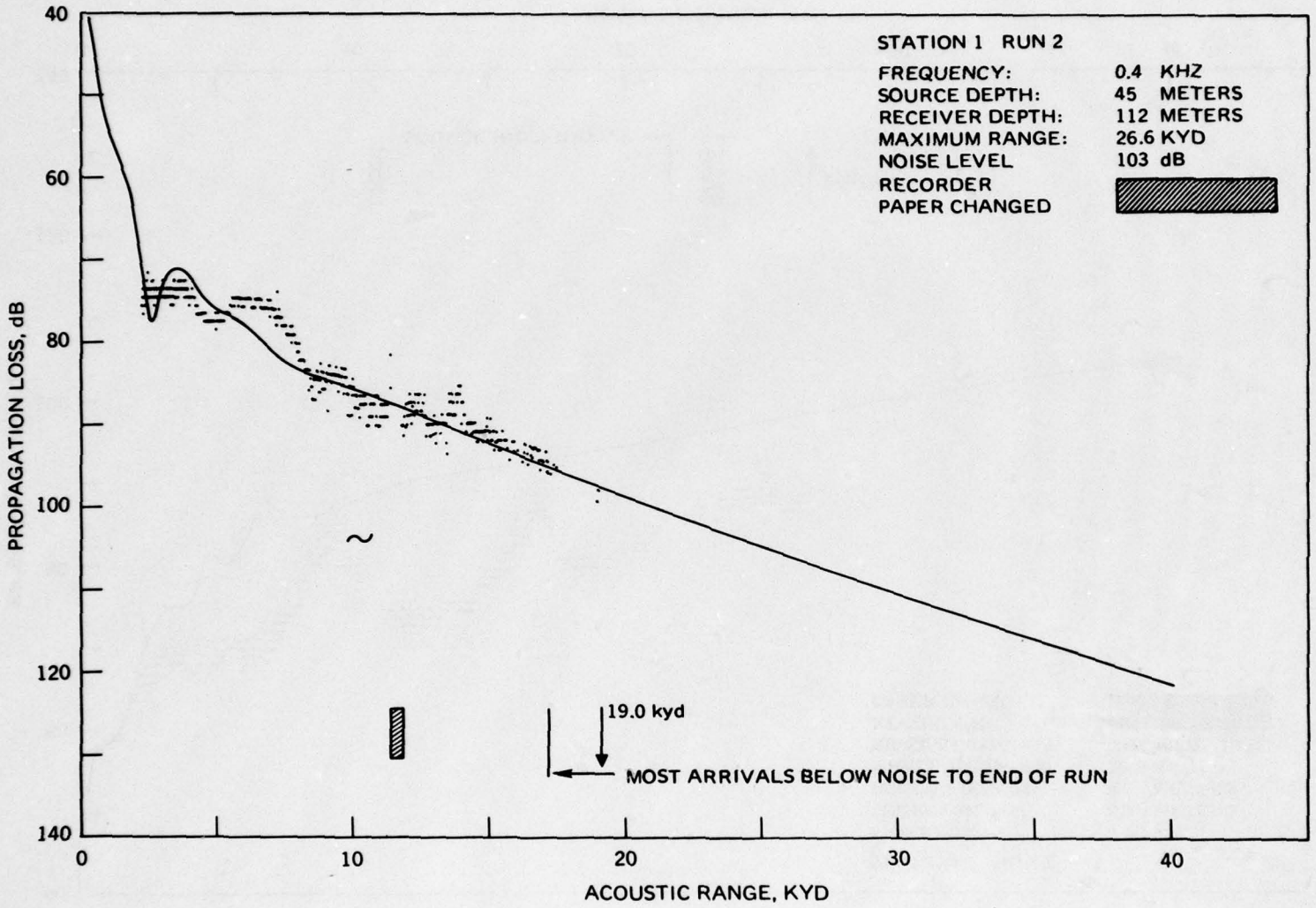
STATION 1 RUN 2
FREQUENCY: 0.4 KHZ
SOURCE DEPTH: 45 METERS
RECEIVER DEPTH: 112 METERS
MAXIMUM RANGE: 26.6 KYD
NOISE LEVEL 103 dB
RECORDER PAPER CHANGED
19.0 kyd
MOST ARRIVALS BELOW NOISE TO END OF RUN
PROPAGATION LOSS, dB
40
60
80
100
120
140
0
10
20
30
40
ACOUSTIC RANGE, KYD

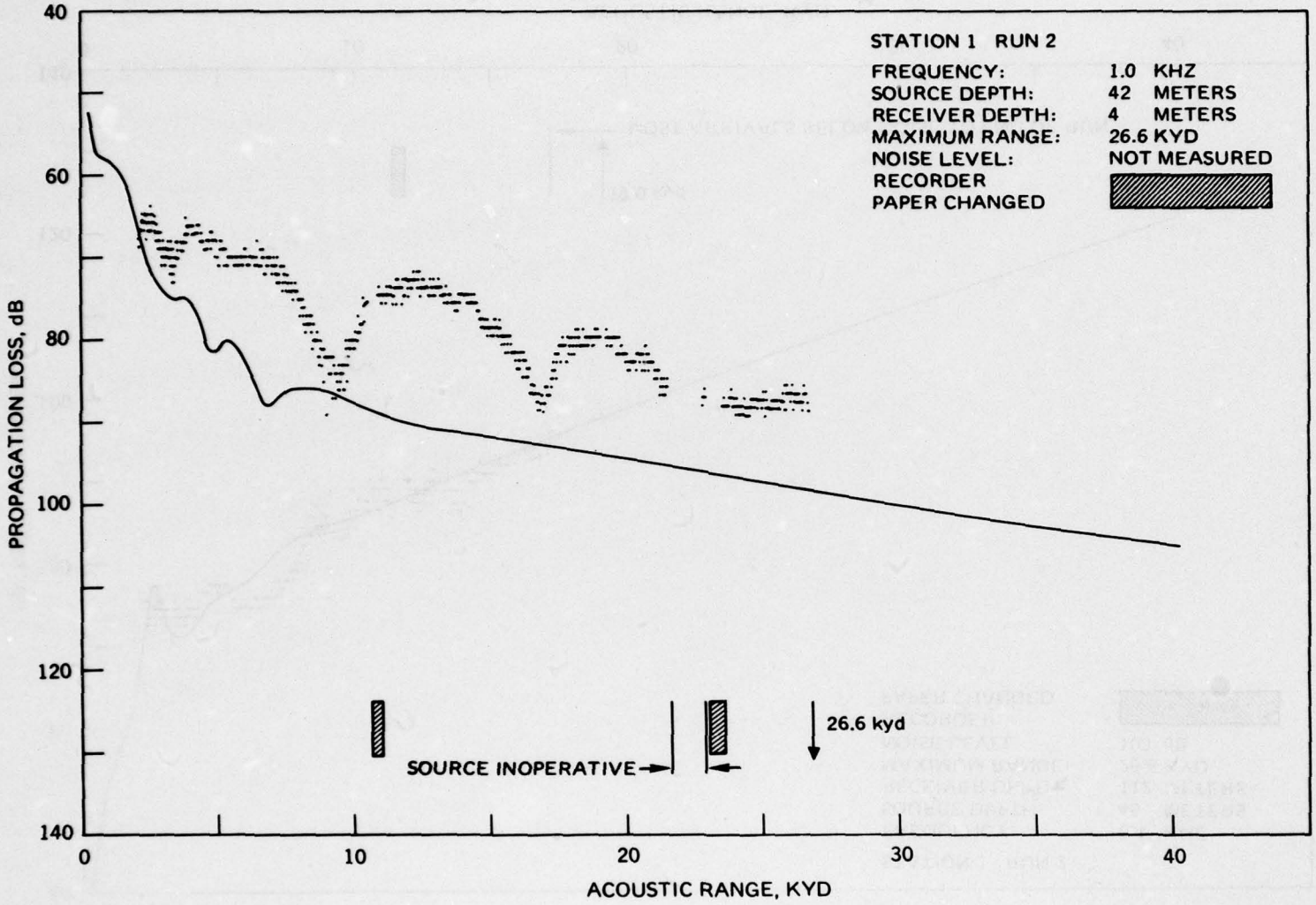
STATION 1 RUN 2
FREQUENCY: 1.0 KHZ
SOURCE DEPTH: 42 METERS
RECEIVER DEPTH: 4 METERS
MAXIMUM RANGE: 26.6 KYD
NOISE LEVEL: NOT MEASURED
RECORDER PAPER CHANGED
PROPAGATION LOSS, dB
40
60
80
100
120
140
0
10
20
30
40
ACOUSTIC RANGE, KYD
SOURCE INOPERATIVE
26.6 kyd

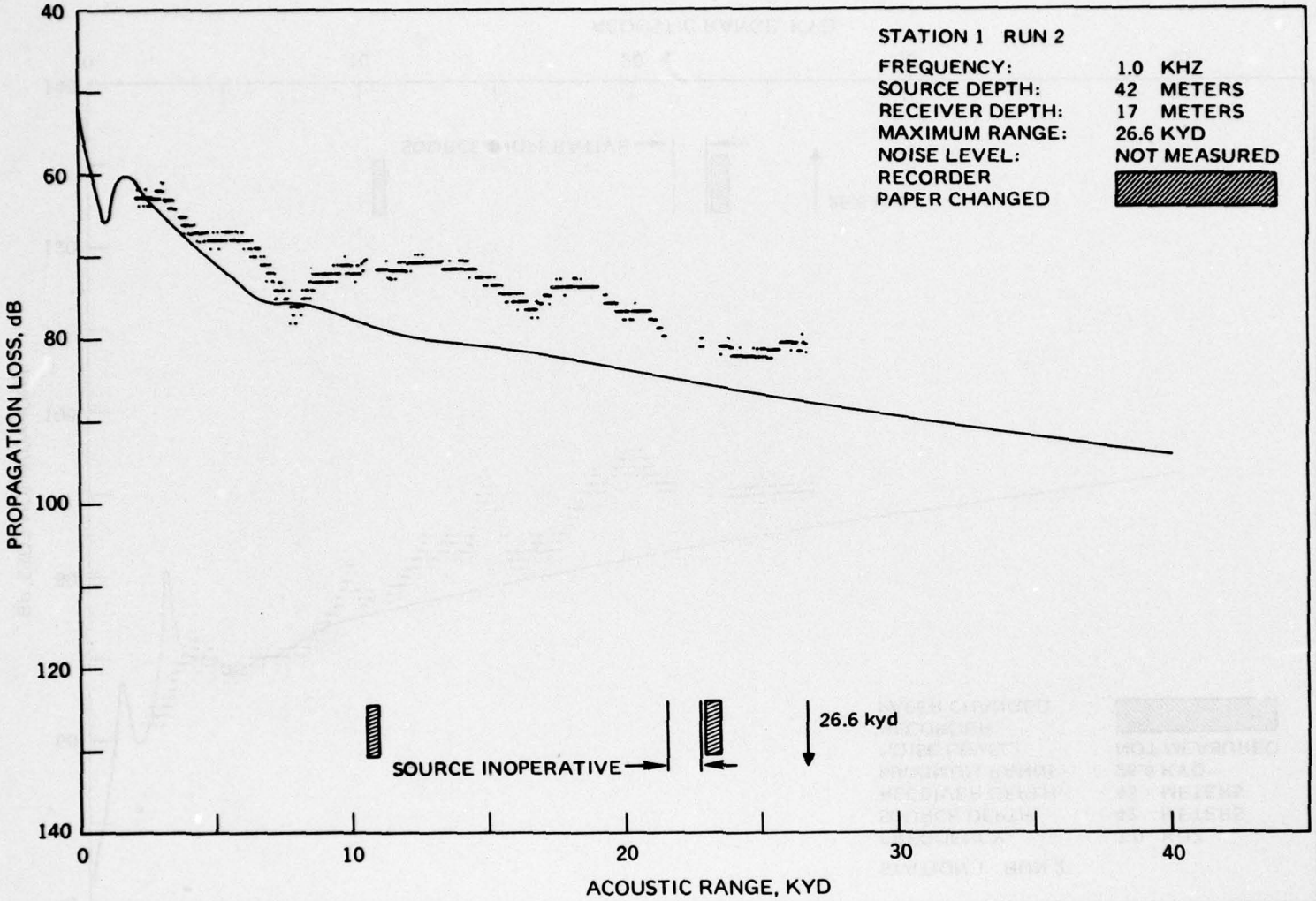
STATION 1 RUN 2
FREQUENCY: 1.0 KHZ
SOURCE DEPTH: 42 METERS
RECEIVER DEPTH: 17 METERS
MAXIMUM RANGE: 26.6 KYD
NOISE LEVEL: NOT MEASURED
RECORDER PAPER CHANGED
PROPAGATION LOSS, dB
40
60
80
100
120
140
0
10
20
30
40
ACOUSTIC RANGE, KYD
SOURCE INOPERATIVE
26.6 kyd

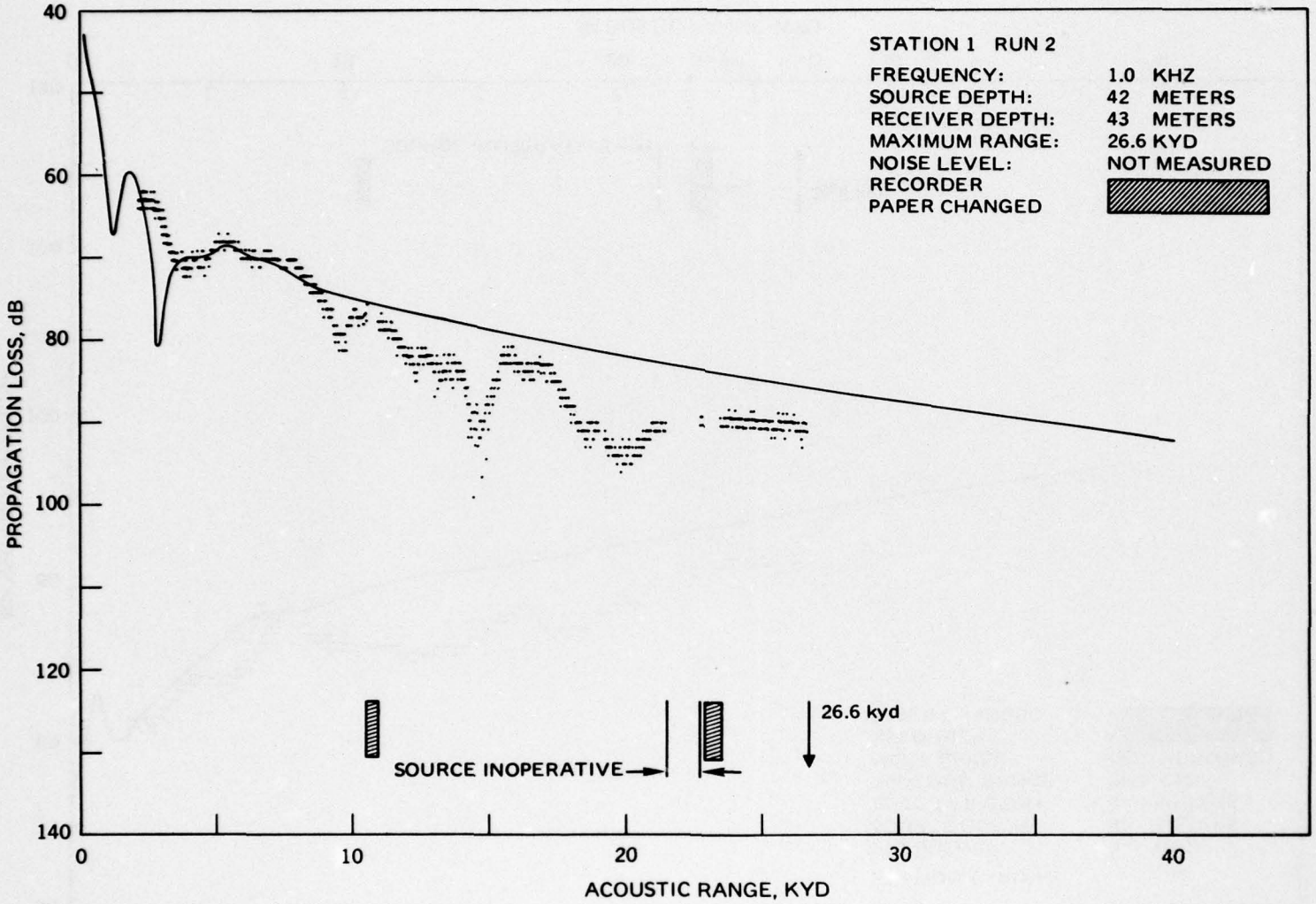
STATION 1 RUN 2
FREQUENCY: 1.0 KHZ
SOURCE DEPTH: 42 METERS
RECEIVER DEPTH: 43 METERS
MAXIMUM RANGE: 26.6 KYD
NOISE LEVEL: NOT MEASURED
RECORDER PAPER CHANGED
PROPAGATION LOSS, dB
40
60
80
100
120
140
0
10
20
30
40
ACOUSTIC RANGE, KYD
SOURCE INOPERATIVE
26.6 kyd

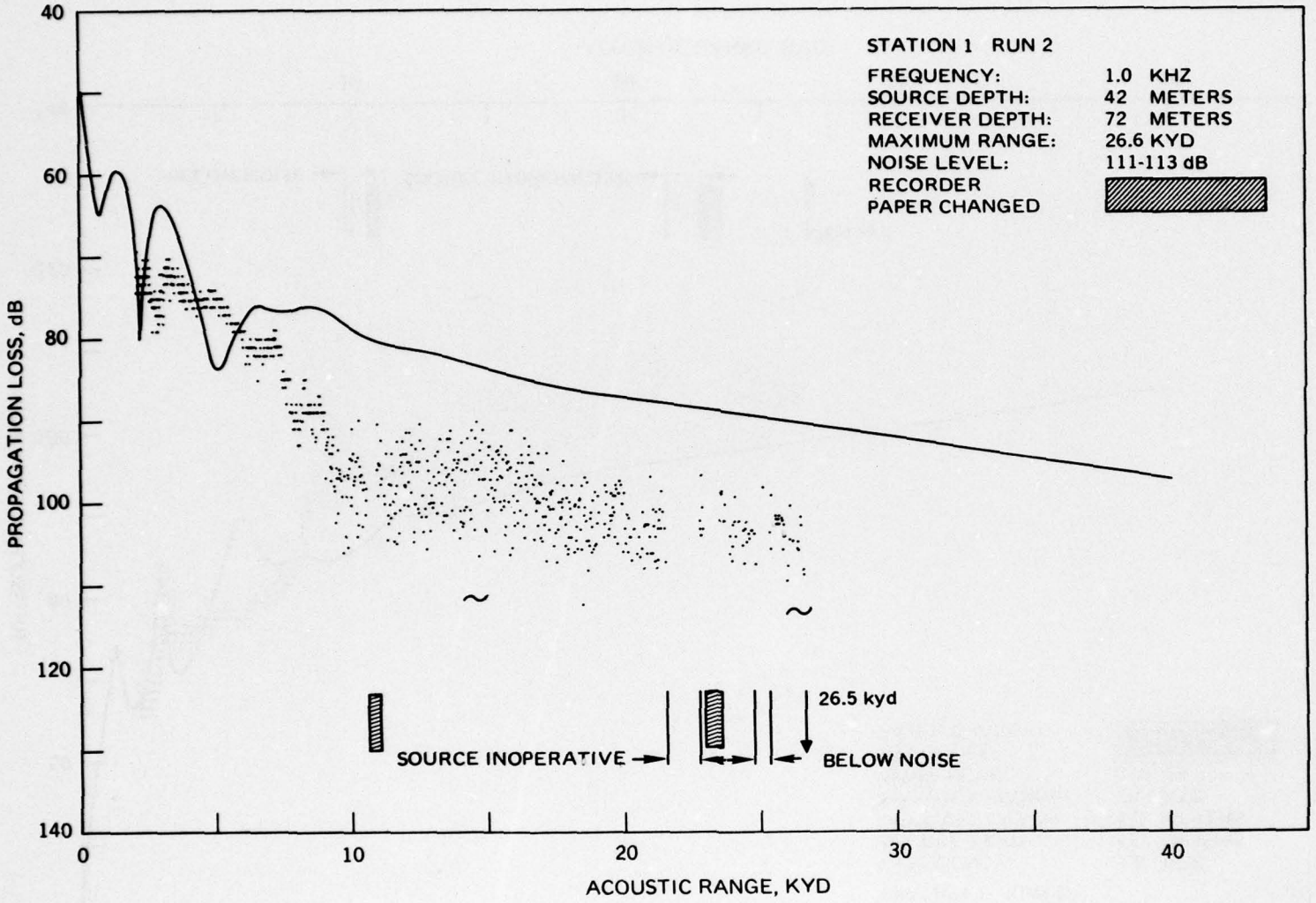
STATION 1 RUN 2
FREQUENCY: 1.0 KHZ
SOURCE DEPTH: 42 METERS
RECEIVER DEPTH: 72 METERS
MAXIMUM RANGE: 26.6 KYD
NOISE LEVEL: 111-113 dB
RECORDER PAPER CHANGED
26.5 kyd
SOURCE INOPERATIVE
BELOW NOISE
PROPAGATION LOSS, dB
40
60
80
100
120
140
0
10
20
30
40
ACOUSTIC RANGE, KYD

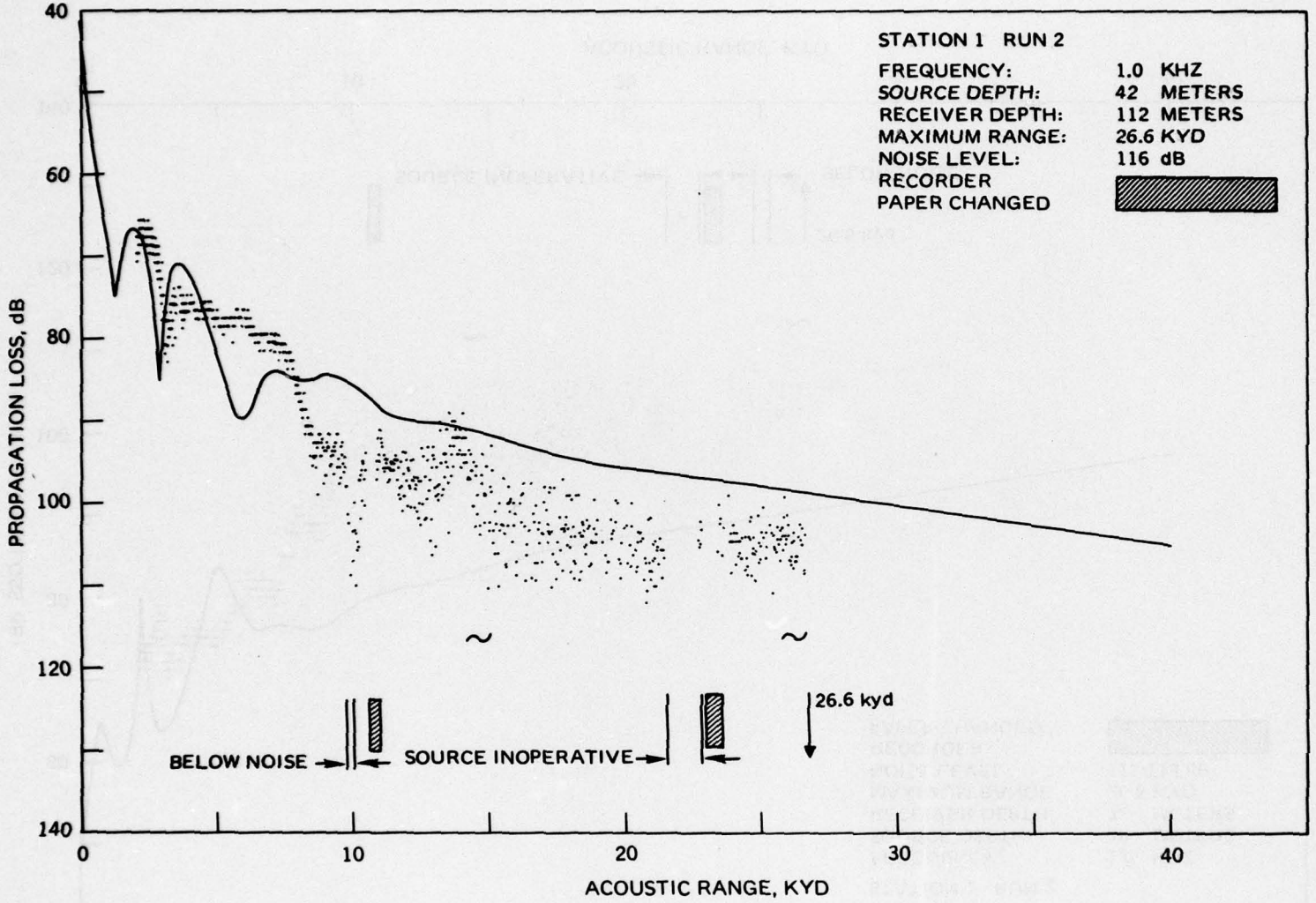
STATION 1 RUN 2
FREQUENCY: 1.0 KHZ
SOURCE DEPTH: 42 METERS
RECEIVER DEPTH: 112 METERS
MAXIMUM RANGE: 26.6 KYD
NOISE LEVEL: 116 dB
RECORDER PAPER CHANGED
PROPAGATION LOSS, dB
40
60
80
100
120
140
BELOW NOISE
SOURCE INOPERATIVE
26.6 kyd
0
10
20
30
40
ACOUSTIC RANGE, KYD